Sheffield Hallam University

Bone Vibration Analysis as a Novel Screening Tool for Long Bone Fractures

---

A thesis submitted in partial fulfilment of the requirements of Sheffield Hallam University for the degree of Doctor of Philosophy

Ridita Ali

January 2019

Director of Studies: Dr Lyuba Alboul

Supervisor: Dr Amaka C. Offiah

Co-Supervisor: Dr Xu Xu

Declaration

I hereby declare this thesis is my own work and effort and it has not been submitted anywhere for any award apart from that of Doctor of Philosophy at Sheffield Hallam University.

The sources used in this thesis apart from my work, has been referenced and acknowledged.

…… ……

Ridita Ali Date

Abstract

The aim of this study is to reduce the number of X-ray scans taken to detect fractures, by developing a bone fracture screening system. When assessing a bone injury, doctors need to decide whether the injury has resulted in a fracture or a sprain so that they can provide appropriate treatments. The current way to differentiate between these is by an X-ray scan. In 2011, the 46,000 children attending Sheffield Children's Hospital Emergency Department had 10,400 X-rays, mostly to help diagnose bone fractures. Roughly half the X-ray scans taken indicate that the injury is sprain. Unnecessary X-ray scan means raising costs and exposing patients to ionising radiation.

Vibration analysis is a well-established technology for condition monitoring for defect detection in industries however; its use in the medical field is still evolving. In bone vibration analysis, periodic or aperiodic oscillations or oscillating signals are introduced, and subsequent responses are recorded followed by using mathematical methods to reach a conclusion. In this study, a computer-controlled mechanism induces a mild vibration and successive responses are recorded via a piezoelectric sensor. To demonstrate the method's feasibility, a preliminary study was carried out on five blocks of wood of different density, with the same dimensions. The tests indicated a significant reduction in the blocks' vibration frequency following their fracture.

After obtaining National Health Services (NHS) Research Approval, appropriate number of bone vibration responses was recorded from adults' wrists and children's wrists and ankles who attended local hospitals following wrist or ankle injuries. Suitable signal processing and pattern recognition techniques were developed on the basis of vibration responses from bones at various stages to interpret the recorded signals. Data were acquired from healthy participants at a local school which were compared with the data acquired from hospital participants to verify the methods. Currently, this study differentiates around 80% of the injuries accurately.

Additionally, both the data acquisition program and the device have been modified to improve the developed procedures. This study made some promising discoveries and the resulting techniques can be used for further explorations.

Acknowledgements

First of all, I would like to thank my Director of Studies, Dr Lyuba Alboul for all her support, guidance and kind advice throughout my PhD research. I would also like to thank my first supervisor, Dr Amaka C. Offiah for her constant support and constructive suggestions. I am thankful to my second supervisor, Dr Xu Xu for her availability and advices.

I would like to express my gratitude to Dr Reza Saatchi for helping me at the initial stage of my PhD study. I am appreciative of the financial support for my research from Children's Hospital Charity. I am grateful to all the participants from Northern General Hospital, Sheffield Children's Hospital, Saturday School ClubOK located at King Edward VII Upper School and Sheffield Hallam University who participated in this study.

Finally, I would like to thank my parents, my sisters (Samira Ali and Sabiha Ali), my husband (Mohammed Rezwan Rahman) and in-laws for all their love and support that encouraged me to continue my research.

List of Abbreviations

1D	One-dimensional
2D	Two-dimensional
3D	Three-dimensional
A&E	Accident and Emergency Department
AF	Attenuation Factor
CAD	Computer Aided Design
CFA	Current feedback amplifier
CM	Contact microphone
CT	Computed Tomography
CWT	Continuous Wavelet Transform
DFT	Discrete Fourier Transform
DSP	Digital Signal Processing
DWT	Discrete-time Wavelet Transform
ED	Emergency Department
FE	Finite Element
FFT	Fast Fourier Transform
GCP	Good Clinical Practice
GP	General Practice
MATLAB	Matrix Laboratory
MOSFET	Metal–oxide–semiconductor field-effect transistor
MPEG	Moving Picture Experts Group
MRI	Magnetic Resonance Imaging
NGH	Northern General Hospital
NHS	National Health Service
NI LabVIEW	National Instruments Laboratory Virtual Instrument Engineering Workbench
OPA	Operational Amplifier(s)
PCB	Printed Circuit Board

PET	Positron Emission Tomography
PVDF	Polyvinylidene Fluoride
QCT	Quantitative Computed Tomography
RMS	Root Mean Squared
RPM	Revolutions per minute
SCH	Sheffield Children's Hospital
SDOF	Single degree of freedom
SOM	Self-organising map
STFT	Short-Time Fourier Transform
US	Ultrasound
WD	Wavelet Decomposition
WCSS	Within-Cluster Sum of Squares
X-rays	X-radiations

Table of Contents

List of Figures

Figures in Chapter 2

Figures in Chapter 3

Figures in Chapter 4

Figures in Chapter 5

Figures in Chapter 6

Figures in Chapter 7

List of Tables

Table in Chapter 2

Table in Chapter 4

Tables in Chapter 5

Tables in Chapter 6

Table in Chapter 7

Chapter 1: Introduction

1.1 Background

The first line of investigation following wrist and ankle injury is radiography which helps to differentiate between fracture and sprain. In cases, where the patients complain of persisting pain in the follow-up hospital attendances, Computed Tomography (CT), Magnetic Resonance Imaging (MRI) or Positron Emission Tomography with nuclear medicines (PET) scans are conducted to reveal any hidden fracture.

Each radiographic examination costs £40 to £120.

- In a study conducted at South Wales Accident and Emergency Departments (A&E), 64% of the radius/ulna injuries were diagnosed as sprains, not as fractures (Lyons, R. A., *et. al.* 2017). Distal radius fractures are by far the most common ones. 35% wrist fractures and 50% are from ulna/radius are undiagnosed on the second visit by radiography. Moreover, 30% patients with significant soft tissue injuries do not get diagnosis (Dussa, C. U., *et. al.* 2006).
- 302,000 new ankle sprains and 42,000 new severe ankle sprain patients attend UK Emergency Departments (ED) each year (Maffuli, N., *et. al.* 2008).

There are also many other cases where injuries in bones have been misdiagnosed as sprains (Guly, H. R. 2002) (Tsyrulnik, A. 2015).

- X-rays are one of the most common diagnostic tests to detect bone fractures and osteoporosis. X-rays are a form of ionising radiation. The resulting image of an x-ray detector is a two-dimensional (*2-D*) image of a three-dimensional structure (*3-D*). While passing through a patient, the X-ray beam is absorbed in proportion to the cube of the atomic number of the numerous tissues through which it passes. Thus, the larger the amount of radiation hitting the detector, the darker the image will be. Hence, materials of low density appear darker than those of high density. The disadvantage of this technique is that x-rays actively divide cells and can

cause genetic mutations. The genetic mutations may cause cancer (Clarke, C. G. D., *et. al.* 2015). Some patients who have been exposed to X-rays can develop cancers 10 to 15 years later (Dana-Faber Cancer Institute 2019). The other problems are that the equipment is non-portable, expensive and performing X-rays requires skilled technicians. The *main* reasons for developing a non-invasive screening method, in this case, vibration analysis, are *reducing time* and *cost of attending hospital*.

The patients who have sprains in their bones are getting exposed to unnecessary radiation. However, the risk of causing cancer by each X-ray is very minimal (Public Health England 2008).

- Quantitative Computed Tomography (QCT) techniques used for monitoring healing are limited to exterior implants as metal embeds could introduce artefacts which could affect the scans (Boer, F. C. D., *et. al.* 1998).
- Ultrasound (US) is a technology to examine the inner organs of the body. However, US images are prone to speckle noise and using it for fracture screening would be subjective and needs highly skilled radiographer and radiologist. US scanning also require the sensing probe to be pressed on the injured site which can be painful. Moreover, bones absorb at least 50% of the incident radiation and the reflected radiation undergoes absorption losses by the cartilage and ligament more than the skin and fat layers surrounding the bone before it reaches the receiver. It also has the problem of heating the surroundings of the bone and thus damaging the surrounding soft tissues (Dawood, M. S., *et. al.* 2012).

1.2 Aims and Objectives

Aims

The aim of the study is to develop and evaluate a system, its associated signal processing and pattern recognition techniques to screen for bone fracture in human subjects.

Objectives

The study objectives were:

i. Designing, developing and testing of required system to induce suitable bone vibration and then measure the required bone vibration responses to differentiate between fracture and sprain in long bones.
ii. Preliminary evaluation of the system on blocks of wood of different density.
iii. Critical evaluation of the system in adult subjects to demonstrate the system acceptability for carrying out the same procedure on children and in addition, evaluate its performance in screening for bone fractures.
iv. Upon successful completion of task (iii), critical evaluation of the system in children to demonstrate the system suitability for real world applications and to evaluate its performance in screening for bone fractures.
v. Improvement of the results for developing the screening technique includes modification of the device, program for acquisition of data and computational techniques for the distinguishing purpose.
vi. Acquisition of vibration responses from healthy children for observing the pattern of results compared to the data acquired from hospital.

1.3 Method Used

In this research, vibration has been applied on suitable bones and data have been captured from long bone (wrists and ankles) injuries. These vibration responses have been analysed appropriately to detect the presence or absence of fracture. Vibration analysis is a popular technique in detecting cracks inside machines and a promising technique in diagnosing metabolic bone disease such as osteoporosis and monitoring fracture healing. Key features of this technique are that it is entirely non-invasive, cost effective, easy to apply and harmless on humans. Most of the publications show that more experiments have been conducted on tibia and femur but much less on ulna and radius. Therefore, this research intends to cover this gap in the experimental studies of the use of vibration analysis on detection of bone fractures. The current study has been carried on both wrists and ankles using vibration analysis to develop a reliable screening tool to detect fracture.

1.4 Research Questions Investigated

There were several questions enquired by different experiments to find out the solutions.

I. Is there any difference in frequencies indicated by intact bones and fractured bones or similar material (wood)?
II. Does it demonstrate that if a bone is fractured then vibration induction using the mechanism suggested will detect the fracture properly and will not cause any pain to the patient (especially to a child), when the bone is fractured?
III. How the difference in frequency or any other property, generated from bone(s) designate a bone to be fractured or unfractured?
IV. Is the vibration study helpful in differentiating ankle fracture from sprain?

1.5 Outline of the Chapters

Chapter 1: Introduction

Chapter 1 introduces to the topic and purpose of the research undertaken. A brief background of the study carried out over four years is provided giving a brief idea why this study is necessary to be conducted including the research questions solved at different stages, the aims and objectives of the project along with the outline of the chapters.

Chapter 2: Overview of Bones structure and their injuries

Chapter 2 presents the Literature Review of the entire project. Various researches related to this study, were carried out at various times with different devices, techniques and mechanisms. All those researches (mostly published articles) give an indication why this study can be a success. The ideas proposed, and studies conducted previously with some of their outputs which are related to this project are all described in the chapter.

Chapter 3: Theoretical background of the Techniques used

Chapter 3 outlines all the theories behind this project. These theories represent an explanatory overview on the method chosen; how the mechanism of the device used in this research, actually works in practice and finally the procedures' descriptions to clarify the reasons for applying the techniques. The official procedures before beginning the project practically have also been discussed.

Chapter 4: Smart Systems and Evaluations

Chapter 4 describes the methodology of this research. It contains figures of the experimental set-ups and the explanations of every stage of this project. The official steps performed before starting the project and also, the practical steps taken to reach the aim are explained. This chapter provides an overview of the hardware and software so far employed used for recording the data and in obtaining current results. The description of the layout of the circuit as well as details of each step for constructing parts of the main circuit has been attached. The modifications performed to the device are accounted with the reasons behind doing so. The techniques for processing the data acquired at different stage of this research are discussed into details.

Chapter 5: Relations and Variations between Fracture and Sprain

Chapter 5 provides the preliminary results and their analyses. This chapter shows how the results were produced, specifying the reasoning behind such results and the possible meanings and impacts related to the aim of this study. Most of the results are displayed using figures and tables.

Chapter 6: Data from Children's Wrists

Chapter 6 presents the results established from the data acquired from children of age between 10 and 15 years old with wrist injury who participated in the study with the parental consent. It also contains the details how the data have been acquired from children's wrists with no injuries from a local school. The analyses and the comparisons of the results and the efficiency of the method and techniques developed have all been described in detail.

Chapter 7: Data from Children's Ankles

Chapter 7 shows the results established from the data acquired from children of age between 10 and 15 years old with ankle injury who participated in the study with the parental consent. The analyses of the data and the suitable techniques applied to the data have been discussed.

Chapter 8: Conclusion and Further Works

Chapter 8 concludes the thesis. It summarises the research findings and suggests further work directions. The significance of the outcomes is discussed. Contributions to knowledge are described in detail. As it has been proven that this study has a strong potential, it has been suggested that how the device can be improved and how different area can be explored with this kind of mechanisms.

1.6 Presentations and Conferences

- Ali, R., Alboul, L., Offiah, A. C., " Development of a non-invasive screening technique for detection of wrist fractures in children" in 32nd International Congress and Exhibition on Condition Monitoring and Diagnostic Engineering Management, Huddersfield, U.K., 2019.

- Fennimore D., Ali R, Alboul L., Offiah A. C., "Assessing the ability of vibration analysis to differentiate wrist and ankle fractures from sprains in children" in International Conference on Children's Bone Health, Salzburg, Austria, 2019.

- Ali, R., Fennimore, D., Alboul, L., Offiah, A. C., “Assessing the ability of vibration analysis to differentiate wrist fractures from sprains in children” in 9th Annual Mellanby Centre Research Day, University of Sheffield, UK, 2018.

- Ali, R., Alboul, L., "Development of a Novel Screening Tool to detect fractures in Long Bones," in MERI PGR Showcase Event: Gathering Together, March 2018.

- Ali, R., Alboul, L., Offiah, A., "Signal Processing Techniques for Accurate Screening of Wrist Fractures," in Doctoral Conference on Computing, Electrical and Industrial Systems, DoCEIS 2017, pp. 175-182, May 2017.

- Ali, R., Alboul, L., Offiah, A., "Clustering and self-organising mapping to analyse Bone Vibration as a method of screening Fracture," Presentation at Sheffield Children's Hospital CHIRPP Meeting, November 2016.

- Ali, R., Offiah, A., Ramlakhan, S., "Fuzzy C-Means clustering to analyze bone vibration as a method of screening fracture," in 2016 10th International Symposium on Communication Systems, Networks and Digital Signal Processing (CSNDSP), pp. 1-5, 2016.

- Ali, R., "Analysis of bone vibration signals in order to screen fracture," at MERI Research Symposium, May 2016.

- Ali, R., Saatchi, R., Offiah, A., Ramlakhan, S., "Frequency Response and Cluster Analysis of Bone Vibration Signals to Screen for Bone Fractures," in MERI/BMRC Winter Poster Event 2015, December 2015.

- Ali, R., Saatchi, R., Al-mafrachi, R., "Bone Vibration Analysis as a Novel Technique for Fracture Screening," in MERI/BMRC Winter Poster Event 2014, December 2014.

Chapter 2: Overview of Bones structure and their injuries

2.1 Introduction

In this chapter, an overview of the bones and fracture mechanics, along with the vibration analysis applications in industries and medical fields, are provided. The following are discussed:

- the related topics for developing the system,
- the relevant techniques for analysing the acquired data.

The system and analysis of data enabled long bone injuries to be screened and differentiated between sprain and fracture. This research is associated with long bones (ulna, radius, tibia and fibula), so an overview of the long bones is provided.

2.2 Structure of a Human Body

There are 206 bones in a human body. Each bone is made up of the complex matrices of tissues. Osteogenic precursor cells, osteoblasts, osteoclasts, osteocytes, and the hematopoietic features of bone marrow are the cellular components that make up the bone. Bone is a dynamic structure that can easily adapt to varying requirements by shifting its structure and mass accordingly (Planell, J. A. 2009). Its major functions include protection of internal organs, offering firm segments for muscles to enable movement and it acts as the main reserve of calcium and phosphate in the body (Hohmann, E. L., *et. al.* 1986).

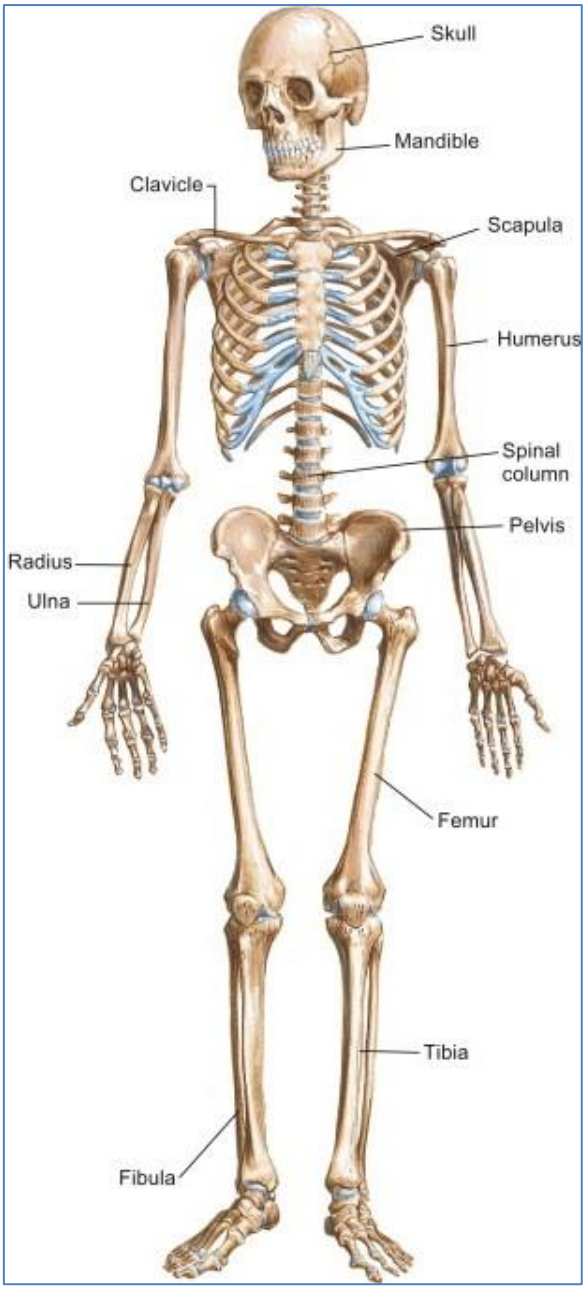

Figure 2.1: Regional anatomy of the whole Skeleton (Treuting, P. M., *et. al.* 2012).

Bone is a composite material and its complex and compact structure mainly consists of minerals, organic matrix, cells, and water. While minerals contribute to making up two-thirds of the dry weight of bones, the relative quantities of all the elements are responsible for the mechanical properties critical to bone function (Feng, X. 2009). The inorganic, organic, and water compounds that enable locomotion, protection of important internal organs, and regulation of mineral homeostasis are about 40%, 30% and 25% by volume, respectively (Feng, X. 2009). Crystalline Hydroxyapatite is the predominant inorganic component whereas collagen makes up 90% of the organic matrix (Auer, J. A., *et. al.* 2011). Collagen is required for the bone's flexibility

while the combination of mineral and collagen gives bone its stiffness (Planell, J. A. 2009).

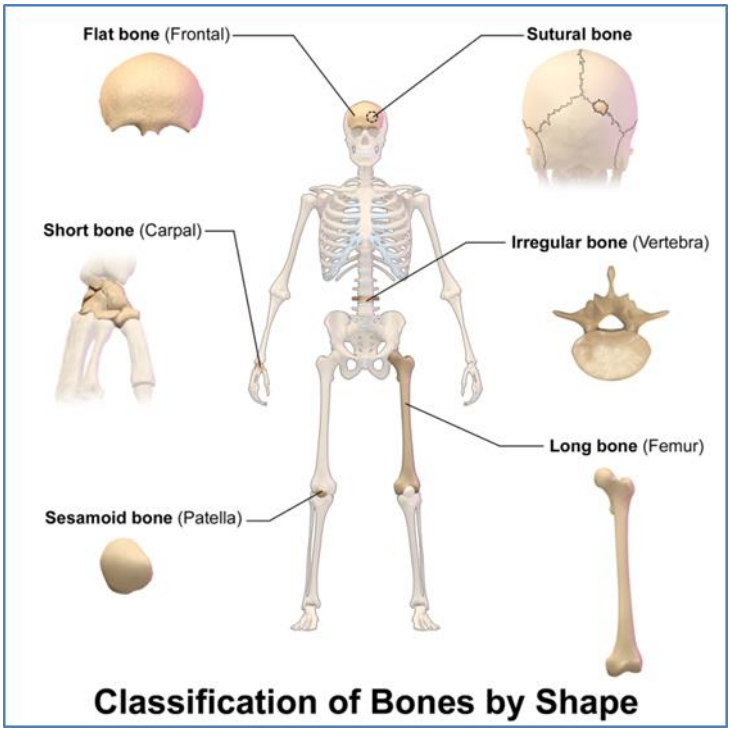

Figure 2.2: Classification of Bones (Blaus, B. 2015).

In order to simplify the understanding of the concept of bones, they have been arranged into different groups through the application of some classification methods. The categorisation can be done as follows: (Planell, J. A. 2009):

- Predominant tissue composition (cortical and trabecular),
- Type (long, short, flat, irregular and sesamoid) and
- Site (axial and appendicular).

During the life span, bone experiences complex patterns of loading. Prediction of behaviour under applied loads necessitates delineating its mechanical properties. The properties and geometry of bones can be found out by mechanical testing. (Rajaai, S. M., *et. al.* 2010).

2.3 Bone Mass, Density and Growth

Fracture risk depends on bone growth and bone loss. Both these factors depend on intake of nutrition, especially protein. (Rizzoli, R., *et. al.* 2001) (Rizzoli, R., *et. al.* 2004). Gender difference in bone mass in adults can be clearly discerned at puberty. The important difference observed during this stage is the difference in bone mass that occurs due to a larger growth in bone size that results from a growth in cortical shell, a property which affects males more than females (Seeman, E. 2003). A longer duration of pubertal maturation is responsible for the notably larger average areal bone mineral density (BMD) detected in young healthy adult males when compared to females in the lumbar spine, also at the mid-femoral or mid-radial diaphysis levels (Theintz, G., *et. al.* 1992). (Avdagic, S. C., *et. al.* 2009) carried out a study and published their report on investigation of how increasing age of young men and women affects skeletal region of peak bone density; additionally, they tested the impact of diet as well as physical activity on bone mass. Sodium, protein, and fibres were nutrients which notably corresponded to BMD. According to their findings, the fact that boys achieve peak bone density after girls and this density variance is the most prominent in the spine.

According to several studies, fractures in childhood, possibly resulting from a deficit in bone mass accumulation throughout rapid longitudinal development, might be related to lower peak bone mass (Ferrari, S. L., *et. al.* 2006).

The vertebral microstructure transforms noticeably from a dense and extremely associated network of rods to a less dense and less well-connected network of plates during growth (0-25 years). While aging (>25 years), the structure changes to a less dense, less well-connected web of rods and trabecular bone volume fraction is lost as well (Thomsen, J. S., *et. al.* 2012).

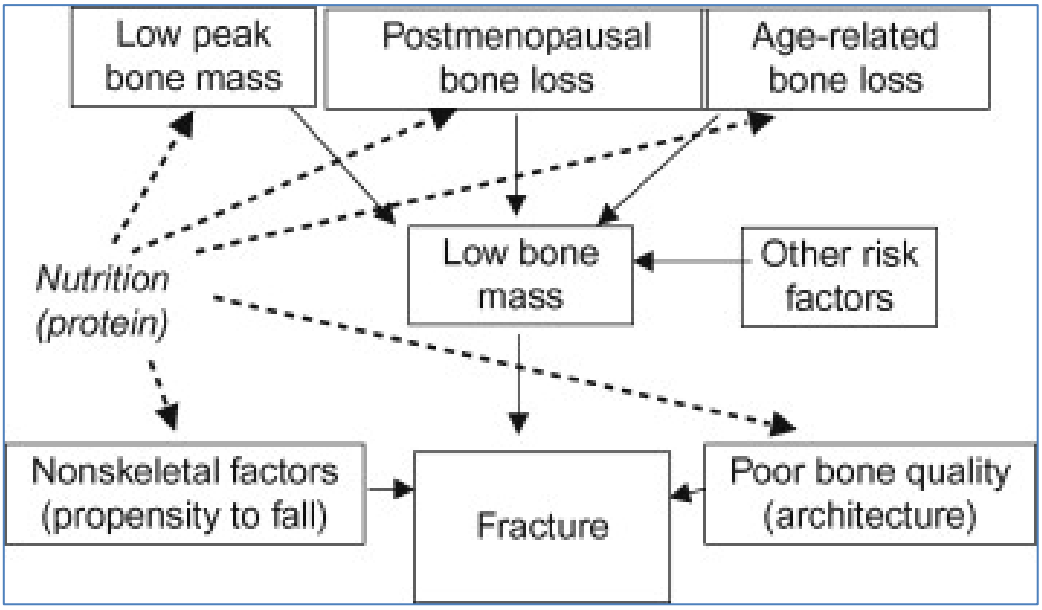

Figure 2.3: Potential influence of protein consumption on several modules of bone fragility (Rizzoli R. 2010) (Rizzoli, R., *et. al.* 2004).

2.4 Fracture Mechanics

A fracture is a break in any bone usually occurring when there is an impact or force applied to it. Name of fractures can be derived from their severity, the shape or location of the fracture line, or sometimes the name of the physician who initially recognised a specific fracture (Tortora, G. J., *et. al.* 2011). The natural reflexive movement for any person falling is to extend their hand to lower the impact of the fall, which is followed by fractured bones. 10% to 25% of all paediatric injuries are made up of fractures (Landin, L. A., 1997). In a study carried out in the United Kingdom, it has been suggested that boys sustained childhood fracture more than girls and 30% of fractures in both sexes occurred in radius/ulna (Cooper, C., *et. al.* 2004).

There are many types of fractures. Some common fractures are described below with their illustrations and radiographs (Tortora, G. J., *et. al.* 2011).

- Open or Compound fracture - The parts of the bone that are broken, protrude (or bulge out) through the skin.

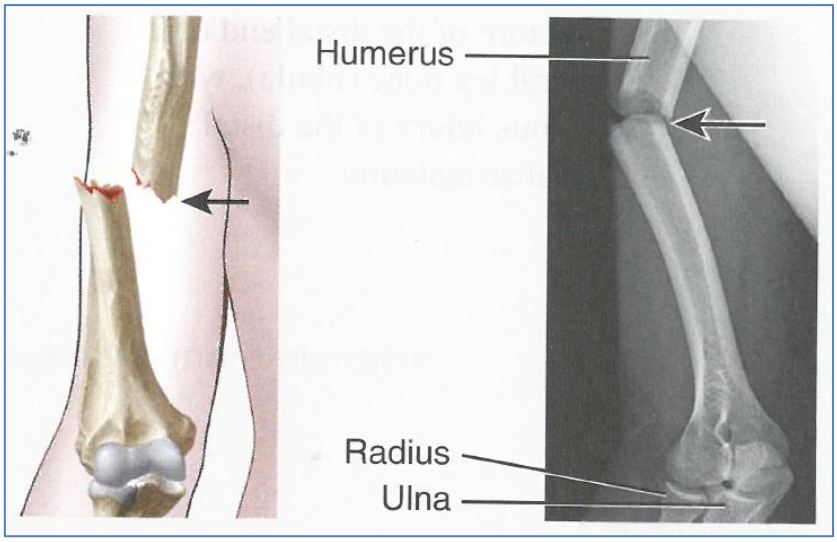

Figure 2.4: Illustration and Radiograph for Open or Compound Fracture (arrows) (Tortora, G. J., *et. al.* 2011).

- Closed or Simple fracture - The broken ends of the bone do not break or come out of the skin.

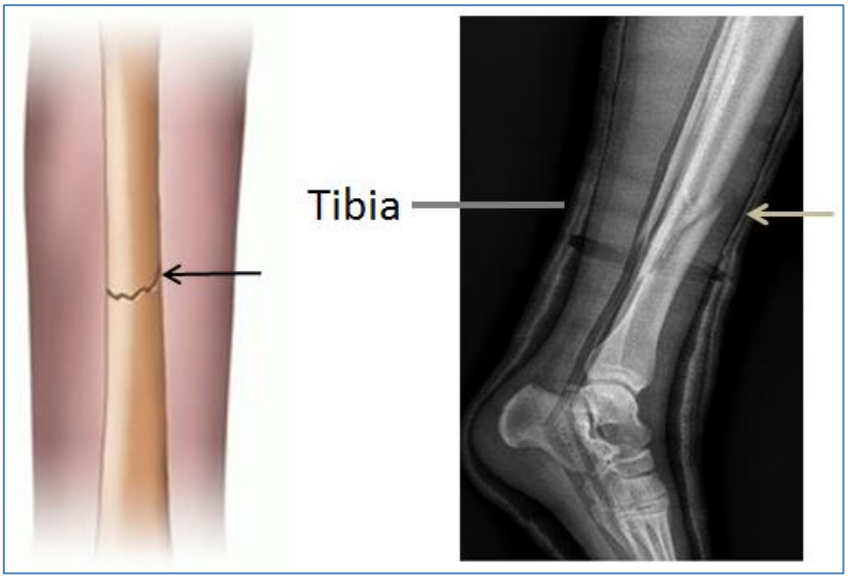

Figure 2.5: Illustration and Radiograph for Closed Fracture (arrows) (Relay Health 2017) (Cole, P. A. 2017).

- Comminuted fracture - The bone is split, or crushed into fragments at the area of collision and small bone pieces remain between the two main pieces.

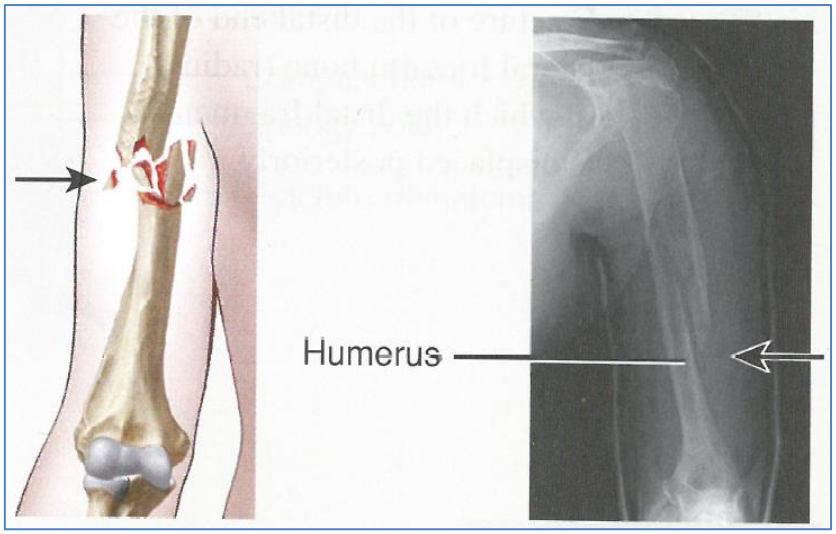

Figure 2.6: Illustration and Radiograph for Comminuted Fracture (arrows) (Tortora, G. J., *et. al.* 2011).

- Greenstick fracture – Like a green twig appears after it breaks, a partial fracture causes the bone to break on one side and the other side to bend due to it. This only occurs in children whose bones are not entirely ossified and consist of more organic elements than inorganic ones.

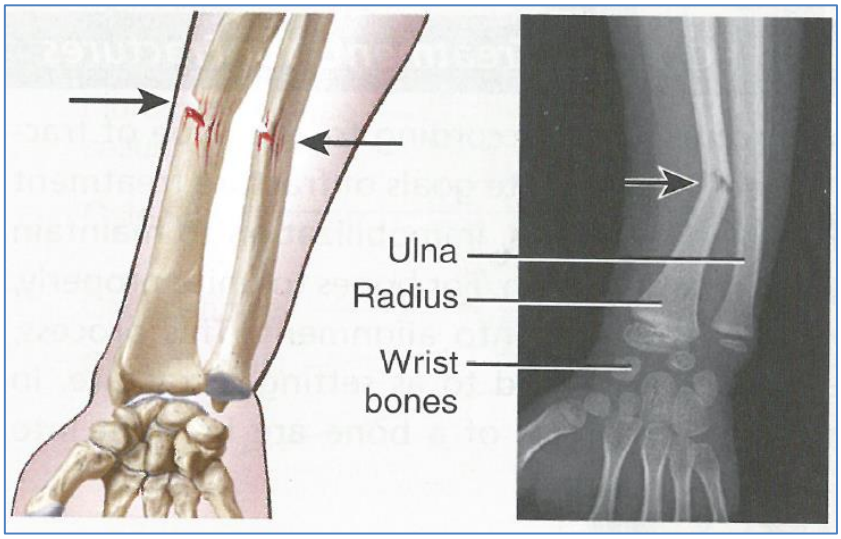

Figure 2.7: Illustration and Radiograph for Greenstick Fracture (arrows) (Tortora, G. J., *et. al.* 2011).

- Impacted fracture – One end of the fractured bone is forcefully driven into the internal end of the other.

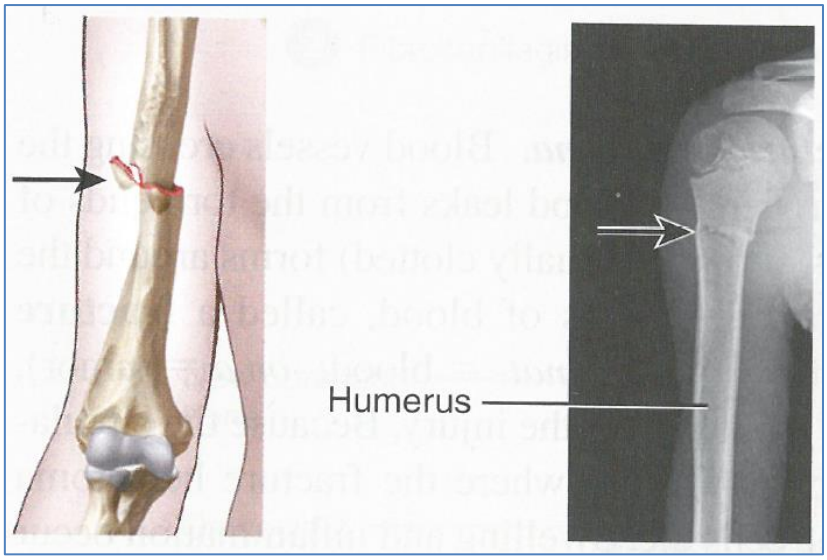

Figure 2.8: Illustration and Radiograph for Impacted Fracture (arrows) (Tortora, G. J., *et. al.* 2011).

- Pott fracture – Fracture of the distal end of the lateral leg bone (fibula), accompanied by acute injury of the distal tibial articulation.

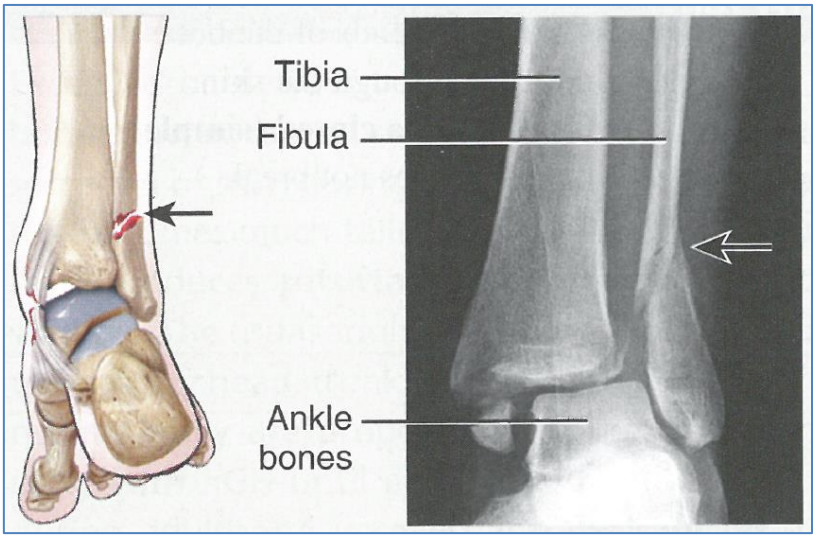

Figure 2.9: Illustration and Radiograph for Pott Fracture (arrows) (Tortora, G. J., *et. al.* 2011).

- Colles' fracture – Fracture observed at the distal end of the lateral forearm bone (radius) where the distal piece is displaced posteriorly.

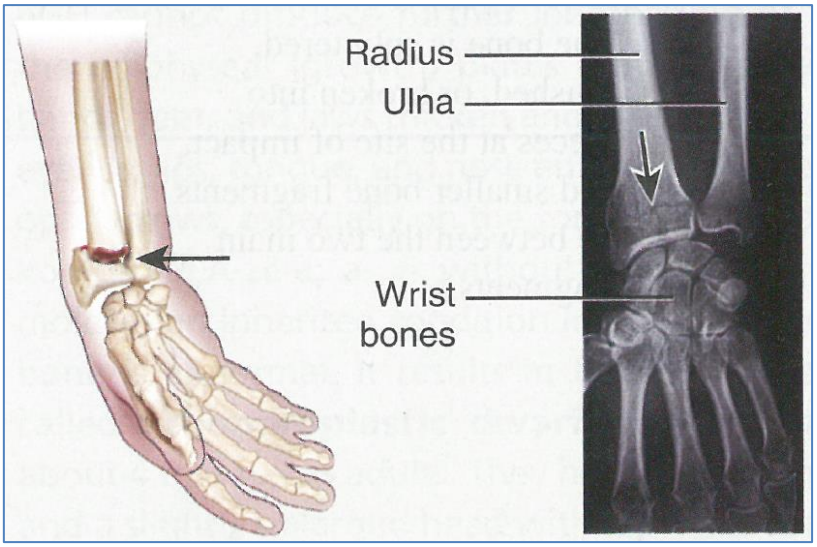

Figure 2.10: Illustration and Radiograph for Colles' Fracture (arrows) (Tortora, G. J., *et. al.* 2011)**.**

2.4.1 Long Bones and Fractures

Long bone fractures are referred to the fractures in the following bones: *humerus*, *radius*, *ulna*, *femur*, *tibia* and *fibula*.

- The two forearm bones are the radius and the ulna (Graaff, V. D. K. M. 1998).
    - The humerus is the longest bone of the upper extremity. It contains a proximal head that forms a joint with the cavity of the scapula, a body and a distal end, modified to articulate with the two bones of the forearm.
    - The ulna is longer and more strongly linked to the humerus than the radius. The coronoid system forms the frontal lip of the trochlear notch, and the olecranon forms the latter part. The styloid process is a knobbed part on the tapered distal end of the ulna, the head and a knoblike projection.

Fracture of the head of the radius is the most common, as it is driven forcefully against the capitulum of the head. If a fall results in landing on an outstretched hand, it may cause a fracture of the neck or the distal end. The radius contributes essentially to the articulation at the wrist joint than does the ulna. It consists of a body with a large distal end and a small proximal end. The distal end of the radius has a styloid process on the lateral tip and an ulnar notch on the medial side that obtains the distal end of the ulna.

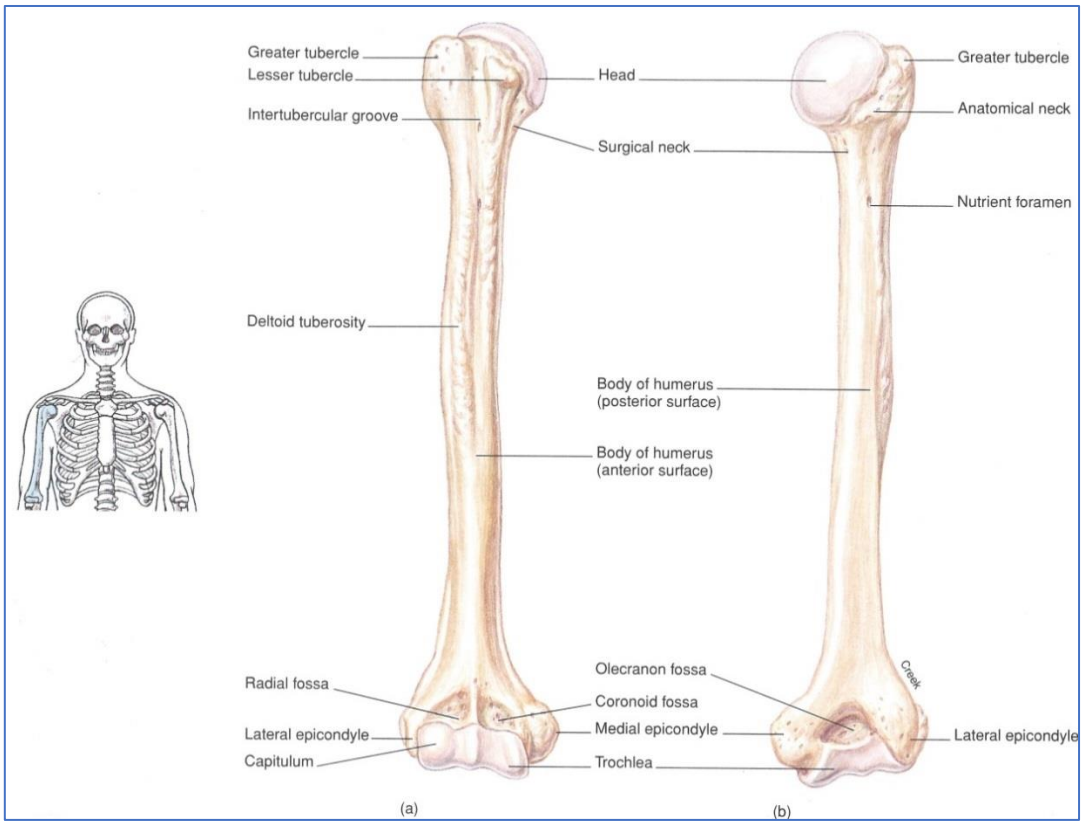

Figure 2.11: The right Humerus. (a) An anterior view and (b) A posterior view (Graaff, V. D. K. M. 1998).

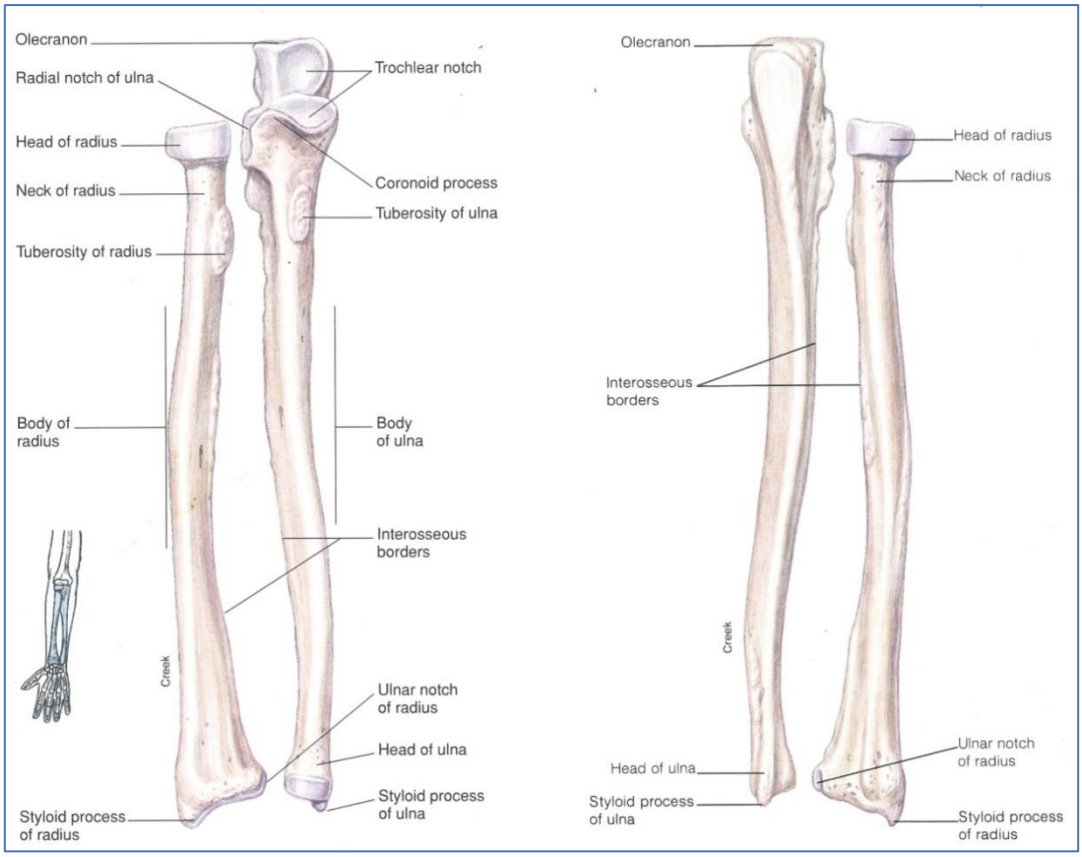

Figure 2.12: An anterior view of the right Radius and Ulna (Graaff, V. D. K. M. 1998).

- The two ankle bones are the tibia and fibula (Graaff, V. D. K. M. 1998).
    - The longest, toughest and heaviest bone in the body is the femur, which is also the only bone of the thigh. The distal end of the femur is prolonged for enunciation with the tibia. The distal end of the femur draws out to join with the tibia and the medial and lateral condyles act as the articular developments for this joint.
    - The tibia pronounces proximally with the femur at the knee joint and distally with the talus of the ankle. It articulates both proximally and distally with the fibula. The medial and lateral epicondyles are located above the condyles, on both sides. The tibia is the weight-bearing bone of the leg and typically bigger in size than the fibula.
    - The fibula is an extensive and slender bone that is essential for muscle attachment rather than for support. The head of the fibula articulates with the proximolateral end of the tibia. The distal end has a projecting knob known as the lateral malleolus.

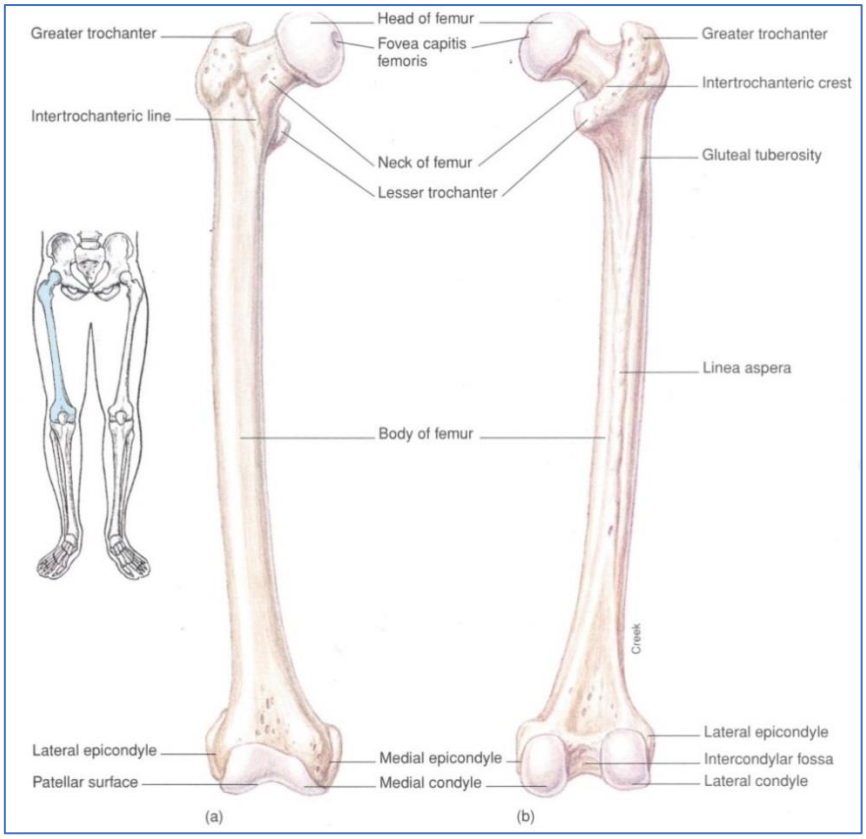

Figure 2.13: The right Femur. (a) An anterior viewpoint and (b) A posterior viewpoint (Graaff, V. D. K. M. 1998).

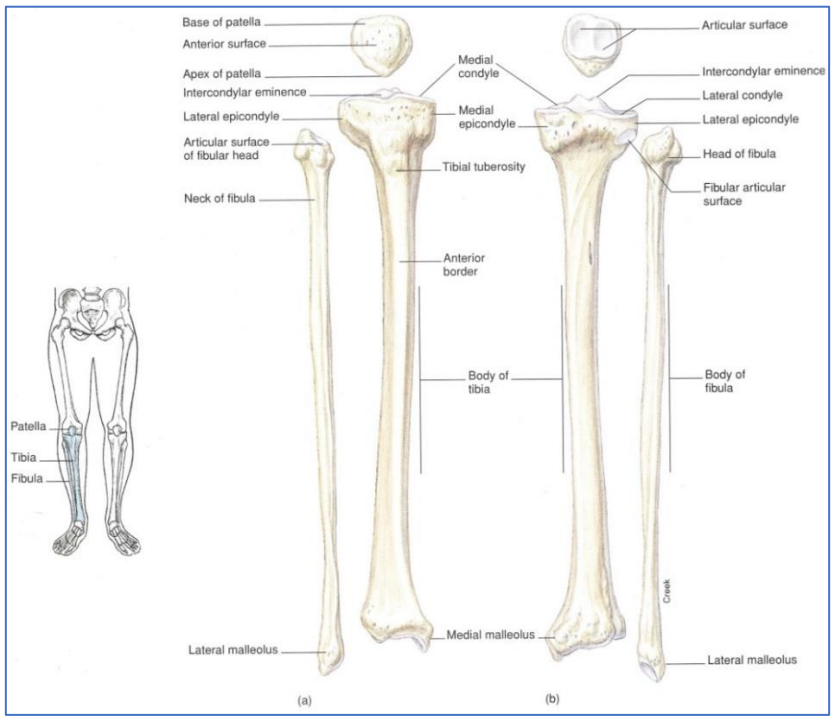

Figure 2.14: The right Tibia. (a) An anterior view and (b) A posterior view (Graaff, V. D. K. M. 1998).

Long bones can be divided into three areas – a relatively cylindrical shaft (diaphysis), two expanded ends (proximal and distal epiphyses) and a developing region called the metaphysis located in between the epiphyses at each end of the bone. The sub-segments of the long bones are shown in Figures 2.11 to 2.14.

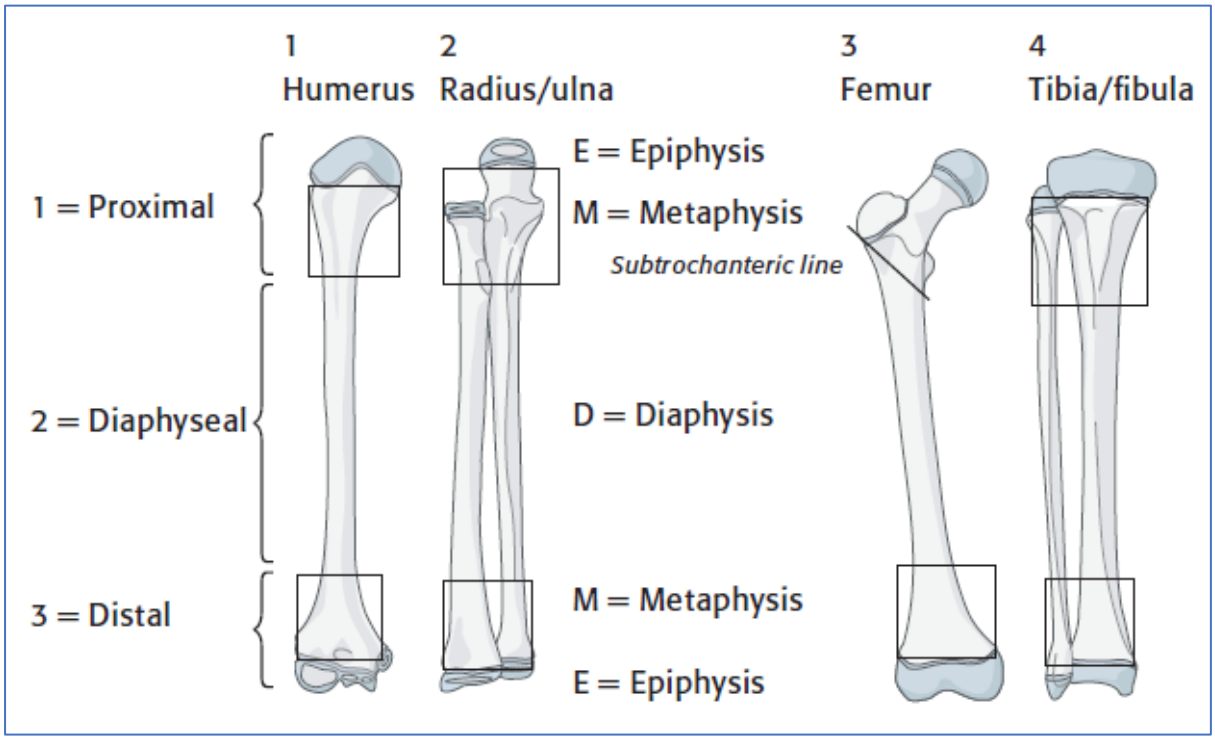

Figure 2.15: Sub-segments of Radius, Ulna, Tibia and Fibula (Slongo, T. 2010).

Breaks in the distal parts of these bones are referred to as wrist fractures. Fractures mostly occur in the distal radius; however, they can occur in combination with an adjacent fracture of the ulna. Occurrence of only the distal ulna being fractured is uncommon (Handoll, H. H. G., *et. al.* 2016). According to (Hedstrom, E. M., *et. al.*, 2010), children are most commonly affected by distal radius fractures. The most familiar cause of distal radius fractures is a fall on an outstretched hand. Depending on the growth plate (physics) and the age of the child, the severity, complexity and location differs. (Handoll, H. H. G., *et. al.* 2016). The mean age of children (aged up to 16 years) presenting with these injuries in 2000 at two Edinburgh hospitals was 9.9 years and 55% were boys (Rennie, L., *et. al.*, 2007).

After the finger and distal radial physeal fracture, ankle fractures are the third most common fractures in children. Around 20-30% of all paediatric fractures are in ankles. Most ankle fractures occur at 8-15 years of age. The peak injury age is 11-12 years and is rare under the age of 5. This type of injury is more common in boys. Most of the ankle fractures is due to a rotational force and is often seen in sports injuries associated with abrupt or swift changes in direction (Blackburn, E., *et. al.* 2012).

2.5 Monitoring of Bone States

The clinical monitoring of *diagnosing fractures* is commonly carried out by observing bone density using X-ray techniques and the fracture may result to a mere sprain instead of a proper fracture. An X-ray can sometimes be unable to display a clear area for the fracture site and it can only become observable after three to six weeks post injury (Bin, S. A. S., *et. al.* 2006) as shown in Figure 2.16.

The procedure of assessing the status of the healing bone, the recognition of complications in the course, and the correct identification of the endpoint of healing is termed as monitoring of *fracture healing.* In a few cases fractures do not heal readily and can result in extensive surgery or even amputation (Ryder, D. M., *et. al.* 1993).

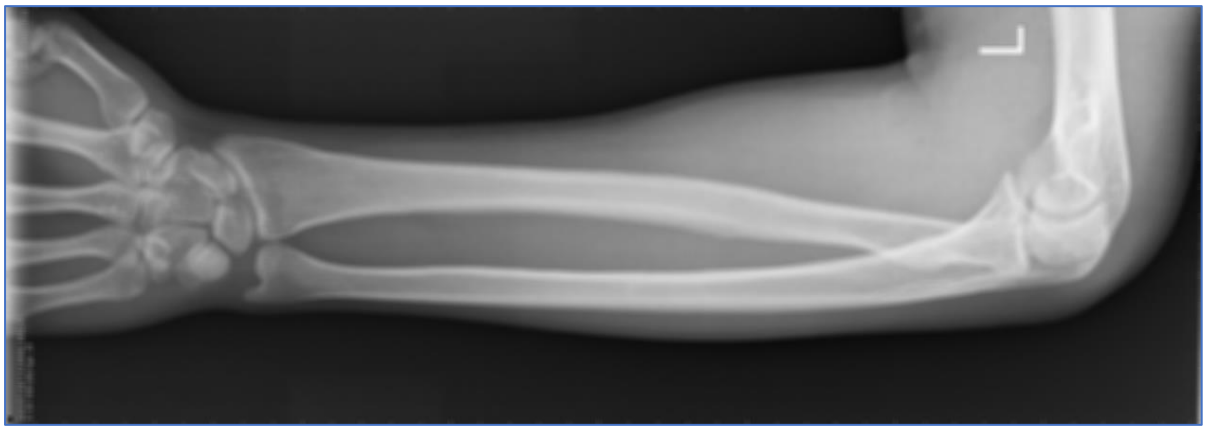

Figure 2.16: Rotated Forearm Image (Mustra, M., *et. al.* 2014).

Medical science or clinical studies involving the investigation of normal anatomy and physiology require images of the human body parts and this is made possible by the method called medical imaging (Yaniv, Z., *et. al.* 2004). It can be quite complicated to recognise similar features in two successive images in medical imaging, since it is difficult to find the anatomical features precisely and reliably (Mustra, M., *et. al.* 2014). The use of X-ray equipment is often not entirely convenient for the diagnostic radiographers and the analysis is unclear (Divya, P., *et. al.* 2012). Additionally, fracture detection and also, evaluation of orthopaedic fractures by X-ray images is still under-explored field so developments of different kind of algorithms are in the process to improve the imaging technique (Vijayakumar, R., *et. al*. 2013) (Bandyopadhyay, O., *et. al.* 2016).

2.6 Screening Tests

According to (Wilson *et. al.* 1968) and (Maxim, L. D., *et. al.* 2014), screening tests are widely used in medicine and are the plausible methods which apply appropriate assessments to detect a disease or any other abnormality. To examine and confirm whether a person has the probability to be affected by a specific medical condition, the screening tests (sometimes termed medical surveillance) are used in clinical practice. The next step is to prepare the screened subject for treatment and in case that the condition is contagious; methods to prevent the affected person from posing a threat to his/her neighbour follow.

A screening test is not intended to be diagnostic. Theoretically, screening can confirm if the subject needs to have the diagnosing tests because it is a commendable means of identifying the condition in its initial stage and thus, enabling an early diagnosis. If the screening tests are positive, then the subject needs diagnosing tests.

Screening tests can be as follows (Wilson *et. al.* 1968):

- Mass screening - indicate the expansive screening of a whole population or a large subgroup.
- Selective screening - screening of groups in the population that are particularly at high risk.
- Multiple screening - this has mainly evolved by combining several single screening tests and is the logical consequence of mass screening.

A clinical test or screening test is assessed based on the technical expressions, sensitivity and specificity. *Sensitivity* defines the ability of the test to accurately identify the people affected by the disease (Placzek, D. A., *et. al.* 2017). *Specificity* is the determination of the capability of the test to properly eliminate the people who are not affected by the condition (Placzek, D. A., *et. al.* 2017). The key terms for calculating sensitivity and specificity are described below.

To illustrate the performance of a diagnostic test, clinicians use the *positive predictive value (PPV)* and *negative predictive value (NVP)* and they rely on the frequency of the condition present in the population of concern.

- True positive (TP) - the patient is affected by the condition and the test is positive.
- False positive (FP): the patient is not affected by the condition, but the test is positive.
- True negative (TN): the patient is not affected by the condition and the test is negative.
- False negative (FN): the patient is affected by the disease, but the test is negative.

$$\text{Sensitivity} = TP / (TP+FN) \quad (2.1)$$

$$\text{Specificity} = TN / (TN+FP) \quad (2.2)$$

$$\text{Accuracy} = (TP+TN) / (TP+TN+FP+FN) \quad (2.3)$$

According to (Lalkhen A. G., *et. al.* 2008), the interpretations of the above terms are detailed below.

- When the test is able to accurately identify all patients affected by the disease, it is said to have 100% sensitivity.
- When a test is able to identify 90% of patients with the disease (true positives) but 10% with the disease appear unidentified (false negatives), it is said to have 90% sensitivity.
- When the test is used to detect a serious but treatable disease (e.g. cervical cancer), it is imperative for the test to have a high sensitivity.
- When a test accurately identifies all patients without the disease, it is said to have 100% specificity.
- When 80% of patients unaffected by the disease are accurately detected as test negative (true negatives) but 20% patients without the disease are inaccurately recognised as test positive (false positives), the test has 80% specificity.
- A test that has high sensitivity, but low specificity can lead to several patients, unaffected by the disease to be informed of the probability of them having the disease and they are then urged to undergo further examination.
- Likelihood ratio is a fundamental term often used with reference to the utility of tests. This term is used to describe how much more a patient who tests positive is prone to be affected by the disease compared to the one who tests negative.

2.7 Vibration Analysis

Vibration analysis is a broadly complex domain that exploits various properties of the testing and diagnosis disciplines (Yi, Q. 2015). This technique allows detecting the origins of machine failures, so that these machines can be replaced or repaired before it leads to a major and expensive fault (Sharpe, D. 2015). This analysis of electrical machinery is a testing method, that provides a rational way for maintenance, simplifies fault detection and fault diagnosis and thus saves time, effort and cost (Jamil, I. A., *et. al.* 2014). The overall level of a vibration measurement - the

state and vibration signals' frequencies can indicate where the location of the problem and what it might be (Neale, M. J. 1996).

Vibration measurement and its real-time graphical representation have a large variety of applications in both domestic and industrial machines, ground, engines, vibration, climate or pre-disaster reading, etc. The analysis makes data collection, storing and processing simple and easy by means of several signal processing methods, thus it is the usual technique for the applications mentioned above (Jamil, I. A., *et. al.* 2014). There are principles and techniques of time-series and fast Fourier transform (FFT) methods in vibrating structures for detecting different anomalies like cracks and defect detection, identification and estimation (Fassois, S. D., *et. al.* 2007) (Patil, S. S., *et. al.* 2014).

Vibration analysis can be grouped into four main domains (Yi, Q. 2015).

- *Time domain* analysis is dedicated to identifying the integral act of the tested parts: peak, average, root-mean-square, cover values of vibration amplitude. These parameters are compared with threshold values to identify latent defects or abnormal performances.
- *Frequency domain* analysis can deliver more information as the measured signal is decomposed into a sequence of frequency components (spectrum) by a Fourier transform calculation (or fast Fourier transform — FFT), described in Chapter 3.10. Local investigation of the various frequency components allows the linkage of a signature with the processed signal, so that the verified part can be recognised precisely by its own signature (signature analysis).
- *Time-varying* characteristics of the signals that comprise computing various spectra on the time observation window can be beneficial via a joint time/frequency technique such as Gabor−Wigner−Wavelet, the Wigner-Ville distribution, etc. Generally, the spectrums are associated to the rotational speed of the verified devices (order analysis), such that the analysis of the single order that is characterised by frequency components changing with the speed can be extracted.

- *Modal* analysis allows studying the dynamic properties of structures under vibration excitation. These systems apply FFT to carry out a transfer function that displays one or more resonances, by means of which it is possible to estimate the characteristic mass, damping, stiffness, and other properties of the tested part.

Due to the success rates in industrial applications, following the usage of signal processing for interpretation of results, vibration analysis is gaining popularity in medical fields. It is considered a non-invasive technique for fracture healing (Roberts, G. S., *et. al.* 2000) (Tan, L., *et. al.* 2017) with bone density and chronic diseases (Vasile, A. *et. al.* 2014) (Pang, M. Y. C. 2010), and the prevention of osteoporosis (Zhu, D., *et. al.* 2010).

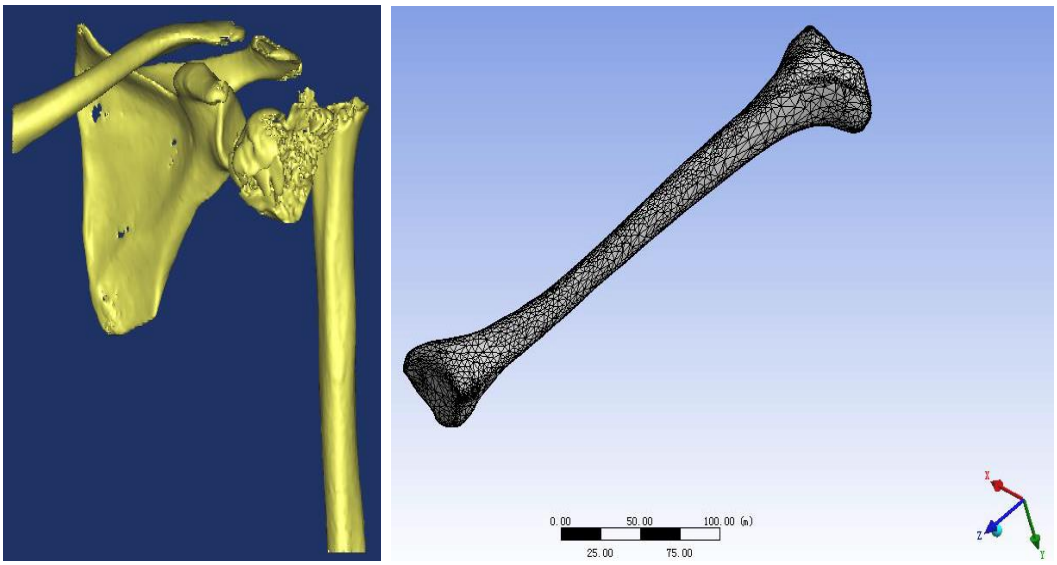

(a) (b)

Figure 2.**17**: A fracture in the comminuted proximal Humerus in combination with shoulder joint subluxation. (a) Antero-posteriorly (Ma, X., *et. al.* 2010) (b) A three-dimensional finite element model of Tibia (Chun-yu, B., *et. al.* 2010).

Applications of Finite Element (Modes) Analysis (FEA) and development of complex 2-D and 3-D models through computational systems and methods have led to determination of the role of natural frequency for describing and predicting the mechanical behaviour and other features of biological systems (Kumar, A., *et. al.* 2014) (Singh, V. R., *et. al.* 1989) (Hobatho, M. C., *et. al.* 1991). FEA had been used in order to numerically tackle dynamic analysis of fracture healing by means of a bone model (Laura, P. A., *et. al.* 1990).

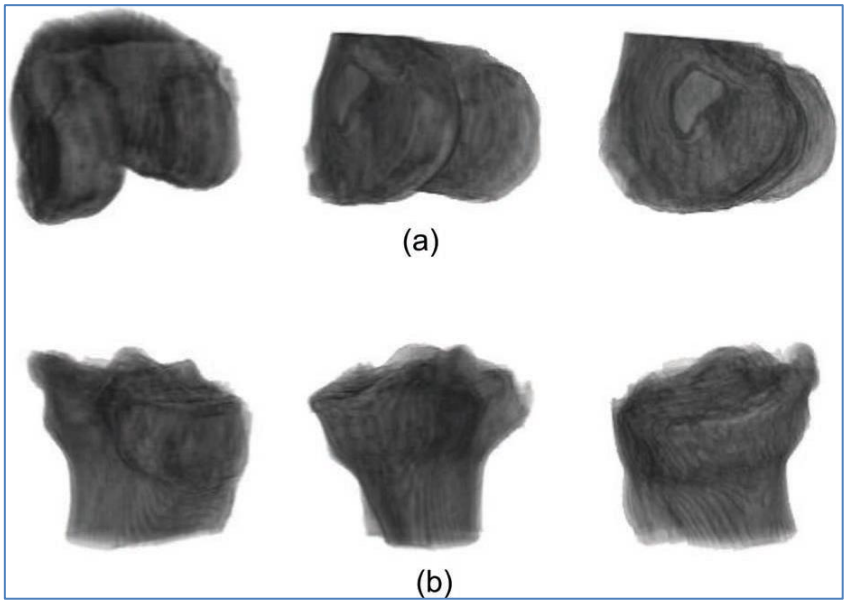

Figure 2.18: The 3D models of (a) Femur and (b) Tibia (Zarychta, P., *et. al.* 2011).

The utility of the computational models is often criticised as there is insufficient number of model verification and validation (V&V). In the field of computational biomechanics, (Anderson, A. E., *et. al.* 2007) presented in detail, the verification, validation and sensitivity researches regarding the construction, analysis and interpretation of models. They have discussed appropriate observations from examples in this area for providing guidance to use V&V principles properly, therefore, improved the peer acceptance of researches using computational models and techniques for creating them.

2.8 Signal Analysis in Vibrational Area

Vibrations and noise are generated by materials with unusual behaviour, such as, those from a road surface, interacting with the tires of a car, or triggered by turbulence around an airplane wing (Brandt, A. 2011). Many signal processing of rotating machines is due to examining the vibrations during a speed sweep, where the machine runs up from a low to a high RPM (revolutions per minute) or runs down from a high to a low RPM. The signals produced because of the speed sweep are nonstationary signals as the frequencies vary over time; these signals are divided into smaller segments and processed via appropriate techniques for finding the spectrum. In order to understand the concepts and applications of vibration analysis, it is imperative to comprehend the characteristics of signal analysis.

Dynamic signals deal with dynamic events in the mechanical field, for example, forces and displacements are expressed as functions of time. A physical entity which varies over time is a signal. Energy is referred to as a quantisation of the size of a signal, in order to compare the infinitely many possible signals. The Root Mean Squared (RMS) value is vital in expressing the energy of a signal properly and it actually describes a type of average signal value (Stein, J. Y. 2001). Some examples of signals are as follows (Brandt, A. 2011):

- The force exerted on a car suspension when the car is on a drive mode on the road.
- The sound pressure from some machine occurring at an operator's ear.
- The displacement of any point in a certain direction on a vibrating handle or on a small machine like in a pneumatic (inflated) drilling machine.

The processing of (dynamic) signals is typically known as *signal analysis*. Signal analysis can be considered as the method of computing and interpreting essential information in a signal, such as, a frequency spectrum followed by some statistical measures. Some of the features of a signal are extracted by sampling which are vital parts for changing continuous-time signals to discrete-time signals.

Signal processing can be inferred as the original process (essentially mathematical or related operations) applied in analysing a signal from one form to another. If signals are to be classified with respect to its frequency properties then the classes are (Brandt, A. 2011):

- Signals which repeat with a period are known as Periodic signals.
- Signals which at each time instant are independent of values at other instants are known as Random signals.
- Signals which last for short duration of time are known as Transient signals.

Signal classification is significant when damaging the effects of vibration, for example, in fatigue testing and in environmental studies.

2.9 Low Frequency Vibration Analysis in Medical Fields

Vibration analysis in orthopaedics was first presented by Lippmann (Lippmann, R. K. 1932). He reported using his finger to create percussion on the clavicle then used a stethoscope to sense the succeeding response. In the early 1970s, published reports on studies done in the field of low-frequency vibration analysis started appearing. With the advancement of the signal processing and the electronic technologies, the development of medical diagnostic and screening tools using vibrational analysis became more credible. This comprised a key European finding from the research led by Professor G. Van der Perre *et. al.*, who investigated vibration analysis in the area of orthopaedics and published several observations effective to medical fields (Cornelissen, M., *et. al.* 1982) (Cornelissen, P., *et. al.* 1986).

(Thomsen, J. J. 1990) performed both theoretical and experimental free vibrations related studies in an excised human tibia. He computed parameters using a Bayesian parameter estimation method (a statistical approach) and performed a sensitivity analysis on a Finite Element (FE) prototype. He established from his observations from vibration analysis that the human tibia is more uniform than what its complex geometry shows.

Vibration analysis is generally divided in three parts:

- the mechanical oscillation of an object,
- the recording of the resulting responses and
- processing these signals.

In theory, both trauma-induced and pathological conditions like osteoporosis, fractures and artificial hip joint loosening can be monitored by applying a stimulus to a bone or bones and analysing the subsequent responses (Nokes, L. D. M. 1999). This method had been used by inducing a partial break to observe different patterns in bone structure. Experiments demonstrated that the information regarding a fracture or healing status of bones can be indicated by resonance frequency (Alizad, A., *et. al.* 2004). Natural frequency of bone fracture fragment had been experimentally determined that made some excellent observations in the assessment of fracture healing (Singh V. R., *et. al.* 1989) (Singh, V. R. 1996). (Jurist, J. M. 1970) has experimented on forearms and determined the elastic response of bones along with the ulnar resonant frequency.

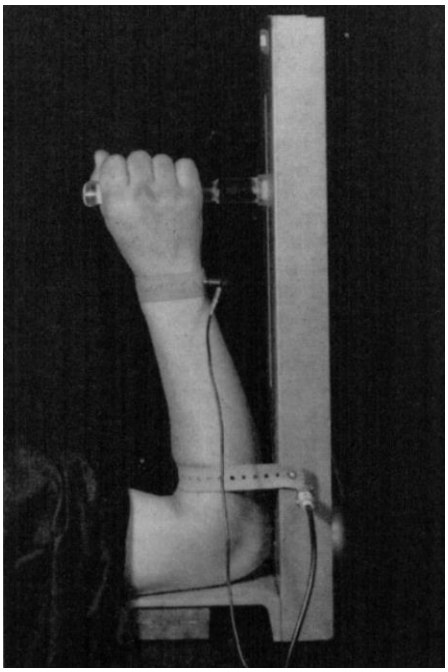

Figure 2.19: Arm support and the illustration of the standard position for recording (Jurist, J. M. 1970).

(Jurist, J. M. 1970) employed a mixture of effects from oscillator and amplifier which energised the modified loudspeaker driver with a range of frequencies. At the olecranon process, the ulna is excited, and the responses were noted at the distal end using an accelerometer. Jurist also listed the difficulties in acquiring the frequencies (Jurist, J. M. 1973).

In order to detect fracture in bones, experimental studies had been conducted where smartphones were placed on ankles or feet. In one study, signals were analysed by "Apps" to indicate the range of vibrational energy (dB/Hz) for detecting presence/absence of fracture (O'Brien, T. 2016). Another study was conducted where bone acoustics had been examined to indicate stress fracture in a patient's bone (Hopman, L. D., *et*. *al.* 2016). This was done by applying a vibration of a selected frequency to a patient at a selected anatomical site and analysing the vibration responses at another anatomical site. The investigations were done based on a database and indicated the presence of a fracture by displaying a probability.

2.10 Methods of Bone Excitation

There are two most general types of stimuli which can be applied to the human skeletal system to induce vibration (Nokes, L. D. M. 1999):

- Impulse Vibration Excitation method,
- Continuous Vibration Excitation method.

2.10.1 Impulse Vibration Excitation Method

Vibrations can be introduced to a bone or several bones by one and/or short duration force; this is called an impulse. This impulse can be generated by devices like a small and light instrumented hammer or a type of small pendulum. There can be periodic excitations. These vibrations are produced due to platform switching operations and external transients like electromagnetic pulses or lightning (Kichouliya, R., *et. al.* 2012).

The example of this method is shown in Figure 2.21. Another example is provided by (Razaghi, H., *et. al.* 2014). They have induced stationary vibration (the speed of the impacts did not change) on turkey bones and after processing their recorded data, they have successfully established the existence of various relationships between vibration frequency responses and bone mass/volume ratio by performing analysis using Digital Signal Processing (DSP). Accelerometers are miniature devices which were used in some of the studies to control the impacts or/and acquire corresponding vibration data. (Collier, R. J., *et. al.* 1994) applied impulsive force on human tibia and recorded the mechanical phase constants of the resultant waves.

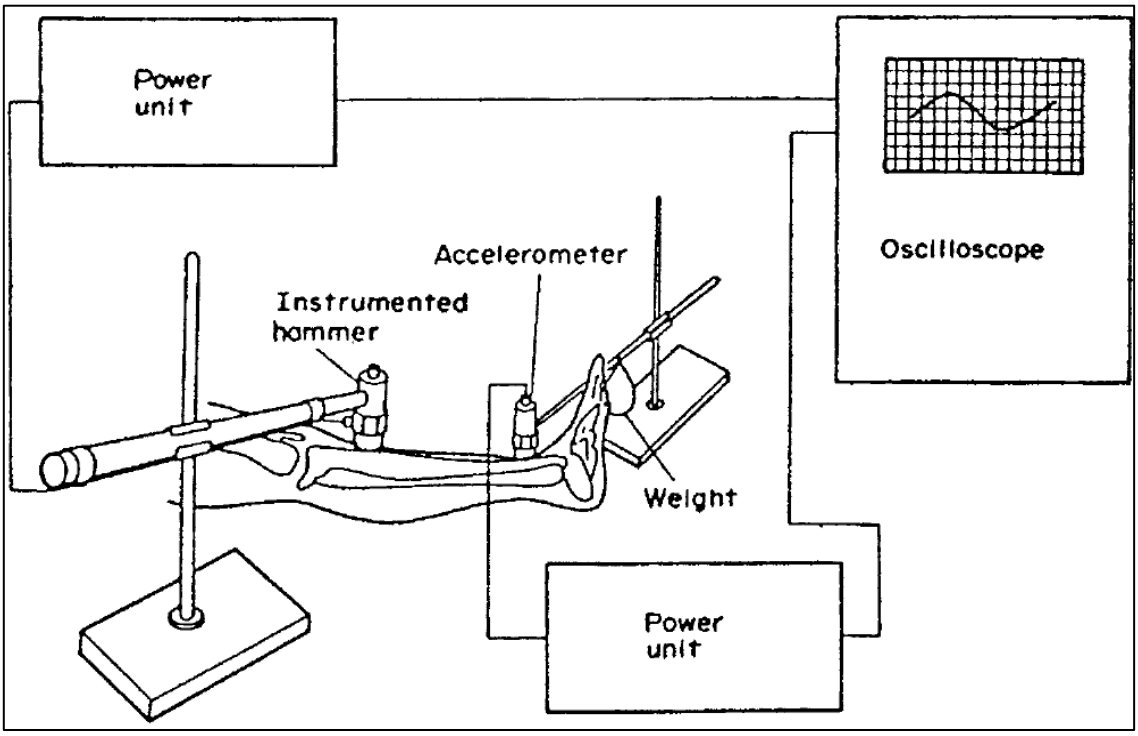

Figure 2.20: Illustration of a technique using instrumented hammer to apply impulsive force to a bone (Collier, R. J., *et. al.* 1994).

2.10.2 Continuous Vibration Excitation Method

When applying this technique, a mechanism (such as a vibration motor or a piezoelectric device) continuously vibrates the bone. Several investigations were conducted using this approach since 1942 (McGraw, N. H. 1942).

This technique was applied in 1967, but the location or fixation of the vibrator was not reported anywhere. The authors vibrated bones at a frequency of *1 kHz* and established a way for analysing femoral and humeral fracture healing (Dencker, H., *et. al.* 1967). (Georgiou, A. P., *et. al.* 2001) utilised this technique to examine efficiency of vibration testing as a non-invasive technique of diagnosing loosening of total hip replacements. They compared the method with radiographs from patients who have hip prosthesis loosening issues. According to their experiments, vibration testing resulted in having a sensitivity of 80% and a specificity of 89% and they concluded that this method can produce more concrete notes on the stability of whole replacements than radiographs in the clinical set-ups displayed in Figure 2.22.

Figure 2.21: A frequency input excitation method using a vibrator (Georgiou, A. P., *et. al.* 2001).

(Nikiforidis, G., *et. al.* 1990) reported where an analytic model was formulated. This model established the parameters at the fracture site. An oscillatory force with frequencies from *200* to *1600 Hz* can be produced by means of an electromagnetic shaker and the parameters derived related to the lateral and axial bone vibration could be studied. There were more studies on continuous vibrational excitation with promising results (Jansson, D., *et. al.* 2013).

2.11 Properties of Bones and Effects of Soft Tissue

2.11.1 Effects of Frequencies on Bones

Establishing various mechanical properties of bones is one of the focal points of many studies and finding natural frequency of bones is one of them. This is basically to see if these properties can be used as a non-invasive diagnostic method in medical field. Vibration tests are done in vivo to extract the properties. Oscilloscope has been commonly used as an observation tool for recognising the signal patterns in order to determine the frequencies.

A study conducted in 1985 for assessing fracture healing applied stimulus vibration on human tibiae - 30 intact tibiae and 22 fractured tibiae (Nokes, L., *et. al.* 1985). The researchers have used an accelerometer for recording the accelerations through the tibiae. They have demonstrated that in a fresh fracture, small amount of vibratory signal is transmitted and the signal at the distal ends has very low amplitude. Additionally, the attenuation factor (AF) was small. As healing progresses, vibration was transmitted with increasing steps across the fracture site therefore, the amplitude of the signal increases, also the AF. On the other hand, in 2010, a group of researchers has established that both parametrical and non-parametrical correlation exists between the BMD of femur and natural frequency of right and left tibia (Bediz, B., *et. al.* 2010). They have demonstrated that natural frequency of the tibia (a long bone) decreases with decrease in bone mineral density.

(Thomsen, J. S., *et. al.* 1990) carried out a study with seven tibiae and established undamped natural frequencies of tibia in the range of 0 to 3 kHz with a high degree of confidence. A study documented frequencies from dry specimens of intact as well as fractured tibiae (Gabrielli, F., *et. al.* 2008). (Gabrielli, F., *et. al.* 2008) have shown that frequency response of fractured bones was much larger than that of the unbroken ones. On application of piezoelectric solicitation, the average of frequency responses produced by unfractured bones equated to 401 Hz compared to the values right after fracture, equal to 1278 Hz. Their results indicated that resonance frequency of broken bones was much larger than that of the normal long bones.

(Bediz, B., *et. al.* 2010) findings showed that the natural frequency of the tibia decreased with reducing BMD and also concluded a weak correlation with the BMD of the femur determined by dual energy X-ray densitometer.

2.11.2 Frequencies of Bones

(Adewusi, S., *et. al.* 2013) used Finite Element (FE) model of the human hand-arm system to note mode shapes and frequencies. They have experimented with six subjects, and then used suitable number of resonant frequencies and damping ratios to calculate the Rayleigh damping coefficients, employed for the harmonic analysis of the model in ANSYS (engineering simulation and 3-D design software). Their results are shown in Table 2.1.

Table 2.1: Figures of natural frequencies from the hand-arm prototypes attached to immobile and mobile shoulder (Adewusi, S., *et. al.* 2013).

	Model with fixed shoulder		Model that permits shoulder motion	
Mode #	**Freq. (Hz)**	**Remarks (highest at)**	**Freq. (Hz)**	**Remarks (highest at)**
1	8.2	Rigid rotation	5.3	Rigid rotation about the shoulder
2	39.0	Elbow	13.4	All parts (z_h-axis)
3	111.3	Palm	34.7	Elbow
4	131.4	All parts (z_h-axis)	96.2	All parts
5	190.2	All parts	107.5	Palm
6	329.4	All parts	123.3	Palm and wrist
7	342.9	All joints	184.1	All parts
8	411.4	Wrist & palm	191.2	All parts (z_h-axis)
9	459.5	Wrist & elbow (z_h-axis)	251.1	All joints
10	576.9	All parts	304.5	Shoulder and elbow
11	642.5	Palm muscle	381.9	All parts
12	700.7	Forearm & palm	385.0	Palm
13	710.4	Palm	402.4	Wrist and palm
14	769.7	Elbow	456.2	Wrist and palm (z_h-axis)
15	815.4	Elbow and palm (y_h-axis)	466.9	Elbow & Palm
16	844.2	Palm (mostly muscles)	549.1	All joints
17	846.4	Upper-arm	553.4	All joints and palm muscles
18	904.6	Palm, wrist and elbow muscles	609.8	Elbow and palm muscles
19	932.3	Upper-arm muscles	616.5	Trunk
20	953.7	Shoulder and elbow muscles	642.6	Palm muscles

(Adewusi, S., *et. al.* 2014) performed modal, harmonic and strain analyses of the FE models in the extended and bent-arm positions to derive strain-based frequency weighting for the palm (hand), wrist, elbow and shoulder.

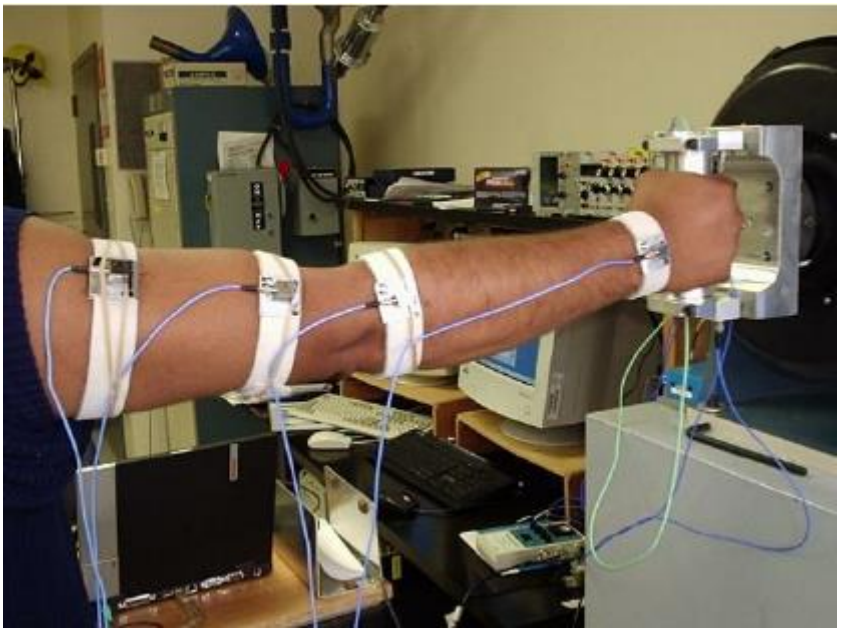

Figure 2.22: Investigational arrangement displaying the extended arm posture (Adewusi, S., *et. al.* 2014).

Their results have revealed that resonant frequencies for the extended arm posture are in the following ranges:

- 10.9 -15,
- 27.7 – 39.9,
- 87.9 – 99.2 and
- 97.8 – 110.0 Hz.

The resonance frequency ranges for the bent-arm posture are:

- 13.0 – 17.3,
- 27.2 – 36.8,
- 53.4 – 62.0,
- 78.1 – 89.9,
- 152.3 – 154.0 and
- 164.0 – 169.9 Hz.

Their further investigations exhibited that the hand-arm is impacted with continuous extension and compression in the 10.9 – 17.3 Hz frequency range that is, approximated to the frequency of maximum value (12.5 Hz). They have suggested based on their results that the hand-arm may suffer injury of the joints (wrist, elbow and shoulder) in the 10.9 – 17.3 Hz frequency range.

The frequencies of upper arms, shoulder, back and neck have been determined by using three accelerometers and one laser vibrometer (Xu, X. S., *et. al.*, 2016). In order to comprehend the transmitted vibration and the biodynamic results, the mass at the palm of each hand was recorded. This research found that

- the resonance frequency of the upper arm equated to 7–12 Hz,
- the resonance frequency of the shoulder resonance equated to 7–9 Hz and
- the resonance frequency of the back and neck resonances equated to 6–7 Hz.

It was noted that the hand-arm posture, vibration magnitude along with the application of hand force had impacts on the subsequent responses.

2.12 Responses to Whole Body Vibration

The responses due to vibration application on whole body were observed and recorded specifying the numerical range of vibration that can be suitably applied (Griffin, M. J. 1990).

- During sinusoidal *vertical* oscillation at frequencies:
  - Below about 2 Hz most parts of the body move up & down together.
  - (For a seated person) above 2 Hz amplification of the vibration within the body is triggered. Usually at about 5 Hz, first major resonance (frequency of greatest amplification) occurs and vibration acceleration often causes highest discomfort.
  - Between about 10 Hz and 20 Hz, the voice may be caused to trill by vibration.
  - Between about 15 Hz and 60 Hz, vision may be affected due to association with resonance of the eye.

- During *horizontal* vibration of the seated entire body at frequencies:
  - Below about 1 Hz, the oscillation tends to cause the body to sway but this may be resisted by muscular action/support from a seat.
  - Ranging between 1 Hz to 3 Hz, it is difficult to stabilise the upper parts of the body.
  - Increasing from 3 Hz to 10 Hz, the horizontal vibration is less well transmitted to the upper body.

- Posture:
  - A small change in position or muscle tension may help to decrease vibration severity.
  - The effects of postural changes increase with increase in frequencies.
  - A variance in body position which changes the contact with a vibrating surface, such as a backrest, also modifies the causes of the vibration.

- Seating:
  - At low frequencies (below 1 Hz), the dynamics of many seats have little influence; but in the region of 4 Hz, they significantly amplify vertical vibration.
  - At larger frequencies than 4 Hz, many seats attenuate vertical vibrations and at more than 10 Hz the influence of the motion is decreased.

- Standing Position:
  - In a normal standing position, the effects of vertical vibration are usually similar to those in the seating position.
  - The influence of frequencies more than 3 Hz may decrease by bending at the knees.
  - Horizontal vibration at frequencies less than 2 Hz tends to raise instability in standing persons which may be decreased by gripping a handhold or, with lateral vibration or, with lateral vibration, placing the legs apart.

- Recumbent Position:
  - The full length of the body (from head to feet) may be exposed to the same vibration or parts may be well isolated from the motion.
  - A couch can either provide stability to resist horizontal movement or allow substantial motion.

2.13 Conclusion of Chapter 2

This chapter briefly describes the Bone structure and how several factors can affect fracture in bone. This chapter gives also an overview of vibration analysis applied in various medical sectors since 1932 till date.

Chapter 3: Theoretical background of the Techniques used

3.1 Introduction

Vibration is repeated displacement of objects from its position of equilibrium, when they are excited by a force (Morgado, R., *et. al.* 2013). The basic principle in the vibration mechanism are time, forces (or masses) and space. This behaviour is simply the exhibition that equates the motion of physical bodies with the forces acting on them. When a disturbance is inflicted on a body to move from its reference point, then it tries to return to its original position as per the elastic properties of the materials of the body. Usually nearly everything in nature vibrates that sometimes might be too small for recognition. Alternatively, sometimes there might be huge vibrations occurring due to natural disasters such as tsunamis, earthquakes and typhoons (Chakraverty, S., *et. al.* 2016).

Vibrations are caused by the situations enlisted in (De Silva, C. W. 2007) (Rao, S. S. 2007):

- A moving or rotating machinery's unequal distribution of forces,
- External forces like wind, earthquakes or explosions,
- When there is friction between more than one body,
- Variation of fields like magnetic or electric,
- Motion of vehicles, etc.

Motion of bodies subject to vibration can be periodic or non-periodic (Wahab, M. A. 2008).

- Periodic motion: a motion that repeats itself at equal time intervals, e.g. a simple pendulum, where the motion repeats *regularly* at equal time intervals.
- Non-periodic motion: a motion that is *irregular* or can be repeated at unequal time intervals, e.g. the response of a structure to an earthquake.

In what follows a brief overview of the basic vibration concepts is given, as the most of vibration phenomena obey these basic principles.

3.2 Free Vibration

Systems with the property of having repetitive motions are simple harmonic oscillators. Distinct particles in any medium vibrate about their equilibrium positions but they do not propagate through the medium. If they are excited by a small amount of force and moved from their resting position, they will begin to vibrate with simple harmonic motion. This is a periodic motion that fluctuates in a sinusoidal manner where the displacement *x*, of the system varies as (Wahab, M. A. 2008):

$$x = A \sin \omega_n t \tag{3.1}$$

In (3.1) *A* is a constant ω_n - angular velocity of the system, *t* - time.

The velocity of the system is calculated by differentiating the displacement with respect to time.

$$\dot{x} = \frac{dx}{dt} = A\, \omega_n \cos \omega_n t \tag{3.2}$$

The acceleration of the system is calculated by differentiating the velocity with respect to time.

$$\ddot{x} = \frac{d^2x}{dt^2} = -\, A\, \omega_n^2 \sin \omega_n t \tag{3.3}$$

A system with a single degree of freedom (SDOF) is known to be the simplest vibrating system.

3.2.1 Undamped Free Vibration

The equation of motion of such systems is derived from the Newton's second law:

$$\sum F_x = m\ddot{x} \tag{3.4}$$

where $\sum F_x$ – the sum of the external forces in the x direction; and

$\ddot{x}$ - the acceleration in the x direction.

The only force acting on the mass is kx in the negative x direction.

$$-kx = m\ddot{x} \tag{3.5}$$

Rearranging Equation in 3.5,

$$m\ddot{x} + kx = 0 \tag{3.6}$$

or

$$\ddot{x} + \omega_n^2 x = 0 \tag{3.7}$$

where $\omega_n = \sqrt{\frac{k}{m}}$ - the system's angular frequency in rad/s.

The solution of such problem called as harmonic oscillator is the sinusoidal wave given in (3.1).

3.2.2 Damped Free Vibration

Damping force formed by a viscous damper is equal to $c\dot{x}$, where c is a viscous damping coefficient in N.s/m. The damping coefficient, c, characterises a simple model for the dissipation of energy in the system due to frictional forces.

Newton's second law can be represented as:

$$-kx - c\dot{x} = m\ddot{x} \tag{3.8}$$

Rearranging Equation in 3.8,

$$m\ddot{x} + c\dot{x} + kx = 0 \tag{3.9}$$

or,

$$\ddot{x} + 2\varsigma\omega_n\dot{x} + \omega_n^2 x = 0 \tag{3.10}$$

where $\omega_n = \sqrt{\frac{k}{m}}$ - the system's angular frequency in rad/s and ς – the damping ratio.

$$\varsigma = \frac{c}{2m\omega_n} \tag{3.11}$$

$$\therefore \varsigma = \frac{c}{c_c} \tag{3.12}$$

where $c_c = 2m\omega_n$ - the critical damping coefficient.

The solution of (3.9) is given as decaying sinusoidal wave which is given further below.

3.3 Forced Vibration

A system experiences forced vibration when excitation force is continuously applied to it. The dynamic force can be externally applied, produced by an unbalanced rotating machine or due to motion of foundation, such as an earthquake. A dynamic force is a function of time. It may have different relationships with time and be accustomed to different shapes, such as," *periodic, non-periodic, harmonic, square, triangle, saw tooth, half sine, step, ramp, impulse, or random* "(Wahab, M. A. 2008).

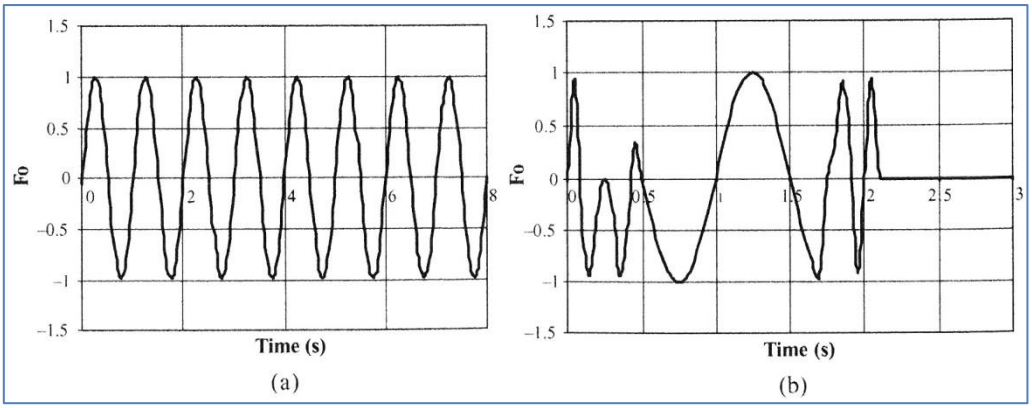

Figure 3.1: (a) Harmonic force and (b) Random force (from Wahab, M. A. 2008).

A force of a harmonic type, that is, $f(t) = F_0 \sin \omega t$, is shown in Figure 3.1(a) where ω is the forcing frequency (also known as the excitation frequency) and a force of a random type is shown in Figure 3.1(b). Using Fourier transformation, any random force can be indicated by the addition of a series of harmonic forces:

$$f(t) = A_0 = \sum(A_i \, sin \, \omega_i \, t + \, B_i \cos \omega_i \, t) \tag{3.13}$$

where A_0, A_i and B_i are all constants.

When a harmonic force is applied to a system with a single degree of freedom (SDOF), the vibration consists of two kinds of motion:

- at the forcing frequency and
- at the natural frequency of the system.

The vibration at the natural frequency decays after some time because of damping, while the vibration at the forcing frequency continues. The vibration at the forcing frequency is called steady state forced vibration.

For more detail on vibration systems we refer to any book that describes dynamics of vibration, for example, (Wahab, M. A. 2008).

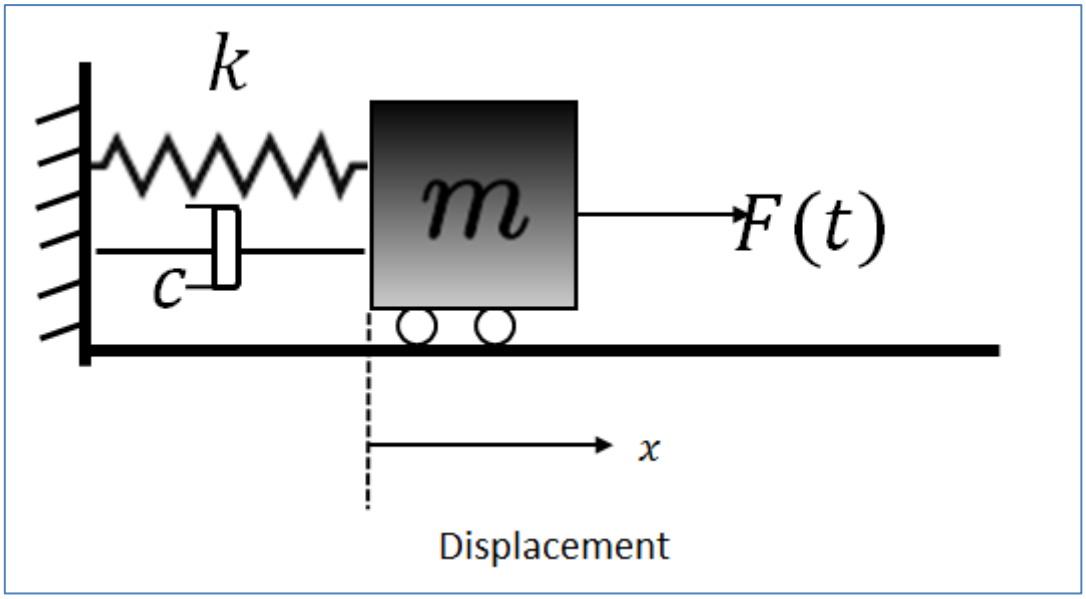

Figure 3.2: A system with a single degree of freedom (SDOF).

3.3.1 Undamped Forced Vibration

For an undamped forced-vibration SDOF system, the damping coefficient, *c* equals zero. The equation of motion, derived from Newton's second law is:

$$-kx + F_o \sin \omega t = m\ddot{x} \tag{3.14}$$

Rearranging Equation (3.14),

$$m\ddot{x} + kx = F_o \sin \omega t \tag{3.15}$$

or

$$\ddot{x} + \omega_n^2 x = \frac{F_o}{m} \sin \omega t \tag{3.16}$$

where

$\omega_n = \sqrt{\frac{k}{m}}$ - the system's angular frequency in rad/s.

3.3.2 Damped Forced Vibration

A viscous damped SDOF system subjected to a harmonic force, $f(t) = F_o \sin \omega t$ is displayed in Figure 3.2, where *c* is the viscous damping coefficient.

From the free-body diagram, Newton's second law can be represented as:

$$-kx - c\dot{x} + F_0 \sin \omega t = m\ddot{x} \tag{3.17}$$

Rearranging Equation (3.17) yields:

$$m\ddot{x} + c\dot{x} + kx = F_0 \sin \omega t \tag{3.18}$$

or

$$\ddot{x} + 2\varsigma\omega_n\dot{x} + \omega_n^2 x = \frac{F_o}{m} \sin \omega_n t \tag{3.19}$$

where $\omega_n = \sqrt{\frac{k}{m}}$ - the system's angular frequency in rad/s and $\varsigma = \frac{c}{2m\omega_n}$ is the damping ratio.

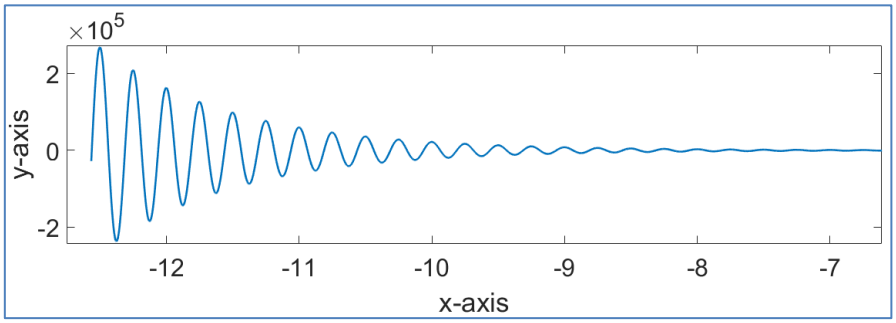

Figure 3.3: x (time) - y (displacement) graphical representation of a damped system to show the effects of friction on a vibrating object.

When the frictional forces are proportional to velocity of an object and the vibrations are damped, these forces become weaker gradually as a result of the lower speeds. The systems conserve the energies and try to lose less, when a lesser amount of energy is left in the system. Consequently, in theory, the vibrations never result to zero, and the loss of energy from the system is exponential according to mathematical calculations. A fixed percentage of its energy/cycle is always reduced by the system, known as the exponential decay.

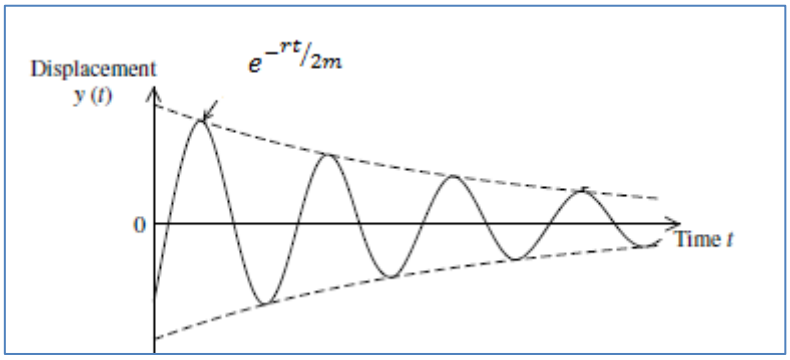

Figure 3.4: Damped Oscillatory Motion (De Silva, C. W. 2007).

3.4 Piezoelectricity and its application in Sensors

Piezoelectricity was discovered in 1880 by two brothers Jacques Curie and Pierre Curie. (Jaffe, B. *et.al.* 2012) have referred to it as "the ability of certain crystalline materials to develop an electric charge proportional to a mechanical stress". Piezoelectric materials convert (Vijaya, M. S. 2012):

- mechanical energy (as external stress or strain) to electrical energy (as surface charge density, electric field or voltage) - known as direct piezoelectric effect.
- electrical energy to mechanical energy - known as indirect piezoelectric effect.

Piezoelectric material is a suitable material for designing smart systems because it has a unique capability of converting energy in both directions, that is, from mechanical to electrical and vice versa (Buxi, R., *et. al.* 2014). The piezoelectric polymer Polyvinylidene Fluoride (PVDF) films are widely known to be good materials for distributed sensors and actuators in the vibration control. This is a high-efficiency and high-power electric-acoustic transducer (Moheimani, S. O. R. 2003) (Ho, Y. S., *et. al.* 2014). Its inner structure is presented in Figure 3.5.

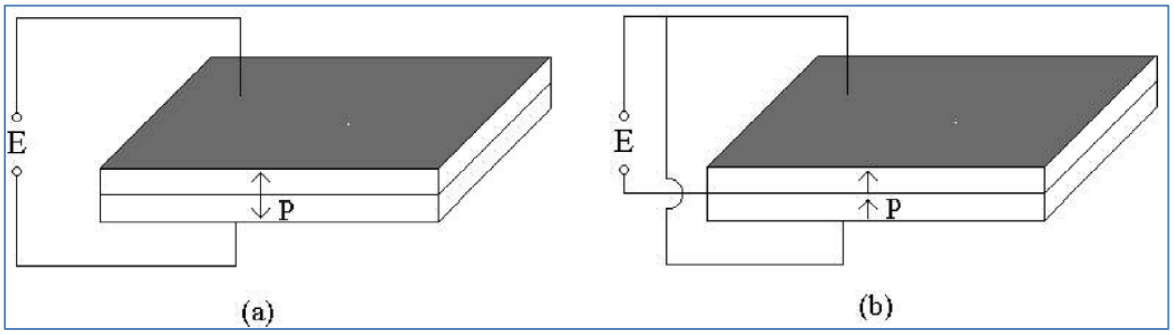

Figure 3.5: Geometrical schematic of a piezoelectric ceramic transducer. (a) Connected in series (b) Connected in parallel (Lin, S. 2004).

Yasuda noticed that bones show piezoelectric properties (Yasuda, I. 1953). Piezoelectric effect of bones has been observed when samples were cut from the femur of a man and an ox and dried fully by heating (Fakuda, E., *et. al.* 1957). As human bones are piezoelectric in nature thus when bones are mechanically excited, there is a rise in AC voltage in whole body as a result of piezoelectric property of

bones and thereby current flows in all the parts of body. (Marino, A. A., *et. al.* 1971) measured the piezoelectric effect in human bone specimens and repeated it with the same samples after demineralisation or decollagenation. The experiments have indicated the organic component gives rise to some or all of the piezoelectric effect in whole bone. (Singh, J., *et. al.* 2014) have investigated the electrical conductivity of bones to demonstrate that there is a maximum voltage of 30-60 Volts in human body which can produce piezoelectric charge and can be utilised for designing human electricity sensor devices. Piezoelectric effect is investigated in several ways to discover relevant properties and have been applied in many medical and industrial devices.

3.5 Sensor Isolation

The utilisation of AC-line-powered medical diagnostic, measurements, and treatment equipment can expose patients and their supporters to the hazard of electrical shock, burns, oxygen saturation, internal-organ damage, and cardiac arrhythmias directly due to leakage current consequently from improper grounding and electrical separation (Been, Y. S., *et. al.* 2007) (Salem, O., *et. al.* 2013).

For sensors built on piezoelectric effects, the application of stress forms dipole charge and produces electrical potential difference on the surfaces that can prove to be harmful for the human body as well as any potential electrical emissions from sensors can worsen the quality of other nearby medical devices; these result in distortions or artefacts on any neighbouring scans (Li, X., *et. al.* 2010). Figure 3.6 is an example of isolation device and Figure 3.7 shows their types.

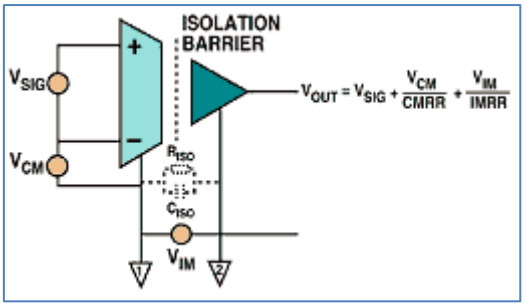

Figure 3.6: An ideal isolation model that would transmit the input signal V_{SIG} across the barrier and reproduce it perfectly at the output. The isolation-mode voltage = V_{IM} (Pickering, P. 2009).

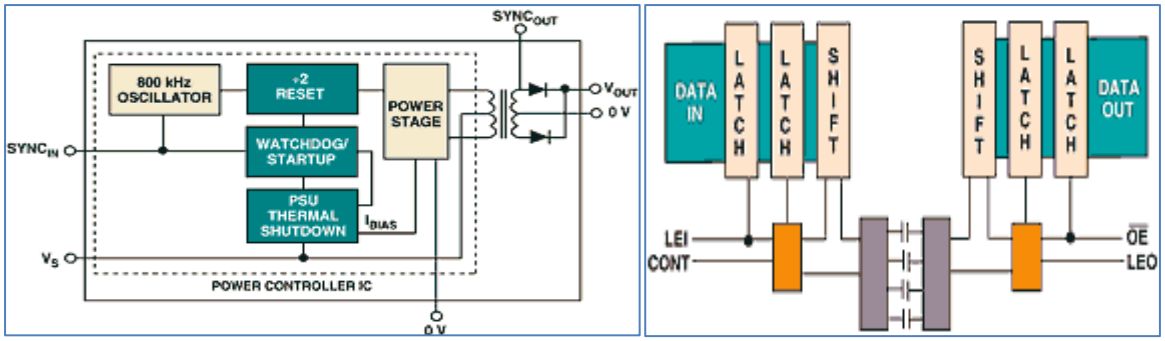

Figure 3.7: (a) Inductive Isolation Device. (b) Capacitive Isolation Device (Pickering, P. 2009).

3.6 Filter

Filters can be used for signal segmentation and removal or attenuation of the unwanted frequencies, so they treat the signals in a frequency-dependent way (Zumbahlen, H. 2011). Different kinds of filters were designed in this research to observe the external disturbance removal and following effects on the resultant signals. In order to understand the filter types in depth, the filters have been discussed below. There are several types of filters: *Bessel, Butterworth, Chebyshev, Inverse Chebyshev, Elliptic, Gaussian and Rectangular filter*. The following section provides a brief description of the most common filters.

3.6.1 FIR Filters and IIR Filters

Finite Impulse Response Filters (FIR)

FIR filters are non-recursive digital filters with impulse response in finite-duration that do not have the feedback.

The FIR filters' have the following advantages:

- Can have linear phase.
- Always stable, even when digitised.
- Usually have linear design methods.
- Efficient applications on hardware.
- Start-up transients have fixed length of duration.

The design aim of a FIR filter is to achieve appropriate coefficients to facilitate its estimated desired magnitude frequency response, subsequently that of a lowpass, high-pass, band-pass, or band-stop filter (Tan, L., *et. al.* 2013). The following observations can be concluded at this stage:

- The ripples or oscillations in the passband and stopband of the frequency response create the Gibbs effect (decaying oscillations) and the behaviour derives from the rapid chopping of the finite impulse response. Window functions are used for recovering from this exact problem and these have been described in *3.7*: Windowing.
- Production of sharp roll-off properties in the transition band is possible when there are a long number of the filter coefficients. A demerit is there might be larger time delay and computational complexity for employing such types of filter will be increased.
- In the passband filters, the phase response is linear that is, all frequency components of the filter input within the passband are exposed to the same time delay at the filter output. It is mandatory for implementing in audio and speech filtering, where removal of phase distortion is necessary.

Infinite Impulse Response Filters (IIR)

IIR filters are digital filters with infinite impulse response. As these filters have the feedback unlike FIR filters so their frequency responses are better than that of the FIR filters of the same order (Milivojević, Z. 2009). Their phase characteristic is non-linear and that might be a problem to the systems that may require phase linearity. They are also known as recursive digital filters. These can be designed in several ways. One of the common methods is by means of the reference analogue prototype filter and is the most suitable for designing all regular forms of filters such as lowpass, highpass, bandpass and bandstop filters.

There can be various procedures to attain a rational approximation for discrete IIR filters: by transformation of analogue filters or by optimisation that provides stability. The discrete filters can be designed by the classical analogue designing processes (Butterworth, Chebyshev, Elliptic, etc.) via the bilinear transformation mapping the analogue s-plane to the z-plane (Chaparro, L. F., *et. al.* 2014).

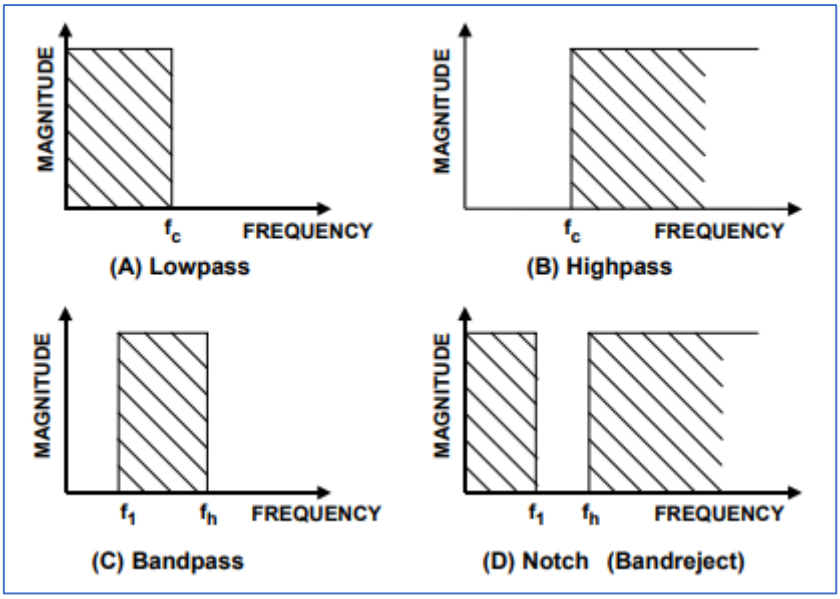

Figure 3.8: Types of ideal Responses by a Filter (Zumbahlen, H. 2011).

All of these filters have real world applications because of certain properties listed below.

- The Butterworth filters => fair amount of amplitude and transient behaviour.
- The Chebyshev filters => amplitude response is better but poor transient behaviour.
- The Bessel filter => optimised to attain improved transient response owing to a linear phase or constant delay in the passband. Thus, frequency response will be relatively worse.

However, in the case when the time domain responses are categorised, the Bessel filter would be best, then the Butterworth filter and followed by the Chebyshev filter (Zumbahlen, H. 2011).

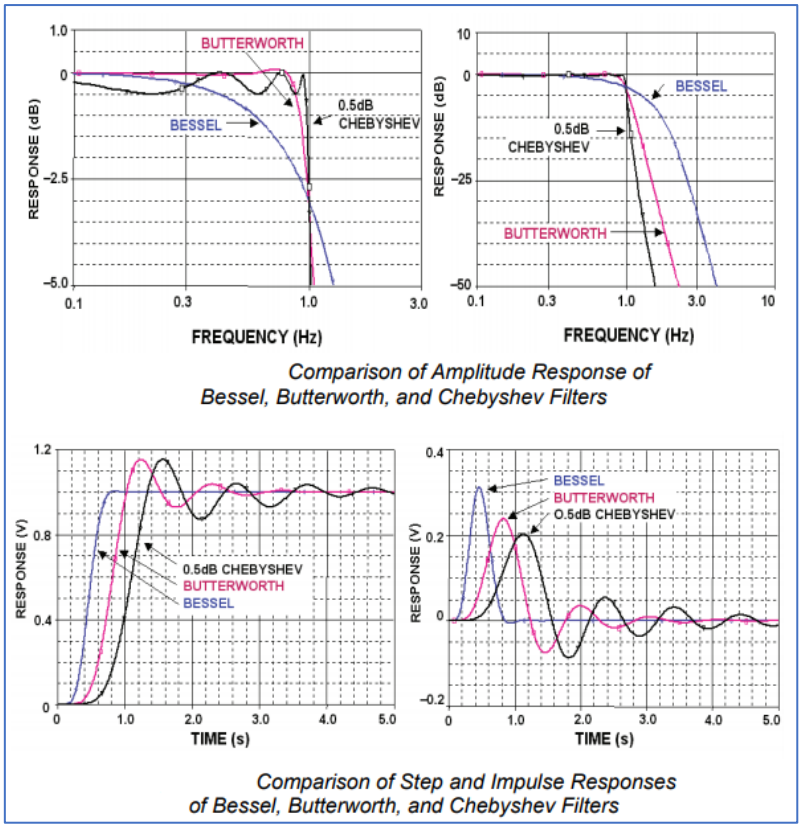

Figure 3.9: Amplitude, Step and Impulse Responses of three commonly used filters for comparisons (Zumbahlen, H. 2011).

According to experiments and analysis of (Kaur, R. *et. al.* 2014), Bessel filter has:

- an exceptional pulse response, i.e. minimal overshoot, as a result of its linear phase response.
- a constant time delay within pass band with the best step response with slight overshoot.
- a slower initial rate of attenuation beyond the pass band when compared to Butterworth and other filters.

The bandwidth of Bessel filter is defined by the range of frequency where the transfer function falls below 3 decibels (dB).

3.7 Windowing

Windowing method has been developed to remove the undesirable phenomenon such as an overshoot occurring at simple discontinuities sometimes known as Gibbs oscillations which usually are found in the passband and stopband IIR filters. The Gibbs oscillations originally take place when there is immediate subtraction of the infinite-length coefficient sequence; at that point, it becomes mandatory to apply a suitable functioning window. These oscillations should be symmetrical additionally that can reduce the weight of the IIR coefficients, laid in a range, to zeros at both ends.

Mostly the inventors named windows after themselves which include Hamming, Von Hann, Kaiser, Blackman, and the like. The window coefficients will taper off between 0 and 1 close to their edges and this type of coefficient variation defines the window properties. This is not like filtration system and generates a set of ideal coefficients. If there is supposedly a finite set of multiplication and addition functions, then to apply suitable filtering, windowing becomes necessary to remove the truncation effects of the sequence.

A window is basically applied to decrease the stopband or passband ripple effects produced in the frequency response, but it cannot make the steepness of the truncation effect larger. Figures 3.10 to 3.12 are some examples of frequency responses with different windows for comprehensive comparison and they are all shown for a band-pass filter. The windows are mainly different on their performance based on the width of the transition band and the stopband attenuation of the frequency response. When designing a filter, truncation lengths, ripples, attenuations are considered to achieve a suitable windowing effect (Parker, M. 2017).

Hamming and Blackman windows are illustrated in Figures 3.11 and 3.12 respectively. It is noticeable that the rectangular window (in Figure 3.10) offers the steepest transition band with large side-lobes and decreases the stopband attenuation. The Hamming and Blackman windows affect the wide transition range but generate a high stopband attenuation. Most of the software programs support windowing for designing all finite impulse response. These windows have same

kinds of effects on the bands and side-lobes when designed for different types of filters.

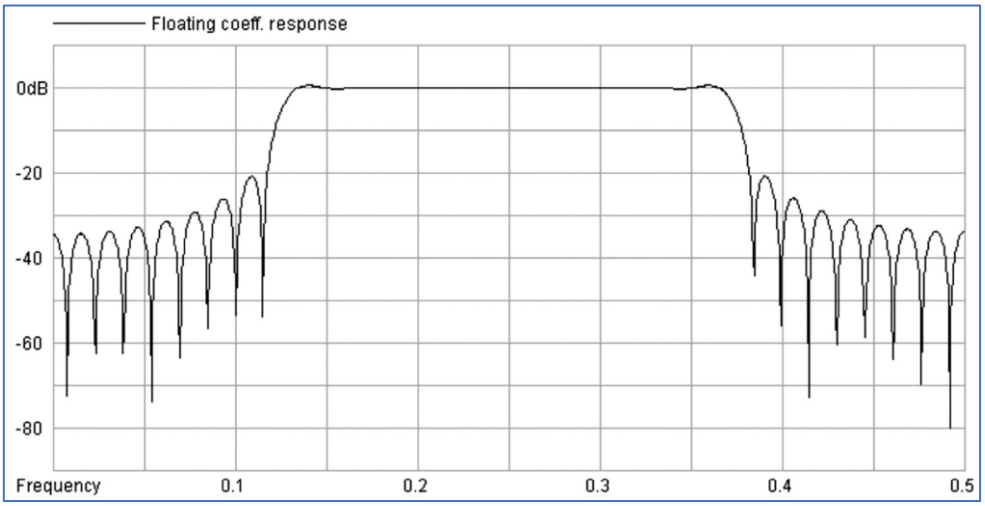

Figure 3.10: Rectangular Window applied to Bandpass filter (Parker, M. 2017).

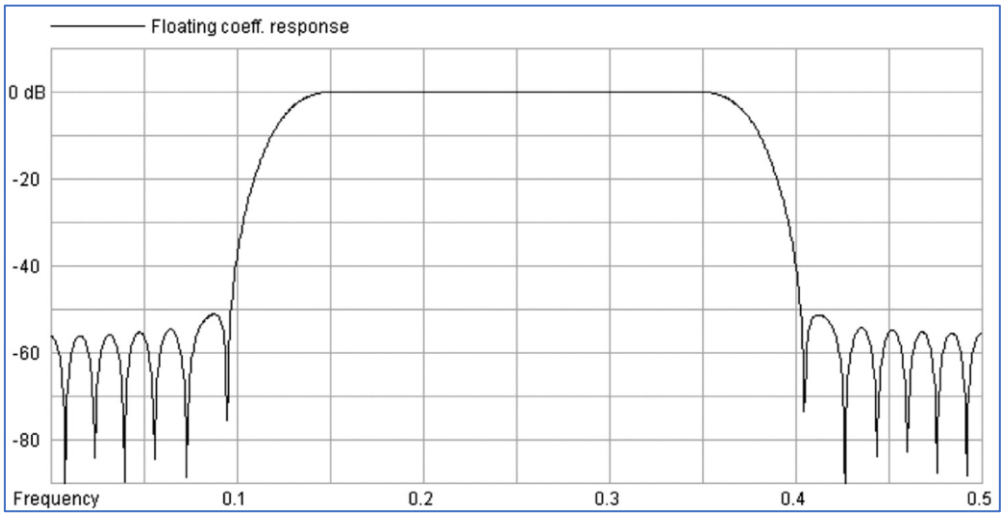

Figure 3.11: Hamming Window applied to Bandpass filter (Parker, M. 2017).

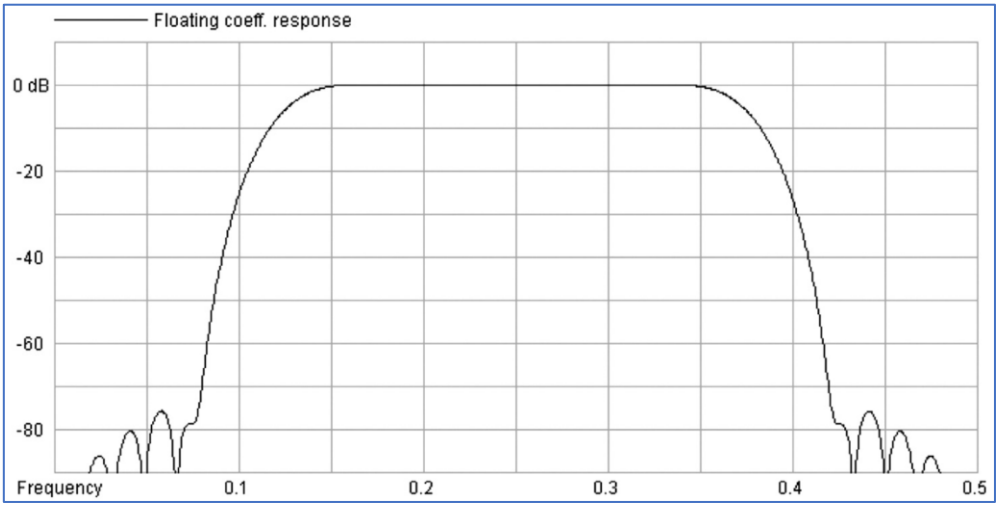

Figure 3.12: Blackman Window applied to Bandpass filter (Parker, M. 2017).

There are several real-world windowing applications where this technique has been applied successfully; such as, minimising side lobes in antenna array, in performing Frequency response analysis of respiratory sounds and some others (Kamble, P. 2016) (Teja, M. V. S. R., *et. al.* 2014).

3.8 Amplifier

The main purpose for designing an amplifier is to increase the level of voltage, current and power. This increased range is known as the gain of the amplifier. The formula for finding out the quantitative range of the increase is significant and should be set according to the amplifier application. A gain is expressed as a ratio of available input power to output power (Pettit, J., *et. al.* 1961).

For example,

- Voltage gain = Ratio of high impedance input to high impedance output, for an oscilloscope amplifier or Output voltage/current by Input voltage/current.
- A telephone repeater amplifier has a limited available input power and should supply power to specified line impedance.

A device that allows a small amount of voltage or current can amplify an electrical signal from any DC source to control the flow of a larger current. Usually the operational amplifier (OPA) is used to amplify loop gain, phase accuracy, bandwidth, noise reduction and bandwidth constancy in different systems. Recently some researchers have proposed that OPA along with CFA(s) (current feedback amplifier) increase the gain with fewer backlashes called *composite amplifiers* (Stephan, G. J. G., *et. al.* 2015). The structure of the amplifier is displayed in Figure 3.13.

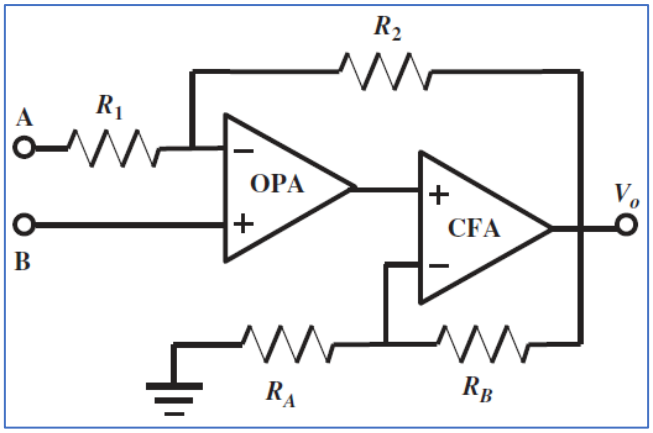

Figure 3.13: Conventional composite amplifier (Stephan, G. J. G., *et. al.* 2015).

3.9 Vibration System interface

Interfacing is done on a system to add features to it and to make it perform better otherwise; it will work with fewer options. Interfacing allows a system to be connected to other microprocessors and make its computation easier and faster. Both the design and implementation of the suitable interfaces handled by a user to control processes like vibration excitation and acquisition, are achieved by the Laboratory Virtual Instrument Engineering Workbench (LabVIEW) software. It is a graphical programming environment which is developed by National Instruments (NI). Scientists and engineers use LabVIEW to design and also implement complex and refined interfaces by means of its built-in extensive libraries that can accomplish purposes like signal processing and data visualisation (Hambley, A. 2011).

3.10 Printed Circuit Board (PCB)

Printed circuit board (PCB) is the typical term but may be referred by “printed wiring boards” or “printed wiring cards”. Former to the industrialisation of the PCB, the lengthy procedure of point-to-point wiring used to be carried out which were often prone to frequent failures at wire junctions and short circuits, in cases, such as, wire insulation began to age and crack.

The contemporary invention relates to method for generating and working data of a PCB inspection apparatus for optically inspecting assembly state of PCB components (Jeong, J. K., *et. al.* 2014). PCB is getting lighter, thinner, shorter, smaller and compact for mounting highly integrated components and is getting more important as a fundamental element enhancing degree of integration. High-speed PCBs have become much more common during the past five years. Today's chip geometries are around 32 nm and continually getting smaller. Those extremely fine geometries are crucial to pack more metal-oxide semiconductor field effect transistors (MOSFETs) onto the silicon so that millions and millions of those transistors or active devices provide the necessary electronics functions or gates to achieve high performance. High performance means higher speeds, and that's the name of the game (Khan, Z. 2014).

A PCB inspection apparatus according to another exemplary embodiment of the current invention comprises generating Gerber data comprising information for pads on the PCB; loading a CAD (Computer-Aided Design) coordinate file comprising a coordinate of a component mounted on the pads; inferring a shape of the component within a pad area by matching the Gerber data and CAD coordinate file; setting an offset based on the inferred shape of the component; and performing offset inspection based on a set value (Jeong, J. K., *et. al.* 2014).

There are many variables and considerations that quickly make an installation very complex. Thus, the design and installation of parts in a system definitely require several options of components to be fitted in any system (Gouldthorpe, B. 2014).

3.11 Theoretical Framework

The Analyses include many types of techniques. A list is given below followed by descriptions.

1. Fast Fourier transform (FFT),
2. Correlation coefficient,
3. Cross correlation,
4. Fuzzy C-means Cluster Analysis,
5. K-means,
6. Dendrogram,
7. Wavelet Decomposition,
8. Short-Time Fourier transform (STFT) and
9. Self-organising map (SOM).

3.11.1 Fast Fourier Transform (FFT)

In 1967, some researchers studied the process called Fast Fourier Transform (FFT) to evaluate its use and they have described it as the computational tool which enables signal analysis such as power spectrum analysis and filter simulation (Cochran, W. T., *et. al.* 1967). When a signal is aperiodic, it can be demonstrated in the form of integral of sinusoids, or harmonically unrelated exponentials. In this way, the resulting spectrum can be continuous and mathematically indicated by the Fourier Transform (Lynn, P. A. 2000).

The FFT is a method for efficiently calculating the Discrete Fourier Transforms (DFT) of a series of data samples (Cochran, W. T., *et. al.* 1967). The DFT is a kind of mathematical process used in numerous processing and applications related to signals. It is a transformation procedure for an ordered sequence of data, generally from the time domain into frequency domain, to recognise the spectral facts regarding the sequence clearly. The DFT is a function of frequency and can be defined as a composition of complex numbers arranged in an ordered set where each number has a real part and an imaginary part. Generally, the real parts are transformed. The DFT is calculated by a method known as the FFT whose output may typically be the similar number of complex values calculated by the DFT. The

FFT process removes many repeated complex parts given by the DFT, and therefore, it requires less execution time. The FFT is sometimes referred to as the implementation of the DFT. If there is a real data set with *N* samples in a signal *x(t)* and *N* is a power of two, then computing time is (Stearns, S. D., *et. al.* 1996):

$$\frac{FFT\ computing\ time}{DFT\ computing\ time} = \frac{1}{2N}\ log_2 N \tag{3.20}$$

This mathematical technique is applied in various fields such as science, engineering and mathematics and these cover power spectrum analyses (Welch, P. 1967), electronics and communications (Yoshizawa, S. 2013), biomedical engineering (Yoganatha, A. P., *et. al.* 1976), geophysical analysis (Zhang, Z. 2011), stock market data (Stadnik, B., *et. al.* 2016) and many more. The Fourier transform (FT) is:

$$H(f) = \int_{-\infty}^{\infty} h(t) e^{-j2\pi ft}\, dt \tag{3.21}$$

and the inverse Fourier transform is

$$h(t) = \int_{-\infty}^{\infty} H(f) e^{j2\pi ft}\, df \tag{3.22}$$

If $f(x)$ = signal (that is, input data) then $F(\omega)$ is equal to the spectra of the signal. If *f* is assumed as a filter's impulse response that produces output data by operating on input data then *F* is known as the filter's frequency response (Brigham, E. O. 1988).

Two key features of FFT:

- Sampling
    - It is simply a method for producing a continuous signal with discrete data set of values. The signals used in the real world, for example, audio signal or our voices, are called "analogue" signals. The signals need to be converted to "digital" form for processing them in computers. An analogue signal is continuous in time as well as amplitude. A digital signal is discrete in time as well as amplitude. Sampling is a technique for converting a signal from continuous to discrete time. The measurement of the signal is determined at particular intervals in time. The values found are called a sample. Additionally, an analogue signal can be quantised in amplitude.

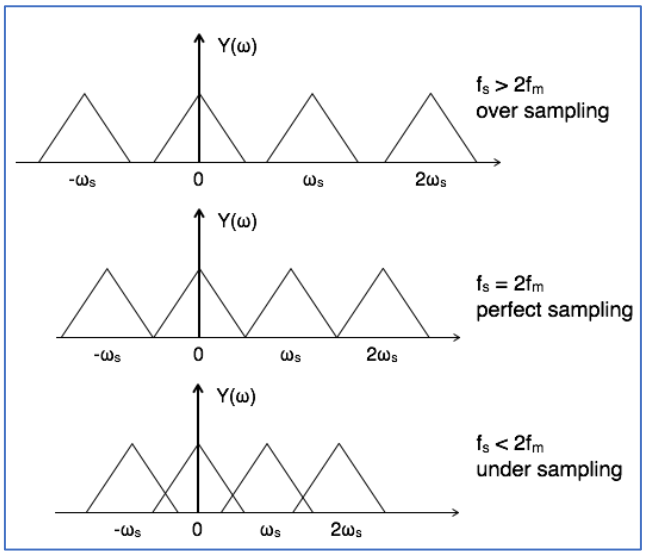

Figure 3.14: Sampling types of a signal where f_s = sampling frequency and f_m = maximum frequency (Tutorials Point 2018).

- Aliasing
    - Aliasing is a phenomenon that is reflected by a signal, when it is reconstructed into a continuous time signal. This phenomenon is due to the occurrence of undesirable components in the converted signal. These parts were absent when the original signal was sampled. As the conversion process takes place, the resulting signal might not have some frequencies of the original signal. If the frequency is lower than a certain level then signal frequencies can overlap and consequently aliasing occurs. These frequencies are sometimes called the folding frequency as they "fold" around half the sampling frequency (Zawistowski, T., *et. al.* 2009).

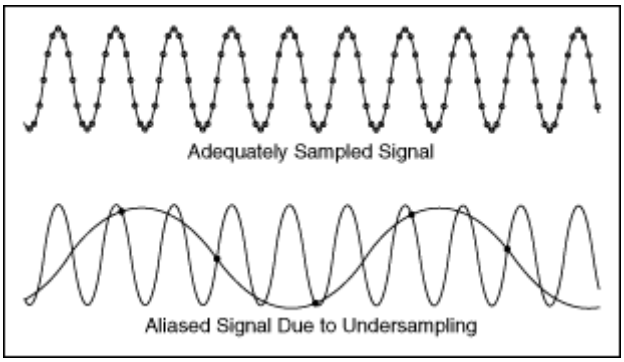

Figure 3.15: Effects of sampling and aliasing of signals (National Instruments, 2018).

Aliasing can be removed by considering f_s (sampling frequency) > $2f$ (natural frequency) and also by using anti-aliasing filters.

3.11.2 Correlation coefficient and Cross correlation

Correlation: It is a typical statistical comparison that determines the length to which two or more variables alter together.

A correlation coefficient: It is a quantitative measure of the correlation.

Relationship: $-1 \leq$ correlation coefficient, $r < 1$ (Deviant, M. S. 2010).

"r" also known as the linear correlation coefficient or the Pearson product moment, specifies the power and the direction of a linear relationship between two variables, *X* and *Y* (Math Bits 2018).

$$r = \frac{n\sum xy - (\sum x)(\sum y)}{\sqrt{n(\sum x^2) - (\sum x)^2}\sqrt{n(\sum y^2) - (\sum y)^2}} \quad (3.23)$$

where,

n is the number of pairs of data,

x and y are the individual sample points.

- A positive correlation is a measure to find out how much those variables increase or decrease in parallel.
- A negative correlation is a measure to find out how much one variable increases along with the decrease of the other one.
- No correlation means that there is no linear relationship (sometimes referred to as a weak link); r is close to 0.

0 => no relationship

+1 => positive relationship

-1 => negative relationship

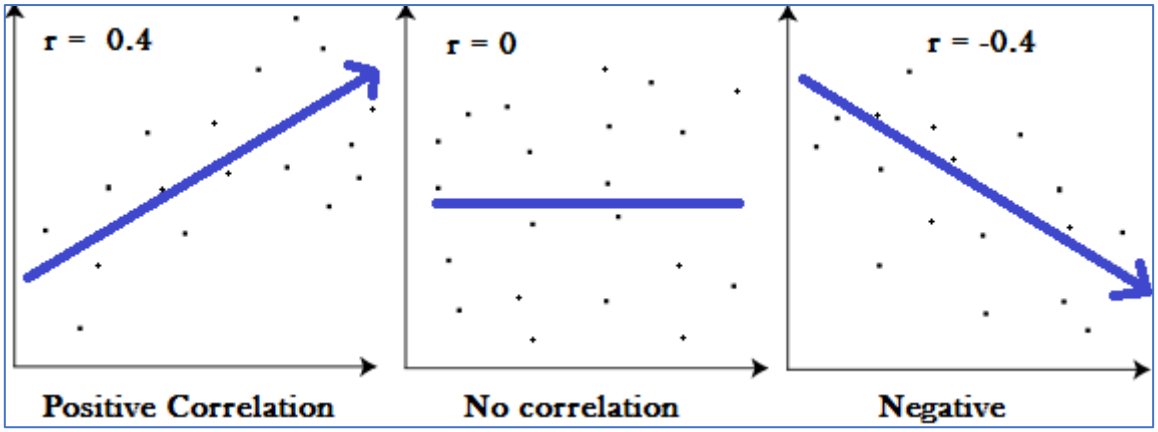

Figure 3.16: Graphs showing a correlation of -1, 0 and +1 (Deviant, M. S. 2010).

Cross-correlation: It is a process to calculate the similarity between two signals and is used between input and output signals to identify an unknown system (Stein, J. Y. 2001). The cross-correlation provides a comparison of two deterministic signals and finds out the similarity between one signal and another signal (or the first signal) that is produced by a time delay (Yarlagadda, R. K. R. 2010).

The cross-correlation between two real signals x and y is given by the following equations (Stein, J. Y. 2001).

$$C_{xy}(\tau) = \int_{-\infty}^{\infty} x(t)y(t-\tau)\,dt \tag{3.24}$$

$$C_{xy}(m) = \sum_{n=-\infty}^{\infty} x_n y_{n-m} \tag{3.25}$$

where the time shift τ or m is called the lag.

3.11.3 Cluster Analyses

Clustering: A common descriptive task in which a finite set of categories is identified to describe the data (Kantardzic, M. 2011). A classification structure may represent a convenient scheme for organising a large data set in order to comprehend relations more easily and to retrieve information more efficiently. If a data set can be labelled by a certain number of groups of objects, then these translations may be classified by certain patterns of similarities and differences in the sets (Everitt, B., *et. al.* 2011).

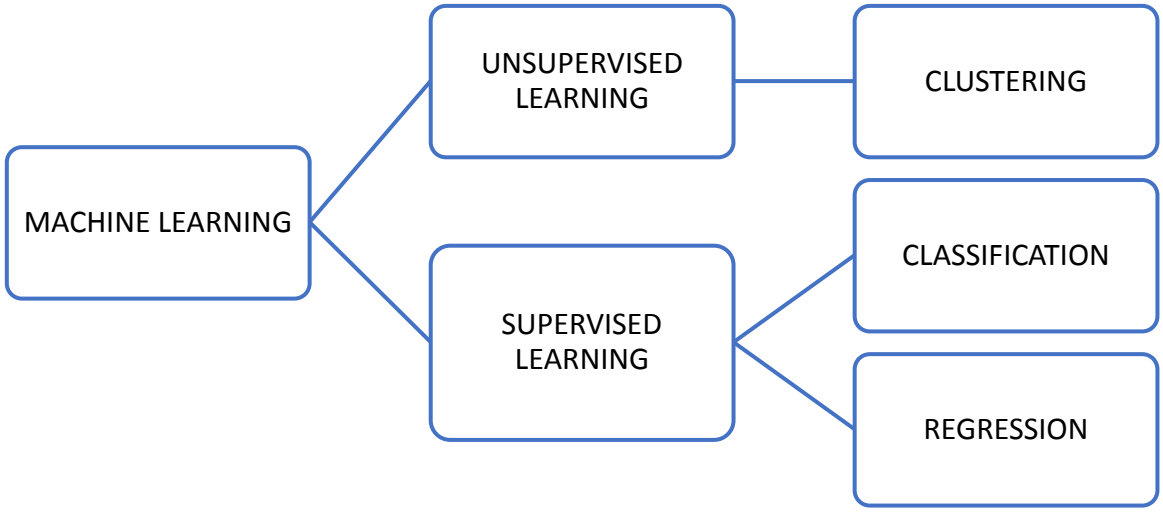

Figure 3.17: Machine Learning Techniques (MathWorks, MATLAB 2017).

Supervised learning is a type of machine learning algorithm which formulates a known dataset (called the training dataset) for making predictions. The training dataset has input data and response values. The learning method tries to make a suitable prototype that predicts the relationship between the dataset and produces the response values. A test dataset is used to validate the model. Greater training datasets produce models with larger predictive power that is able to generalise better for new datasets. In this type of algorithm, the machine is provided with sequential desired outputs y1, y2, and so on and where its aim is to learn to yield the accurate output when a new set of input is supplied (Ghahramani, Z. 2004).

Supervised learning includes two groups:

- Classification: for categorical responses, where the inputs can be divided into particular “classes” and
- Regression: for continuous responses.

Some of the categorisation processes are:

- *Support vector machines (SVM),*
- *Neural networks (NN),*
- *Naïve Bayes classifier,*
- *Decision trees,*
- *Discriminant analysis and*
- *Nearest neighbours (kNN).*

Common regression algorithms include:

- *Linear regression,*
- *Nonlinear regression,*
- *Generalized linear models,*
- *Decision trees and*
- *Neural networks.*

Unsupervised learning is a type of machine learning algorithm that draws interpretations from datasets containing of input data with no labelled responses. Cluster Analysis is the most general technique intended for investigative data analysis to locate classes or hidden patterns inside the datasets (MathWorks, MATLAB 2017).

Common clustering algorithms include:

- *Hierarchical Clustering,*
- *Fuzzy C-means Clustering (Technique used in this research),*
- *K-Means Clustering (Technique used in this research),*
- *Gaussian mixture models,*
- *Self-organising maps and*
- *Hidden Markov models.*

3.11.4 Fuzzy C-means Clustering

Data clustering is usually classified into four ways:

- partitioning approach,
- hierarchical approach,
- grid-based approach and
- density-based approach.

Hierarchical along with partitioning methods are more common than the density-based and grid-based method. Partitioning method is more widespread because hierarchical method takes time to process in comparison when there is a large set of data to be classified (Jain, A. K., *et. al.* 2000). The partitioning algorithm is sectioned

into K-means, Fuzzy C-means (FCM), Gaussian expectation maximisation, etc. FCM is comparatively efficient, easy to implement and converging fast. As the usage of classification in data mining is increasing, several scholars have researched with FCM and the results are all satisfactory. There have been a number of publications on proficient data mining by utilising FCM.

FCM assigns a membership value or a certain ratio to each dataset where a relative cluster centre is yielded between the data and the clusters. Hence, the membership values are drawn closer to the specific cluster centre, if the observatory points are nearer to the grouped centres. The summation of the “degrees of membership” of each data point must be "one". The formula is subjected to the minimisation of the resulting neutral function (Frunza, M-C. 2016):

$$J_m = \sum_{i=1}^{N} \sum_{j=1}^{L} \mu_{i,j}^{m} \left\| x_i - c_j \right\|^2, 1 \leq m < \infty \qquad (3.26)$$

where

N = number of data

L = number of clusters

$\mu_{i,j}$ = degree of membership of x_i in cluster j

|| * || = any distance metric (Euclidean) between an input and the centroid allocated to the cluster.

3.11.5 K-means

K-means has proved to be a very influential data mining algorithm and has been used in various sectors such as, in medical, networking, etc. For clustering a particular set of data into a number of stated numbers of clusters, k-means is the perfect technique. An example is provided below (Hasan, M. K., *et. al.* 2015).

This process has been applied to separate "n" genes into "k" classes, in order to reduce the space between the cluster’s genes and its resultant centroid, illustrative of the cluster. The aim is to separate “n” into "k" sets *Si*, i = 1, 2…, k for minimising the within-cluster sum of squares (WCSS),

$$WCSS\ or\ I_{k-means}(C) = \sum_{j=1}^{k} \sum_{i=1}^{n} || x_i^j - c_j ||^2 \qquad (3.27)$$

where $||x_i^j - c_j||^2$ is equal to the distance between a gene and the cluster's centroid.

In the grouping processes, the first cluster centroids are chosen unsystematically, then each gene is allocated to the nearby cluster centroid. After that, each cluster centroid is relocated to the average of the points assigned. This algorithm converges if the allocations do not vary anymore which is indicated by iterations in any software which calculates "k-means" value.

However, there is a fundamental drawback of this type of partitioning system - storing and run-time linked with long clusters for keeping quantisation errors low and model fidelity large. Few methods on how to reduce these problems have been published by studies (Norouzi, M., *et. al.* 2013) (Dalton, L. A. 2014).

3.11.6 Dendrogram

The Dendrogram is a hierarchical method that can be presented via both a mathematical and a graphic depiction. It can be divisive or agglomerative. Therefore, the dendrogram is often a reference for the results of the hierarchical clustering.

Some terminology for a dendrogram is listed as following; Figure 3.18 is an illustration:

- The starting point of the tree is at the root.
- The nodes of the dendrogram denote clusters. The internal nodes symbolise all observations that are classified built on the type of linkage and distance used. For most of the cases of dendrograms, terminal nodes contain a single observation.
- The stem or edge displays the link with the clusters underneath them. The length of the edge symbolises the distances at which the clusters are linked.

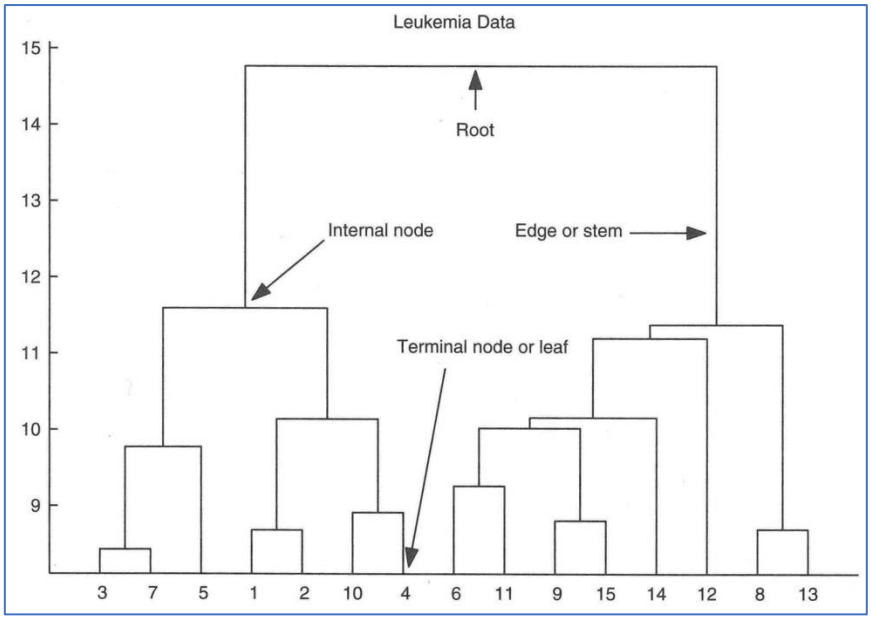

Figure 3.18: Dendrogram example of an agglomerative clustering to Leukaemia data (Martinez, W., *et. al.* 2005).

The dendrogram demonstrates the procedure of building the classes, along with the internal nodes designating certain groups, when it has been cut at a suitable level.

3.11.7 Self-organising map (SOM)

Self-organised learning repetitively updates neural network (NN) synaptic weights as a response to application of inputs, until a final configuration is achieved, as per a set of prescribed procedure (Barner, K. E., *et. al.* 2004). It contains *m* number of neurons positioned at an ordered low-dimensional (usually a 2-D) map. According to the topologies allocated, the adjacent neurons are related in a neighbourhood fashion. This indicates the shape of the Kohonen map. The distance function calculates the Euclidean distance (gap between the neurons) starting from a neuron to any other neighbouring neuron. If neuron, *i* has a d-dimensional weight vector, known as $w = (wi_1, wi_2, ..., wi_m)$, where $i = 1, 2 \ldots .m$, which has the similar aspect as the input space. The formulae followed for developing SOM learning algorithm (Chaudhary, V. *et. al.* 2014):

a. Initialise the *wi's* of the *m* × *n* neurons.
b. Choose *x(t) as* any input which can be considered as the input to all the neurons simultaneously in parallel.
c. Finalise the output *c*.

$$c = arg(min_{1 \le i \le mn}\{\|w_i(t) - x(t)\| \}) \quad (3.28)$$

where ||.|| = the Euclidean distance measure where *x(t)* = the input and *wi(t)* = weight vector of neuron *i* at *t* number of iterations.

d. The weight of the neurons is updated by means of the following equation:

$$w_i(t+1) = w_i(t) + h_{c,i}(t)x(t) - w_i(t) \quad (3.29)$$

where $h_{c,i}(t)$ = Gaussian neighbourhood which specifies the learning rate and width of the neighbourhood radius.

e. For all the inputs, the stages starting from (b) to (d) are repeated.

3.11.8 Wavelet Decomposition

The wavelet transformation is based on wavelets that are frequency changing and particular time length allocated small waves. In comparison with the FFT, they provide both frequency contents of a signal and its temporal information. The wavelet transforms deal with time-frequency analysis of non-periodic signals and provides the means to analyse non-stationary signals (Ifeachor, E. C., *et. al.* 2002). Wavelet transforms have several applications, in filtering signals, denoising-signals, data compression, image processing, etc. All wavelets are derived from a basic (mother) wavelet.

The continuous wavelet transforms (CWT) is defined as

$$CWT(a,b) = \frac{1}{\sqrt{a}} \int g * \left(\frac{t-b}{a}\right) dt \quad (3.30)$$

Wavelet transforms show signals by decomposing them into many components that are derived from a single mother wavelet through shifting and scaling. Some popular wavelet functions are Morlet, Haar, and Daubechies. The CWT is typically executed in discrete time, giving rise to the discrete-time wavelet transform (DWT) (Hamdy, N. 2009).

According to (Meyer-Baese, A., *et. al.* 2014), a filter bank can be defined as a number of filters, connected mainly via sampling operators and sometimes via delays. The analysis filters are typically lowpass and highpass filters in case of two-channel filter bank.

There are two components of the filter banks:

- analysis: Here the signal is decomposed.
- synthesis: Reconstruction of the decomposed signal takes place in this part.

The lowpass filter takes “averages” and the high-frequency contents are smoothed out by the process. The highpass filter takes “differences” and smooths the low-frequency components. The procedure of down-sampling or decimation becomes compulsory when decreasing the number of the data for transmission. Down-sampling must be carried out on the filters’ outputs as well. For reconstruction of the signal, up-sampling or interpolation is required. Zeros are placed instead of the removed components.

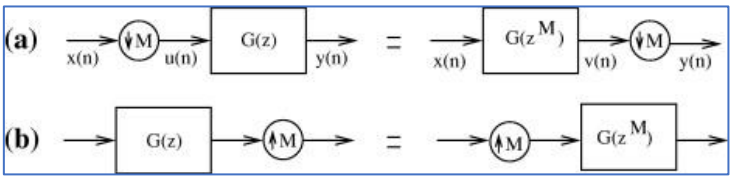

Figure 3.19: Equivalent structures: (a) equivalence for down-sampling, (b) equivalence for up-sampling (Meyer-Baese, A., *et. al.* 2014).

In Figure 3.20, the analysis filters are $H_0(z)$ and $H_1(z)$. The synthesis filters are $G_0(z)$ and $G_1(z)$ and should be adapted to the analysis filters order for cancelling the errors formed in the analysis bank or for achieving efficient reconstruction.

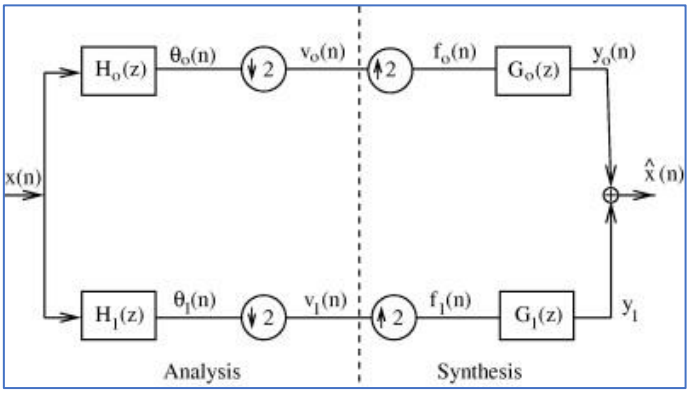

Figure 3.20: Two-channel filter bank (Meyer-Baese, A., *et. al.* 2014).

The outputs θ_0 and θ_1 are down-sampled by 2, and these are in the analysis bank, the sub-band signals are $v_0(n)$ and $v_1(n)$. These signals are quantised by means of a sub-band coder, then coded, and sent to a receiver. Under ideal conditions, $v_0(n)$ and $v_1(n)$ are expected to be received at the synthesis section. Then the signals are interpolated by 2, and the new signals are indicated by $f_0(n)$ and $f_1(n)$. The newly obtained signals are treated by $G_0(z)$ and $G_1(z)$ which are filters for interpolation. The final output $x(n)$ is produced by summing up the signals $y_0(n)$ and $y_1(n)$.

3.11.9 Short-Time Fourier Transform (STFT)

The goal of the Short-Time Fourier transform (STFT) is to divide a signal into overlapping frames by processing it via a moving window then run the DFT at newly formed frames. Therefore, this transformation actually falls in the category of short-term processing techniques. As has already been explained, the length of the moving window plays a vital role because it defines the frequency resolution of the spectrum, given the sampling frequency. Longer windows provide better frequency resolution at the expense of decreasing the quality of time resolution. Alternatively, shorter windows lead to a thorough illustration in the time domain, but generally, provide poor frequency resolution (Giannakopoulos, T., *et. al.* 2014).

In audio analysis applications, the short-term window length typically ranges between 10 and 50ms. The Moving Picture Experts Group (MPEG7) audio standard is usually a multiple of 10ms. If the DFT coefficients of each frame are placed into a separate column of a matrix, the STFT can be characterised as a matrix of coefficients, where the column index denotes time and the row index is associated with the frequency of the respective DFT coefficient. If the magnitude of each coefficient is calculated, the resulting matrix can be referred as an image consequently, it can be visualised. This image is known as the spectrogram of the signal and presents the signal evolution in the time frequency domain.

According to MATLAB, the formula for a signal's spectrogram = spectrogram (signal, window, no-overlap, number of FFT points, sampling frequency), that can plot the spectrogram and return the matrix of STFT coefficients, along with the respective time and frequency axes. An example of spectrogram is given in the Figure 3.21. Each frame is typically multiplied on a sample basis by a suitable window type which

aims at attenuating the endpoints of the frame while preserving the signal around the centre of the frame. This calculation is done before determination of the DFT coefficients takes place.

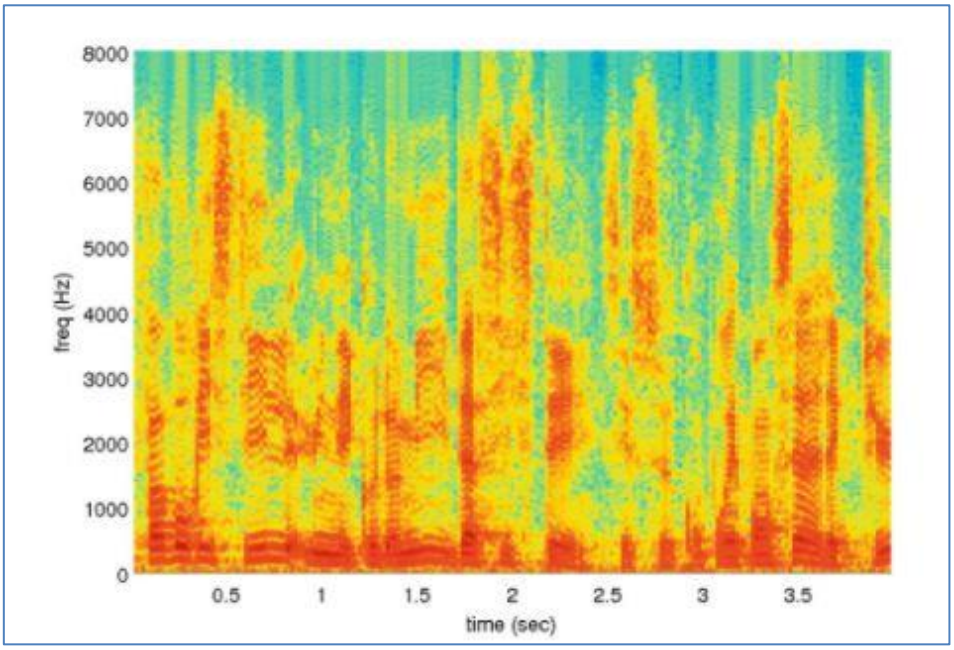

Figure 3.21: The spectrogram of a speech signal. The frames are non-overlapping, 20ms (Giannakopoulos, T., *et. al.* 2014).

The STFT is a solution for finding out the frequency spectra of signals with time-varying frequency spectra. Some drawbacks of this technique are described as follows (Wallisch, P., *et. al.* 2013):

- A slight amount of frequency fluctuations is not clearly detectable as the signal subsets are supposedly stationary.
- As the processing of the entire window produces distribution of frequency at a time point so selecting a shorter length of windows permits improved localisation in time. The disadvantage is if a window is smaller, then fewer samples are obtained by Fourier transform that consequently decreases frequency resolution, essentially in cases of lesser frequencies.

Briefly, there is an adjustment in the middle of the localisation of time and frequency. The application of this method is the finest if frequency varies over a consistent time scale allowing a single window size with no significant information lost.

3.12 Official Steps

3.12.1. Initial Procedures

In order to start the experiments on the university premise, a risk assessment had been filled up.

As this study was carried out in the Accidents and Emergency Department in the Northern General Hospital on Adults, so the consent was taken from the NHS South Yorkshire region. It is a NRES Committee Yorkshire & the Humber - South Yorkshire. In the form, it was clearly stated that 24 patients are to be recruited, of age 18 years old and above. Moreover, one consent form was produced to record the comfort level to take this research on forwards. The researcher who carried out this study (me):

- went through an enhanced DBS (Disclosed and Barring Service) check to check any criminal convictions.
- went through clinical examinations to receive a medical certificate that I am not going to contract any disease to the participants.
- gave an online examination and received a Good Clinical Practice (GCP) certificate.
- research passport was filled up with the official information.

GCP training is a mandatory qualification designed for Health and Social Care by the Research Governance Framework 2005 enclosing every study taking place in the England NHS, and in law (SI 2004/1031, Schedule 1, Part 2, 8) aimed at the individuals involved with medical studies. This training is taken to make sure that anyone who is related to the trials/study has relevant competency to perform the study (NHS, 2017).

3.12.2 Risk Assessment

Performance measurement has a vital part for ensuring success of a project along with its benefits towards the sponsoring organisation. (Pillai, A., *et. al.* 2002) demonstrates how much both the project and organisational performance can impact the metrics measurement in a controlled environment. Hence it is very important to devise appropriate performance measurement system to suite the researcher's safety along to increase the outputs and attainments of the project (Cordero, R. 1990).

There can multiple types of risks in a project (Mustafa, M. A., *et. al.* 1991). This study has two types of risks: Physical and Environmental which are to be controlled. As this study has some soldering and electrical setups to be performed for the instrument to function properly and as desired, thus some precautions for electrocution and protection from harmful fumes were suggested for those tasks. Additionally, there are risks handled by the researcher while working with the computers and also during the practical experiments, like falling of the objects on the feet, etc.

3.12.3 Ethics Approval

When ‘‘ethics’’ is mentioned somewhere, then it is referred to maintain a morally permissible and appropriate standards of conduct to the participants in a study (Davis, M., *et. al.* 2012). Ethics are both collective and individual constructs which can be adopted or imposed (Fellows, R., *et. al.* 2004). It helps to combat pressures on researchers as well as ensures appropriate standards of practices for the study.

This study had firstly been carried out at Accident and Emergency (A&E) Department of Northern General Hospital (NGH) on Adults and later at Emergency Department of Sheffield Children's Hospital (SCH). The consents were taken from the NHS South Yorkshire region. This study was proposed to be developed for children; however, the Ethics board was not convinced whether the device would be too painful for the children to endure, in case, of presence of a fracture. Thus, the study was approved to be carried out on adult patients who came with a wrist injury at NGH A&E to ensure the comfort and discomfort level from them. In the first Ethics form, it was

clearly stated that 24 patients are to be recruited, of age 18 to 24 years old. This first Ethics approval was only for recording on adults in the presence of an approved consultant and radiographer.

There would be two groups of people to be investigated:
16 people with fractures and 8 people with no fracture.
These 16 people will again be divided in two groups: 8 people with wrist bone fracture and 8 people with ankle bone fracture.

The consultant approved for this study at NGH was there on duty only on Fridays, so the recruitment went very slow and the procedure was conducted only on wrists.

After recording from 6 adult patients successfully with the programmed computer results matching that of the X-ray, an application was given for getting the Ethics Approval to carry the study with children at Sheffield Children's Hospital (SCH). The Ethics Approval was given for carrying out the study on 50 children's wrists and 50 children's ankles, aged 10 to 15-year olds.

The participants of aged between 10 and 12 year olds were given different information sheets than that to the 13 to 15 year olds, choosing suitable words, in order for them to understand.

3.13 Conclusion of Chapter 3

The theories for using the components in this study have been verified giving an idea regarding their practical applications previously. The mathematical techniques have also been discussed so that their concepts can be clear for selecting the methods in the next few chapters. Some of the Official steps taken for initiating the research have also been detailed.

Chapter 4: Smart Systems and Evaluations

4.1 Smart Systems

Smart systems are defined as devices that incorporate the functions of sensing, actuation, control and adaptation. These can describe and analyse situations and take decisions based on the available data in a predictive or adaptive manner, thereby performing smart (intelligent) actions (Wan K., *et.al.* 2014). Smart systems are used in many applications such as manufacturing, automotive, energy, environment and health care. These systems have the definite ability to resolve very complex problems, nonetheless, taking over human cognitive functions (Glesner M., *et. al.* 2013).

In the case of health care and medical applications, smart systems are primarily used to improve the quality of diagnosis and treatment. The system described in this study shows the usage of miniature smart hardware devices to produce and procure energy through a medium. The first prototype of the device has been tested to find correlation between vibration frequency and bone density and has been developed by the Medical Electronics Engineering Group at Sheffield Hallam University's Centre for Automation and Robotics Research facility (Razaghi, H., *et. al.* 2014). The device has been modified suitably for distinguishing between wrist fractures and sprains and our group is trying to make it more efficient for the real-world and for others to use. The data acquired from this method is stored and analysed using complex programmed routines through specific software.

4.2 System Design

4.2.1 Sensor

In this study, since the vibration responses generated from the impact excitation process is very small and occurs only for a very short period of time, a highly sensitive sensor with a buffered output was needed to pick-up the vibration responses so CM-01B contact microphone[1] was used in this case to detect and record the vibration signals. It uses a low-noise electronic preamplifier combined with robust Polyvinylidene Fluoride (PVDF) piezo film to deliver a unique sound or vibration pick-up with buffered output. The design lessens external acoustic noise while contributing extremely high sensitivity to vibration applied to the central rubber pad. The CM-01B is suitable for detecting body sound signals. Its datasheet is attached as Appendix A.1. Figure 4.1 displays the schematic as well as the mechanical structure of the sensor used.

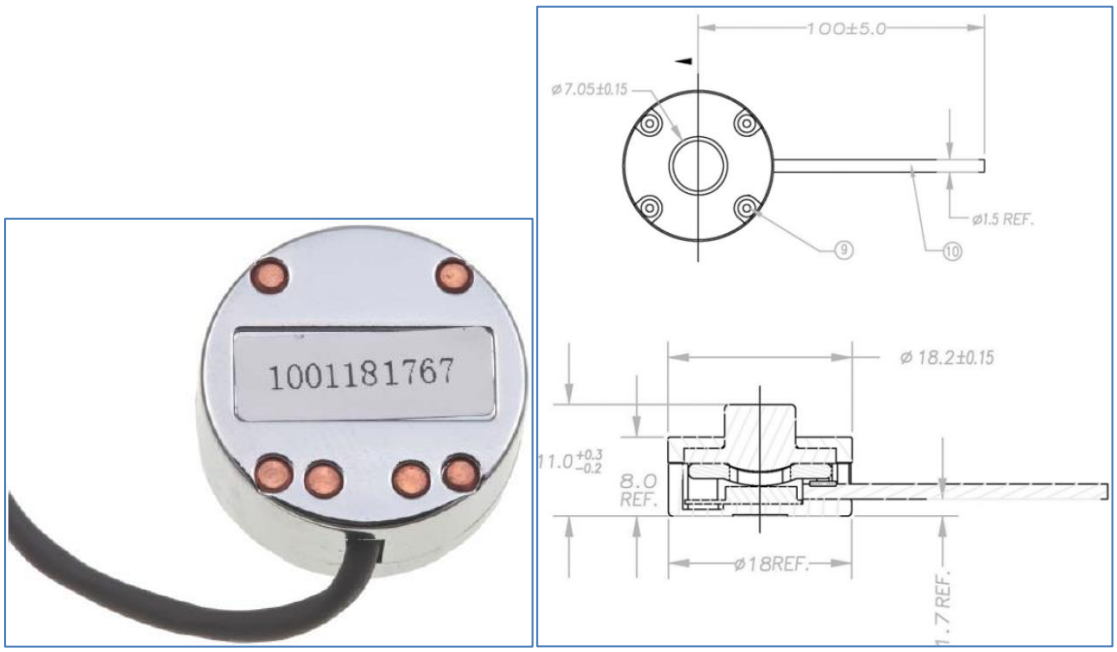

Figure 4.1: (a) Schematic of CM-01B (b) Mechanical layout with dimensions shown (Datasheet, 2011).

[1] http://scsembeddedtech.com/pdffiles/measpec/Contact_Microphone.pdf

For this study, the sensor was enclosed by a plastic body to cover the outer metallic part of the sensor, to avoid it being in contact with the patients directly and to make it look nicer.

Figure 4.2: Piezoelectric Sensor used for the acquisition of data.

4.2.2 Analogue-to-Digital Conversion

The digital signal generated by the computer required to be converted in the analogue form in order to control the small electrical inducer that was used in the excitation system. This conversion process was achieved by using an interface board called National Instrument (NI) myDAQ which is a portable data acquisition board for analogue-to-digital conversion and vice versa (myDAQ, 2010). Interfacing is conducted to move information from one device to another to make the devices function properly.

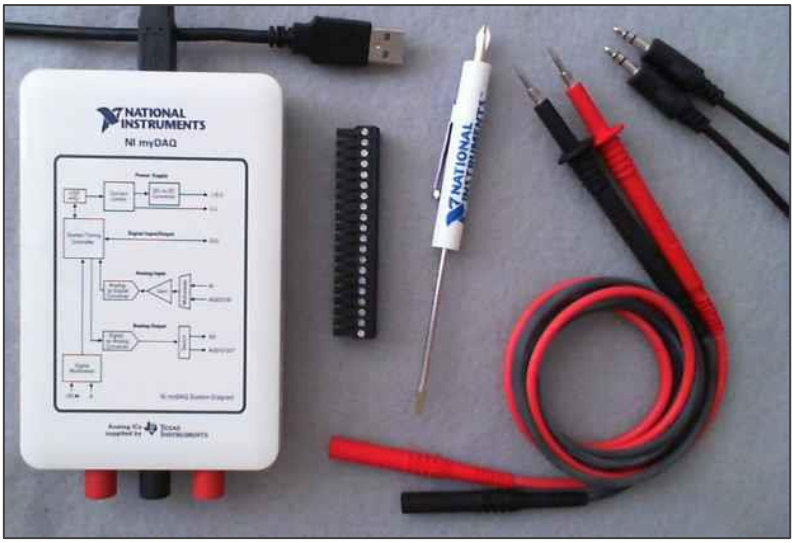

Figure 4.3: The myDAQ NI Instrument and its components.

4.2.3 Initial Set-up

The entire device in Figure 4.4 had been powered up by a power supply and the data were stored in a desktop computer as a result the entire setup was quite large and not portable at all.

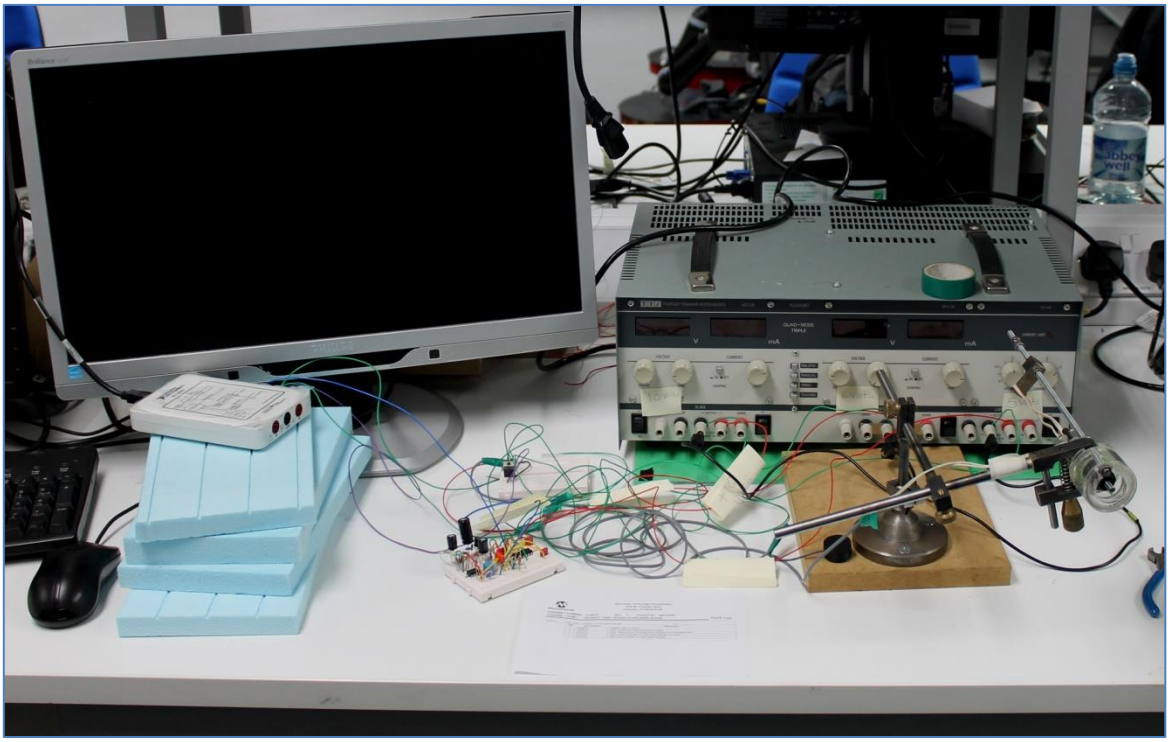

Figure 4.4: Entire Set-up.

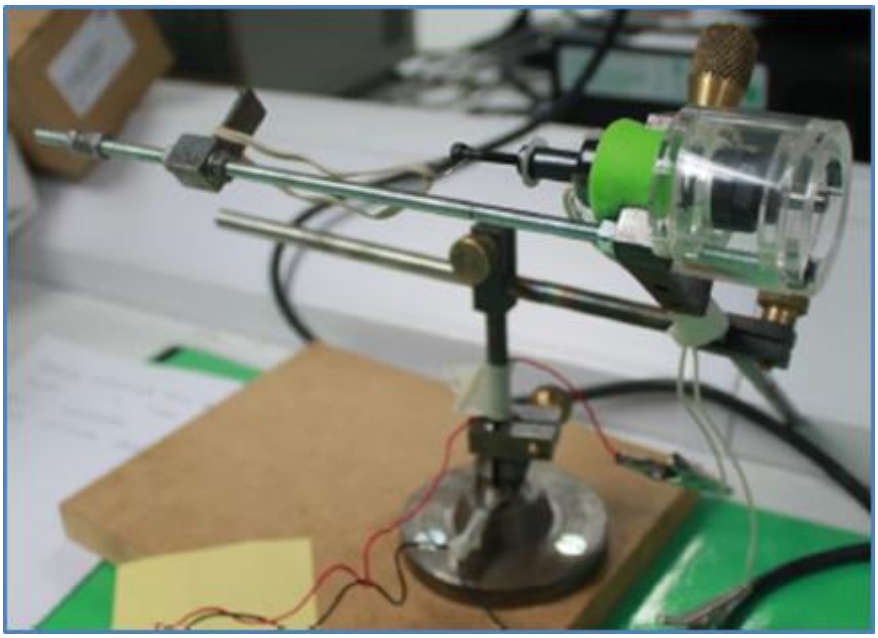

Figure 4.5: Vibration Inducing Unit.

As mentioned in section *4.1*, the device used in this research was initially developed in the Medical Electronics Research Centre of Sheffield Hallam University to assess bone density, so the device and the program were updated for our study. The device has been made more compact so that it is hand-held. Some other modifications made are listed below.

- The desktop computer was replaced by a laptop.
- A small battery of 12 V size was brought to power up the entire system.
- Most of the electronic circuit design was made precise by printing it on a board.

4.2.4 Printed Circuit Board (PCB)

4.2.4.1 Amplifier

The set-up for this study gave an output of 0.5 V so the signal was amplified by the circuit design shown in Figure 4.6. This was done by means of selecting a suitable an Operational Amplifier (Op-Amp). Some of the capacitors were chosen polarised and some were non-polarised. They can be seen in the Figure 4.11.

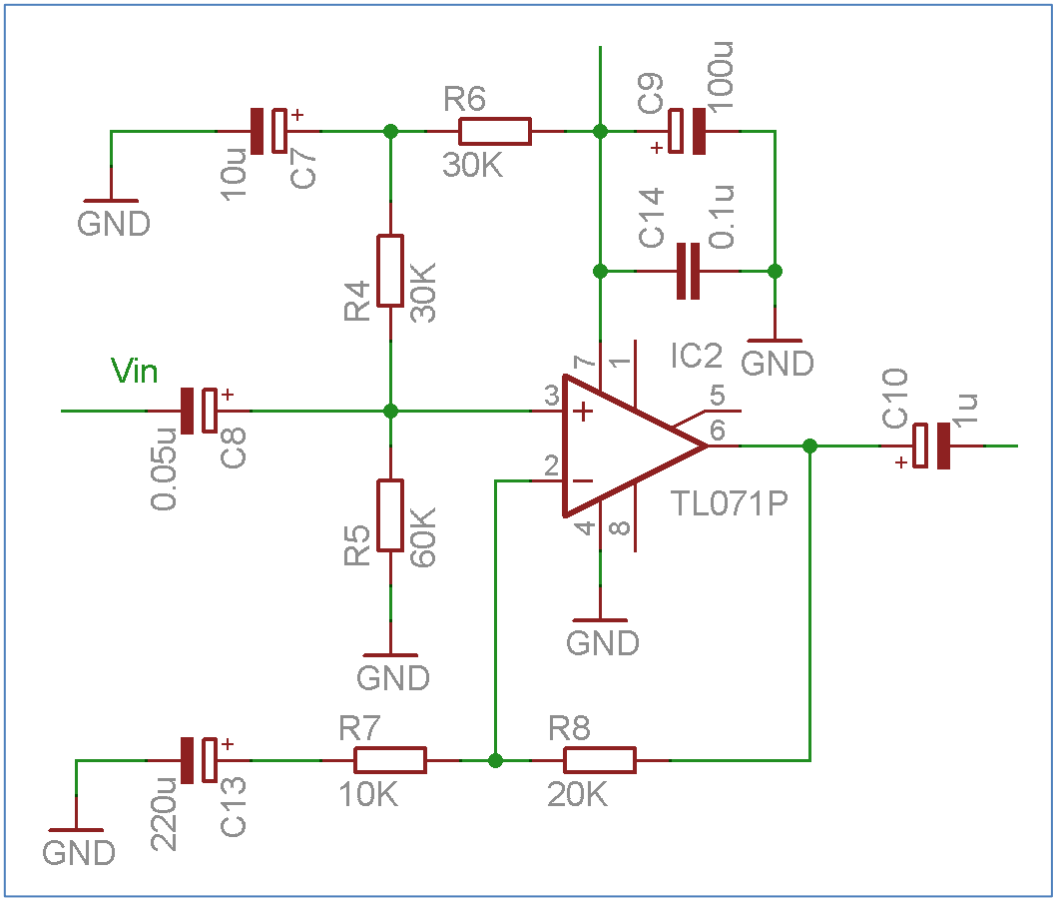

Figure 4.6: Schematic Diagram of the Amplifier.

4.2.4.2 Filter

Then the next step was to use a filter which in this case was a Bessel Filter. The reason for using this was discussed in *Subsection 3.6*. 4th order filter had been used in this study where the circuitry had been made by the addition of two 2nd order ones shown in Figure 4.7.

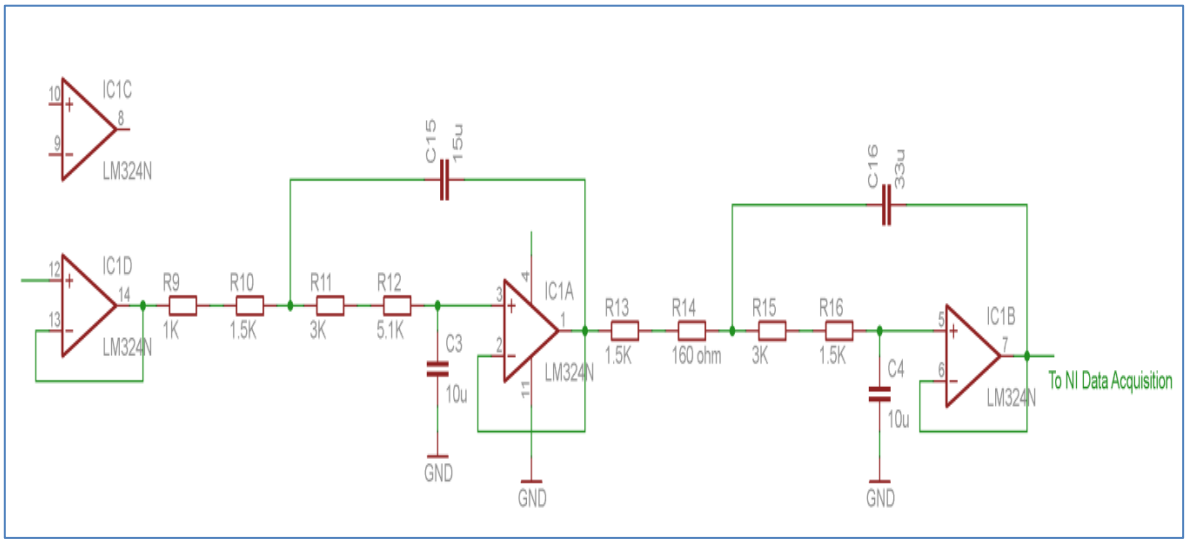

Figure 4.7: Schematic Diagram of the 4th order Bessel Filter.

4.2.4.3 Power Regulator

The vibration excitation and acquisition system were designed to work with a single-12V supply battery which offered reduced power consumptions, costs and increased design life. Since the vibration system consists of different components (Hammer control unit, myDAQ system and the entire circuitry) with different voltage requirements, voltage regulators were required to supply suitable voltage to each section of the system for that part to function properly, as shown in Figure 4.8.

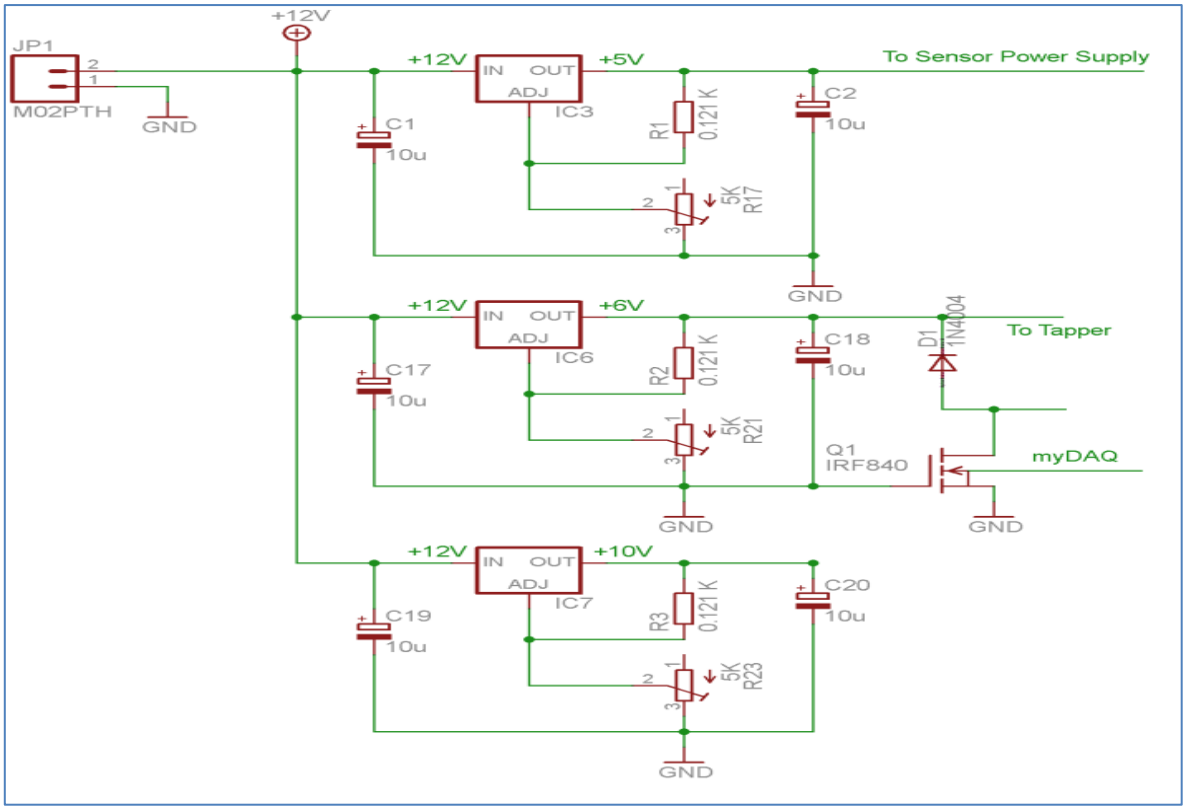

Figure 4.8: Schematic Diagram of the Power Regulator

4.2.4.4 Entire Schematics and Layout

Figure 4.9 shows the entire circuit as the schematics shown in Figures 4.6 (Amplifier), 4.7 (Filter) and 4.8 (Power Regulator) were assembled altogether. This was done to generate the layout for developing the circuit in PCB practically. Figure 4.10 is the layout generated due to the schematic diagram shown in Figure 4.9.

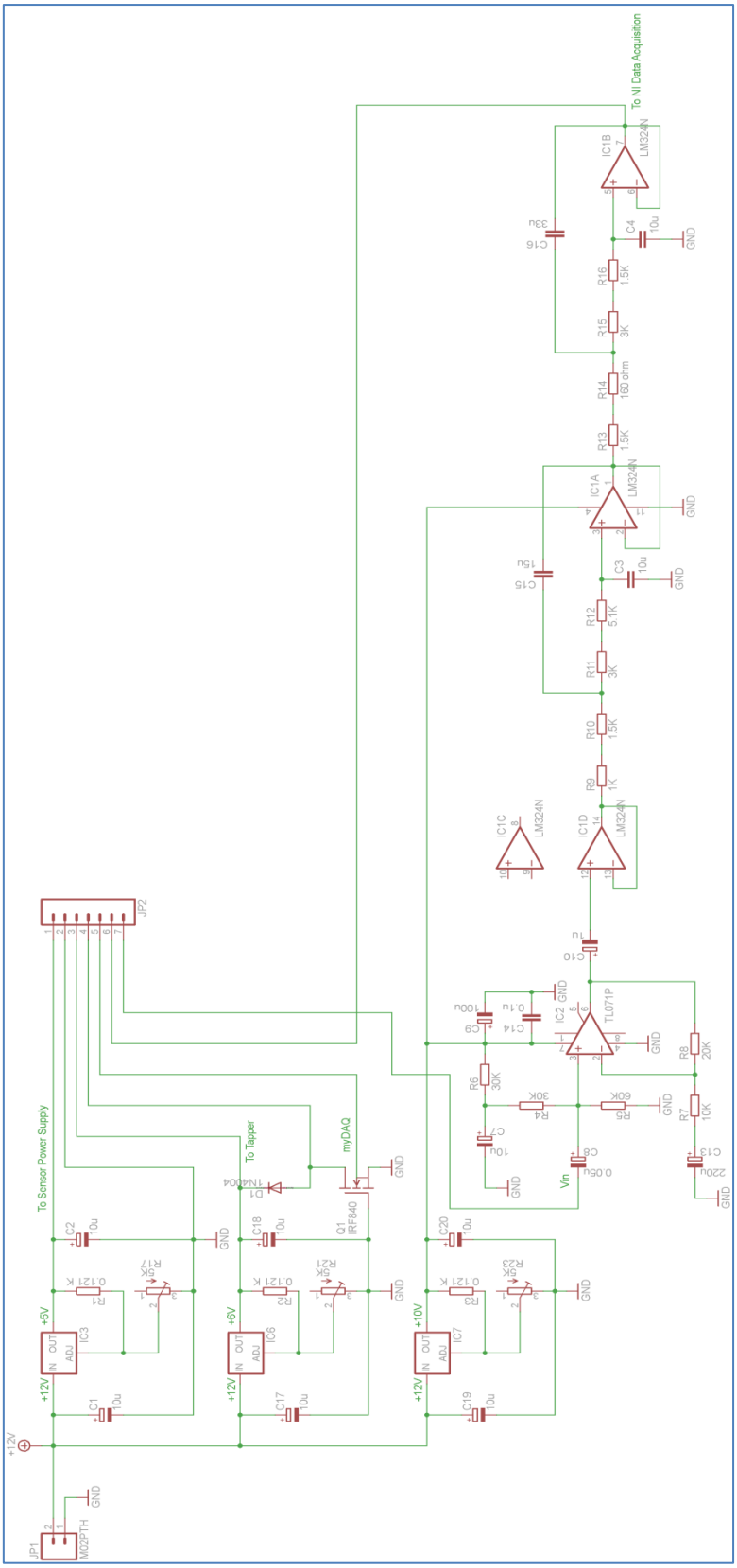

Figure 4.9: Main Circuit Schematics.

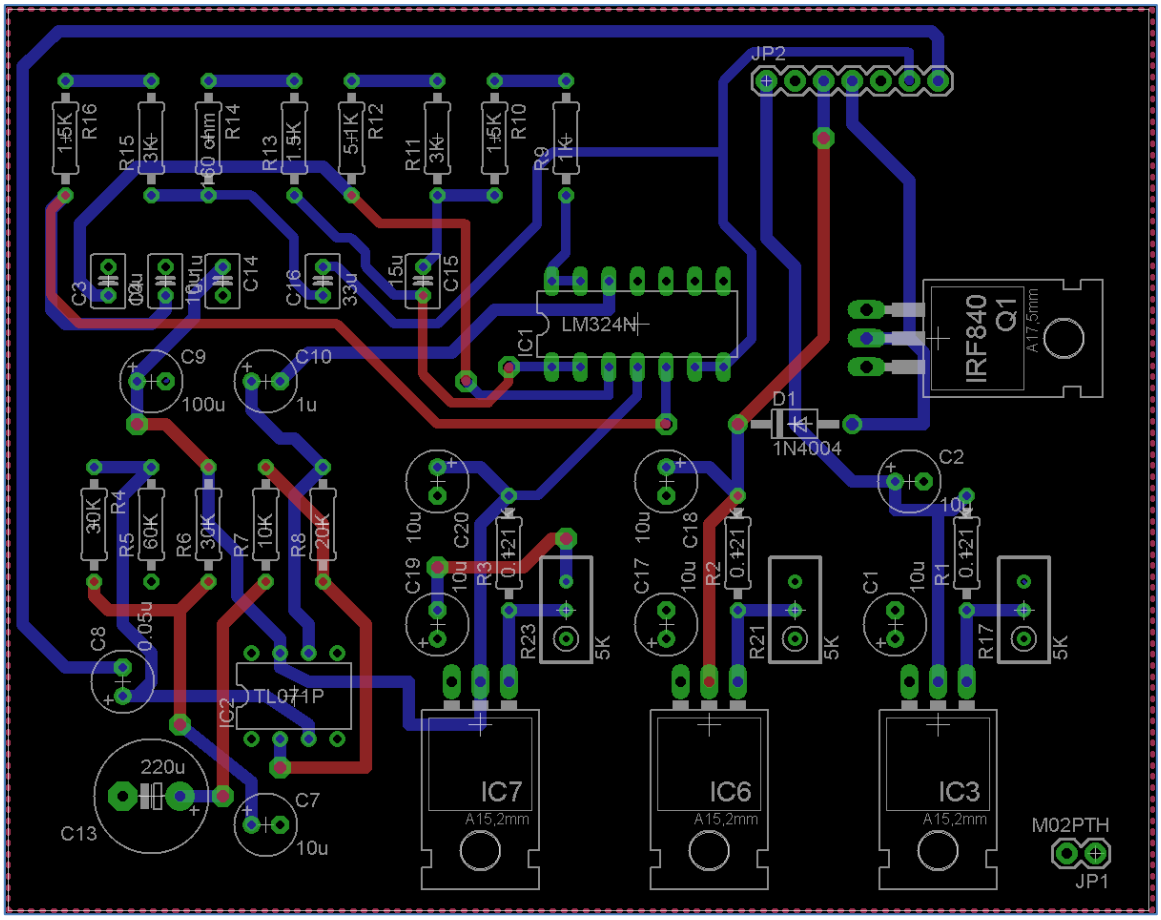

Figure 4.10: Main Circuit Layout for PCB.

Figure 4.11 shows the original photo of the PCB which has all the resistors, capacitors, Integrated Circuits (ICs) soldered for using it throughout the study.

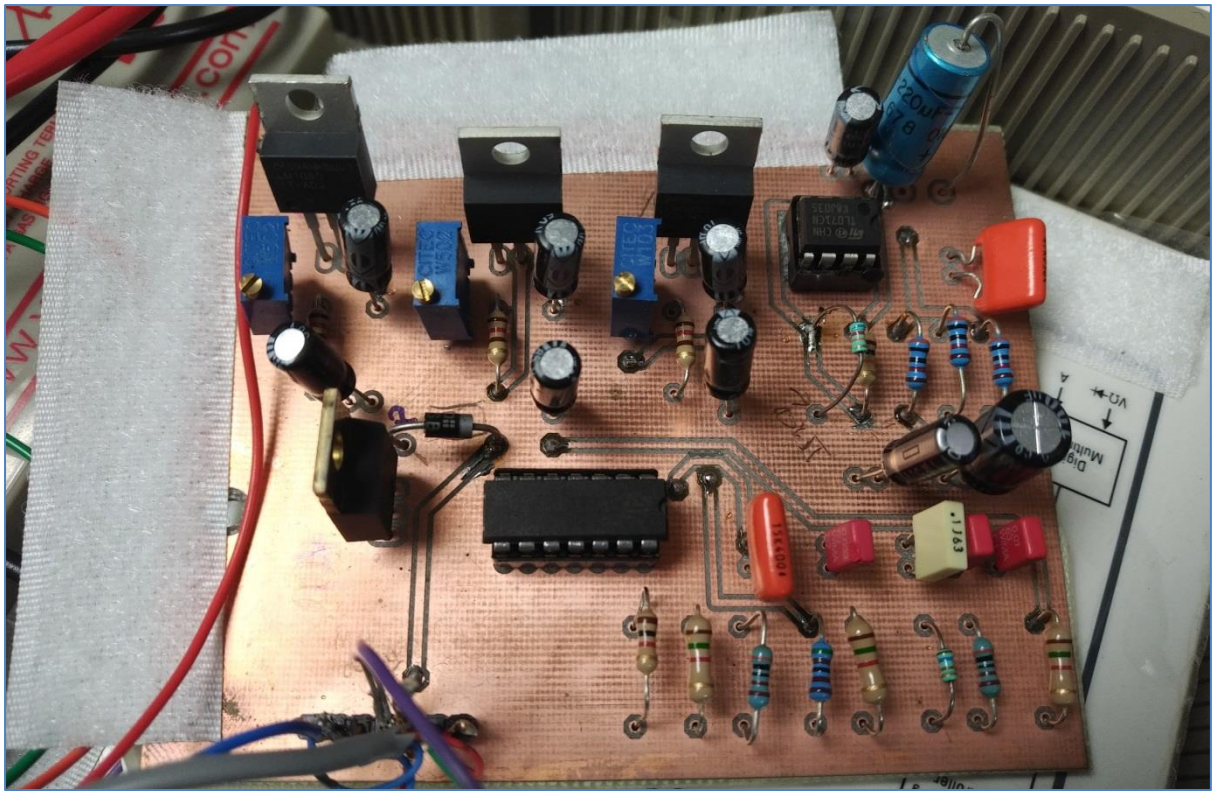

Figure 4.11: Practical photo of the PCB developed for the study.

4.3 LabVIEW and NI myDAQ

4.3.1 Front Panel

The LabVIEW designs displayed in Figures 4.12, 4.13 and 4.14 had been designed by another student in the LabVIEW version 2011 for a previous project in the university. It can be seen in Figure 4.12 that there is a folder option for "saving the sensors data". This option means that the data acquired by the sensor would be saved inside the folder of choice for further use.

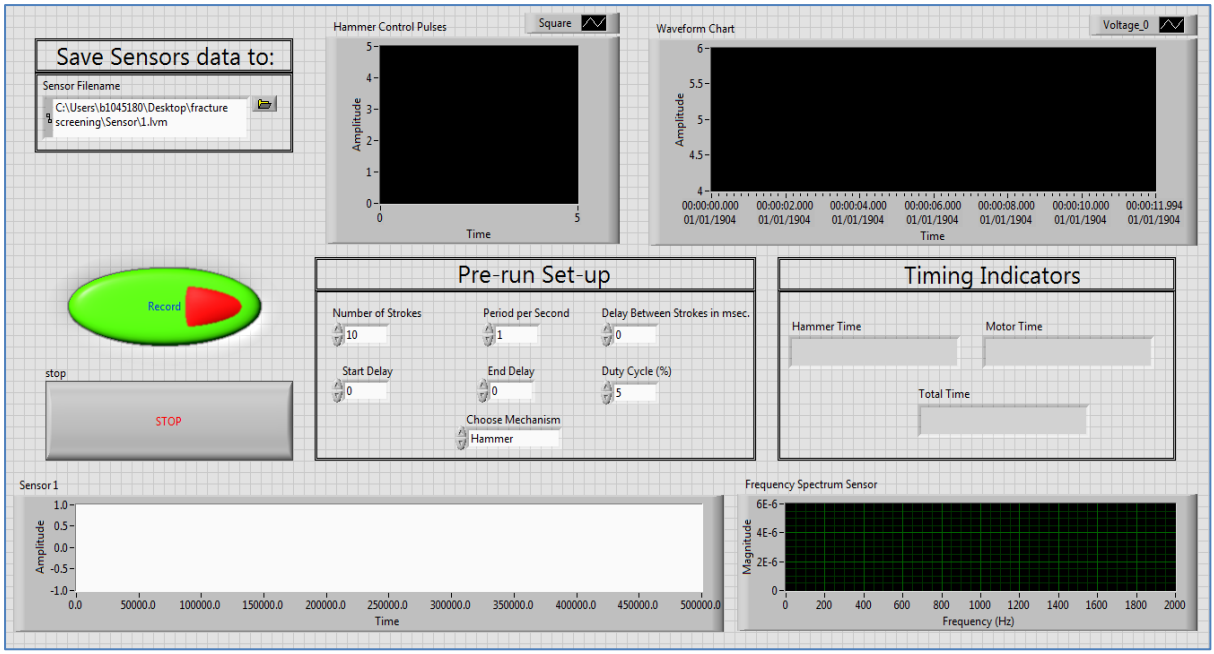

Figure 4.12: The Vibration System Interface (Front Panel).

In the LabVIEW design for this study, three settings were altered.

- The “Duty Cycle” was considered to be 5% (kept as small as possible).
- A delay was preferred, so that after instructing LabVIEW to "run", time is needed to hold the sensor on the target so 5s or 7s was added to the “Delay”. In practice, after pressing “Start”, the vibration mechanism waits for 5s before it starts running.
- “No. of Impacts” was set to 10 so that the vibration mechanism hit the target in front of it, 10 times in 10 seconds. This was determined by experiment in order to balance between sufficient amount of data for analyses and not too much to keep patients comfortable.

The data recording was repeated twice to avoid any error. According to Figure 4.12, the number of hammer impacts, their duty cycle and the delay time between each cycle, can be programmed. Moreover, the interface allows both, the acquired vibration and the hammer control signals to be visualised and their duration time to be displayed. The duty cycle was considered to be no more than 5% to reduce disturbances to the sensor as much as possible and avoid any uneasiness of the participants since the main purpose for carrying out this study at NGH was to check the comfort level.

4.3.2 Data Capture Unit

There were two blocks to be programmed in this project to make them work in parallel:

- The inducer control block diagram.
- The vibration signal acquiring block diagram.

The vibration inducer control unit: This section is responsible for generating a sinusoidal waveform with adjustable periods and duty cycles to control the operation of the vibration inducer. In addition, it is responsible for synchronising the operation of the inducer with the signal acquisition block.

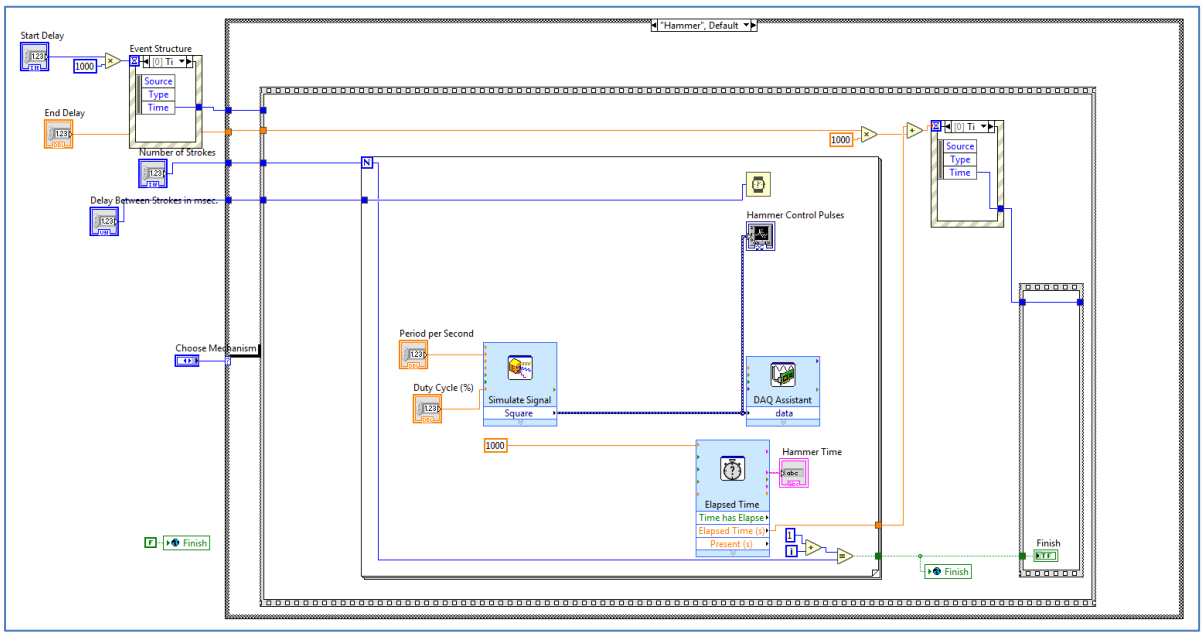

Figure 4.13: Inducer control programming block diagram.

Signal Acquisition: This section is responsible for acquiring the vibration signals from the NI myDAQ board via the myDAQ assistant driver and recording them in a measurement file. This was executed in a “while” loop which acts like a control flow statement that allows code to be executed repeatedly. This loop executes the code block once, before checking if the condition (the hammer impacts) is true or continues. It repeats the loop as long as the condition is true. The waveforms are generated as soon as each impact takes place. The data is passed through a lowpass filter and sampled at a rate of 50,000.

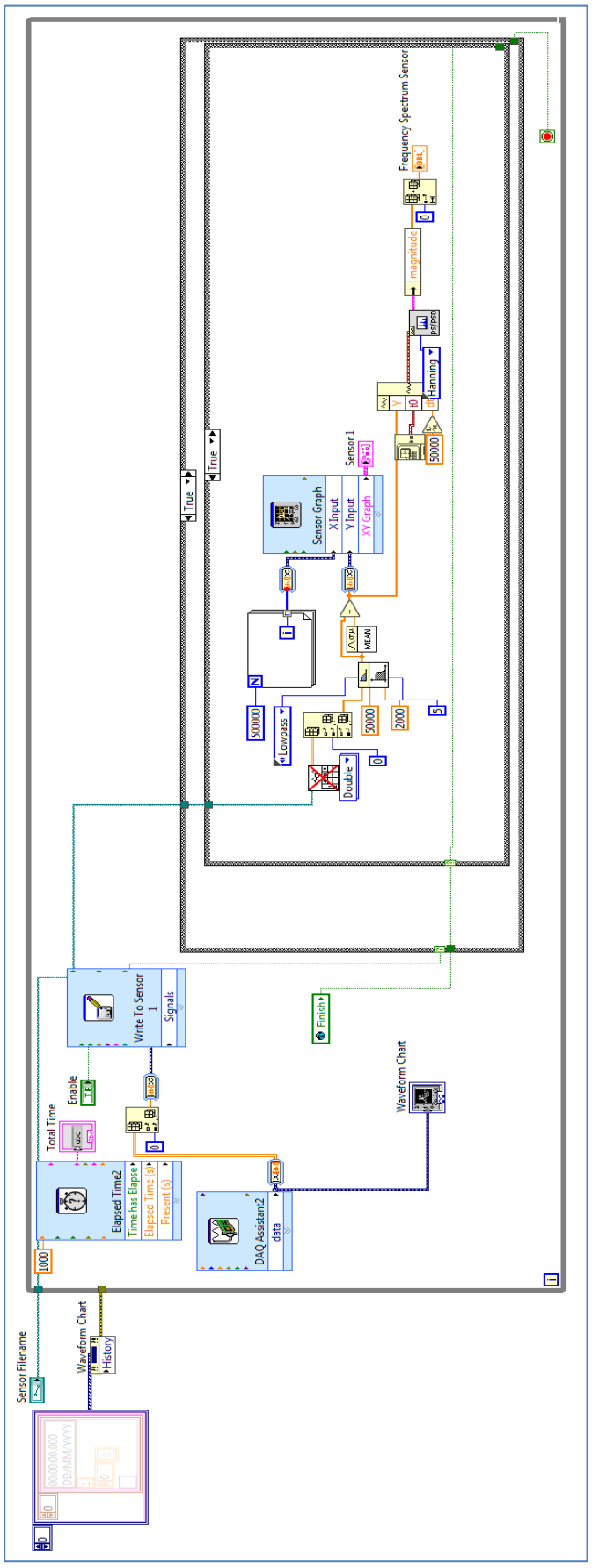

Figure 4.14: Signal acquisition block diagram.

The implemented diagram for acquiring the signals in Figure 4.14 works in parallel with the inducer control block (in Figure 4.13) and it 'stops' either when 10 vibrations had been induced or terminated manually by the user.

4.4 Practical Experiment

This study made the use of the impulse excitation to induce vibration on the subject which was electrically controlled by the mechanisms all discussed in detail in the upcoming sections. The device developed for this study (screening fracture) had been used in three stages:

1. Preliminary study on blocks of wood
    - At the university premises, to observe the patterns on normal and fractured objects and how some properties change with density.
2. On adults
    - At Northern General Hospital (NGH), to verify how comfortable, the procedure will be on both normal and injured wrists.
3. On children, aged from 10 to 15 years old
    - At Sheffield Children's Hospital (SCH), to observe the suitability and accuracy of the procedure for future use on children.
    - At Sheffield Children's Hospital, a pilot study on children's ankles to get references of suitability of methods to be used.
    - At a school in Sheffield, to observe how the pattern of the data acquired from healthy children varies and to compare and distinguish the results with those achieved from SCH.

4.5 Data Collection: First Stage

The experiment was initially performed with five distinct blocks of wood for being acquainted with the set-up as well as to build the expertise to work with humans. Figures 4.4 and 4.5 (*in subsection 4.2.3: Initial Set-up*) show the devices used for this stage of data acquisition.

Owing to health risks associated with animal or human tissues, the preliminary experiments were not carried with raw bones. The wood was chosen because, according to (Mariolani, *et. al.* 2013), it is easily accessible and provides a uniform mechanical property. Both bones and woods are heterogeneous anisotropic materials (Naylor 2014), that is, both having a physical property that has a different magnitude depending on the direction of measurement. Some types of wood share a lot of similarities with bones, like low-weight, flexibility and strength that make them great potential replacements for skeletons (Chant 2012).

Five different samples of wood (shown in Figure 4.15) of approximately 32cm x 2.5cm x 2.5cm were selected. Their densities are listed in Table 4.1.

Table 4.1: Types of Wood with their Dimensions and Densities.

Wood Type	Dimension (cm)	Density (g/cm^3)
Walnut	32.3 x 2.6 x 2.6	0.700
Mahogany	32.1 x 2.6 x 2.4	0.668
Oak	32.2 x 2.5 x 2.5	0.660
Maple	32.3 x 2.5 x 2.5	0.546
Beech	32.3 x 2.5 x 2.5	0.655

Figure 4.15: Five different samples of wood.

Each data recording was repeated five times to avoid any type of error in the data when processing later. These errors may be introduced by any external vibration or the absence of a suitable distance between the target and the hammer.

Each block was attached to a clamp. The distance between the vibration inducer and the wood was 0.5cm. The sensor was attached to the wood so that it was 7cm from the end of the wood. The vibration inducer was set at 1cm (measured by a ruler) from the end of the wood. In this study, the myDAQ instrument was connected to the vibration inducing circuit as well as the computer. Thus, the inducing instrument was controlled by simple instructions like "Start" and "Stop".

All the above steps were repeated twice with different surfaces of the wood samples. These two processes were carried out in order to determine the efficient position of the vibration induction and the sensor location.

Test 1: The inducer was placed at one side of the piece of wood and the sensor was placed on the other side. Figure 4.16 gives a set-up picture for carrying out Test 1.

Figure 4.16: Placement of Tapper at one side and Sensor at the other.

Test 2: The inducer was fixed at the same position as previously described, but the sensor was moved to the top of the wood block to be experimented. The sensor was moved further away from the inducer and then observed how the signal differed in that case. Figure 4.17 gives a set-up picture for carrying out Test 2.

Figure 4.17: Placement of the Tapper and the Sensor for signal detection vertically.

4.5.1 Fractures in the blocks of wood

In order to investigate the effects of a fracture on the vibration responses of the blocks of wood, the blocks of wood were vibration tested prior and after fracture. To fracture a block of wood, it was placed inside an oil-controlled Servo Hydraulic Mechanical Testing Machine. A load was placed on the block and was gradually increased by computer-controlled software till the point where it fractured. Figure 4.18 shows the machinery used for this purpose.

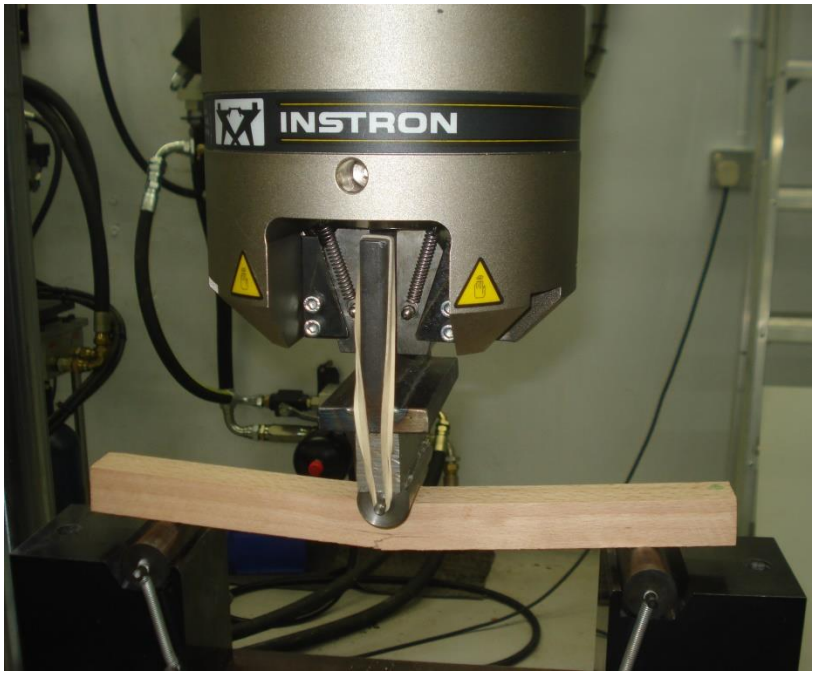

Figure 4.18: Machine giving load to induce cracks in wood.

The speed was 1mm/minute. Load was 100N initially and stroke (distance travelled by piston in each cycle) was 100um.

Figure 4.19 shows how much load at what distance is applied, to produce the fracture in each piece of wood.

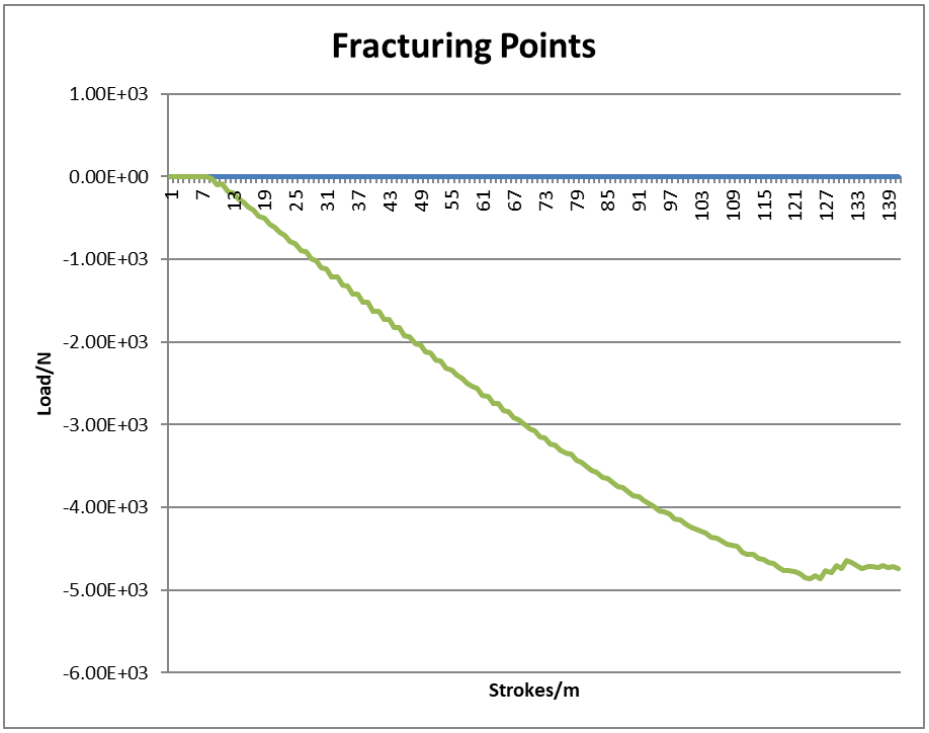

Figure 4.19: Increase of Load to Mahogany wood for fracturing it.

As the force was applied downwards so the load is represented by negative sign in Figure 4.19. The graphs for fracturing all the other kinds of woods are attached in the Appendix A.2.

- The Peak Load which provided the fracture point to Maple wood = 3.084kN.
- The Peak Load which provided the fracture point to Walnut wood = 3.621kN.
- The Peak Load which provided the fracture point to Mahogany wood = 4.877kN.
- The Peak Load which provided the fracture point to Beech wood = 5.739kN.
- The Peak Load which provided the fracture point to Oak wood = 4.787kN.

As the blocks of wood did not have same molecular structure, same density and same mechanical strength, thus they were fractured with a different force. Figure 4.20 shows the fractures in the blocks of wood.

Figure 4.20: Five samples of Fractured Woods.

4.5.2 Processing of the Data from blocks of wood

Initially, magnitude frequency spectra of the vibration responses acquired were calculated. Frequency analysis simplifies the understanding and interpretation of the effects of various time-domain operations, both linear and non-linear. For instance, comparing frequencies eliminated any time related errors. The frequency spectrum is generated via a Fourier transform of the signals.

4.6 Data Acquisition and Processing from Adult Participants

4.6.1 Data Collection from Adults

Following the approval of the Health Research Authority and the National Research Ethics Service, this study was carried out in Northern General Hospital (NGH) Accident and Emergency Department (A&E) on adults, in order to check the pain level caused by vibration induction. Six adult patients (aged between 18 and 70 years) who came to NGH A&E with a wrist injury for assessment participated in this study. The data collected are highly confidential therefore; they have not been shown anywhere in this thesis.

While carrying out the procedure on adult patients, they all sat on a chair. The sensor was put on the skin above either radius or ulna. Vibration was induced via the most prominent bone in their elbow. The data were recorded twice from each hand. They all had X-rays, so a consultant had records of the injury type: fracture or no fracture. The data were processed without the knowledge if the patients had fracture or sprain and at the end of the study, the outcomes produced from cluster analyses derived by means of the signal processing techniques, were matched with the consultant's results to confirm the accuracy of the methods.

The device shown in Figure 4.5 had been clamped to a certain position in experiments with woods, but this could not be the case with patients as they might not be able to keep their hands to a particular position, if they have a major injury. Thus, the device had been removed from the clamp and it was made hand-held. However, the first participant, recruited at NGH, commented that the device looked unattractive and it might drive the children patients away from participating in the study. The device had been taken to the university's Mechanical workshop immediately. It was reshaped so that the resulting instrument has a smaller feature and a steel covering was applied outside the solenoid. The photo of it is shown in Figure 4.21.

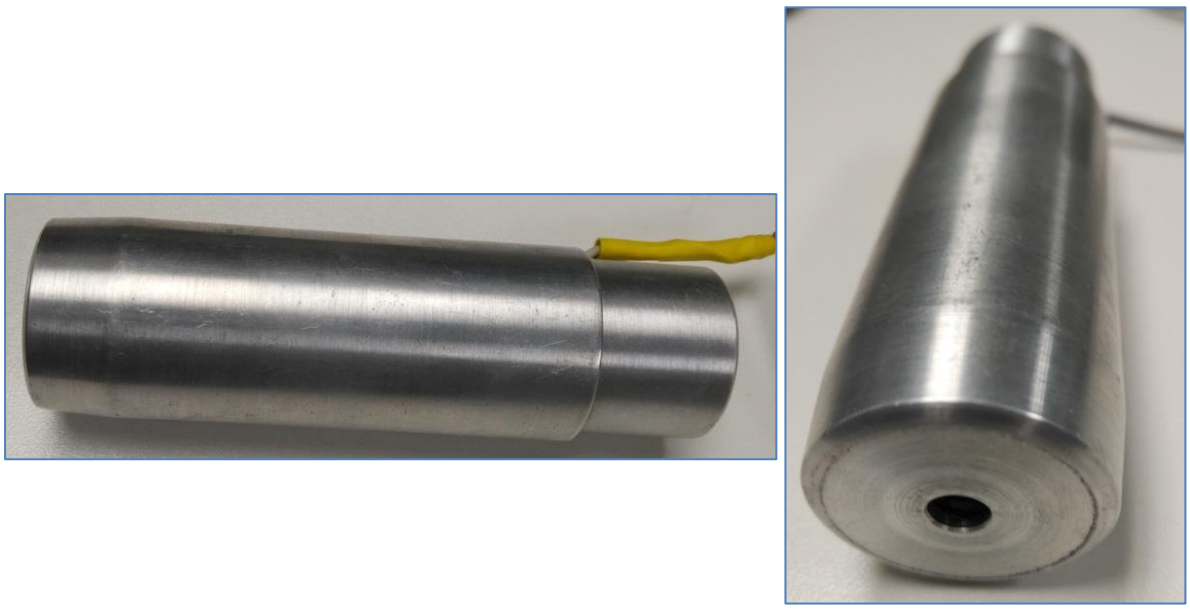

Figure 4.21: Photo of the modified Inducer.

4.6.2 Adults' Data Analyses

Initially the 500,000-data had been acquired and were processed to calculate the Magnitude Spectrum by means of the FFT like that with the blocks of wood. The raw data acquired were all aligned by subtracting the mean values of the total data like shown below. These types of average signal are more aligned for further processing methods.

data = data - mean(data)

The signal produced by the procedure above and data filtered by a lowpass Butterworth filter are shown in Figure 5.7.

Properties of Butterworth filter applied:

- order (maximum delay, used in creating each output) = 5 (a standard value).
- cut-off frequency (a limit in a system's/signal's frequency responses when energy flowing through the system starts to attenuate) = 2000 Hz.
- sampling frequency of the filter = 50,000 samples/s.

The Magnitude Spectra and zoomed magnitude spectra over a smaller range are both shown in Figure 5.8. It can be seen from Figure 5.8 that the Magnitude Spectrum produced against 500 Hz, had higher values and the rest of the values were close to "zero". Thus, only the first 500 points from the Magnitude Spectrum were considered for further processing.

The first 20 data were left out when determining the features in order to avoid the error due to spectral leakage (unwanted frequency components). There were 500,000 data in total, 20 data are actually a very small ratio, equal to 0.004% of the total data.

These features were then compared to determine the "Correlation Coefficients". Correlation coefficients of the magnitude frequency spectra of both left and right wrists were initially calculated then compared. The correlation values were between 0 and +1. The values those were greater than 0.5 corresponded as an indication of a strong positive relation between left and right wrists' frequencies. The values which

were less than 0.5 were considered as weak positive relation between both wrists' frequencies.

The frequencies were classified via k-means (the technique is fully described in *Chapter 3*) as well. This method allocated each patient's frequencies to one class. If one patient had similar frequencies with that of the other patient then the class would be similar.

The results produced by the methods, mentioned above, display a type of distinction of the sets of data but the values produced were much related to each other. Thus, the features were cluster analysed via a clearer distinction process called "Fuzzy C-means (FCM)" (explained in *subsection 3.11.4*) to see if there are patterns between the sets of frequencies which can show that there is a similarity between the data from the uninjured wrists with the injured wrists. The results from the FCM and the radiologist's reports are shown in the *Chapter 5*.

After comparison of the results with those from the radiologist, the results were extracted using one more major signal processing technique called "Wavelet Decomposition (WD)". This was performed to find out the method more efficient to go further. The results produced by both the FFT and the WD were plotted via a "Dendrogram" as well. Finally, the FCM values were tabulated. Figures and Tables are shown in the *Chapter 5*.

This experiment with Adult participants was done solely to find out the comfort level of the procedure but it produced promising results which was encouraging to move forward with the study.

4.6.3 Efficiency of Different Techniques

Wavelet Decomposition (WD) is a well-established technique in the field of Digital Signal Processing. FFT has been applied on the data to classify the signals. However, the efficiency of the methods was tested by applying the WD on the same sets of data.

The application of WD was applied on each of the patient's data in the following method:

- The acquired data were decomposed by level 5 sampling (input shifting, and scaling explained in *subsection 3.11.8*).
- Derivation of the method on the signal was performed by means of a scaling function "Daubechies 5 (db5)" wavelet family.
- The coefficients were extracted.
- Two-degree polynomials were plotted to find the best fitted curve among the number of coefficients derived from the WD shown in the *Chapter 5*.
- The equation for each of the polynomials was finally obtained.

Now these results can be compared with those from FFT.

The frequency spectra produced from the FFT and the constants resulting from the best fitted polynomial curves' equations, were classified using the "dendrogram" (a hierarchical cluster tree diagram) to investigate how similar the groups are. The "dendrogram" was plotted using an association of Euclidean distance between each data set.

As some results were already produced by FCM so they were presented to the radiologist so these were compared with the radiographs' result. Hence, it was already known which data should be going to which branch of the dendrogram. The diagrams produced by both the FFT and the Wavelet Decomposition were similar shown in *Chapter 5*.

However, the probability of the results (from FFT and WD) of falling into separate or appropriate groups was not known. This was done by means of FCM to find out the membership ratios for each data set to belong to a particular cluster, both being tabulated in *Chapter 5*. The techniques were compared from the Tables 5.4 and 5.5.

4.7 Main Set-up

Figures in 4.22 and 4.23 display the box with its lid opened as well as closed, containing the PCB, the vibration inducer and the myDAQ Acquisition Instrument.

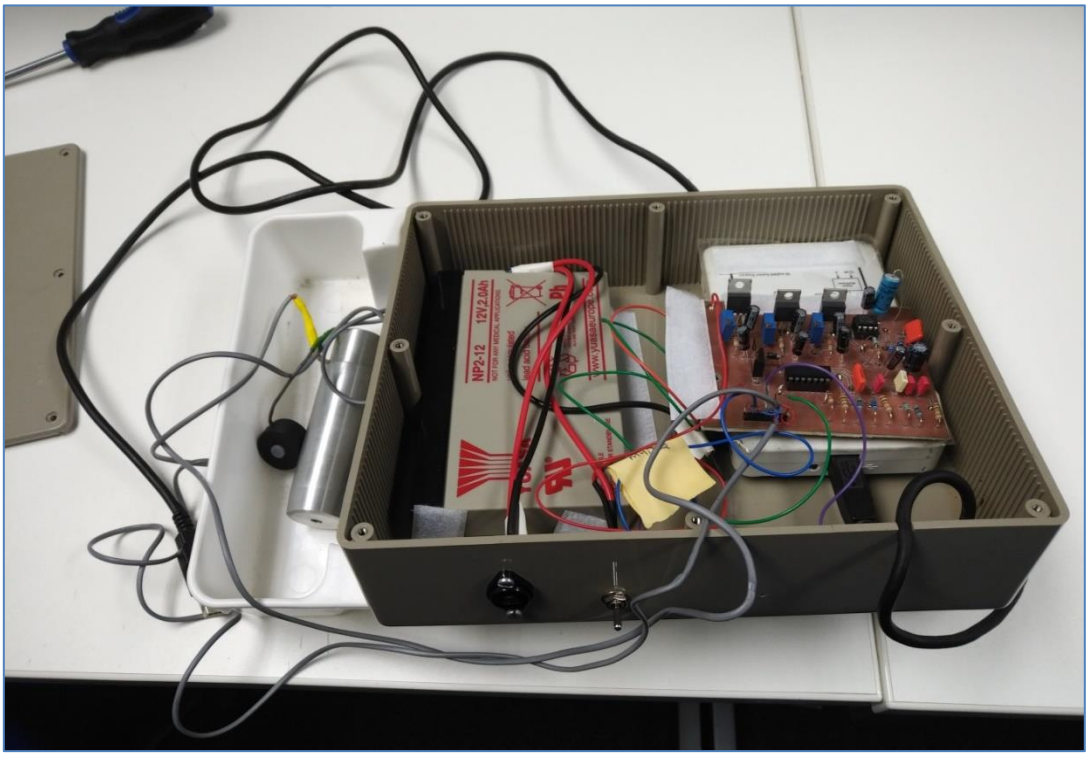

Figure 4.22: Box with lid opened.

Figure 4.23: Box with lid closed.

4.8 Data Acquisition and Processing: Wrist Injury

The adults, who participated in the study at NGH, filled up a questionnaire at the end after recording vibration responses saying that the vibration induction procedure was not painful and can be carried on a 5-year-old child. The Ethics Board approved this study to be carried out on 50 children's wrists and 50 children's ankles and it was made mandatory that all the children participating in the study must be between 10 and 15 years old.

The patient(s) came to the ED of SCH with a wrist injury. If they were advised to have an X-ray, they qualified for participating in this study. They were given the Information Sheets, Consent Forms and Assent Forms to ensure they know about the study and they are ready to participate in the study.

With the wrists, the recording procedure was quite the same as that at NGH. The participants sat on a chair, placed their hands on the same bed that the devices were kept on. The data were recorded from either ulna or radius, placing the sensor on the wrists.

4.9 Data Collection and Processing: Ankle Injury

The procedure was slightly different, in the case of ankle injury. The patients following an ankle trauma attended Emergency Department, all required ankle radiographs as part of routine clinical care and they were all between the age of 10 and 15 years old. They all participated voluntarily, following full informed assent/consent. Parental consent was also obtained. Each child was asked to sit on a chair with their feet on the ground. Two children could not put their feet on the ground because of their level of ankle pain. Their injured legs were kept free in the air.

Vibration was induced via the hand-held device at a point approximately 5 cm above the ankle which created 10 impacts over 10s. The sensor was held on the skin above the tibia (ankle bone on the medial (inside) aspect of the ankle) and was used to capture the data.

4.10 Modifications of the Device

The mechanism was not completely error-free, so some modifications were done to the device at different stages of the study to fix problems faced while recording and various parts have been altered, as listed below.

- *Alteration made to the device after the 2nd patients' data capture.*
  The parts of the inducer could be moved up and down to make its vibration inducer head come out, as shown in Figure 4.21. But a rubber was put beneath to make it tighter than before. The rubber could be removed to make it loose, if necessary.
- *Alteration made after the 10th patients' vibration responses were acquired*.
  The wire coming out of the box that connects with the solenoid was too long. It altered the capturing of the data, when it was touched with a slight force while holding the inducer. A tiny slit was made through the outer covering to make the wire go via the slit, the wire was shortened and wrapped as much as possible with an insulated tape.
- *Alteration made after the 1st ankle data acquired*.
  The wire should be fixed to the wall of the outer covering of the inducer and should not interrupt the solenoid at any point, when it is running. But the wire was getting caught. Therefore, the wire had been glued to the wall to keep it fixed and not be able to move when the device was running.

4.11 Conclusion of Chapter 4

This chapter is a broad discussion on all the experimental set-up details starting from the required hardware and software. The device has been modified at several steps while performing the study. Additionally, some programs that were involved to run the vibration inducer have been modified to make it perform better for further study. These have all been discussed in detail in this Chapter 4 with the reasons behind them.

Chapter 5: Relations and Variations between Fracture and Sprain

5.1 Preliminary Results from blocks of wood

Several types of analyses were performed with the data acquired from the vibration induction to the blocks of wood to observe:

- Surface Distinctions,
- Frequencies at different densities,
- Find out the relations between densities and frequencies.

5.1.1 Surface Distinctions

The results found from testing the mahogany wood are reported first. The data recorded have been processed to produce two kinds of graphs shown in Figures 5.1 and 5.2.

- The first graphical representation gives the amplitude of the data recorded in terms of voltage versus the time taken to record.
- The second subplot shows the magnitude frequency spectrum of the signals presented in the first subplot when processed by the fast Fourier transform (FFT) discussed in *3.11.1*.
- Figures 5.1 and 5.2 are the vibration responses and its associated frequency spectrum processed from the data collected during the Tests 1 and 2 mentioned in *4.5*.

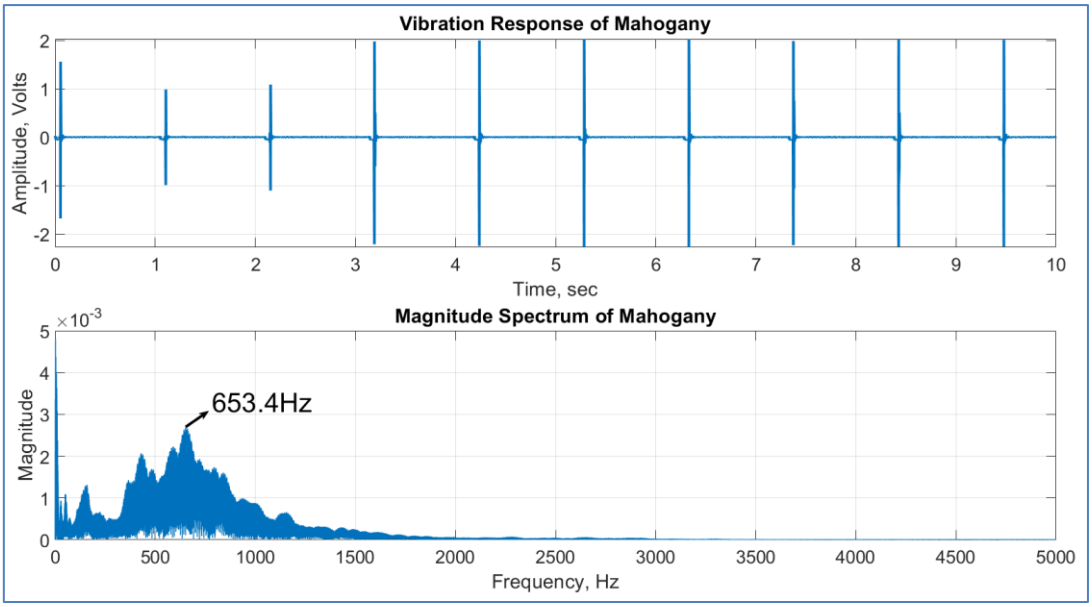

Figure 5.1: Two graphical plots in Surface 1. a) Amplitude vs Time b) Frequency Spectrum with Peak Frequency = 653.4Hz.

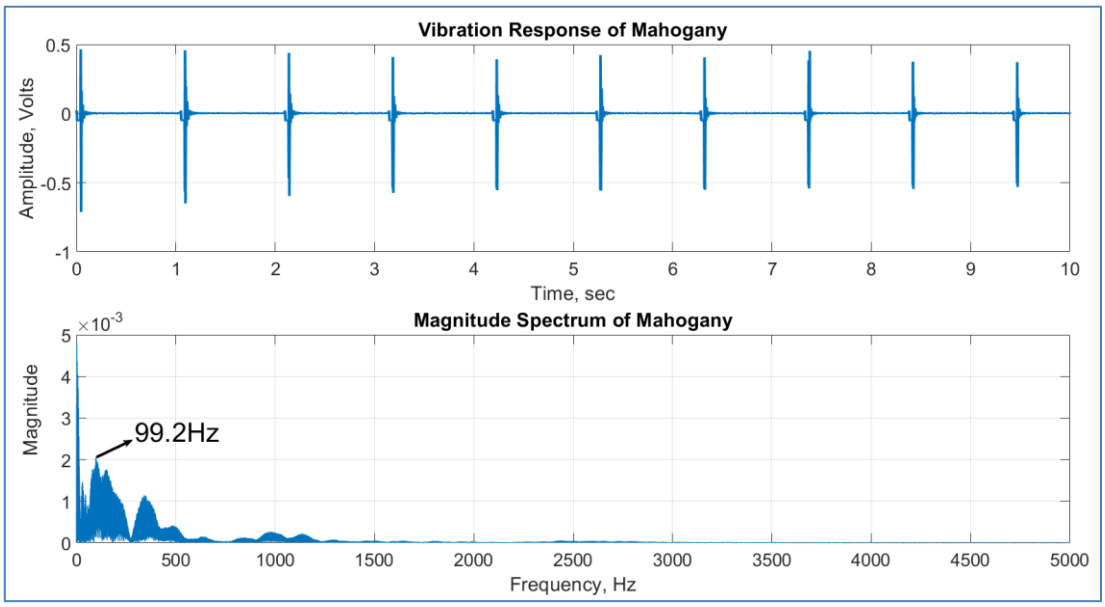

Figure 5.2 Two graphical plots in Surface 2. a) Amplitude vs Time b) Frequency Spectrum with Peak Frequency = 99.2Hz.

It is indicated in Figures 5.1 and 5.2 that the frequency *falls significantly* (from 653.4Hz to 99.2Hz) due to the change in the placement of the sensor between the surfaces where vibration had been induced demonstrated in Figures 4.16 and 4.17.

5.1.2 Frequencies and Densities

As demonstrated in the *subsection 4.5.1*, the data were acquired from 5 different samples of wood. The graphical representations have been produced for all the five different blocks and the peak frequencies were all noted. The frequency spectrum as shown in Figures 5.1 and 5.2 along with each sample's density were listed in Table 5.1 to establish a relation between the density and frequencies.

Table 5.1: Changes in Peak Frequencies with Densities.

Wood Types	Densities(g/cm^3)	Peak Frequency(Hz)
Walnut	0.700	726.7
Mahogany	0.670	653.4
Oak	0.660	497.6
Beech	0.655	490.1
Maple	0.546	466.9

A bar representation has also been plotted to observe the relations between density of the wood and the recorded peak frequency and the relation can be seen in Table 5.1 that samples of wood with higher densities and higher frequencies.

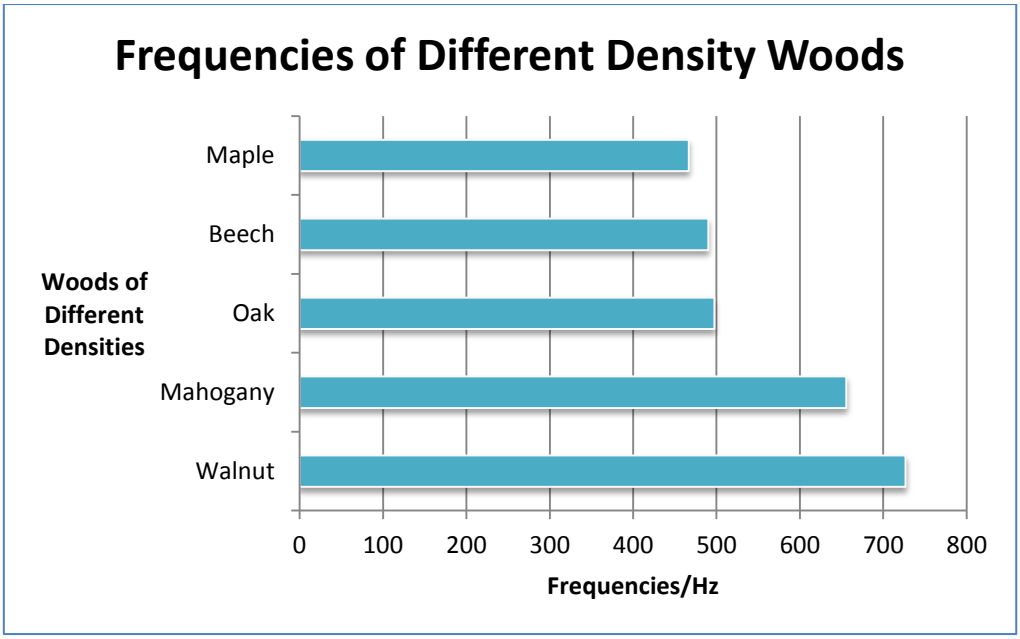

Figure 5.3: Representations of woods with different densities and different frequencies.

5.1.3 Frequencies of Fractured blocks of wood

As the blocks of wood did not have:

- same molecular structure,
- same density,
- same mechanical strength and
- above all, cut along the same grain.

thus, they have been fractured with a different force. Figure 5.4 shows the fractures induced in the blocks of wood.

Figure 5.4: Five samples of fractured blocks of wood.

The data collected from the fractured blocks of wood had been processed and the peak frequencies for each of them had been noted to differentiate between the fractured and non-fractured blocks of wood. Figure 5.5 shows the vibration response and its associated frequency spectrum of mahogany after fracturing process.

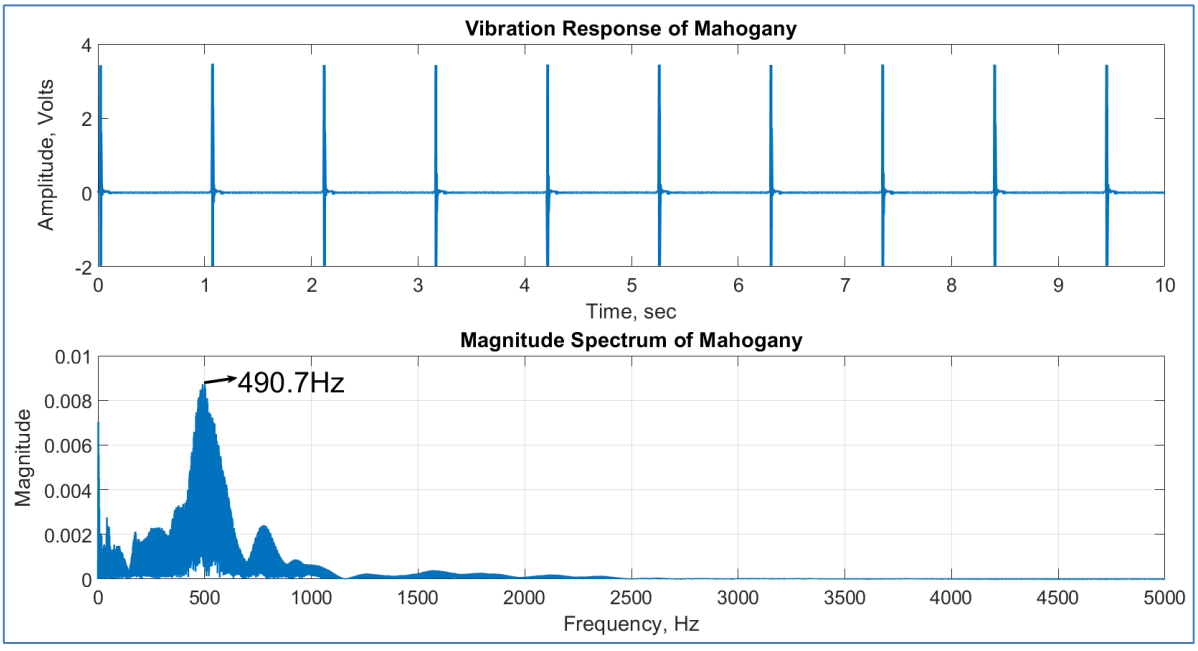

Figure 5.5: Graphical Representation of Fractured Mahogany block.

Table 5.2: Peak Frequencies and Densities.

Wood Types	Densities(g/cm^3)	Peak Frequency (Hz) before fracture	Peak Frequency (Hz) after fracture
Walnut	0.700	726.7	640.1
Mahogany	0.670	655.6	501.2
Oak	0.660	497.6	435.2
Beech	0.655	490.1	410.0
Maple	0.546	466.9	451.2

The variations from intact to fractured blocks of wood depending on the densities have been determined according to the Bar plots (in Figure 5.6) shown below.

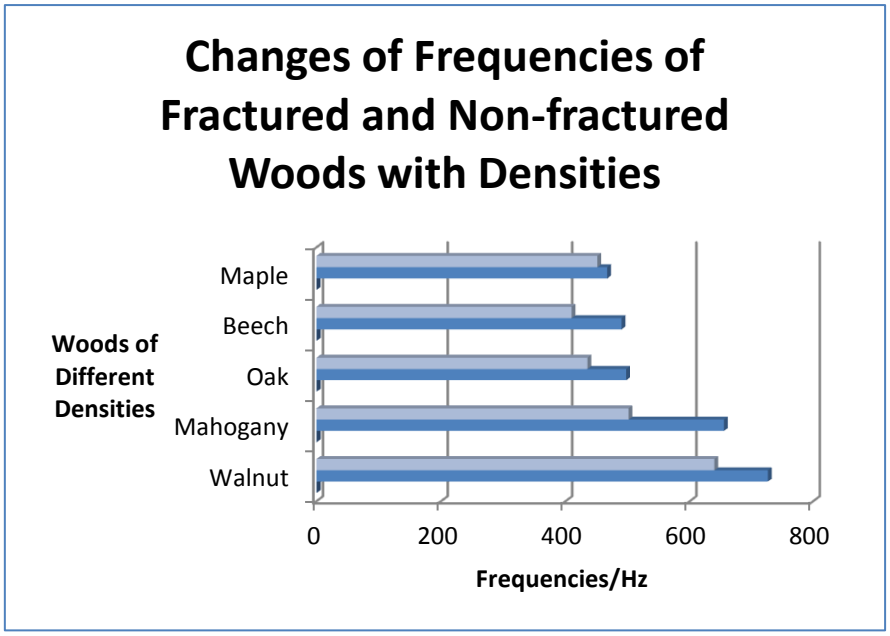

Figure 5.6: Representation of woods with different Densities having different Frequencies in Fractured (light blue) and Non-fractured (dark blue) states.

Figure 5.6 evidently established the woods with higher densities have higher frequencies. After fracture had been induced, the frequencies *decrease* noticeably.

5.2 Results and Discussions on Data from Adults

5.2.1 Frequency Spectra from FFT

The Magnitude Spectra produced by means of Fast Fourier Transform (FFT) along with the initial data and the data that underwent lowpass Butterworth filtering process. If the vibration responses are zoomed, they appear noisy, so Butterworth filters are added in an attempt to filter the unwanted noise which is in the nature of high frequency signals.

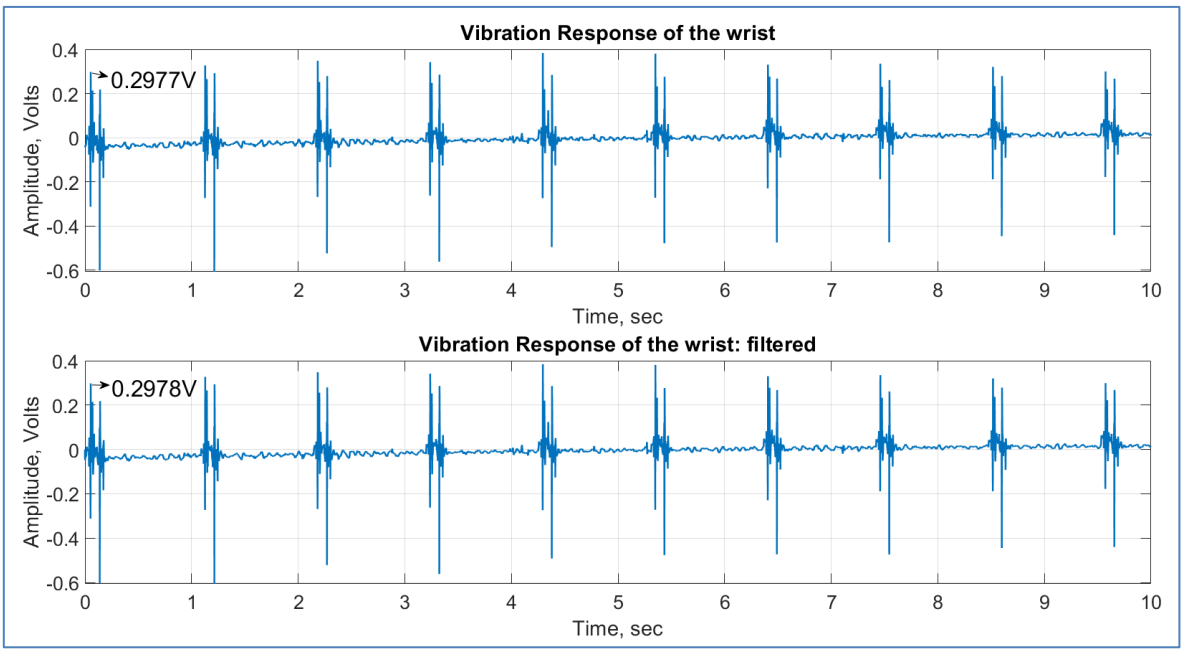

Figure 5.7: Vibration Responses unfiltered and filtered.

The peak amplitude of the Vibration Response from the initial data (unfiltered) = 0.2977 V.

The peak amplitude of the Vibration Response from the filtered data = 0.2978 V.

The amplitudes appear to be very similar with minor changes. However, as there were changes noticed and also because the filter is well-known for its applications, so the resulting data produced by the filter has been used for further analyses.

Figure 5.8 illustrates the Frequency Spectra of the signals in Figure 5.7.

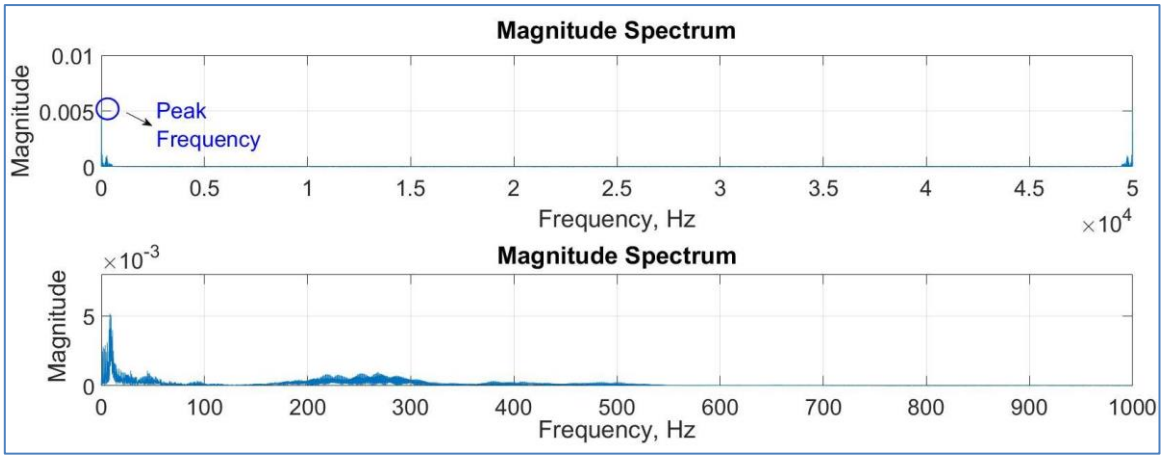

Figure 5.8: (a) Original Magnitude Spectra and (b) Magnitude Spectra over a specified x-axis range.

In Figure 5.8, it is seen that the first plot appears very unclear and Peak Frequency (has been indicated) is small which cannot be used to comprehend and apply further analysis thus; the Spectra have been drawn over a shorter range of x-axis.

5.2.2 K-means, FCM and Radiographs

As mentioned in *subsections 3.11.4 and 3.11.5*, that Fuzzy C-means separate data into classes assigning membership ratios and k-means classify the data according to the neighbourhood similarity among them. These two methods were selected for determining the results.

Table 5.3: Classified Results and X-ray diagnosis of Adult Participants.

Participants Recorded at Hospital					
Subject	Age (years)	Correlation between Left and Right Wrist's Frequency	k-means classification of the Injured wrists only	FCM values of the Injured wrists' likelihood of being fractured	X-ray diagnosis
1	58	0.5037	1	0.2367	Not Fractured
2	26	0.6328	1	0.0562	Not Fractured
3	69	0.2907	2	0.9941	Fractured
4	55	0.3702	2	0.9554	Fractured
5	41	0.5489	1	0.0380	Not Fractured
6	59	0.3439	2	0.9686	Fractured

Table 5.3 states:

- The results from the left and right wrists are more similar for patients 1, 2 and 5 as their correlation values are higher.
- Patients 1, 2 and 5 are in class number 1 and the rest of the patients are in class number 2, according to the k-means values.
- Patients 3, 4 and 6 have more than 90% chances to be in the same group (according to k-means, the class is number 2).

As the radiographs showed that patients 3, 4 and 6 were fractured and the above results showed that patients 3, 4 and 6 were in same clusters, therefore, it was concluded that class 1 was for sprained wrists and class 2 was for fractured wrists and strong membership values were produced by FCM.

5.2.3 FFT or WD: Better Technique?

Figure 5.9 shows the results generated by Wavelet Decomposition (WD) with the Best fitted curve among the coefficients extracted.

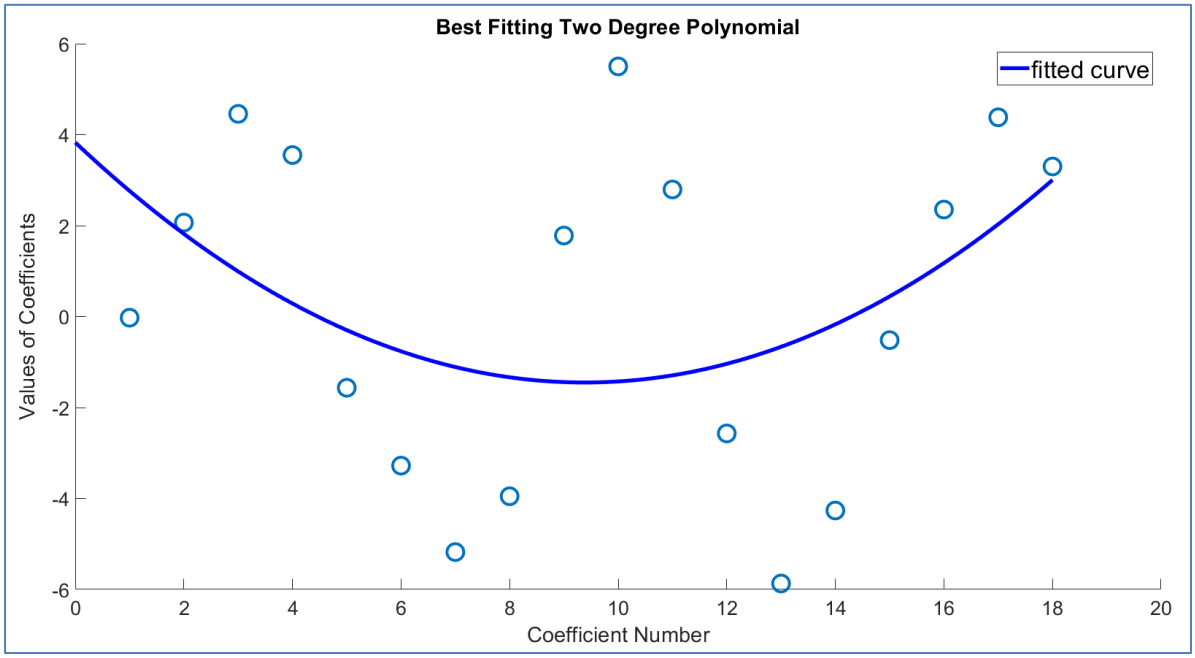

Figure 5.9: Best Fitted Two Degree Polynomial.

The outcomes of FFT and WD are separately drawn by Dendrograms illustrated in Figures 5.10 and 5.11. The Dendrograms reflect some properties of clusters.

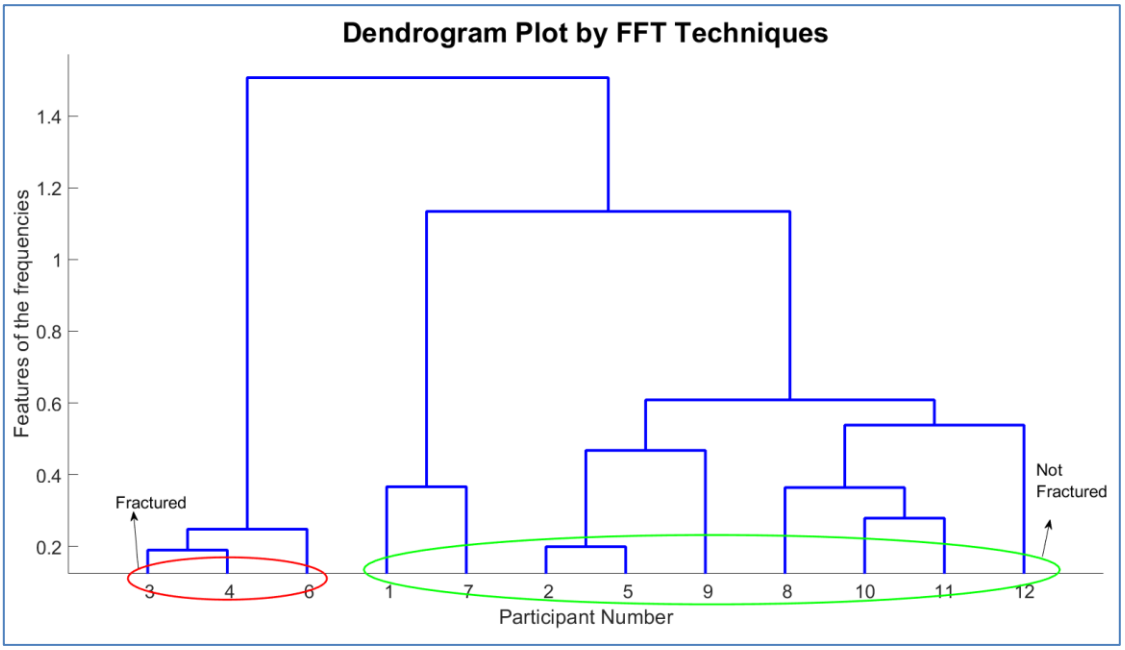

Figure 5.10: Dendrogram Plot produced by Fast Fourier Transformation results.

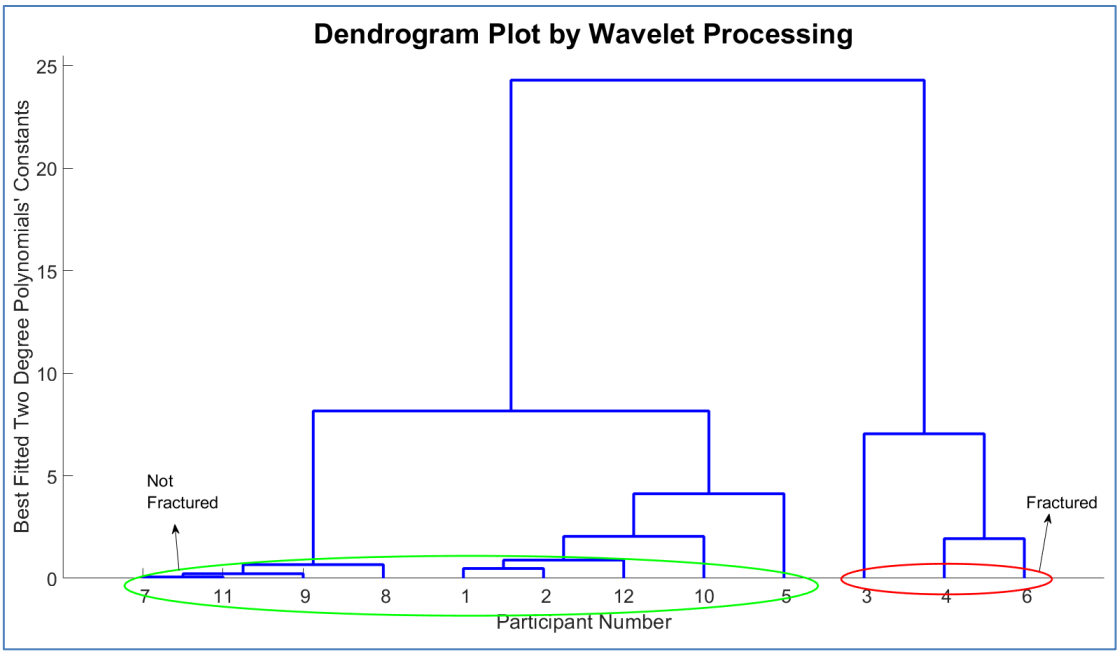

Figure 5.11: Dendrogram Plot produced by Wavelet Transformation results.

The dendrogram plots show that the fractured wrists are in a separate branch than the sprained and normal wrists' branches.

It was supposed that the uninjured wrist's data will be matching to the no-fractured data. However, when higher degree polynomials were calculated, the dendrogram plot could not properly separate the uninjured wrist's data from the fractured group.

The results of Fuzzy C-means produced from both FFT and WD are tabulated.

Table 5.4: FCM analysed results of the FFT features.

Subject	Type	Gender	Probability of having fracture	X-ray results
1	Injured	Female	0.3397	No Fracture
2	Injured	Male	0.3227	No Fracture
3	Injured	Female	*0.9836*	Fracture
4	Injured	Male	*0.9624*	Fracture
5	Injured	Female	0.2429	No Fracture
6	Injured	Female	*0.9275*	Fracture
1	Normal/Uninjured		0.2758	
2	Normal/Uninjured		0.0733	
3	Normal/Uninjured		0.3699	
4	Normal/Uninjured		0.0520	
5	Normal/Uninjured		0.1240	
6	Normal/Uninjured		0.1854	

Table 5.5: FCM results from the constants of the best fitted curve among the WD coefficients.

Subject	Type	Gender	Probability of having fracture	X-ray results
1	Injured	Female	0.0488	No Fracture
2	Injured	Male	0.0068	No Fracture
3	Injured	Female	*0.9820*	Fracture
4	Injured	Male	*0.6210*	Fracture
5	Injured	Female	0.0424	No Fracture
6	Injured	Female	*0.9970*	Fracture
1	Normal/Uninjured		0.0077	
2	Normal/Uninjured		0.0011	
3	Normal/Uninjured		0.0086	
4	Normal/Uninjured		0.2311	
5	Normal/Uninjured		0.0189	
6	Normal/Uninjured		0.0177	

The outcomes generated by WD were very similar to FFT, when using both the dendrogram and Fuzzy C-means. However, there are some disadvantages and unreliable results of using the WD technique listed below.

- WD provides both Frequency and Time related information which makes it difficult to use. The design that induced 10 vibrations must generate the vibration responses similar to each other over the 10s to ensure that results can be processed by WD, that is, each response must have similar time range of its time-dependency.
- In order to make sure that the above reason does not affect the accuracy of the data acquired, the first and last few sets of data are left out when doing the necessary analyses which is similar to some extent, to the leaving the data in the case of FFT. But in WD, approximately 10,000 data were left then FCM produced the desired classification (the clusters were known in this case).
- Additionally, there are substantial numbers of steps before reaching the concluding stage of Fuzzy C-means cluster.

On the other hand, the frequencies produced by the FFT can easily be fed into the Fuzzy C-means code (FCM) already built, to produce membership values. In other words, fewer steps were involved in the case of FFT codes.

5.3 Conclusion of Chapter 5

This chapter is an elaborated description to classify the signals received from intact and fractured samples of wood and adult injured wrist bones. There is an indication from the samples of wood that the signals are dampened faster, if the density is higher. Additionally, the frequencies are lower in the fractured samples than that in the intact ones. From analyses performed on data collected from injured adult wrists, the Fuzzy C-means is an acceptable technique to divide the signals according to the fractured and non-fractured group.

Chapter 6: Data from Children's Wrists

6.1 Introduction

Results of the adult study suggested that vibration analysis using this device, may be used for further processes. Moreover, the adult patients gave positive feedback on the lack of discomfort of vibration on both injured and uninjured wrists. On this basis, the NHS Health Research Authority (Yorkshire & The Humber - South Yorkshire Research Ethics Committee) permitted this study to go ahead with children aged between 10 and 15 years old, following full informed consent from the parent/carer and assent from their parents/legal guardians. An information sheet was provided to the parent(s)/guardian(s). Appropriate age information sheets were provided to children as follows:

- children between 10 and 12 years old,
- children between 13 and 15 years old.

This ensured full understanding of the study by children and parents/guardians prior to recruitment.

The study moved on to children from adults and been conducted at Sheffield Children's Hospital (SCH) between November 2016 and May 2017. This chapter is an in-depth description of data acquisition from children's wrists. The modification of LabVIEW program has been detailed. The techniques to separate the data into classes were amended several times to determine the most precise and efficient methods and these have also been explained.

6.2 Improvements of the Programs

The program windows (Front Panel and Block Diagram) displayed in Figures 4.12 to 4.14 was giving an error with its waveform chart. When the study was carried out at NGH, sometimes, the computer had to be restarted to make the LabVIEW design run properly. The error was due to the software version. The program was developed in LabVIEW version 2013. However, the version of LabVIEW in the laptop which was taken to hospital was 2014 so there was a complete mismatch. Thus, an entirely new program has been designed in the LabVIEW keeping the parameters almost

identical but altering the duty cycle between 7% and 10%, in addition to the alterations of the sample rate of 60,000 so the total data acquired were 600,000 in duration of 10s. The new designs are shown in Figures 6.1 and 6.2.

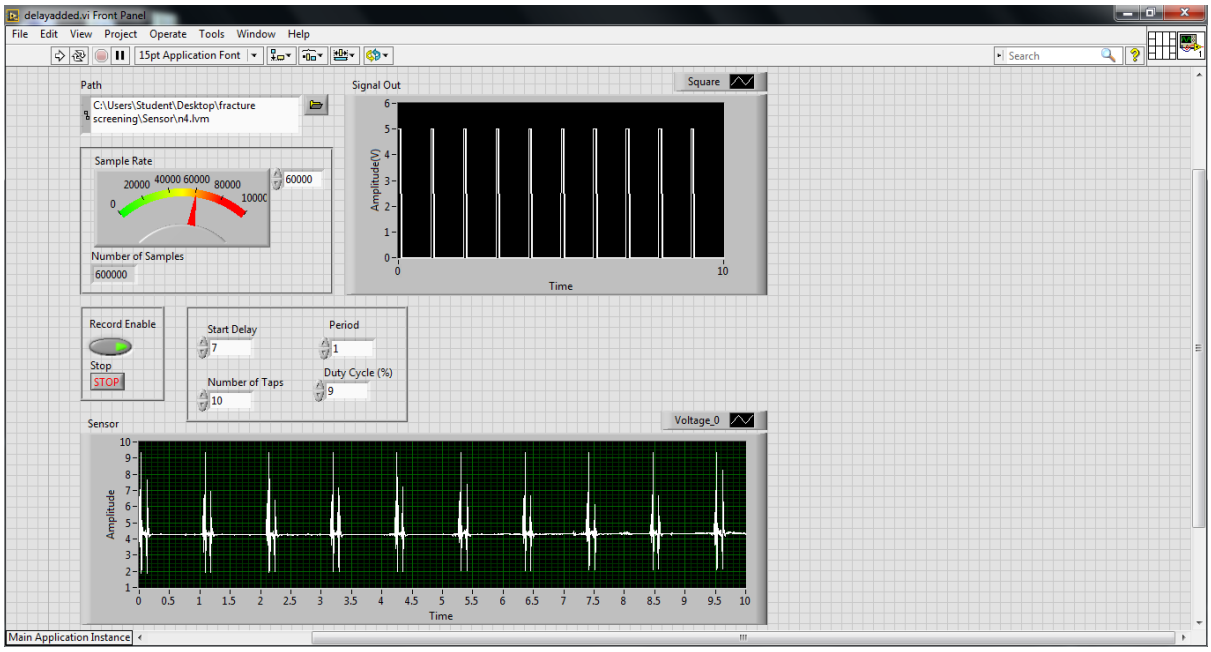

Figure 6.1: New LabVIEW Design - Front Panel.

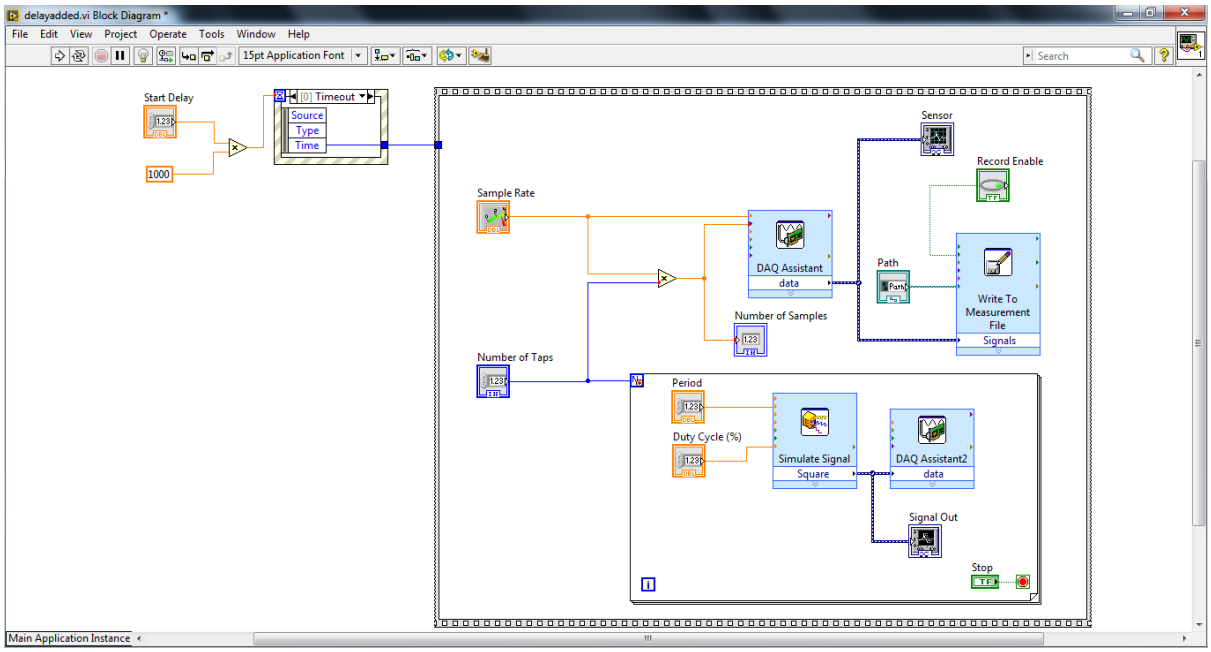

Figure 6.2: New LabVIEW Design - Block Diagram.

All the parameters like the inducer running time and number of vibrations to be induced were kept the same except that of the sampling rate. It was increased from 50,000 to 60,000 samples/second.

Figure 6.3 shows how the entire device looked like for the controlling of the vibration inducer and also, for recording and storing the vibration responses.

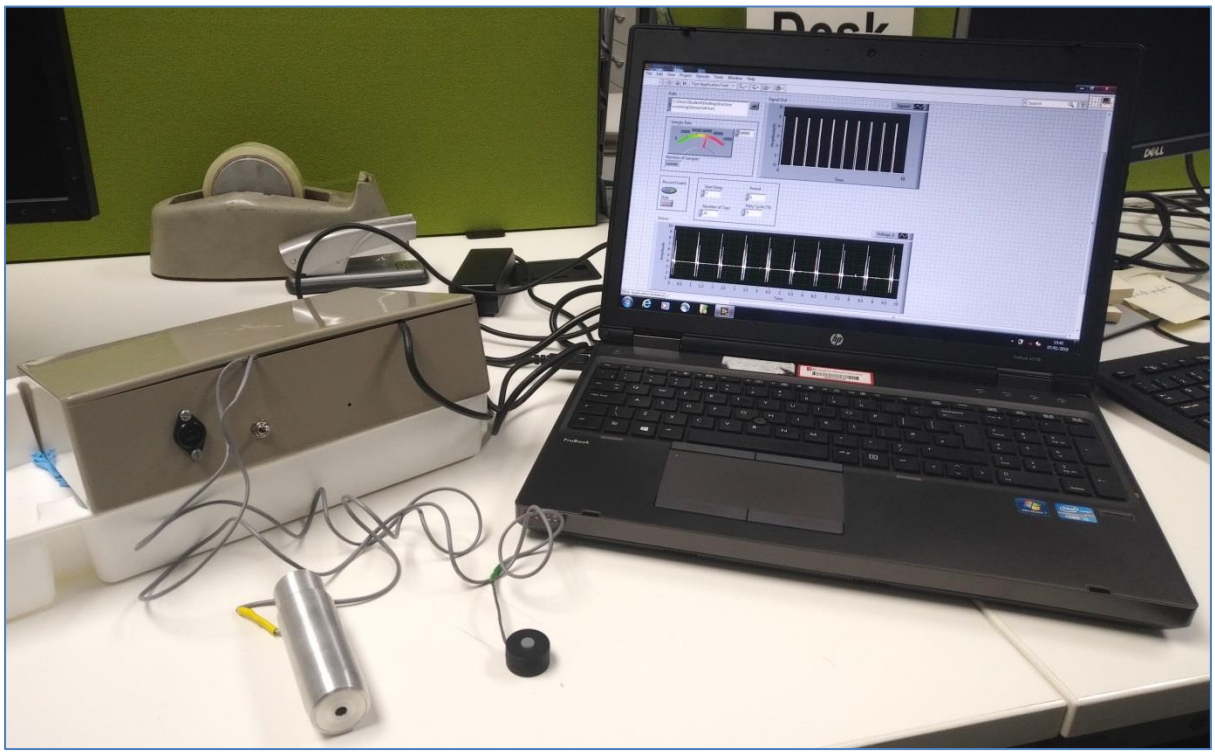

Figure 6.3: Entire Modified Set-up.

6.3 Data Recording

The device was checked by the technicians of Sheffield Children's Hospital to make sure the wires are not dangling outside of the box, in other words, there is no chance that children are in direct contact with power supply.

The acquisition procedure was the same as with adult patients. The children who attended the Emergency Department at Sheffield Children's Hospital checked in with the Triage nurses who would call the researcher. The researcher would briefly describe the study to the parents and if they agreed for their child to participate in the study, the researcher would present the relevant forms to sign and make copies. 1 out of 10 parent(s) would agree for their children to participate in the research to

have a non-invasive technique developed soon. Following the administrative and consent processes, vibration analysis was performed in the time interval between the patient being seen by the ED doctor and having their radiograph(s) performed.

The children would sit on a chair while recording, placing both of their hands on a bed where the entire device had been set-up. The sensor was placed on each wrist. Initially, it was proposed to record once from “ulna” and once from “radius”. The sensor was placed on “ulna” of both hands while recording because of two reasons:

- The first patient complained about causing pain when sensor was placed on “radius”.
- It is a known fact among the clinicians that the “radius” is more likely to be injured in most of the cases of wrist injuries.

The vibration was induced via the most prominent bone of the elbow. The inducer was held not very tightly otherwise, it will not be able to move to and fro. The device would be commanded to be run after 7s after pressing an instruction key on the LabVIEW screen. Figure 6.4 shows the "arrow" that is required to be clicked in the LabVIEW to run a program.

Figure 6.4: Button "Run" in the Front Panel of LabVIEW.

As exactly 10 vibrations were induced, the device would stop recording automatically. The patients were taken for X-ray after the vibration acquisition procedure. The hospital number would be recorded to present it to the radiologist later for matching the result produced by the analysing technique(s) with the radiographs. As the patients would finish having the X-ray and they have also participated in the vibration test, they were asked to fill up a questionnaire, to find out, if the device caused any discomfort and if the children will prefer X-ray or vibration method.

Table 6.1: Questionnaire Response of the Child Participants.

Preferred Method	Number of Participants
X-ray	13 (26%)
Vibration	13 (26%)
No Preference	24 (48%)

Their preferences are represented in terms of percentages by the following diagram.

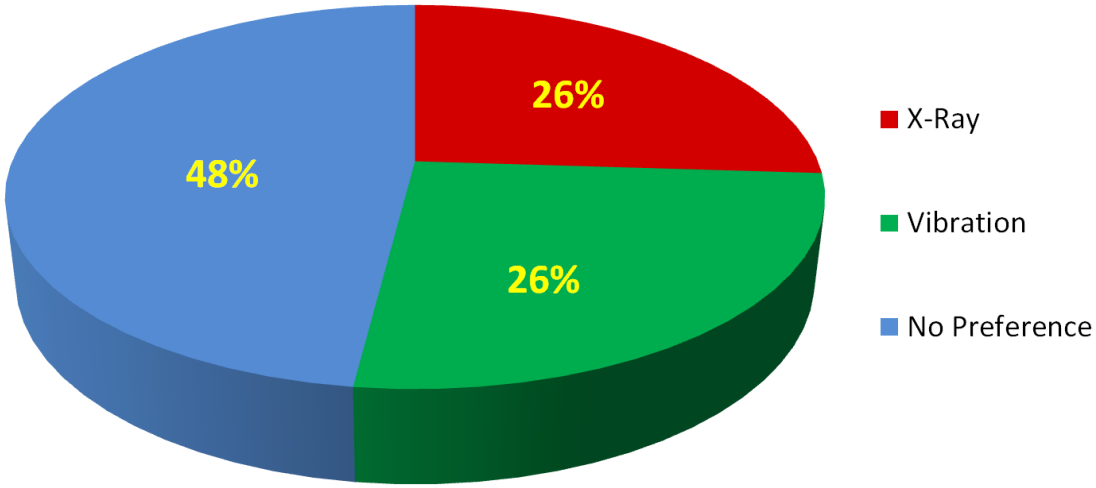

Figure 6.5: Pie Chart representation of the preferences.

As one can observe in Figure 6.5, the majority did not have any preference. The children who preferred X-ray commented that they did not like the tingling sensation created by vibration inducer. In fact, acquisition of radiographs is known to cause discomfort as injured wrists/ankles must be held in certain positions. Nevertheless, from the majority of the participants, the feedback was positive.

6.4 Data processing by Fuzzy C-means

The frequency response along with the filtered signal (obtained by similar methods applied on data acquired from adult patients) and the frequency spectra from the children are displayed in Figure 6.6 to 6.8.

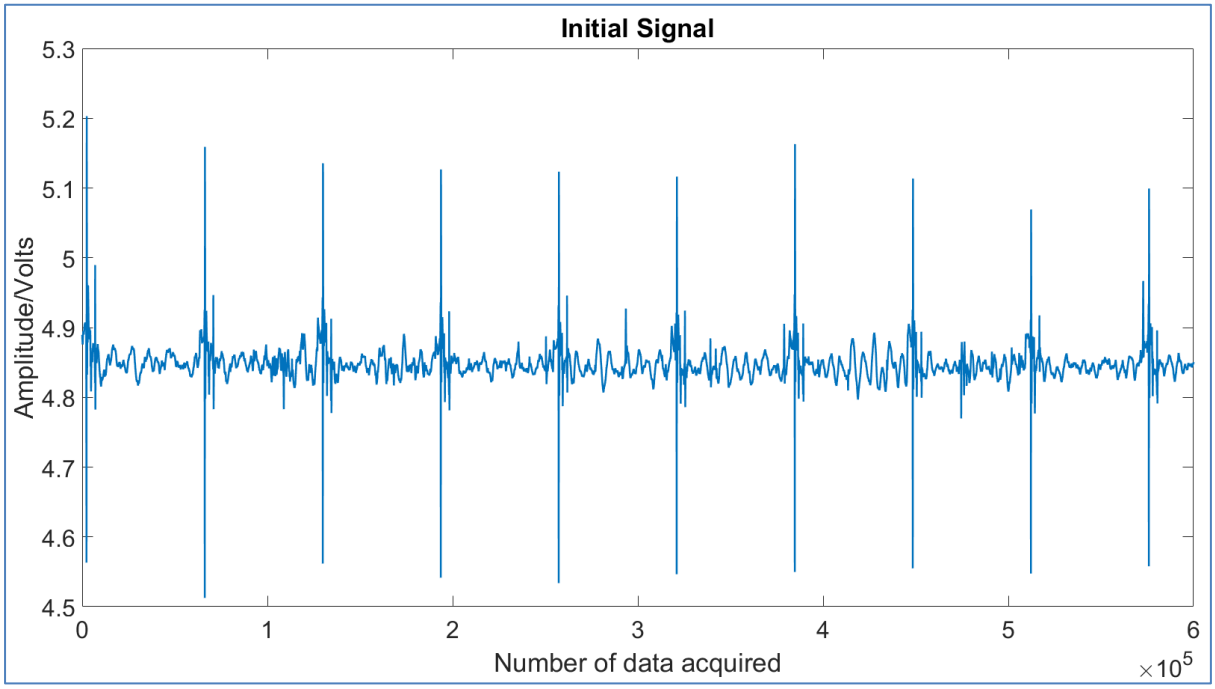

Figure 6.6: Initial Signal.

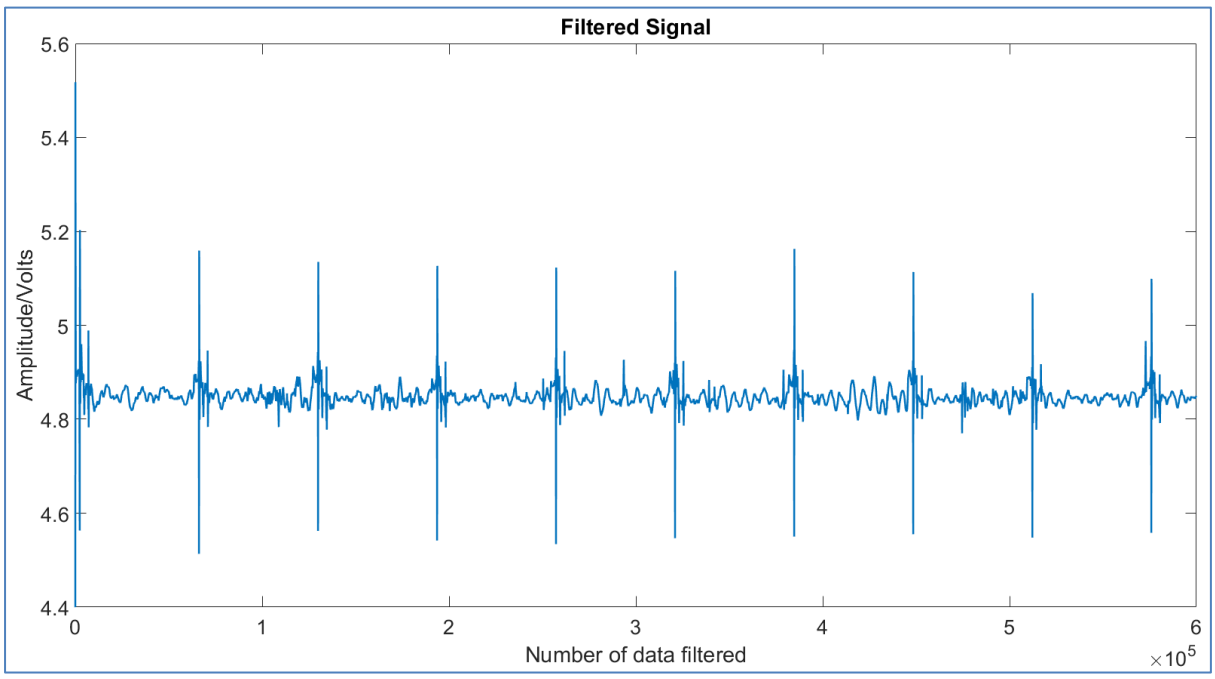

Figure 6.7: Filtered Signal.

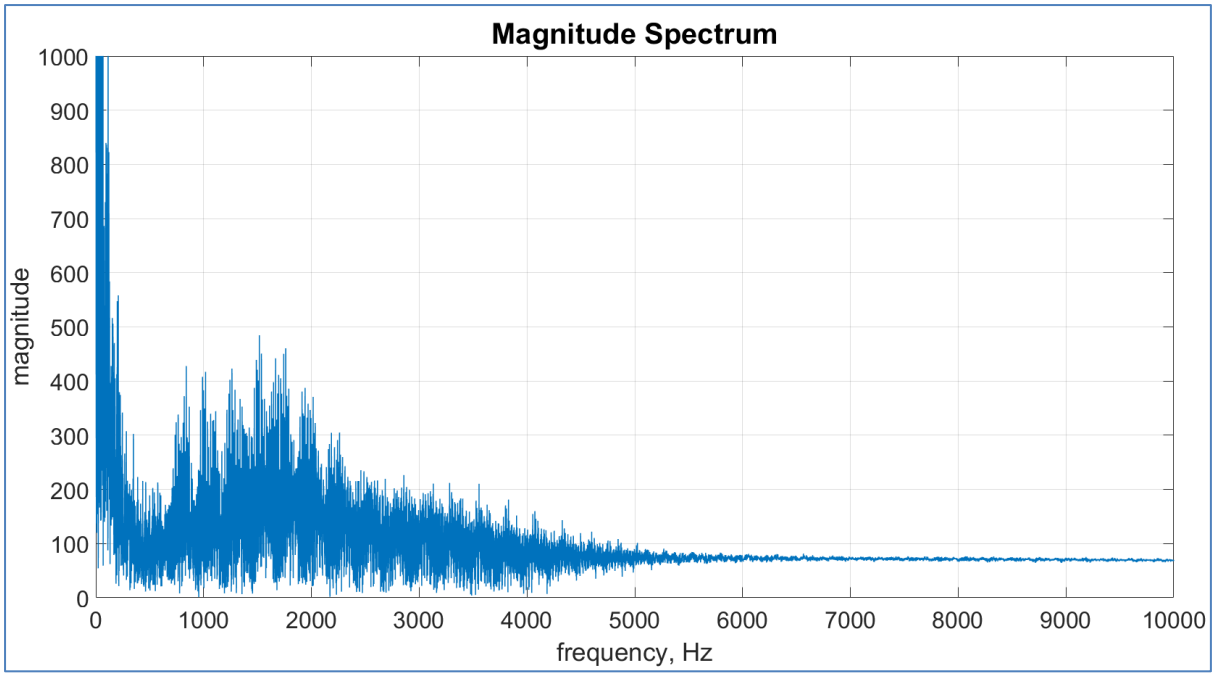

Figure 6.8: Magnitude Spectra over a range of 10,000Hz.

The data from children's wrists were analysed in a similar manner as with the adults' data:

1. Composing the frequency spectra and
2. Processed with the Fuzzy C-means.

14 sets of data were fully processed. Results were sent to the radiologist, from whose reports of the radiographs (fracture/no fracture) were concordant with vibration results in 10 out of 14 cases.

Table 6.2: Initial comparisons of Vibration analyses' results with X-rays.

Participant Number	Results by X-ray	Results by Fuzzy C-means (with membership values/likelihood of being fractured)
1	No fracture	Fracture (0.8969)
2	No fracture	Fracture (0.9111)
3	Fracture	Fracture (0.9529)
4	No fracture	No fracture (0.2121)
5	No fracture	No fracture (0.1664)
6	No fracture	No fracture (0.1906)
7	No fracture	No fracture (0.2159)
8	Fracture	Fracture (0.8415)
9	No fracture	Fracture (0.9606)
10	Fracture	No fracture (0.3036)
11	Fracture	Fracture (0.7551)
12	Fracture	Fracture (0.9923)
13	No fracture	No fracture (0.2887)
14	Fracture	Fracture (0.9749)

The results in Table 6.2 showed *4* results produced by the Fuzzy C-means which did not match with the radiographs. Vibration suggested 3 false positive and one false negative fracture. This means that one out of 14 patients would leave the hospital without being diagnosed accurately while saving 5 out of 14 patients from unnecessary radiation exposure. This technique would likely to be amended for further cases because:

- With this technique, 1 out of 14 patients would not have X-ray, in spite of having fracture.
- The Fuzzy C-means was calculated for the children keeping the adults' data present, in order to compare and observe which group is fractured and which group not. However, these adults' data were acquired via *different LabVIEW programs* (displayed in section: 4.3) and *different sampling rate* (50,000 samples/second).

6.5 Data processed by Magnitude of Frequencies

After recording 50 sets of data, the mean frequencies were plotted via a scattered diagram and observed if the frequencies can be classed such that the sprained one is higher than the fractured ones. Three other changes were made to the signal displayed in Figure 6.6 to observe the effects on results:

- A lowpass Infinite Impulse Response Filter with order "5" (maximum delay for producing maximum output) has been designed. It has been assigned Passband frequency of 5000Hz and a sampling rate of 60,000samples/second.
- A Parzen (de la Vallée Poussin) window has been applied.
- About 8000 of the data from each of the taps was removed to see if there were any effects of introducing the vibration responses.

The resulting graphs are illustrated in Figures 6.9 and 6.10 with the response of the vibration induction after removal of some data and the magnitude spectra.

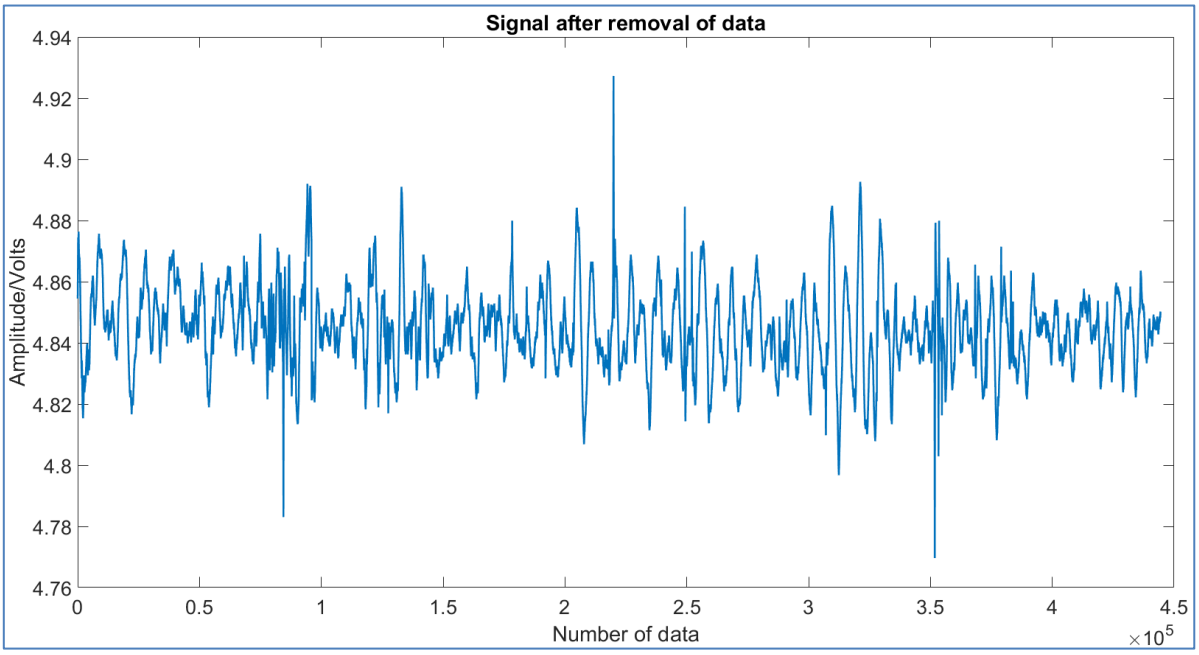

Figure 6.9: Responses after data removal.

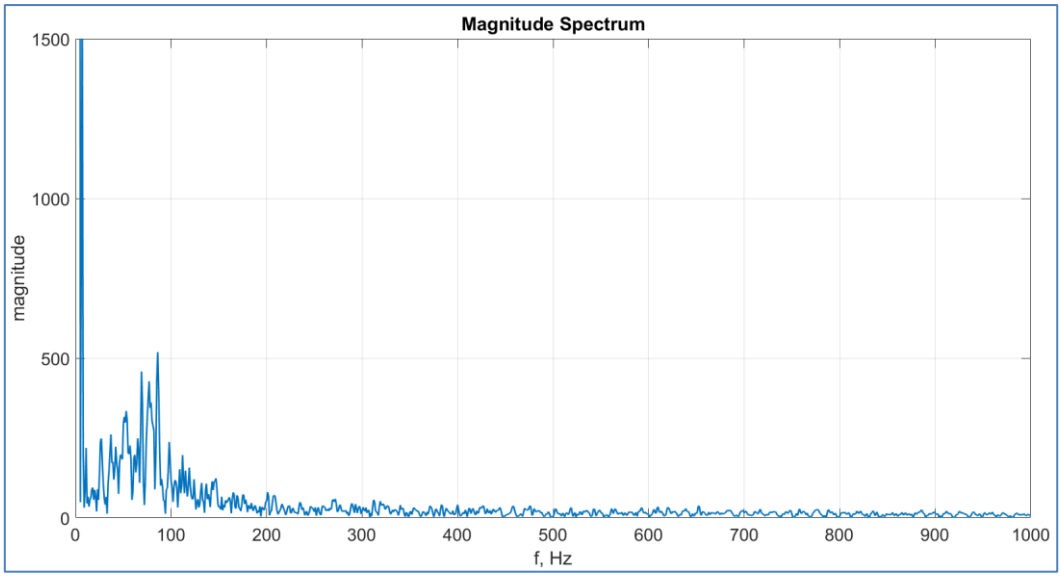

Figure 6.10: Magnitude Spectra over a range of 1000Hz.

- The "Mean Frequencies" from the first 1000 Hz of data were drawn via scatter plots. As 14 results were already known so a line was drawn in the middle of Figure to separate the known sprained data from the known fractured ones. In that way, some of the data whose states were to be determined fell below the line and some were above the line.

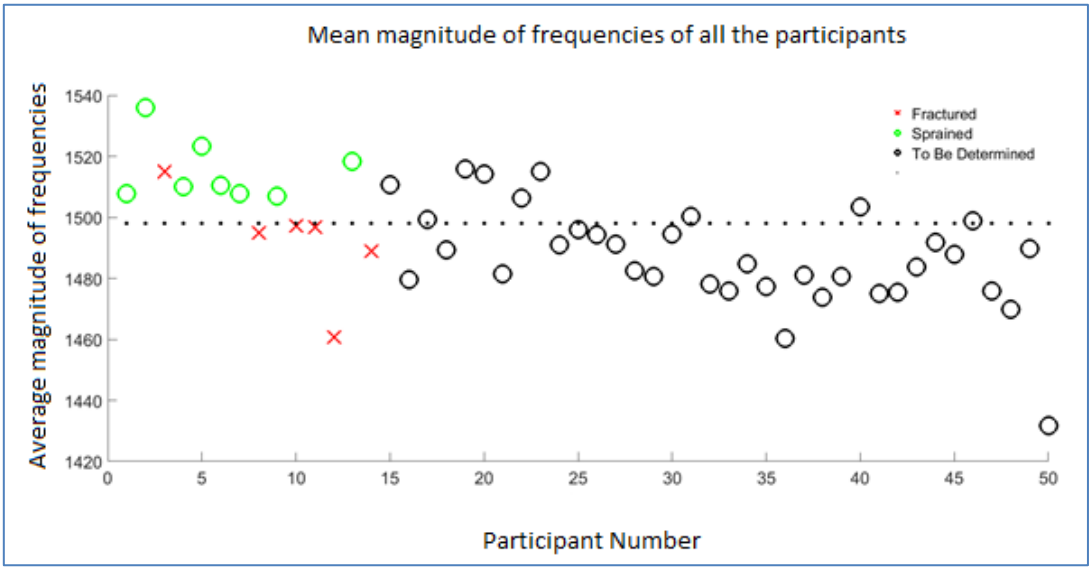

Figure 6.11: Bone mean magnitude of each FFT component of the signals of all the participants.

The results were matched with the radiographs and are shown in Table 6.3. The incorrect results inferred by the “Mean Frequency Components” technique have been italicised and depicted in red font for clarification.

Table 6.3: Total number of vibration analyses' results matched with radiographs.

Number of Participants	Gender	Injured Wrist	Injury Outcome by radiography	Injury Outcome by Mean Frequencies
1	Girl	Right	No Fracture	No Fracture
2	Girl	Right	No Fracture	No Fracture
3	Boy	Right	Fracture	*No Fracture*
4	Girl	Right	No Fracture	No Fracture
5	Boy	Left	No Fracture	No Fracture
6	Girl	Left	No Fracture	No Fracture
7	Boy	Left	No Fracture	No Fracture
8	Boy	Left	Fracture	Fracture
9	Boy	Left	No Fracture	No Fracture
10	Girl	Left	Fracture	Fracture
11	Boy	Left	Fracture	Fracture
12	Boy	Left	Fracture	Fracture
13	Boy	Right	No Fracture	No Fracture
14	Boy	Left	Fracture	Fracture
15	Boy	Right	No Fracture	No Fracture
16	Girl	Right	Fracture	Fracture
17	Boy	Right	Fracture	Fracture
18	Boy	Right	No Fracture	*Fracture*
19	Boy	Right	No Fracture	No Fracture
20	Boy	Right	Fracture	*No Fracture*
21	Girl	Right	No Fracture	No Fracture
22	Boy	Left	No Fracture	No Fracture
23	Boy	Right	No Fracture	No Fracture
24	Girl	Right	Fracture	Fracture
25	Boy	Left	Fracture	Fracture
26	Boy	Left	No Fracture	*Fracture*
27	Girl	Left	No Fracture	*Fracture*
28	Boy	Left	No Fracture	*Fracture*
29	Girl	Right	Fracture	Fracture
30	Boy	Left	Fracture	Fracture
31	Girl	Left	Fracture	Fracture
32	Girl	Left	Fracture	Fracture
33	Girl	Left	No Fracture	*Fracture*
34	Girl	Left	Fracture	Fracture
35	Boy	Left	Fracture	Fracture
36	Girl	Left	No Fracture	*Fracture*
37	Boy	Left	Fracture	Fracture
38	Boy	Left	No Fracture	*Fracture*
39	Boy	Left	Fracture	Fracture
40	Girl	Left	No Fracture	No Fracture
41	Boy	Left	Fracture	Fracture
42	Boy	Left	No Fracture	*Fracture*
43	Girl	Right	No Fracture	*Fracture*
44	Girl	Right	No Fracture	*Fracture*
45	Girl	Right	No Fracture	*Fracture*
46	Girl	Right	Fracture	Fracture
47	Boy	Right	Fracture	Fracture
48	Boy	Right	No Fracture	Fracture
49	Girl	Left	No Fracture	Fracture
50	Boy	Right	Fracture	Fracture

It can be noted that around 50% of the sprains were deduced as fractured by the “Mean Frequency” technique. These were just clear average frequencies without leaving any spectral leakage and moreover, it came into light that total number of data removed for determining the results was too many (around 13% of the total data) so removal of data should not be an option for analyses.

6.6 Modifications of the Programs/Techniques

6.6.1 2-D and 3-D Scatter Diagrams

The Mean values are considered with the frequencies generated in last section but assuming there might be some effects or grouping from the changes of Median, Modal and Maximum frequencies, they were computed as per two-dimensional and three-dimensional scatter diagrams such as,

- Bone mean magnitude components of the frequency spectra of the signal vs Bone median magnitude components of the frequency spectra of the signal (shown in Figure 6.12).
- Bone mean magnitude components of the frequency spectra of the signal vs Bone maximum magnitude components of the frequency spectra of the signal (shown in Figure 6.13).
- Bone mean magnitude components of the frequency spectra of the signal vs Bone median magnitude components of the frequency spectra of the signal vs Bone modal magnitude components of the frequency spectra of the signal (shown in Figure 6.14).
- Bone mean magnitude components of the frequency spectra of the signal vs Bone median magnitude components of the frequency spectra of the signal vs Bone maximum magnitude components of the frequency spectra of the signal (shown in Figure 6.15).

The 2-D diagrams are displayed below.

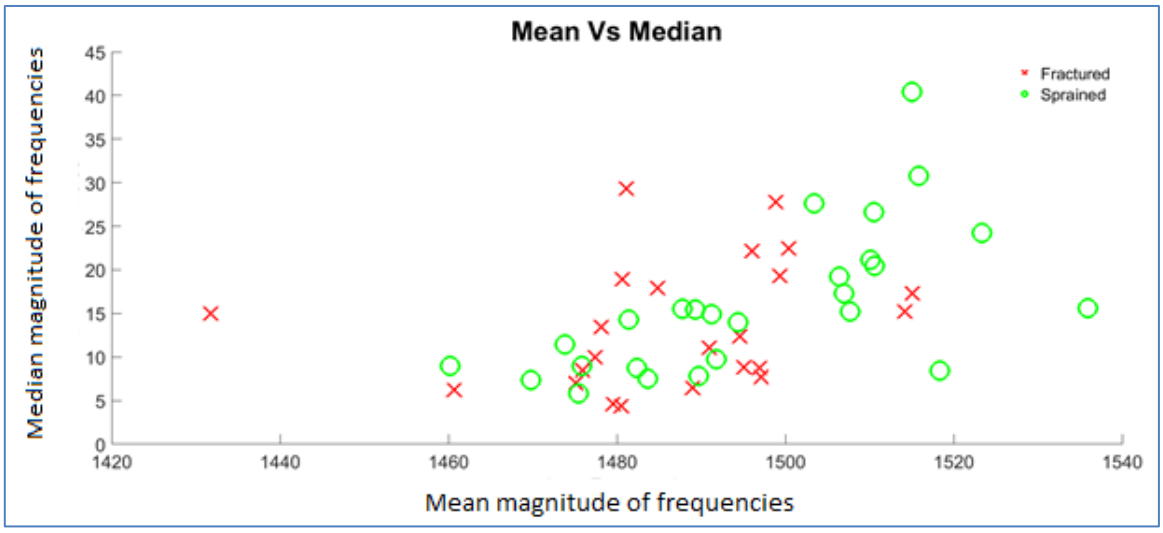

Figure 6.12: 2-D illustration of Bone Mean magnitude components (V/Hz) vs Bone Median magnitude components (V/Hz).

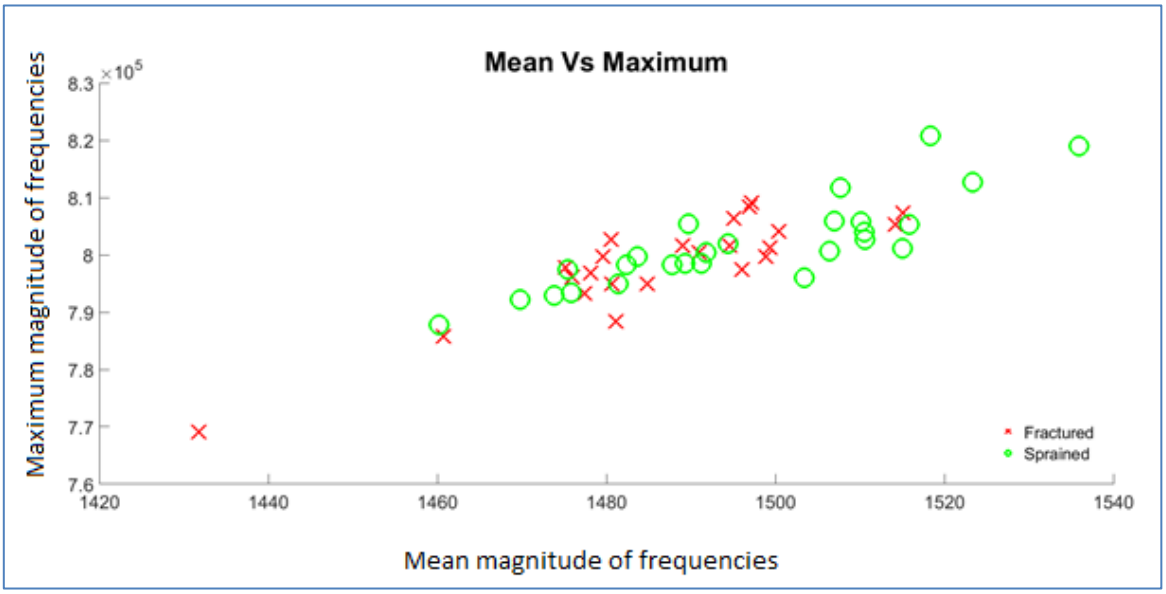

Figure 6.13: 2-D illustration of Bone Mean magnitude components (V/Hz) vs Bone Maximum magnitude components (V/Hz).

The 3-D diagrams are displayed below.

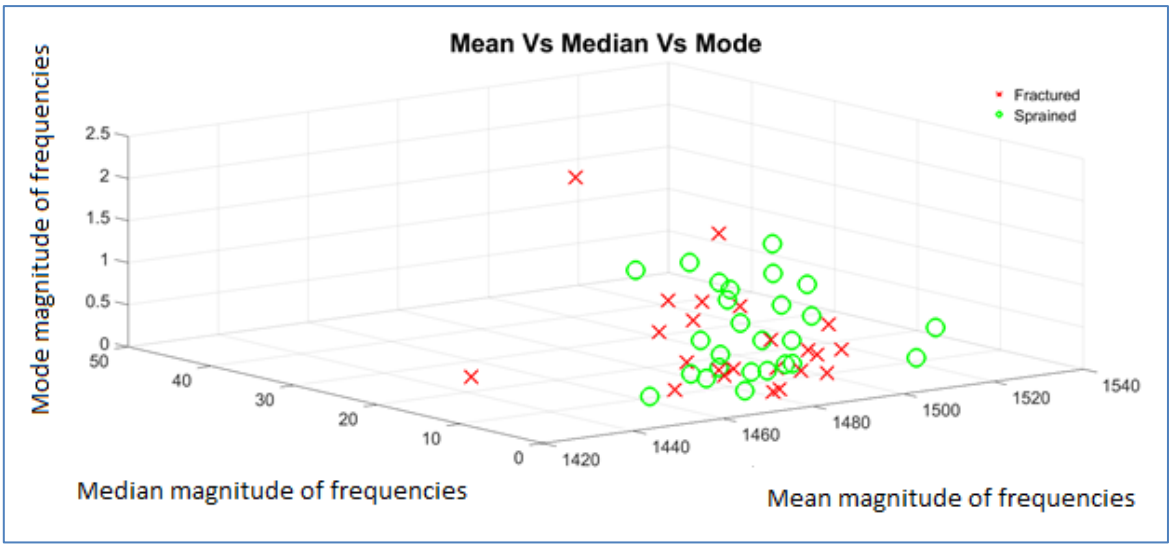

Figure 6.14: 3-D illustration of Bone Mean magnitude components (V/Hz) vs Bone Median magnitude components vs Bone Mode magnitude components (V/Hz).

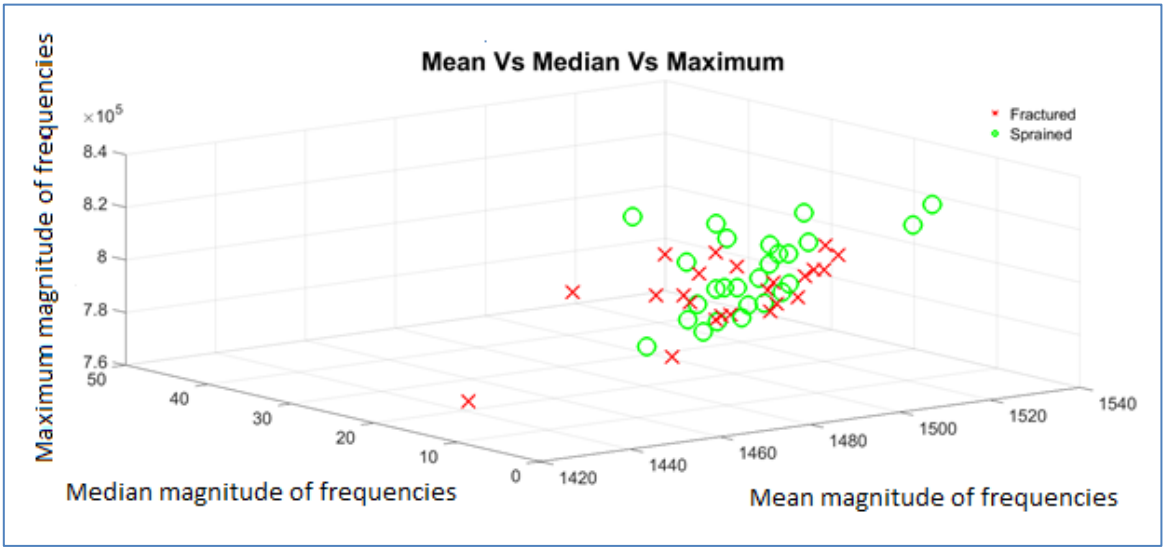

Figure 6.14: 3-D illustration of Bone Mean magnitude components (V/Hz) vs Bone Median magnitude components (V/Hz) vs Bone Maximum magnitude components (V/Hz).

It was impossible to separate the data between the fractured and sprained classes neither in 2-D nor in 3-D diagrams.

6.6.2 Cross-correlation Effects

The “cross-correlation” of two discrete signals measures the similarity between them as explained in the Theoretical Framework in Chapter 3. The injured wrists’ spectra and the uninjured wrists’ spectra produced from FFT were compared by generating cross-correlation as shown in Figure 6.16.

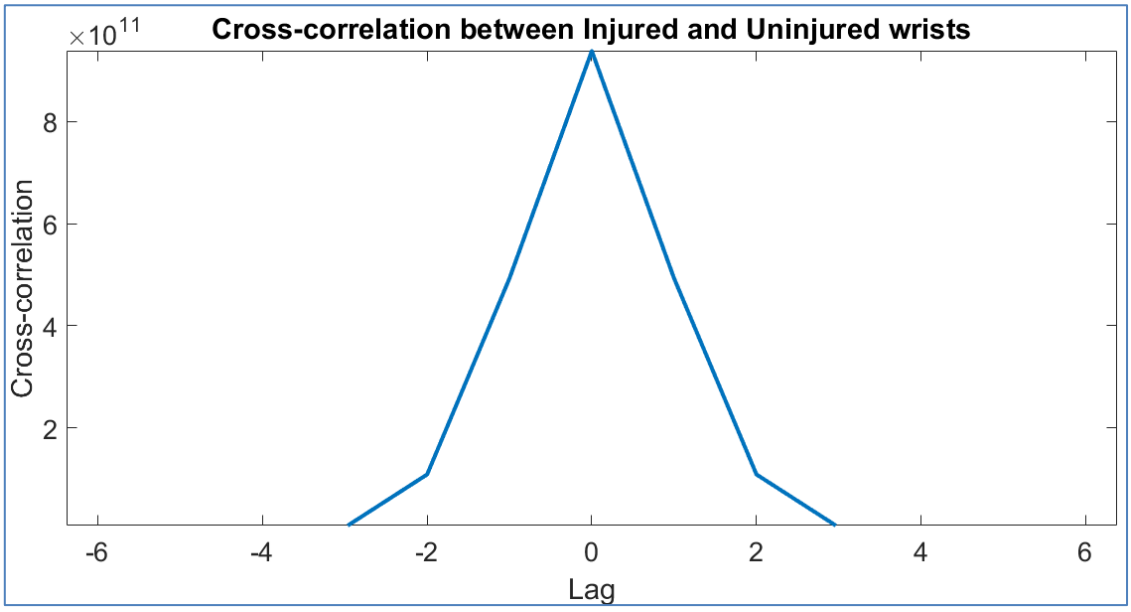

Figure 6.15: Cross-Correlated values.

As Figure 6.16 shows that the peak reflects the highest degree of similarity and that is why, the “maximum value” from the correlated spectra has been found out. These points have been displayed in scatter diagram in Figure 6.17.

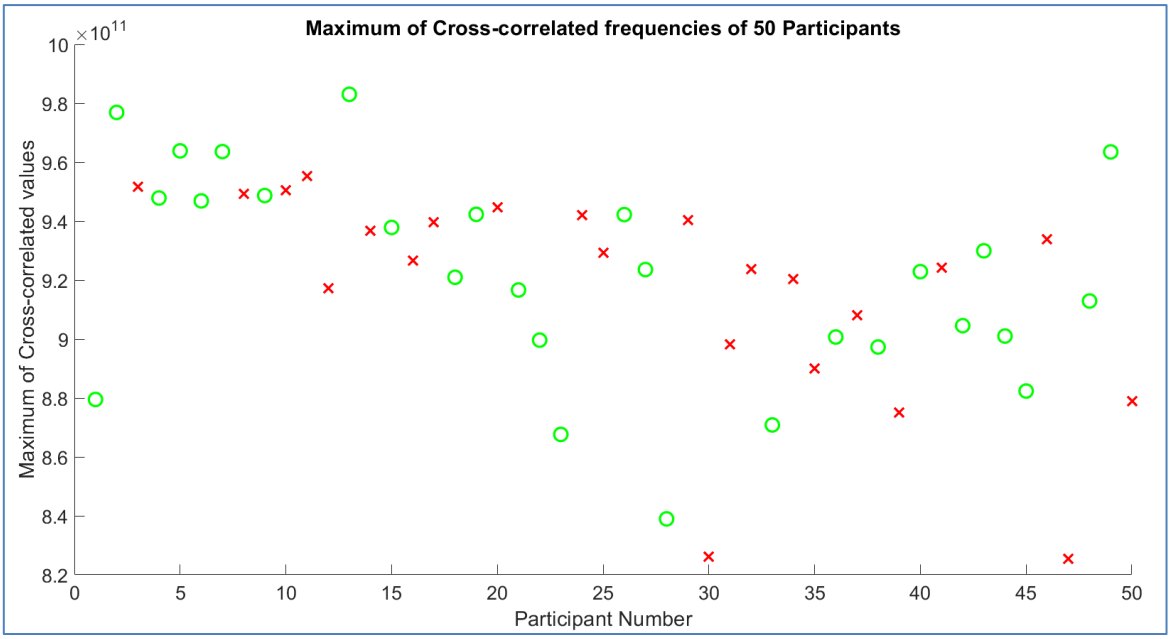

Figure 6.16: Maximum Cross-Correlated values between injured and uninjured wrists where the participants with fractured wrists are denoted by red-crosses and unfractured wrists by green-circles.

The layout in Figure 6.17 could not divide the data into separate classes and so, new methods have been investigated as discussed in the next subsection.

6.6.3 Coherence

In MATLAB, the common frequency points between left and right wrists were found out by the function "coherence". It determines how much the signals are in phase. The results were processed via FFT as previously to find out the spectral values of those points. Assuming the fractured wrists and sprained wrists will not have a large number of common points leading to uncommon frequencies, they will separate from each other. Figure 6.18 displays the features.

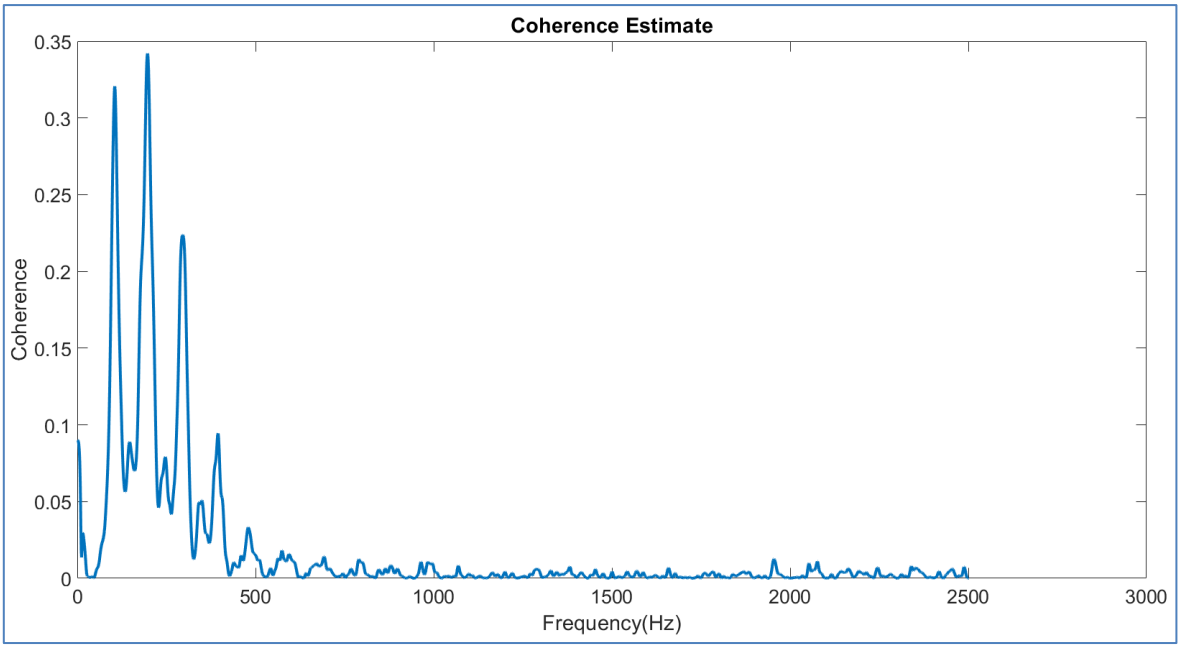

Figure 6.17: Magnitude Spectra after Coherence.

It can be seen from Figure 6.18 that the frequencies were produced only up to 2500Hz. The scatter diagrams for the mean, median and maximum values of the common points were plotted and illustrated in Figures 6.19, 6.20 and 6.21 respectively.

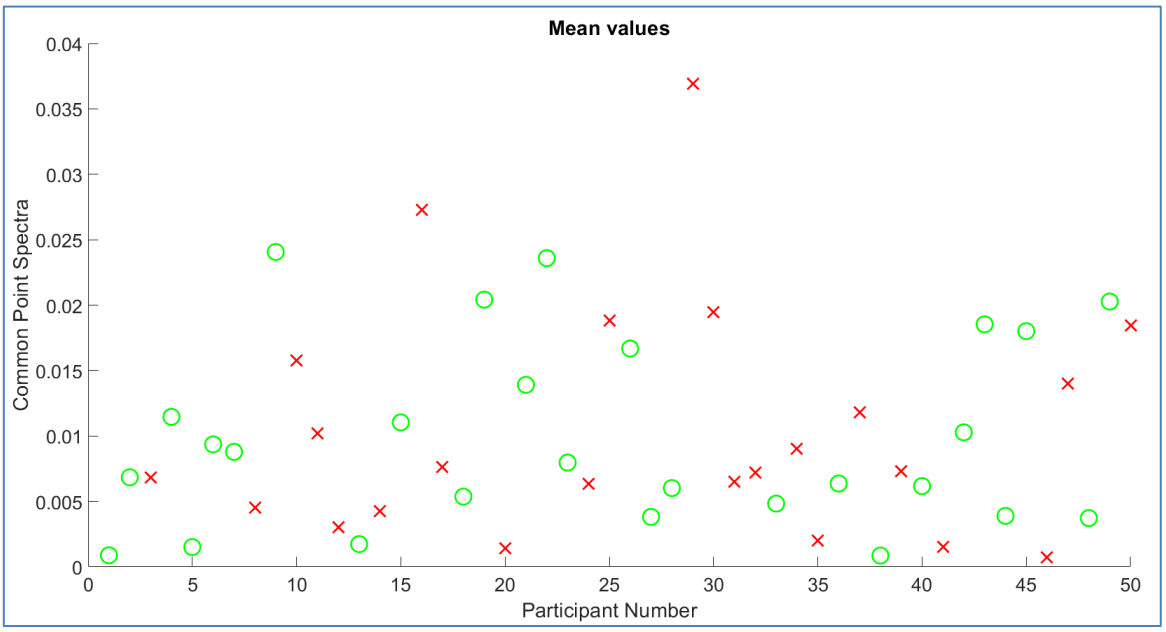

Figure 6.18: Mean Coherence between injured and uninjured wrists where the participants with fractured wrists are denoted by red-crosses and unfractured wrists by green-circles.

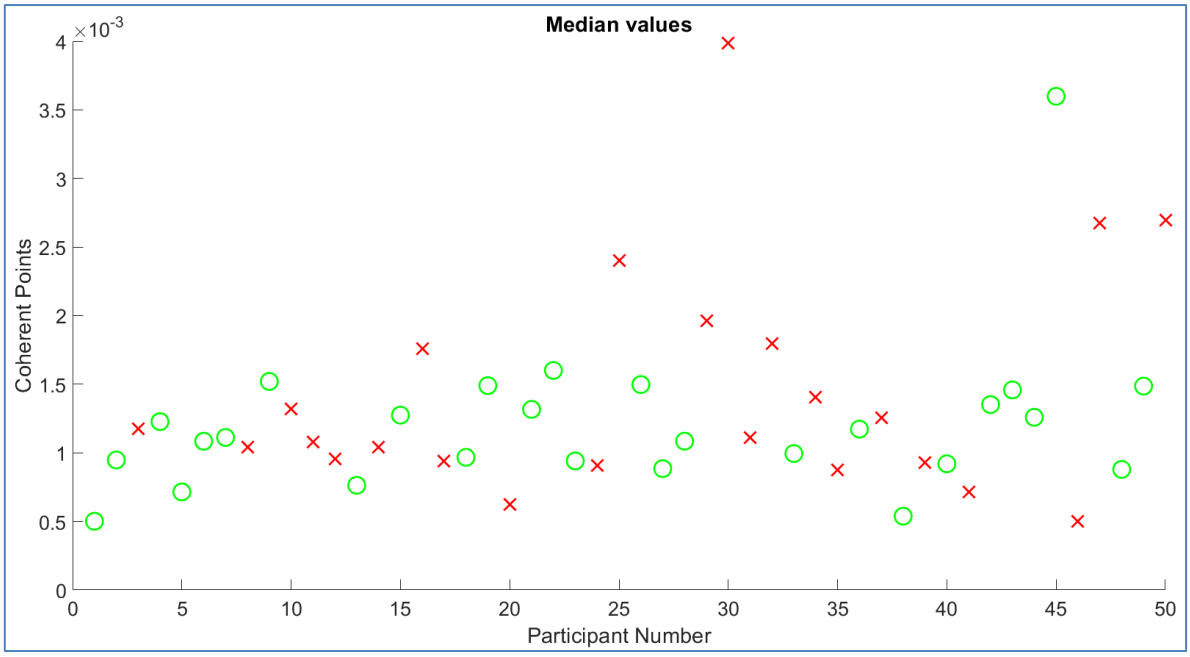

Figure 6.19: Median Coherence between injured and uninjured wrists where the participants with fractured wrists are denoted by red-crosses and unfractured wrists by green-circles.

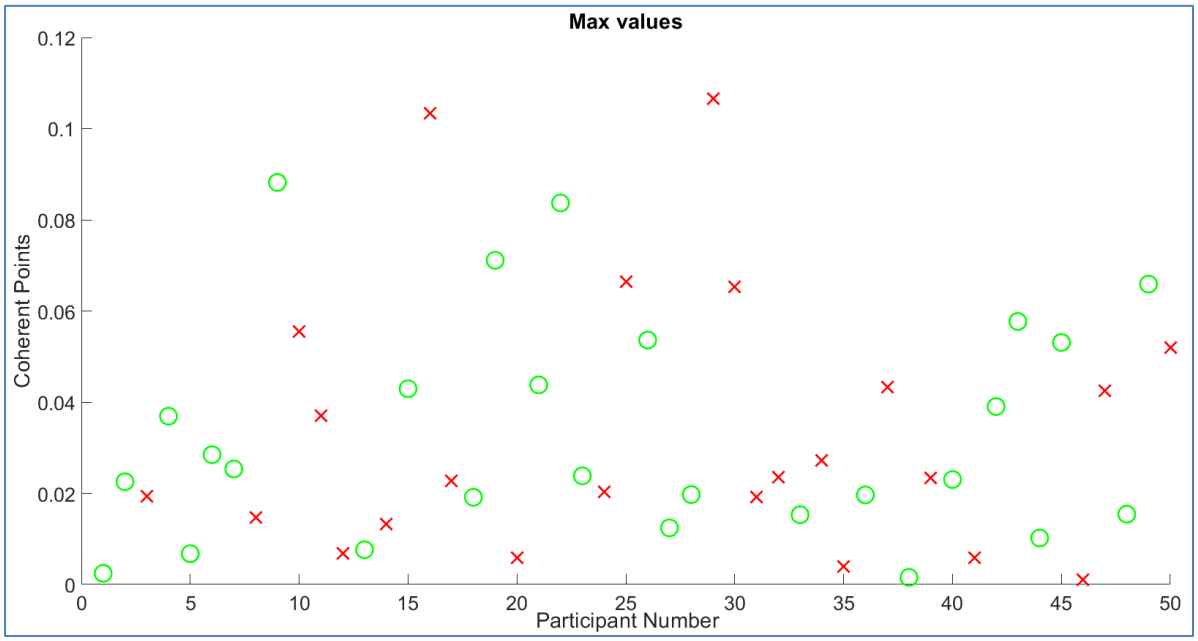

Figure 6.20: Maximum Coherence between injured and uninjured wrists where the participants with fractured wrists are denoted by red-crosses and unfractured wrists by green-circles.

It can be seen from all the three scatter diagrams that there is no pattern of the common points' frequencies for the fractured and sprained wrists.

The "Maximum values" were all produced in a line which reflected the fact that the values had similar peak frequencies. However, there were different "Mean values", that is, there were a range of peaks produced with different values and when they were averaged, and they resulted in various "Mean values".

The fractured and sprained data had different Mean values but if compared to existing theories, the fractured wrists' data should have lower values than that of the sprained ones. That was not the case according to the plots in Figure 6.17, 6.19, 6.20 and 6.21. We had to address another problem. The bones of the wrists have many properties which changed during the recording. The significant and known factor was "fractured" and "sprained". Nonetheless, the difference of sex might have some effect on the recordings. According to (Avdagic 2009) and (Almudhaffar 2014), there is an effect of sex on the bone strength and bone density. Findings of (Bediz, B., *et. al.* 2010) indicate that there is a direct relation between the changes of bone density and bone natural frequency.

Thus, the participants' data were separated according to the sex of the participants which was recorded previously between male and female. There were 29 male participants and 21 female participants. The Mean values according to the sex difference are illustrated in Figures 6.22 and 6.23.

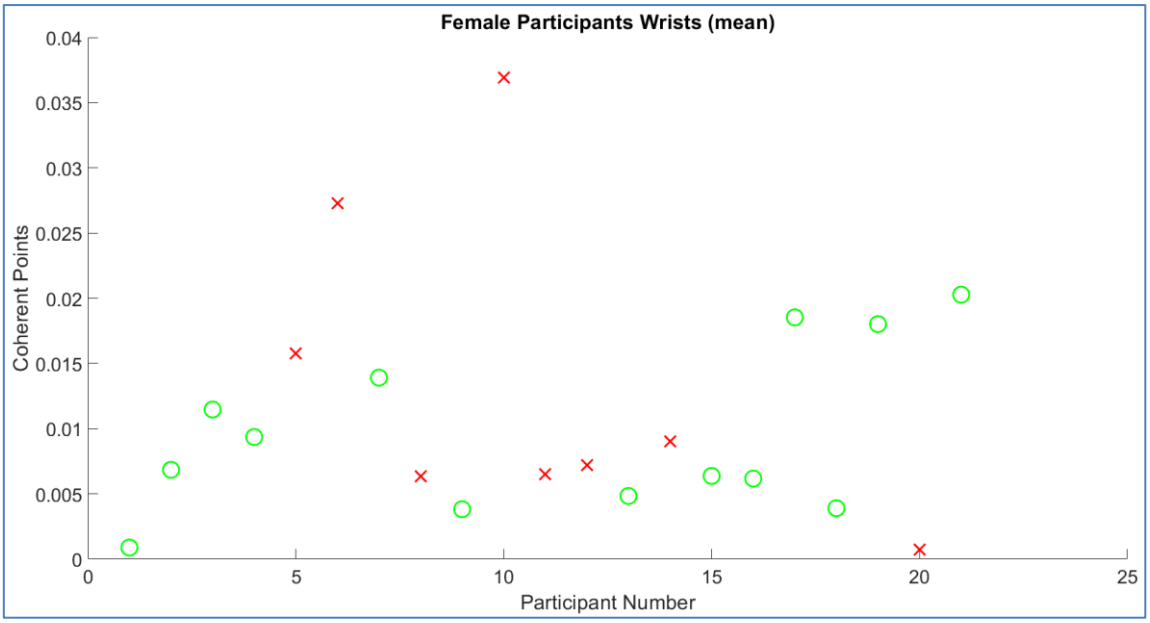

Figure 6.21: Bone Mean frequencies of Female participants with fractured wrists (red-crosses) and sprained wrists (green-circles).

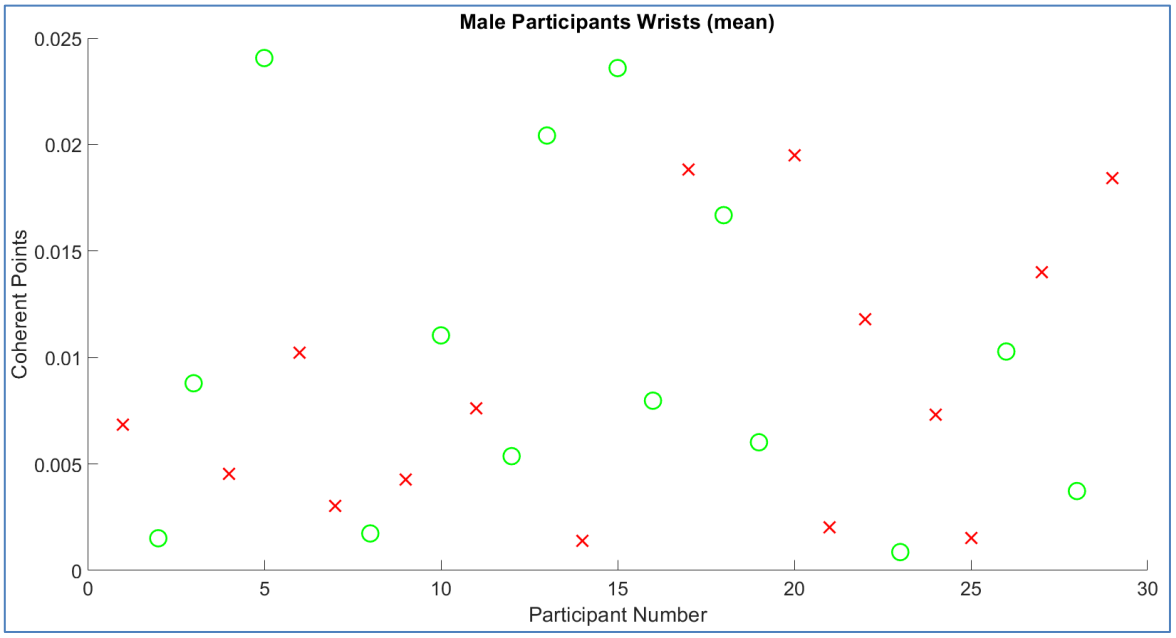

Figure 6.22: Bone Mean frequencies of Male participants with fractured wrists (red-crosses) and sprained wrists (green-circles).

If the mean values are noted of the male and female participants, then it can be clearly seen that there were significant differences of values. The common point in spectra can go up to 0.04 for female participants whereas the value is around 0.025 for the male participants. However, fractured and sprained data did not get

separated from each other as expected, so some more amendments were to be made to observe if any difference occurs.

6.6.4 Median Magnitude from the Frequency Spectra

Considering the above amendments and seeing the results comparing the techniques presented above, the analysing techniques were improved in the following ways:

- Data (Let's name the data as A) = A – rms(A) (as explained in *Chapter 2.8* why it might be advantageous).
- An Infinite Impulse Response type filter (better for analysing techniques explained in *Chapter 3*) has been designed by assigning order of 16 and applied to the data named as "A". This is actually the same procedure as that described in *Subsection 6.5*.
- The entire length of A was processed via a Hamming window (a popular window selected as the default window type in many functions in MATLAB).

  Figure 6.24 displays the initial signal and the spectra after application of filter and Hamming window on the signal.

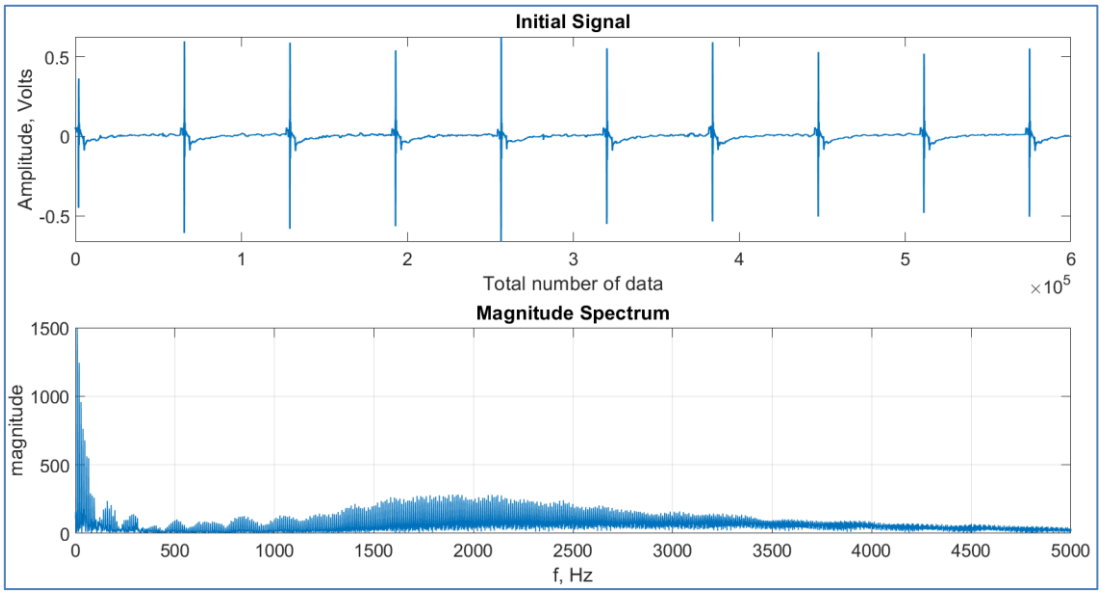

Figure 6.23: Initial Vibration Responses and its Frequency Spectra.

- 400 (=0.067%) of the data from the frequency spectra were left to minimise the spectral leakage. As the sampling rate was increased from 50,000 to 60,000 (in the case of children from adults) so there is a chance that spectral leakage occurs more.
- As illustrated in Figure 6.24, there are no high magnitude frequencies after 4000 Hz so up to 4000 Hz has been included in the amendment.
- Median (middle) frequencies have been considered due to the presence of various *peak* frequencies.
- As explained in the *Chapter 2*, there might be some effects of the sex (male and female) on the frequencies generated from bones so the data were separated based on the sex of the participants.

All displayed by the scatter diagrams in Figures 6.25 and 6.26.

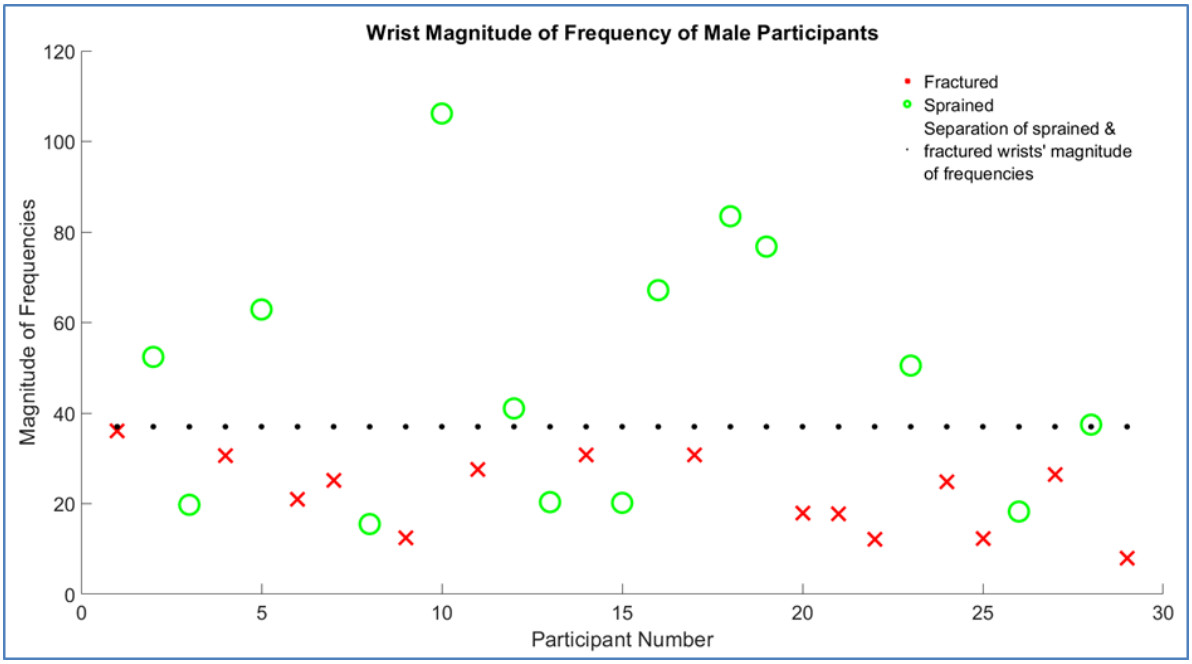

Figure 6.24: Bone Median magnitude components (V/Hz) of the Frequency Spectra of Male Patients.

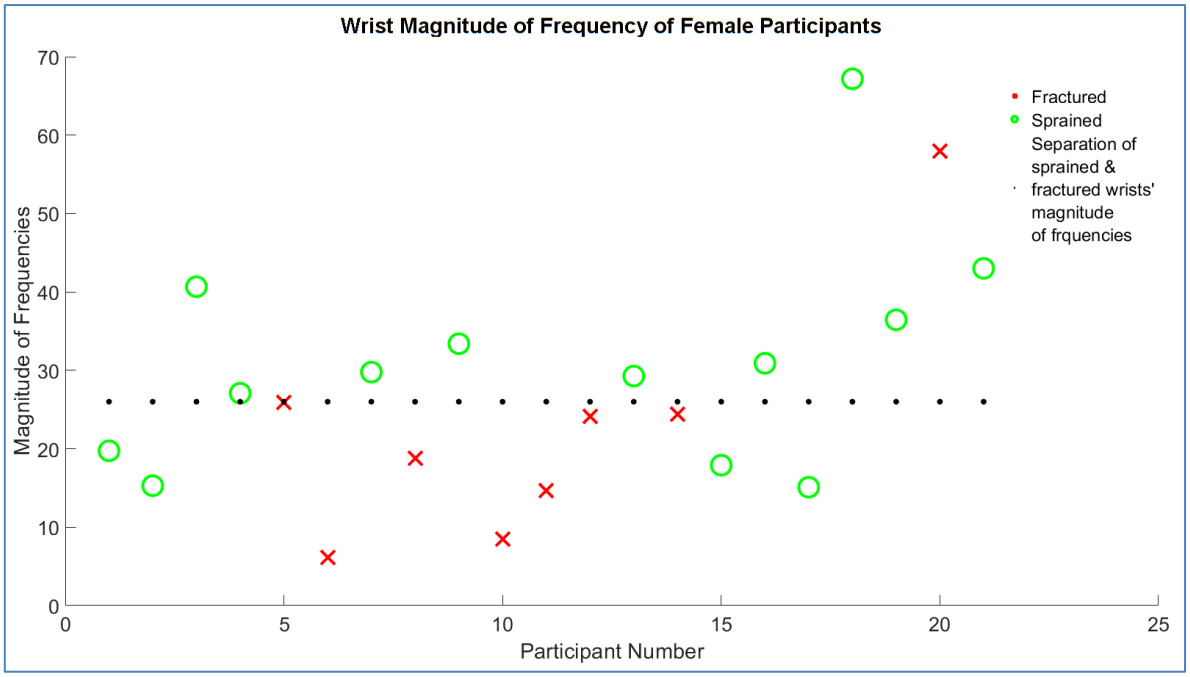

Figure 6.25: Bone Median magnitude components (V/Hz) of the Frequency Spectra of Female Patients.

Using this technique, 9 males and 9 females would have been spared unnecessary exposure to radiation.

- Filters have been designed starting with filter order ‘5’ up to ‘20’ to test the effects of filtration of signals on the frequencies. Filter with order ‘16’ drew the best separation between the fractured and non-fractured data.
- The same techniques have been applied leaving 300, 350, 450 and 500 data to check if the spectral leakage can be reduced. It is observed that low frequencies can be separated due to removal of 300 and 350 data. However, removal of 450 and 500 data does not in fact, give any difference.

Tables 6.4, 6.5 and 6.6 show the participants' test results with their sensitivity, specificity, positive predictive, negative predictive and accuracy of detection of presence and absence of fracture by this method.

Table 6.4: General Decision Matrix of Male patients.

	Truth or Target			
Diagnostic Test Result		Fracture	No Fracture	Total
	Positive	A = 15 (True Positive)	C = 5 (False Positive)	$T_{Test\ Positive}$ = 20
	Negative	B = 0 (False Negative)	D = 9 (True Negative)	$T_{Test\ Negative}$ = 9
		$T_{Fracture}$ = 15	$T_{No\ Fracture}$ = 14	29

Table 6.5: General Decision Matrix of Female patients.

	Truth or Target			
Diagnostic Test Result		Fracture	No Fracture	Total
	Positive	A = 7 (True Positive)	C = 4 (False Positive)	$T_{Test\ Positive}$ = 11
	Negative	B = 1 (False Negative)	D = 9 (True Negative)	$T_{Test\ Negative}$ = 10
		$T_{Fracture}$ = 8	$T_{No\ Fracture}$ = 13	21

As explained in section 2.6,

- *Sensitivity*: the probability that will indicate 'fracture' among those with a fracture.
- *Specificity*: the fraction of those without fracture that will have a negative test result.

Table 6.6: Fracture/Sprain Accuracy Measurements for Males and Females.

	Male (%)	***Female (%)***
Sensitivity	100	87.5
Specificity	64.29	69.23
Prevalence of Fracture	51.72	28.01
Positive Predictive Value	75	63.64
Negative Predictive Value	100	90
Accuracy	82.76	76.19

Interpretation of Table 6.6:

- There were 29 male and 21 female participants and among them 15 males and 8 females had fractured wrists, so prevalence is 51.72% and 28.01% respectively. It shows how common were the cases of fracture in population.
- Sensitivity is 100% (for males) and 87.5% (for females), so the test is supposedly able to detect all the males with fracture and 87.5% of the females with fracture. The test misses 12.5% of the females who have fracture.
- The test has 64.29% specificity for males and 69.23% for females.
  - For males, 9 persons out of 14 persons with negative results were truly negative and 5 individuals test positive for a fracture which they did not have.
  - For females, 9 persons out of 13 persons with negative results were truly negative and 4 individuals test positive for a fracture which they do not have.
- For the clinicians, the "Positive predictive values" are important. Positive predictive value and Negative predictive value state:
  - The males who tested positive, 75% (=15/20) of the males had fracture and the ones who tested negative, none of them actually had fracture.
  - The females who tested positive, 63.64% (=7/11) of the females had fracture and the ones who tested negative, 90% (=9/10) of them did not have fracture.
- The screening test is 82.76% accurate with males and 76.19% accurate with females.

From Table 6.6 and Figures 6.25 to 6.26, it can be concluded that frequencies separated the fractured data from the sprained ones and the test was accurate for most of the participants. However, one female participant (46th patient) had fracture which could not be classified accurately.

6.7 Normal wrists

The Ethics Application was further amended in order to acquire data from healthy uninjured children. The data were acquired on a Saturday in April 2018 from 7 boys and 8 girls at Saturday School ClubOK located at the King Edward VII Upper School.

The procedure for acquiring the data was kept same without changes. The LabVIEW setting has also been kept the same while capturing the vibration responses as that conducted at SCH.

The data were processed in the same way keeping the parameters same as described in the *subsection 6.6.4*. The frequencies were noted down and displayed in the scatter diagrams separating the boys' and girls' plots and including details of previous fracture, frequencies of left wrists and frequencies of right wrists pointed.

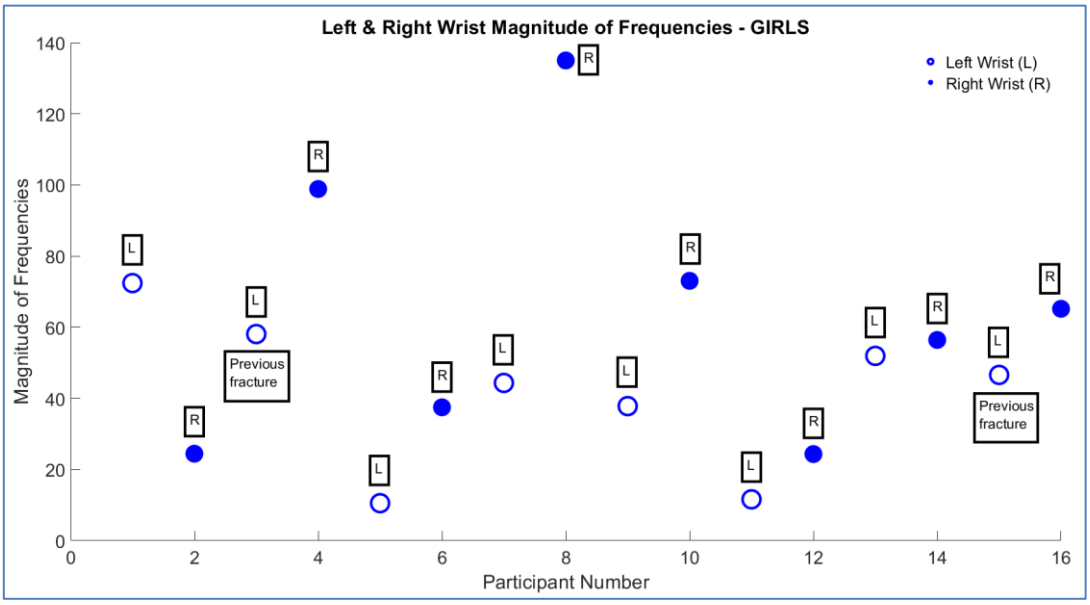

Figure 6.26: Bone magnitude components (V/Hz) of the Frequency Spectra of Female participants.

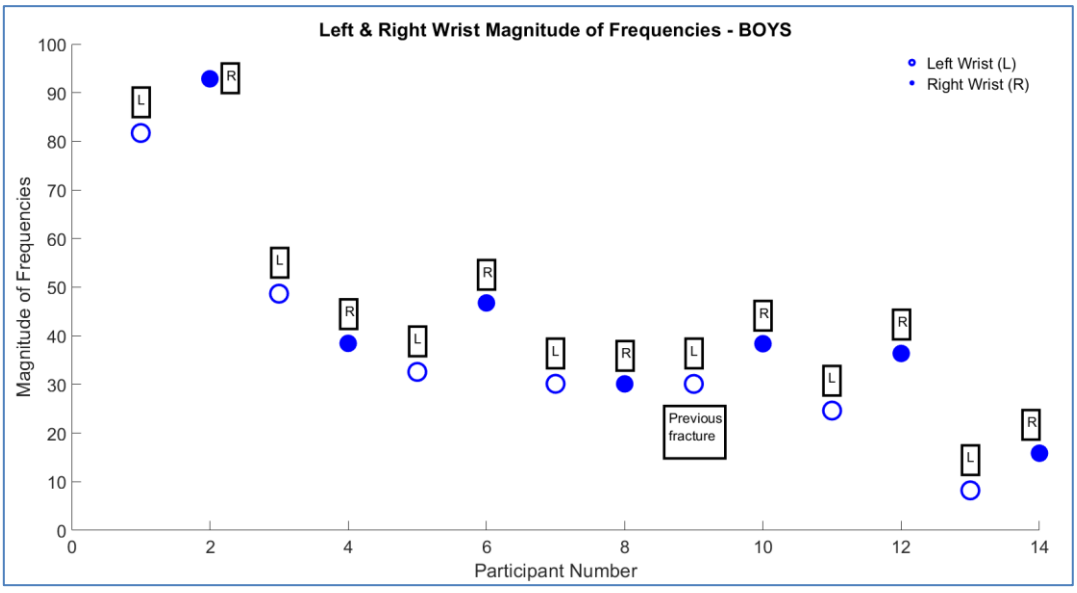

Figure 6.27: Bone magnitude components (V/Hz) of the Frequency Spectra of Male participants.

Table 6.7: Mean, Standard Deviation, Variance, Median and Modal features of the Normal Participants' Vibration Signals based on the Magnitude of their Frequency Spectra.

Measure of central tendency	Boys (V/Hz)	Girls (V/Hz)
Mean	40.5299	46.6294
Standard deviation	20.6731	14.5725
Variance	427.3769	212.3571
Median	36.3760	45.4692
Mode	15.8530	24.3470

Data from Figures 6.27 and 6.28 and Table 6.7 reveal:

- The frequencies of both boys and girls are higher in their right wrists than their left ones. All the participants were right-handed so, dominant wrist or the wrist which is used frequently in daily life might have higher frequencies.
- 2 female and one male participants had fractured their *left* wrists 2 years or more (at a younger age) preceding the study and because left wrists always had lower frequencies than right wrists, it could not be determined if the earlier fracture had any effects.
- The female participants have higher magnitude of frequencies than that of the males and there is increased probability of higher left/right variation in magnitude of frequencies in boys than in girls.
- Males and females have dissimilar wrist bone frequencies. As seen in previous studies (Bediz, B., *et. al.* 2010) and the study conducted with samples of wood during this research, the bones frequencies can vary with the change in bone density. The male and female participants can have different bone density even if they are of the same age. Hence, it suggests that it is always better to classify them separately.

6.8 Statistical comparisons

6.8.1 Maximum Likelihood of Frequencies

The command "poissfit" in MATLAB returns the maximum likelihood estimate (which is referred as the MLE) of the Poisson distribution of a set of data. This function can produce the likelihoods based on the confidence levels. Thus, in order to find out the relevant frequencies to be measured in the future, the command has been applied to the:

- Sprained, fractured, uninjured (SCH) and normal (participants from school) wrists of male participants.
- Sprained, fractured, uninjured (SCH) and normal (participants from school) wrists of female participants.
- The uninjured data were recorded from the patients' uninjured wrists who participated in this study with one wrist injured at SCH.

Table 6.8: Estimations of the Bone Mean magnitude of frequencies calculated with 90% confidence level.

Category	Maximum Likelihood of Magnitudes of Frequencies
Fractured male patients' wrists (SCH)	*30.3 to 35.2*
Sprained male patients' wrists (SCH)	57.0 to 63.9
Uninjured male patients' wrists (SCH)	48.1 to 52.4
Healthy male participants' wrists (School)	51.4 to 60.7
Fractured female patients' wrists (SCH)	*29.1 to 35.7*
Sprained female patients' wrists (SCH)	38.4 to 44.3
Uninjured female patients' wrists (SCH)	51.0 to 56.3
Healthy female participants' wrists (School)	51.1 to 59.7

Table 6.9: Estimations of the Bone Median magnitude of frequencies calculated with 90% confidence level.

Category	Maximum Likelihood of Magnitudes of Frequencies
Fractured male patients' wrists (SCH)	*20.2 to 24.2*
Sprained male patients' wrists (SCH)	44.9 to 52.4
Uninjured male patients' wrists (SCH)	37.9 to 41.7
Healthy male participants' wrists (School)	37.6 to 45.6
Fractured female patients' wrists (SCH)	*19.8 to 25.3*
Sprained female patients' wrists (SCH)	28.7 to 33.8
Uninjured female patients' wrists (SCH)	40.4 to 45.1
Healthy female participants' wrists (School)	42.7 to 50.6

In both cases, the MLE values clearly show that the frequencies (whether mean or median) are lower in the case of presence of a fracture. The uninjured wrists' frequencies of the participants from SCH are similar to that of the participants from the school. In addition, the frequencies for the uninjured and normal wrists determined by MLE are very similar, so recording more data may produce a concrete range of frequencies.

From Figures 6.25 and 6.26, the boundary for classifying fractured and sprained wrists is 37 V/Hz and 26 V/Hz for males and females respectively.

From Tables 6.8 and 6.9, the classifying boundaries for fractured and sprained wrists are:

- 24.2 to 44.9 V/Hz for males (the variance and standard deviation are large according to Table 6.7)
- 25.3 to 28.7 V/Hz for females.

The classifying limits from the scatter diagrams fall within the boundaries generated by MLE. From Figures 6.25 and 6.26, *18* children could have avoided radiographs. Thus, the classification technique by observation of frequencies merits further study. The frequencies noted in Table 6.7 and results from further calculations as shown in Tables 6.8 and 6.9 indicate similar outcomes produced by the FE experiments performed on human hand-arm system by (Adewusi, S., *et. al.* 2014) and vibrations transmission experiments by (Xu, X. S., *et. al.*, 2016) (described in *subsection 2.11.2*).

6.8.2 Normal Distribution

The male and female participants' bone frequencies have been normally distributed with 95% confidence level. An additional plot called "probability plot" has also been added which compares the frequencies to the normal distribution. The plot includes a reference line useful for judging whether the data follow a normal distribution.

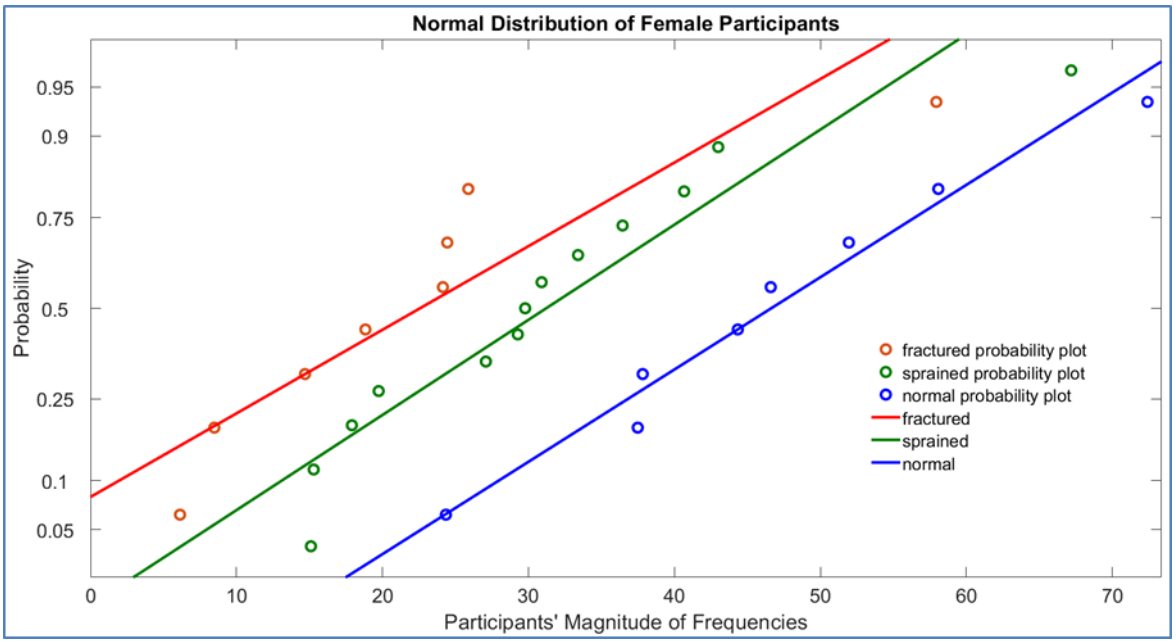

Figure 6.28: Probability plot of Bone magnitude of frequencies (V/Hz) of Female participants normally distributed.

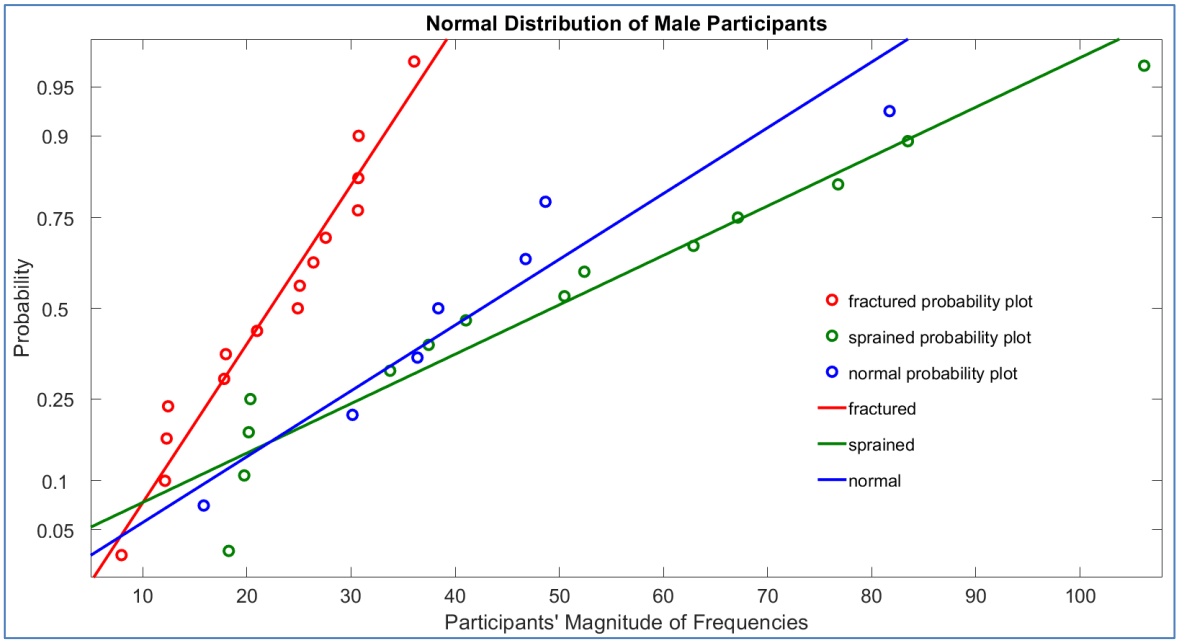

Figure 6.29: Probability plot of Bone magnitude of frequencies (V/Hz) of Male participants normally distributed.

If chances of frequencies occurring are to be allocated between 0 and 1, then it is more convenient to observe the best fitted line plotted through the probability of the frequencies as displayed in Figures 6.29 and 6.30. There is a clear difference between the fractured, sprained (no fracture) and normal states. The frequency of normal wrists is further away from that of the fractured wrists. This can be interpreted in such a way that if a child sustained a minor injury and definitely not a fracture, then the frequencies will not be assigned near the fractured best fitted line.

In order to broaden and justify the interpretation, *sprained* frequencies (displayed in Figures 6.25 and 6.26) which fell into the fractured frequencies' region were removed from Figures 6.29 and 6.30 and the new distributions have been illustrated in Figures 6.31 and 6.32.

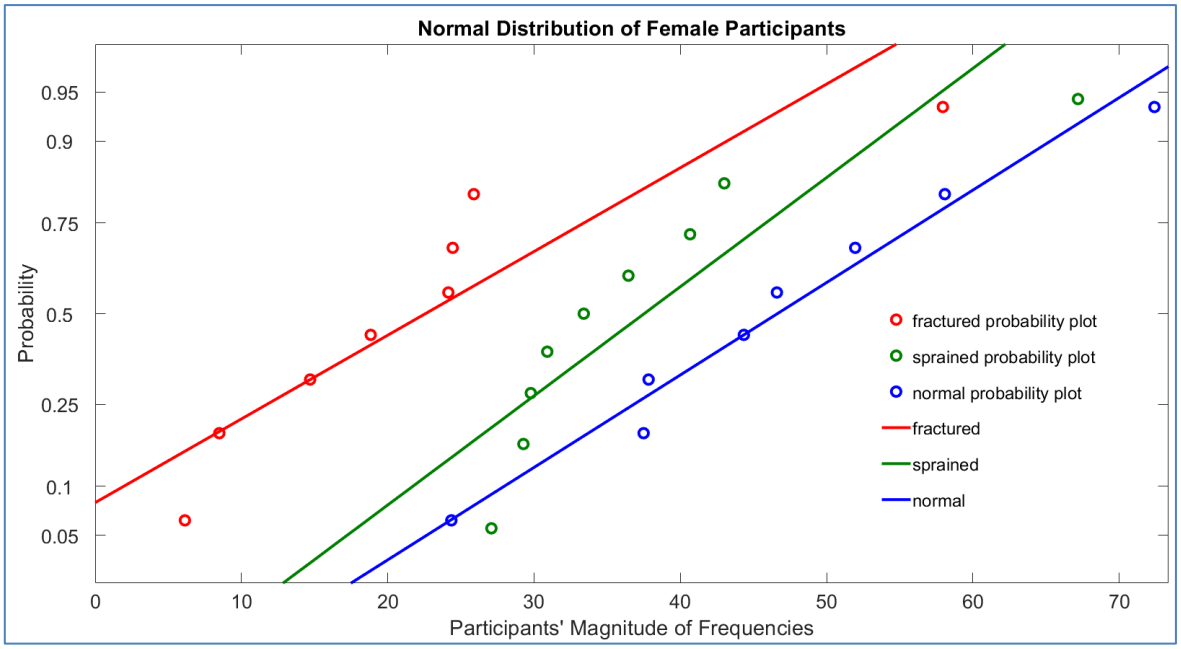

Figure 6.30: Probability plot of Bone magnitude of frequencies (V/Hz) of Female participants normally distributed after removing the incorrect sprained frequencies.

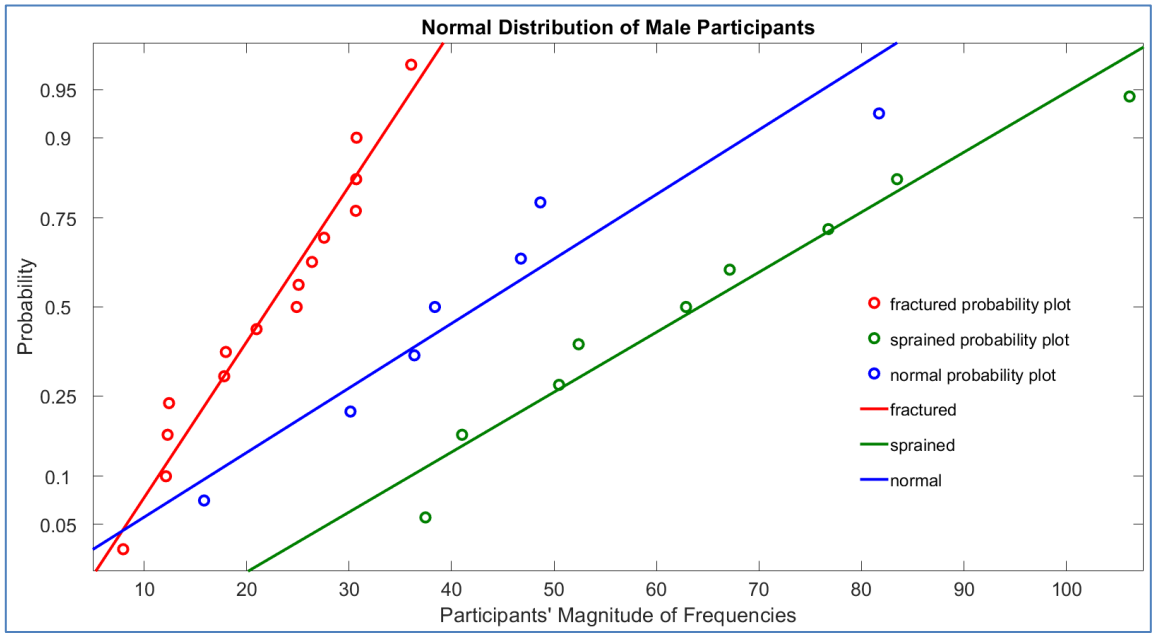

Figure 6.31: Probability plot of Bone magnitude of frequencies (V/Hz) of Male participants normally distributed after removing the incorrect sprained frequencies.

Table 6.10: Mean (mu) and Standard Deviation (sigma) values from Normal Distribution.

Normal Distribution	Mean (V/Hz)	Standard Deviation (V/Hz)
Fractured male patients' wrists (SCH)	*22.243*	*8.480*
Sprained male patients' wrists (SCH)	*49.2902*	*27.238*
Healthy male participants' wrists (School)	42.556	20.459
Fractured female patients' wrists (SCH)	*22.569*	*16.092*
Sprained female patients' wrists (SCH)	31.213	14.139
Healthy female participants' wrists (School)	46.630	14.573

Figures 6.31 and 6.32 illustrate that the removal of the erroneous data brings the sprained and normal frequencies closer. This interprets that if a child comes to the hospital with a fractured wrist then that wrist's frequency should be around the "red" region/best fitted line in Figures 6.29 to 6.32. Table 6.10 shows that the males participants' data are more likely to deviate from the average frequencies and similar to the observations reflected by Table 6.7.

6.9 STFT and Cluster Analyses

6.9.1 Short-Time Fourier transform (STFT)

Further analyses were done by converting the data by Short-Time Fourier Transform (STFT). This processing was performed because for two reasons:

- To verify if other signal processing techniques can recognise the properties discovered in *subsection 6.6*.
- To find out more efficient methods for classification of the data.

The default operation of spectrogram in MATLAB calculates the power of a signal by dividing the entire signal into eight portions with overlap and windowing each part with a Hamming window (Pascal 2013).

Steps/numeric values provided to transform the wrists' data with STFT:

- Data, A = A – rms(A)
- the specified window size = 256
- sampling frequency = 60,000
- default window overlap = length(window)/2
- FFT size = 256.

The figure produced by STFT, displays the results as a thermographic image where the default operation extracts the power spectral density over time using "hotter" colours like red, yellow, etc. to designate frequency bands of greater energy. If the sampling frequency is not specified, the time scale will be incorrect.

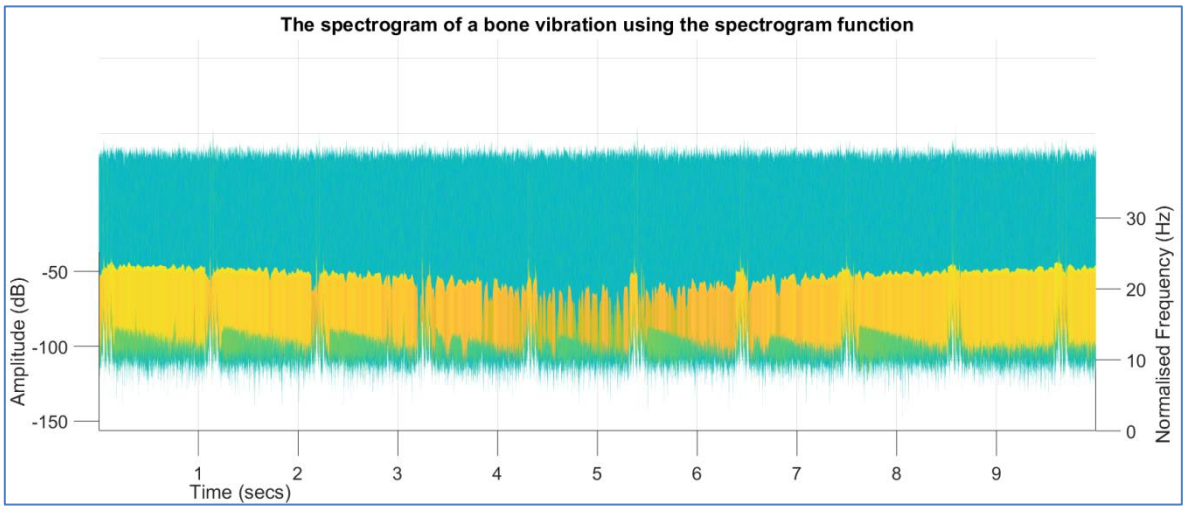

Figure 6.32: Spectrogram of the wrist of an injured subject.

The values produced by the spectrogram analyses in MATLAB are called "s-values". These "s-values" are points that have particular amplitude, time and frequency. The above diagram/spectrogram which is a signal analysis does not generate any classification of data between fracture and sprain. Thus, the technique known as Self-organising map has been applied to observe if it can differentiate the data properly.

6.9.2 Self-organising map

Short-Time Fourier Transform generates a number of segments based on the number of data to be analysed as s-values. The average of s-values has been extracted and Self-organising map (SOM) analyses (described in *subsections 3.11.7* and *3.11.9*) were performed on them.

In case of SOM, male and female participants' data have been separated. As it is already known which patients had fractured wrists and which did not, so the fractured data reflected by SOM, had been drawn separately. This was done to mark the groups to see if any noticeable patterns could be produced to go ahead with using this technique as shown in Figures 6.34 and 6.35.

The neurons in the layer in Figures 6.34 and 6.35 are arranged in physical positions according to a topology function. The function used in this study, is known as the "gridtop" which means the map arranges the position of the neurons in a square shape. The figures show the neuron locations in the topology and indicate how many of the training data are associated with each of the neurons (cluster centres). The topology selected here is 10-by-10 grid.

Figures 6.34 and 6.35 illustrate how many of the trained samples fall into each group. The gap with no hits is an indication of a separation between clusters with no intermediate class of subjects. In the figures, the red circled hits are from the samples, collected from the fractured wrists. The next group of hits are from the sprained (no fracture), all plotted together. In order to understand which data were from the fractured or sprained wrists, they were plotted separately, as attached in the Appendix A.5.

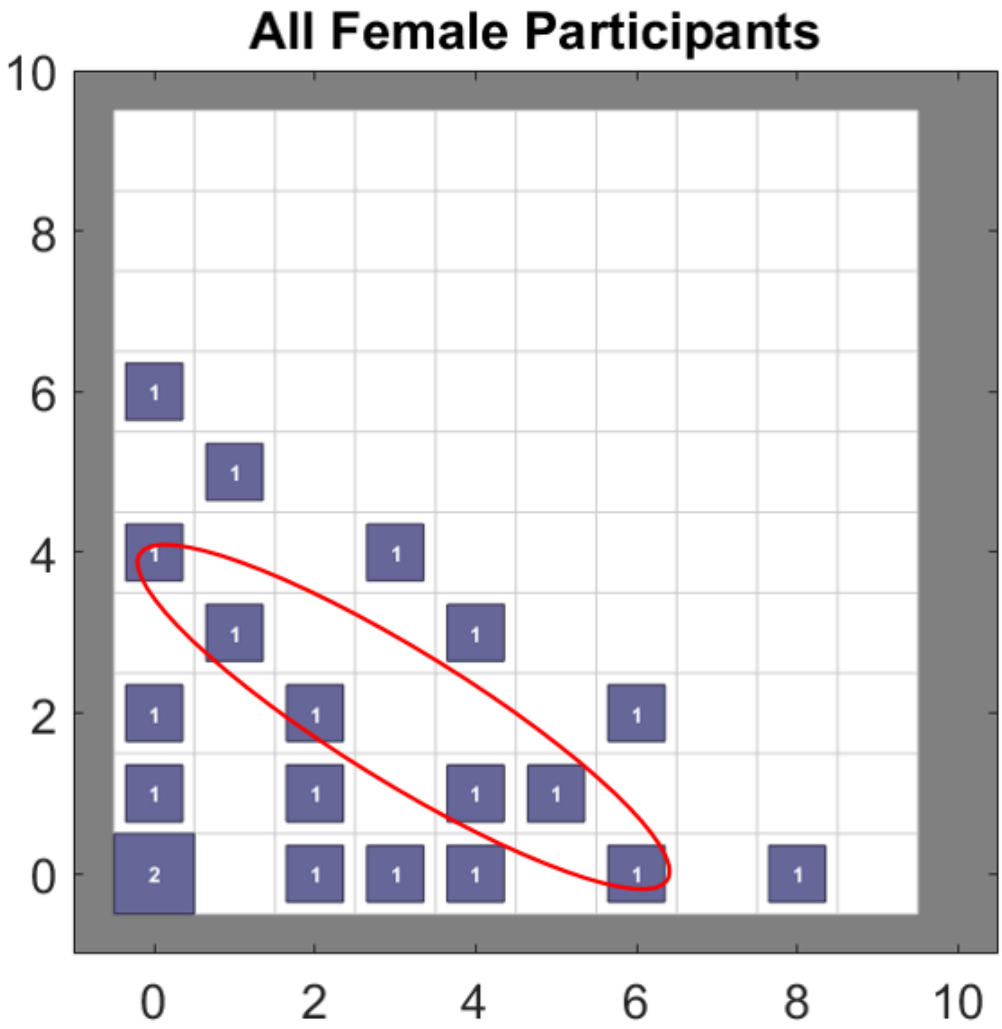

Figure 6.33: s-values of the Female Participants by SOM.

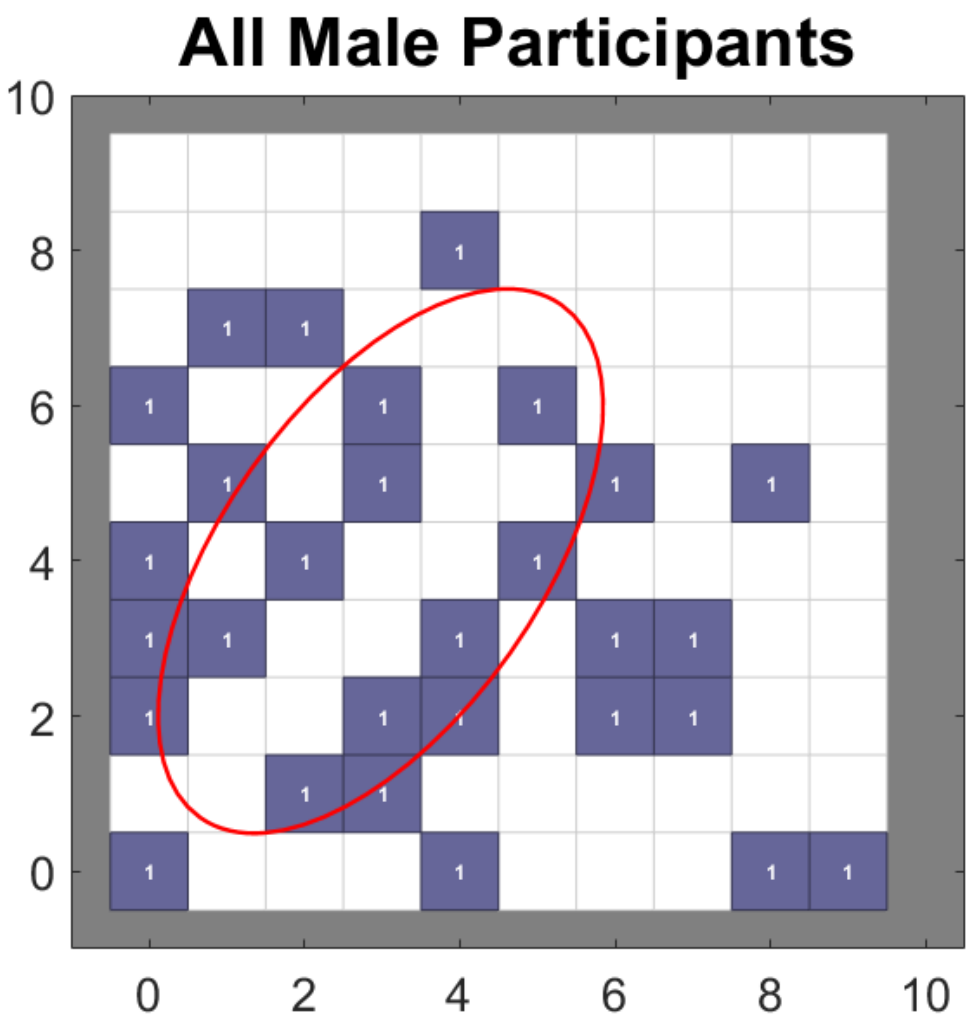

Figure 6.34: s-values of the Male Participants by SOM.

Table 6.11: SOM Results.

	Male Participants	Female Participants
s-values of fractured patients in one cluster	13/15	6/8
Sprained data which fell inside the fractured s-values cluster	2/14	0/13
Total number of participants	29	20

It is quite clear that most of the fractured data are clustered together. However, one set of data from the female participants (46th patient) was not included before analysing via SOM. According to Figures 6.34 and 6.35, the sprained data are not allocated very far away from the fractured data. If more data can be collected and the size of the Kohonen map maximised, then the fractured data might be classified more visibly. Hence, it is currently better not to use this method alone without the frequency determination techniques.

6.10 Conclusion of Chapter 6

This chapter discusses the steps starting from acquiring the data from children's wrists at SCH and at a local school to the processing of the vibration responses. The data processing was performed by several techniques with theoretical expectations described. The results produced have been demonstrated concisely and presented visually. Generation of incorrect results led to the establishment of appropriate techniques, that is, indication of magnitude of frequencies from frequency spectra, to be used in future studies. Some machine learning has also been applied to verify the outcomes.

Chapter 7: Data from Children's Ankles

7.1 Introduction

Studies conducted by (Libetta 1999) have shown that 91% patients who visit the Accident and Emergency (A&E) Departments with ankle and mid-foot injuries receive radiography. But only less than 15% of those radiographs show that the patient has a fracture. This is unnecessary exposure of radiation. Thus, a screening tool that can determine the presence/absence of an ankle fracture in order to reduce the number of avoidable X-rays would be welcome. For this reason, the device and the techniques discussed in the previous chapters have been applied on children, aged between 10 and 15 years old at SCH and observed if the method works with ankle injuries.

7.2 Acquisition of data

This study was conducted on the ankles of 10 children aged between 10 and 15 years old after obtaining local Research Ethics Approval. The participants all attended the Emergency Department of Sheffield Children's Hospital following ankle injury and all required ankle radiographs as part of routine clinical care. They all participated voluntarily, following full informed assent/consent and parental consent.
The device used for this study for data acquisition purpose is the same as that used for wrist study. Thus, the wire connecting the myDAQ instrument and the vibration inducer was shorter than that required for ankle data acquisition. For this reason, the device had to be shifted closer to the ankles for the inducer to be placed properly when the device was "run" (as shown in Figure 6.4). This step had to be repeated every time there was a participant with ankle injury for this study. As this study was continued simultaneously with the wrist study so it was better not to waste time to fix the wire length and solder the connecters again. For this reason, only 10 sets of data were collected.

Each child was asked to sit on a chair with his/her feet on the ground. Two participants' feet (2nd and 9th) could not touch their feet to the ground because of their level of ankle pain. Their injured legs were kept free in the air. Vibration was induced by the hand-held inducer at a point approximately 5 cm above the ankle which created 10 impacts over 10s. The piezoelectric sensor was held on the skin above the tibia (ankle bone on the medial (inside) aspect of the ankle) and was used to capture the data.

The data were acquired from both the injured and uninjured ankles, selecting the following parameters on the acquisition software (similar to the wrist study):

- period of 10 seconds (s),
- 60,000 samples per second,
- 1 Hertz (Hz) frequency,
- starting delay time was provided (waiting time of the inducer before it starts to run) = 7s.

7.3 Results and Analyses

Each signal was graphically presented to understand the shape.

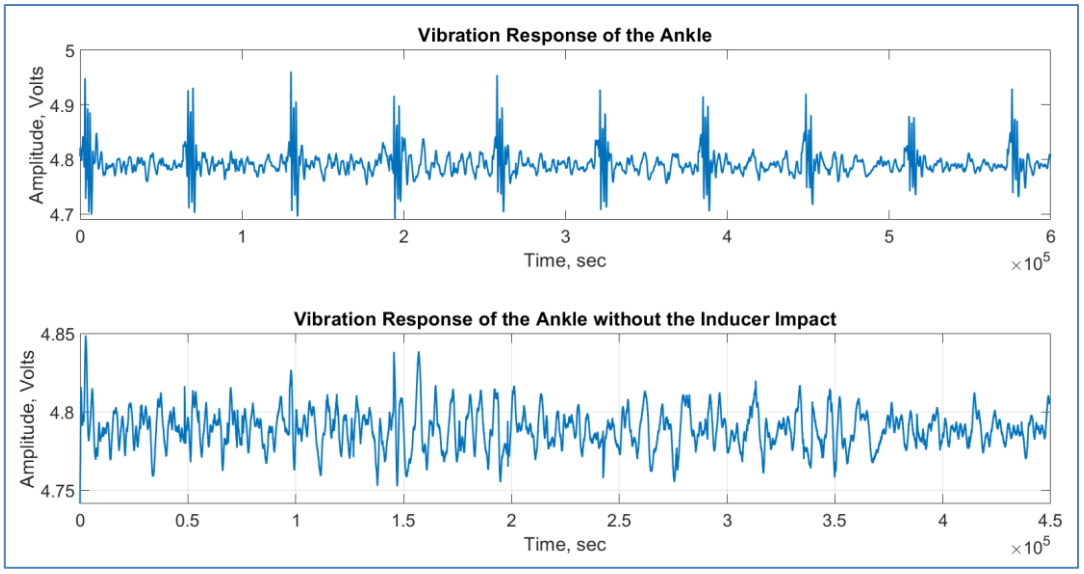

Figure 7.1: (a) Vibration Responses of the ankle bone (b) Vibration Responses after removal of the Inducer Impacts.

The peaks produced by the inducer impact were very unclear and distorted, not revealing any perfect shape, either sinusoid or squared, etc. Thus, 7% of the data (which is the data around the peaks due to the impacts in each second) produced in each second, were subtracted from the data set displayed in Figure 7.1.

The following steps were applied to the signals to produce Frequency Spectra:

- Smoothing - The signal was smoothed using a "loess" method. It means local regression of data using linear least squares and a 2nd degree polynomial.
- Filtering - A lowpass Infinite Impulse Response (IIR) filter with:
    - a passband frequency of 5000Hz,
    - a filter order of '5'.
- Sample rate of 60,000/second.
- Windowing - The smoothed and filtered signal was passed via a Parzen window. Parzen window, named after its originator, is piecewise-cubic approximations of Gaussian windows. The key role of this window is to reduce the effects produced as a result from truncation of signals.

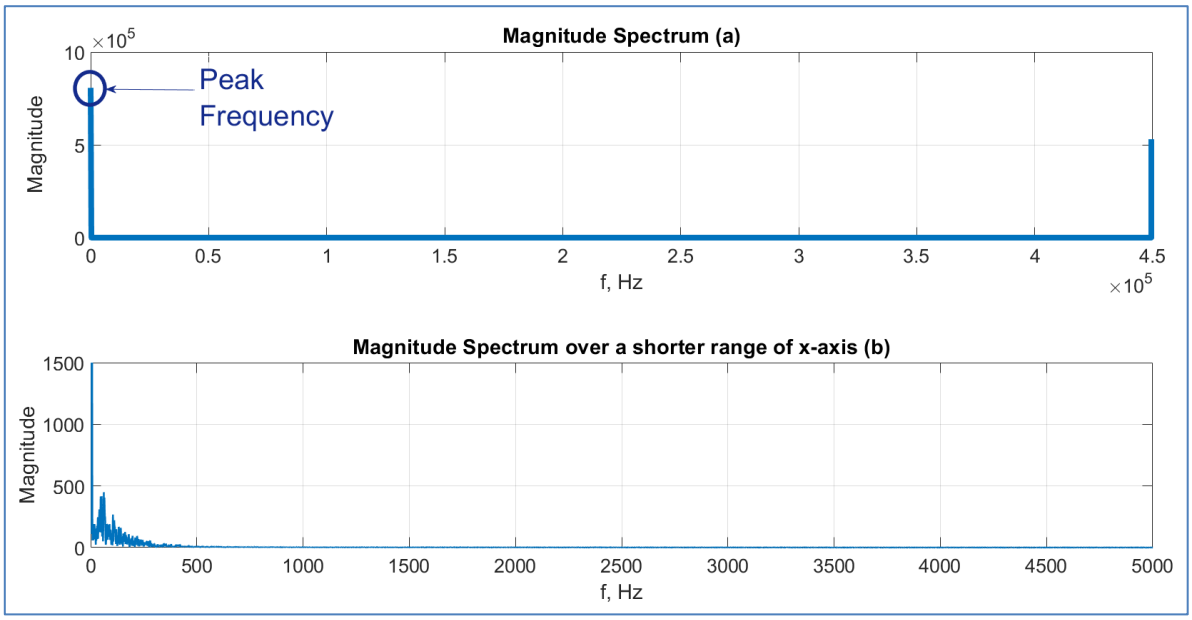

Figure 7.2: (a) Original Frequency Spectra and (b) Frequency Spectra over a shorter range of x-axis.

The Magnitude Spectrum plotted as shown in Figure 7.2(a) does not reveal any frequencies because the range of x-axis is too large thus it has been plotted over a smaller range of x-axis illustrated in Figure 7.2(b). Theoretically, there should be some peak frequencies.

The frequencies of all the participants' injured and uninjured ankles were noted and represented in Figure 7.3. A three-degree (cubic) and a four-degree polynomial have been drawn between the uninjured ankles' frequencies to determine how many points are separated by the line. They have both been represented in Figure 7.3.

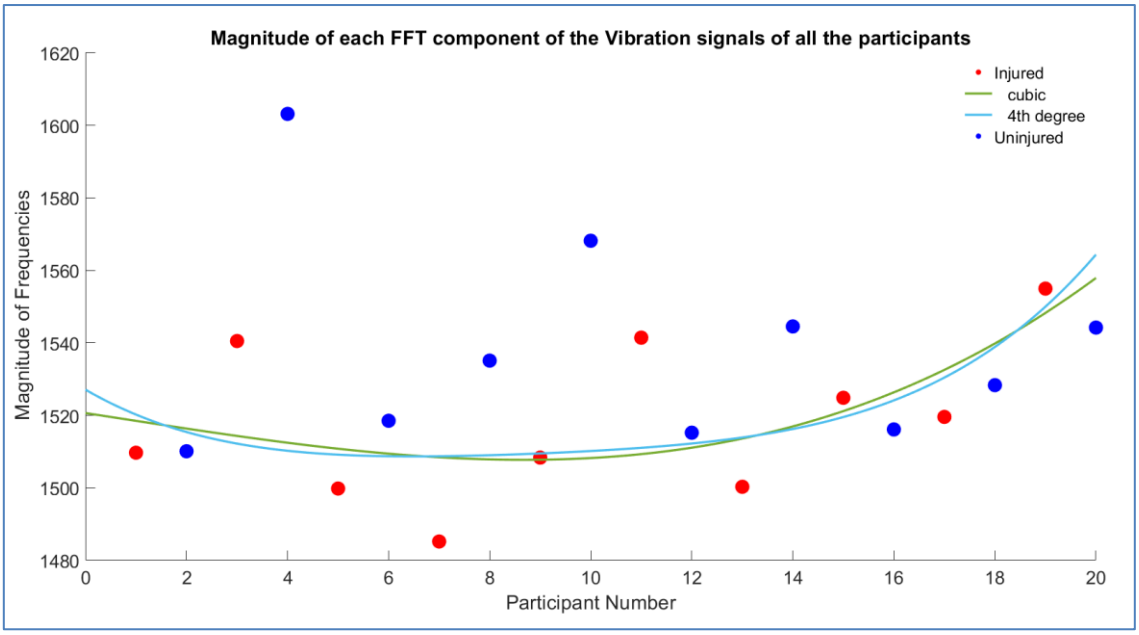

Figure 7.3: Bone magnitude components of the frequency spectra separated by polynomials.

The frequencies which fell below the polynomial were predicted as fractured and above the polynomial as unfractured. The results were sent to the radiologist to match with the reports of the radiographs. The results are tabulated below.

Table 7.1: Maximum of Cross-correlated magnitude of frequencies.

Number of Participants	Sex	Injury Type by X-ray	Injury Type by Cubic Polynomial	Injury Type by 4-degree Polynomial
1	Female	No Fracture	Fracture	Fracture
2	Male	No Fracture	No Fracture	No Fracture
3	Female	No Fracture	Fracture	Fracture
4	Female	No Fracture	Fracture	Fracture
5	Female	No Fracture	No Fracture	Fracture
6	Female	No Fracture	No Fracture	No Fracture
7	Female	No Fracture	Fracture	Fracture
8	Male	No Fracture	No Fracture	No Fracture
9	Female	No Fracture	Fracture	Fracture
10	Male	No Fracture	No Fracture	No Fracture

The *problem* encountered with the polynomial method was that the best fitted polynomial shape can change at any time based on the value of the frequencies when more injured patients are required to be assessed. Thus, there is no fixed way of applying the technique to determine the injuries.

There was another technique applied for the assessment. The signals from both injured and uninjured ankles were cross-correlated with each other. It is actually a technique which has been developed for assessing the wrist injuries. The maximum values of the cross-correlated frequencies were calculated and then scattered again. The results are represented in Figure 7.4.

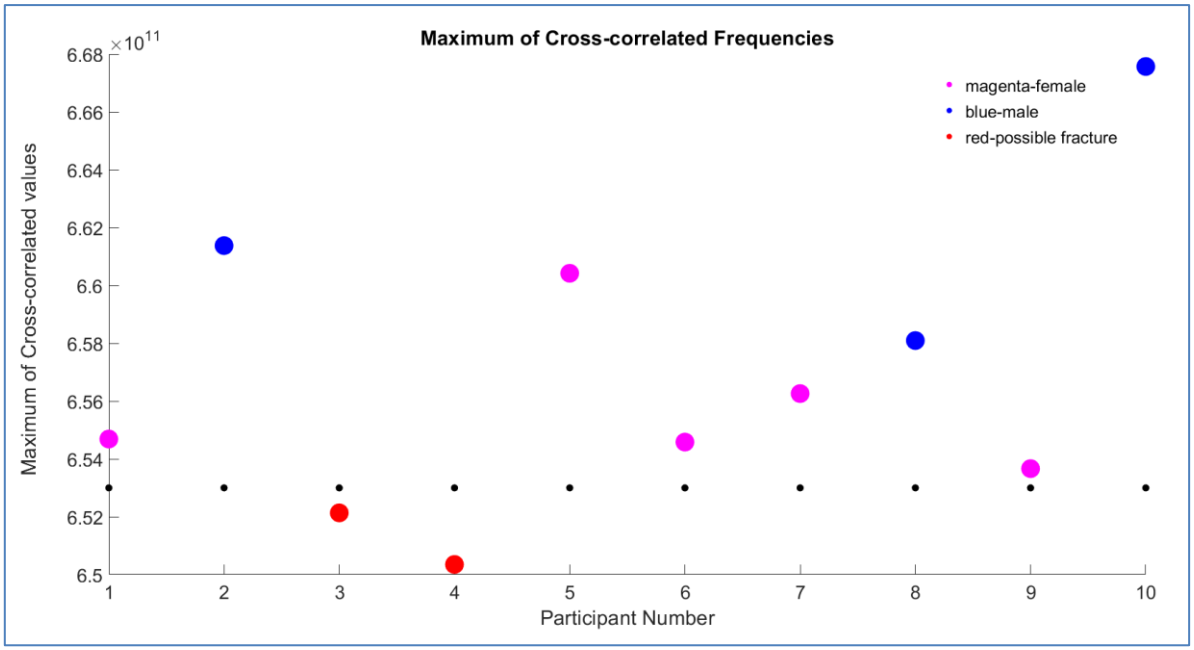

Figure 7.4: Maximum of Cross-correlated Bone magnitude of frequency spectra.

7.4 Conclusion of Chapter 7

Although this was a pilot study, yet Figures 7.3 and 7.4 suggest:

- higher ankle frequencies in males and
- significant variability between patients.

Both of the above points indicate that the study with ankle injuries needs further investigation.

Chapter 8: Conclusion and Further Works

8.1 Review of the study

The purpose of this study was to develop a screening tool for detecting Long Bone fractures in children. This study is affiliated with Sheffield Children's Hospital. The current situation is that most of the children are sent for having X-rays following an injury as this is the only way for the doctors to assess an injury. However, 60+% of the X-rays done on Long Bone injuries show that there is no fracture.

Each X-ray costs around £40 to £120. The patients must wait for the doctors to see them (sometimes 4 to 6 hours) following an injury. Without radiographs, it is impossible for the doctors to determine if an injury is a sprain or a fracture. Thus, the patients are regularly having X-ray. Although X-ray does not cause much ionising or harmful radiation exposure while taking radiographs, but no radiation is better than some radiation.

An existing device in the Centre of Automation and Robotics Research (CARR) was used at the beginning of this study and several modifications were made to the device to facilitate this study. This is a pilot study to develop a suitable screening technique. Data have been acquired from

- samples of wood,
- adults with wrists injuries who attended NGH,
- children with wrist or ankle injuries who attended SCH and
- children with no injuries at a local school.

Vibration has been induced for 10s by a suitable device via the most prominent bone in the elbow and the corresponding responses have been captured by a piezoelectric sensor attached to the wrists and ankles. Additionally, suitable acquiring programs have been improved for further studies along with proper modifications of the device. The vibration responses have been analysed using several techniques like Fast Fourier Transform, Short-Time Fourier Transform and Wavelet Decomposition. The

results demonstrate that production of frequency spectra by a particular method and parameters can classify between bone fractures and sprains well.

8.2 Research Questions with Answers

I. *Is there any difference in frequencies indicated by material similar to bones (wood) when they are intact or in fractured state?*

As described in Chapter 4, the research was initially carried out on 5 samples of blocks of wood with different densities. Data have been acquired by inducing vibration in their intact states and also in their fractured states. The variations in the peak frequencies, extracted from the composition of the frequency spectra, in both the states have been compared. Chapter 5 illustrates the results and concludes that the frequencies fall due to the variations of densities, that is, the less the densities, the less the frequencies.

II. Does it demonstrate that if a bone is fractured then vibration induction using the mechanism suggested will detect the fracture properly and will not cause any pain to the patient (especially to a child), when the bone is fractured?

According to the Chapter 4 and 5, vibration responses have been recorded from adult patients who attended A&E of NGH due to a wrist injury. 6 patients volunteered for this study. 10 vibrations have been induced for 10s and subsequent responses have been captured by placing a piezoelectric sensor on the wrists of both hands. The data were processed by finding frequency spectra and then classified by Fuzzy C-means, K-means and Correlation coefficients. The patients all had X-rays. 3 of the patients had fracture and 3 of them had sprains. The outcomes of the radiograph reports have been compared with the findings of the cluster analyses and it showed 100% match.

III. How the difference in frequency or any other property, generated from bone(s) designate a bone to be fractured or unfractured?

Vibration responses have been recorded from 50 children wrists who all attended Emergency Department of SCH with a wrist injury. All of them were between 10 and 15 years old. They all had X-ray. Their data were appropriately processed and compared with the results of the X-rays. The techniques were evaluated in several ways to yield an appropriate method for determining injury states. Data were acquired from 15 normal children also from Saturday School ClubOK located at King Edward VII Upper School to analyse with the same techniques as done with those from SCH and compare the effectiveness of the techniques. The patterns produced by the data from both SCH and school children suggested that:

- the male and female participants have different magnitude of frequencies,
- right hands might have higher magnitude of frequencies than left hands or the hand, which is dominant in use might have higher frequencies; most importantly, fractured wrists have lower frequencies than intact wrists and their variations from their mean values are larger for the males than that of females.

IV. Is the vibration study helpful in differentiating ankle fracture from sprain?

There were only 10 recruitments conducted with the ankle injuries. The wire of the inducer connected with the battery and all the electronic components attached to it, was relatively short as this device have been initially developed for the evaluation of wrists' injuries. The frequencies were generated by the FFT then categorised by polynomials and cross-correlation. The X-rays showed that there was no fracture present in any of the 10 patients. Some conclusions were drawn, like how the techniques can be applied for the further data acquisition. However, more number of recruitments is required for the study and the wire needs to be extended before carrying out the acquisition of the data. Additionally, some fractured ankles would definitely be advantageous for making concrete conclusions.

8.3 Summary of the research performed: main steps and findings

There have been several studies conducted previously to determine the natural and resonant frequencies of bones and also suggestions have been made that these can be utilised for determining fracture as discussed in Chapter 2. Such works have been done on hip bones as well. But there have been no concrete studies done on long bones (especially wrists) and to the best of our knowledge, no development of screening techniques. This research was performed as a pilot study to initiate the development of screening techniques utilising vibration signals. There are several other methods that need to be explored to increase the accuracy of the technique and also to find the reliable method for considering this technique in practice. The contributions made by the author with the help of the supervisors have been listed below:

- The device developed previously by the Sheffield Hallam University researchers, has been further modified in order to appropriately induce vibrations for a short period of time and extract corresponding bone vibration responses. In particular, some parts have been changed to make the device portable and the design of the device has been improved as well.
- Suitable control program has been designed to induce vibrations.
- Suitable acquisition program has been designed to save the vibration responses.
- All the modifications done to the device, suggestions made for alterations and the modification done to the programs have been discussed in Chapter 4.
- Preliminary studies have been conducted with samples of wood that have similar structures to bones to understand the properties that can be differentiated after introduction of fractures. The blocks of wood of different density have been collected and fractured by the help of the technicians of the University Mechanical Workshop.
- Online examinations were accessed and passed very well to be allowed to carry the data acquisition from patients attending Emergency Departments in local hospitals.

- Data were acquired from 3 (three) places: Northern General Hospital, Sheffield Children's Hospital and Saturday School ClubOK. The researcher visited those places and performed experiments on the subjects who consented to participate in the study. Appropriate Consent forms, Assent forms and Feedback questionnaires were collected.
- The data were recorded and securely saved to a laptop allocated to this study.
- The collected vibration responses were processed by means of various methods and observed whether the techniques can be efficiently utilised for differentiating between fractures and sprains.
- The main processing and differentiating methods chosen were fast Fourier transform, Wavelet Decomposition, Short-Time Fourier Transform, K-means, Fuzzy C-means and Self-organising map.
- The filtering methods included were Butterworth filters and newly designed IIR filters specifying the order of filters.
- The windowing methods chosen for this study were Hamming and Parzen windows, however, several other windows have been studied before deciding which windows should be used.
- Statistical methods developed for determining the efficiency of the methods were Correlation, Maximum Likelihood Estimate and Normal Distribution.

8.4 Contributions to Knowledge

Our study contributed to knowledge in several areas: to fundamental research, to applied science and to health services.

• Contribution to fundamental research: We introduced several new methods in processing vibration signals that could be applicable to signals obtained from different media. Several new algorithms have been explored and updated for data analysis. The details are given in *8.3*.

• Contribution to applied science: significant modification of a working device to generate vibration signals. The device was made portable, hand-held and minimum power consuming that would potentially allow its use by non-clinicians and in non-hospital settings.

• Contribution to health services: potential reduction of unnecessary X-ray examinations, reducing the waiting time in emergency departments and the number of unnecessary visits to hospitals.

8.5 Future Research

This research revealed some properties, for example, the sex of the participants might have impacts on frequencies. But there are other properties which need to be explored as well, for example, height of the participant, length between the sensor data and the vibration inducer, etc. Some data analyses showed that the dominant wrists (used more often) can have frequencies different from that of the other wrist (used less often). However, this factor needs to be explored in detail with a larger number of participants. Most importantly, this study produced some promising data and provided several ways to analyse the data that can be considered in further study.

The device and the associated acquiring methods have been modified according to the study steps. But for further research, it will be better to build a new prototype with longer wires and fixes suggested then to start collection of corresponding data for evaluations.

The methodology has to be improved further. There are various techniques that need to be implemented to check whether vibration signals from long bone injuries can be divided between sprains and fractures. More spectral analyses need to be taken into account before reaching any conclusion. Advanced techniques like *Spectral Kurtosis*, *Power Spectral Density Estimate* etc. can prove to be more useful in bringing out features that can be analysed further for differentiating. Attenuation of the oscillations or attenuation of the acoustic of the waves can be composed and compared among the fractured, sprained and normal signals to observe the rate of decrease of the signals. More learning techniques can be involved to differentiate further rather than estimating the cut-off frequencies.

While working on the improvements, one test needs to be conducted. The patients, especially the children get very frustrated very easily so they sometimes move their hands or legs which can hamper vibration induction followed by the recording. Thus, it should be observed carrying the same analyses for first 5 signals acquired, if they produce the same result as by the 10 signals (acquired in 10s). If they are the same, then the induction time can be reduced to make the data collection more effective. Moreover, if more data can be involved and better comparisons can be made

between the fracture and sprain then normal recording from normal wrists and ankles can be spared.

The study should be taken further considering the age of the participants, that is, this research to be conducted on younger children and analyse the data collected. The results of this study so far showed that ages of the participants did not have any effect on the results and the participants did not mention of any pain or discomfort due to the vibration inducer. However, a higher number of participants provide a more solid basis and therefore, a more reliable data set for analysis. Thus, the result will be more conclusive.

The entire study was regarding the development of a novel screening tool to reduce the unnecessary exposure of X-rays on children's bones. This study is conducted for the first time and many areas have been investigated. However, it will be better to examine further by recruiting new participants with different age group involving analysis of data via learning techniques; that will automate the process. It has already been demonstrated that the non-invasive tool is painless.

References

5 – Skeletal System. (2012). In: Treuting, Piper M. and Dintzis, Suzanne M. (eds.). Comparative Anatomy and Histology, A Mouse and Human Atlas. Elsevier.

Adewusi S., Thomas M. and Vu V.H. (2014). Resonances of the Human Hand-Arm System using Finite Element and Operational Modal Analysis Methods. Test transaction on control and mechanical systems, 3, 11-18.

Adewusi S., *et. al.* (2014). Modal Parameters of the Human Hand-Arm using Finite Element and Operational Modal Analysis. Mechanics & industry, 15 (6), 541-549.

Alizad, A., *et. al.* (2004). The effects of fracture and fracture repair on the vibrational characteristics of an excised rat femur. In: Ultrasonics symposium, 2004 IEEE, 1513-1516.

Almudhaffar, M., Nassar, A. A. and Kareem, H. A. H. A. (2014). Vibration of Bones: A Case Study on Human Femur. Basrah journal for engineering sciences, 14 (2), 229-239.

Analog Devices Inc. Engineeri (2011). Chapter 8 Analog Filters. In: Zumbahlen, Hank (ed.). Linear Circuit Design Handbook. Newnes, 8.1-8.144.

Anderson, Andrew E., Ellis, Benjamin J. and Weiss, Jeffrey A. (2007). Verification, validation and sensitivity studies in computational biomechanics. [online]. Computer methods in biomechanics and biomedical engineering, 10 (3), 171-184.

Auer, . Jorg, A. and Stick, John, A. (2011). Chapter 74 Bone Biology and Fracture Healing. In: Lopez, Mandi J. and Markel, Mark D. (eds.). Equine Surgery. 4th ed., Saunders, 1025-1027.

Avdagic, S. C., *et. al.* (2009). Differences in peak bone density between male and female students. Arh hig rada toksikol, 60(1), 79-86.

Bandyopadhyay, Oishila, Biswas, Arindam and Bhattacharya, Bhargab B. (2016). Long-bone fracture detection in digital X-ray images based on digital-geometric techniques. Computer methods and programs in biomedicine, 126, 2-14.

Barner, Kenneth E., Barner, Kenneth E. and Arce, Gonzalo R. (2004). Chapter 11: Self-Organizing Maps and Their Applications in Image Processing, Information Organization, and Retrieval. In: Nonlinear signal and image processing theory, methods, and applications. CRC Press, 387-445.

Bediz, Bekir, Özgüven, Nevzat H. and Korkusuz, Feza (2010). Vibration measurements predict the mechanical properties of human tibia. Clinical biomechanics, 25 (4), 365-371.

Been, Yeo Siok, Khan, Jamshed Namdar and Hui, Derek Chng Peng (May 2007). Designing medical devices for isolation and safety. EDN avago technologies, 75-78.

Bin Sediq, A. S., Qaddoumi, N. and Al-Nashash, H. (2006). Novel near-field microwave bone healing monitoring using open-ended rectangular waveguides. In: GCC conference (GCC), 2006 IEEE, 1-5.

Blackburn, E., *et. al.* (2012). Ankle fractures in children. J bone joint surg am, 94, 1234-1244.

Blaus, Bruce (2015). Classification of Body. [online]. Last updated 14 January 2015. http://blausen.com/.

Boer, FC den, *et. al.* (1998). Quantification of fracture healing with three-dimensional computed tomography. Archives of orthopaedic and trauma surgery, 117 (6-7), 345-350.

Brandt, Anders (2011). Noise and Vibration Analysis: Signal Analysis and Experimental Procedures. First ed., John Wiley & Sons, Ltd.

Brigham, E. Oran (1988). Chapter 2: The Fourier Transform. In: Oppenheim, Alan V. (ed.). The Fast Fourier Transform and its Applications. US, Pearson; US ed edition, 9-29.

Buxi, D., Redoute, J. and Yuce, M. R. (2014). A frequency-sensing readout using piezoelectric sensors for sensing of physiological signals. In: Engineering in

medicine and biology society (EMBC), 2014 36th annual international conference of the IEEE, 1420-1423.

Chakraverty, S. (2009). Vibration of Plates. USA, CRC Press.

Chakraverty, Snehashish and Pradhan, Karan Kumar (2016). Vibration of functionally graded beams and plates. Odisha, India, Elsevier.

Chant, Ian (2012). Researchers Propose Wood As A Next Generation Bone Replacement. [online]. https://www.themarysue.com/wood-bone-replacements/.

Chaparro, L. F. (2014). Signals and Systems Using MATLAB. 2nd ed., Academic Press.

Chaudhary, Vikas, Bhatia, R. S. and Ahlawatb, Anil K. (2014). A novel Self-Organizing Map (SOM) learning algorithm with nearest and farthest neurons. Alexandria engineering journal, 53 (4), 827-831.

Chun-Yu, Bao and Qing-Hua, Meng (2010). Three-dimensional finite element analysis of the tibia stresses during jumping moment. In: 2010 international conference on computational and information sciences, Chengdu, China, 756-759.

Clarke, Christopher, G. D. and Dux, Anthony, E. W. (2015). 1. About X-rays. In: Abdominal X-rays for Medical Students. John Wiley & Sons, 1-3.

Cochran, William T., *et. al.* (1967). What Is the Fast Fourier Transform? Proceedings of the IEEE, 55 (10), 1664-1667.

Cole, Peter, A. (2017). How would you treat a 14-year-old football player with closed fracture of the right tibia? [online]. https://www.healio.com/orthopedics/news/blogs/%7B308c56a9-0504-4258-a4fd-aa24afb17bf6%7D/ask-the-experts/how-would-you-treat-a-14-year-old-football-player-with-closed-fracture-of-the-right-tibia.

Collier, R. J. and Ntui, J. A. (1994). In vivo measurements of the phase constants of transverse mechanical waves in a human tibia from 100 to 1000 Hz. Medical engineering & physics, 16 (5), 379-383.

Cooper, C., *et. al.* (2004). Epidemiology of childhood fractures in Britain: a study using the general practice research database. Journal of bone and mineral research, 19 (12), 1976-1981.

Cordero, Rene (1990). The measurement of innovation performance in the firm: An overview. Research policy, 19 (2), 185-192.

Cornelissen, M., Cornelissen, P. and Van Der Perre, G. (1982). A dynamic model of a healing fractured tibia. Journal of biomechanics, 15 (10), 806.

Cornelissen, P., *et. al.* (1986). Assessment of tibial stiffness by vibration testing in situ—II. Influence of soft tissues, joints and fibula. Journal of biomechanics, 19 (7), 551-561.

Crowell, Benjamin (2003). Vibration and Waves. 2.1st ed., Fullerton, California, Light and Matter, 3.

Dalton, Lori, A. (2014). On the Optimality of k-means Clustering. In: Houston, USA.

Dana-Farber Cancer Institute (2019). Can X-Rays Cause Cancer? [online]. https://blog.dana-farber.org/insight/2019/01/can-xrays-cause-cancer/.

Davis, Michael and Feinerman, Alan (2012). Assessing Graduate Student Progress in Engineering Ethics. Science and engineering ethics, 18 (2), 351-367.

Dawood, Munqith S., Wael, Farah and Habeeb, Fadel (2012). Study the Effect Of Laser And Ultrasound On The Healing Of Bones Fractures. i-manager's journal on future engineering and technology, 7 (4), 21-26.

De Silva, Clarence W. (2007). Vibration Damping, Control, and Design. Vancouver, Canada, CRC Press.

Deviant, Mat, S. (2010). The Practically Cheating Statistics Handbook. 2nd ed., Createspace.

Divya, P., Geetha, R. and Kavitha, P. S. (2012). Semi-automatic detection of fracture in wrist bones using graph-based grammar approach. In: Computing communication

& networking technologies (ICCCNT), 2012 third international conference on, Coimbatore, July 26-28, 2012. 1-7.

Dussa, C. U., *et. al.* (2006). Wrist Injury with normal X-Rays – Which is better investigation? Orthopaedic proceedings, 88-B (SUPP I 186-187).

Everitt, Brian, *et. al.* (2011). Cluster Analysis. 5th ed., Wiley.

Fakuda, E. and Yasuda, I. (1957). On the piezoelectric effect of bone. Journal of the physical society of Japan, 12 (10), 1158-1162.

Fellows, Richard, Liu, Anita and Storey, Colin (2004). Ethics in construction project briefing. [online]. Science and engineering ethics, 10 (2), 289-301.

Feng, Xu (2009). Chemical and Biochemical Basis of Cell-Bone Matrix Interaction in Health and Disease. Current chemical biology, 3 (2), 189-196.

Ferrari, SL, *et. al.* (2006). Childhood fractures are associated with decreased bone mass gain during puberty: an early marker of persistent bone fragility? Journal of bone and mineral research, 21 (4), 501-507.

Frunza, Marius-Christian (2016). Chapter 2G - Fuzzy Methods. In: Solving Modern Crime in Financial Markets. Academic Press, 183-191.

Fung, Ellen B., *et. al.* (2012). The effect of whole body vibration therapy on bone density in patients with thalassemia: A pilot study. American journal of hematology, 87(10), E76-E79.

Gabriellia, F., *et. al.* (2008). Bone integrity described by resonance frequency signature. Computer methods in biomechanics and biomedical engineering, 1, 95-96.

Georgiou, A. P. and Cunningham, J. L. (2001). Accurate diagnosis of hip prosthesis loosening using a vibrational technique. Clinical biomechanics, 16 (4), 315-323.

Ghahramani, Zoubin (2004). Unsupervised Learning. In: Bousquet, O., Von Luxburg, U. and Rätsch, G. (eds.). Advanced Lectures on Machine Learning. 1st ed., Springer-Verlag Berlin Heidelberg, 72-112.

Giannakopoulos, Theodoros and Pikrakis, Aggelos (2014). Introduction to Audio Analysis: A MATLAB Approach. 1st ed., Academic Press.

Girdhar, Paresh (2004). Practical Machinery Vibration Analysis and Predictive Maintenance. Newnes. Practical Machine Vibration Analysis and Predictive Maintenance.

Graaff, Van De Kent M. (1998). Chapter Seven Skeletal System: The Appendicular Skeleton. In: Human Anatomy. 5th ed., McGraw-Hill, 168-188.

Griffin, M. J. (1990). Handbook of Human Vibration. San Diego, CA, Academic Press Inc.

Guly, HR (2002). Injuries initially misdiagnosed as sprained wrist (beware the sprained wrist). Emergency medicine journal, 19 (1), 41-42.

Hambley, A. (2011). Electrical engineering principles and applications. 5th ed., New Jersey, Person Education, Inc.

Hamdy, Nadder (2009). 8 Discrete-Time Transforms. In: Applied Signal Processing: Concepts, Circuits, and Systems. United States of America, CRC Press, 399-432.

Handoll, Helen, H. G., *et. al.* (2016). Interventions for treating wrist fractures in children. Cochrane database of systematic reviews, (12), 1-10.

Hasan, Mohammad, Shabbir and Duan, Zhong-Hui (2015). Chapter 4 – Hierarchical k-means: A Hybrid Clustering Algorithm and Its Application to Study Gene Expression in Lung Adenocarcinoma. In: Tran, Quoc, Nam and Arabnia, Hamid (eds.). Emerging Trends in Computational Biology, Bioinformatics, and Systems Biology. Elsevier Inc., 51-67.

Hedström, E. M., *et. al.* (2010). Epidemiology of fractures in children and adolescents: increased incidence over the past decade: a population-based study from northern Sweden. Acta orthopaedica, 81 (1), 148-153.

Ho Yeon Son, *et. al.* (2014). Flexible Fibrous Piezoelectric Sensors on Printed Silver Electrodes. Nanotechnology, IEEE transactions on, 13 (4), 709-713.

Hobatho, Marie Christine, *et. al.* (1991). Development of a Three-Dimensional Finite Element Mode of a Human Tibia using Experimental Modal Analysis. J. biomechanics, 24 (6), 371-383.

Hohmann, E. L., *et. al.* (1986). Innervation of periosteum and bone by sympathetic vasoactive intestinal peptide-containing nerve fibers. Science, 232 (4752), 868-871.

Hopman, Lance David, Scheinberg, Samuel and Fox, William Henry (2016). Acoustic Detection of Bone Fracture. United States Patent.

Ifeachor, Emmanuel C. and Jervis, Barrie W. (2002). 3 Discrete Transforms. In: Digital Signal Processing A Practical Approach. 2nd ed., Prentice Hall, 133-150.

Jaffe, Bernard, Cook, W. R. Jr and Jaffe, H. (eds.) (2012). Piezoelectric Ceramics. 3rd ed., New York, Academic Press. Piezoelectric Ceramics.

Jain, A. K., DUIN, R. P. W. and MAO, Jianchang (2000). Statistical Pattern Recognition: A Review. Ieee transactions on pattern analysis and machine intelligence, 22 (1), 4-4-37.

Jamil, I. A., *et. al.* (2014). Vibration data acquisition and visualization system using MEMS accelerometer. In: Electrical engineering and information & communication technology (ICEEICT), 2014 international conference on, Dhaka, 10-12 April 2014. 1-6.

Jansson, D. and Medvedev, A. (2013). Visual stimulus design in parameter estimation of the human smooth pursuit system from eye-tracking data. In: American control conference (ACC), 2013, 887-892.

Jeong, Joong-Ki and Lee, Seung-Jun (2014). Koh Young Technology Inc.; Patent Issued for Method for Generating Task Data of a PCB and Inspecting a PCB. Journal of engineering, 8051.

Jurist, J. M. (1973). Difficulties with measurement of ulnar resonant frequency. Physics in medicine & biology, 18, 289-291.

Jurist, John M. (Physics in Medicine & Biology). In Vivo Determination of the Elastic Response of Bone I. Method of Ulnar Resonant Frequency Determination. 1970, 15(3), 417-426.

Kamble, H. and Phadke, G. S. (2016). Frequency response analysis of respiratory sounds and comparative study for windowing techniques. In: 2016 international conference on signal processing, communication, power and embedded system (SCOPES), Paralakhemundi, India.

Kantardzic, Mehmed (2011). 1 Data - Mining Concepts. In: Data Mining: Concepts, Models, Methods, and Algorithms. 2nd ed., New Jersey, John Wiley & Sons, Inc., 3.

Kaur, Komal Preet, Randhawa, Rajneesh and KALER, R. S. (2014). Performance analysis of WDM-PON architecture using different receiver filters. Optik - international journal for light and electron optics, 125 (17), 4742-4744.

Khan, Zulki (2014). Uncovering Assembly Problems of High-Speed PCBs. SMT (online), 29 (2), 74-78.

Kichouliya, R., *et. al.* (2012). Investigating the effects of impulse excitations on instrumented electro-explosive devices. In: Electromagnetic compatibility (APEMC), 2012 Asia-Pacific symposium on IEEE, Singapore, May 2012. 988-992.

Kumar, Ashwani, *et. al.* (2014). Free Vibration Modes Analysis of Femur bone Fracture Using Varying Boundary Conditions based on FEA. Procedia materials science, 6, 1593-1599.

Lalkhen, Abdul Ghaaliq and Mccluskey, Anthony (2008). Clinical tests: sensitivity and specificity. Continuing education in anaesthesia critical care & pain, 8 (6), 221-223.

Landin, Lennart A. (1997). Epidemiology of Children's Fractures. Journal of pediatric orthopaedics, 6 (2), 79-83.

Laura, PA, Rossi, RE and Maurizi, MJ (1990). Dynamic Analysis of a simplified bone model during the process of fracture healing. J. biomed eng., 12 (2), 157-160.

Li, Xiaoyang and Kan, Edwin C. (2010). A wireless low-range pressure sensor based on (PVDF-TrFE) piezoelectric resonance. Elsevier journals: Sensors and actuators A: Physical, 163, 457-463.

Libetta, Carole, *et. al.* (1999). Validation of the Ottawa ankle rules in children. J accid emerg med, 16, 342-344.

Lin, Shuyu (2004). Piezoelectric ceramic rectangular transducers in flexural vibration. Ultrasonics, ferroelectrics, and frequency control, IEEE transactions on, 51 (7), 865-870.

Lippmann, Robert K. (1932). The use of auscultatory percussion for the examination of fractures. J bone joint surg, 14 (1), 118-126.

Lynn, Paul A. and Fuerst, Wolfgang (2000). Introductory Digital Signal Processing with Computer Applications. 2nd ed., West Sussex, England, John Wiley & Sons Ltd.

Lyons, Ronan A., *et. al.* (2017). Children's fractures: a population based study. Injury prevention, 5, 129-132.

Ma, Xing, *et. al.* (2010). Application of Computer-assisted Novel 3D Reconstruction and Simulation in Orthopaedic Surgical Treatment of Complex Proximal Humeral Fractures. In: 2nd international conference on computer engineering and technology, Chengdu, China, 16-18 April 2010. 743-746.

Maffuli, Nicola and Ferran, Nicholas A. (2008). Management of Acute and Chronic Ankle Instability. Journal of the American academy of orthopaedic surgeons, 16 (10), 608-615.

Manfred Glesner, Francois Philipp (2013). Embedded Systems Design for Smart System Integration, 32.

Marino, Andrew, A., Becker, Robert O. and Soderholm, Sidney C. (1971). Origin of the piezoelectric effect in bone. Calcified tissue international and musculoskeletal research, 8 (1), 177-180.

Mariolani, José Ricardo Lenzi and Belangero, William Dias (2013). Comparing the In Vitro Stiffness of Straight-DCP, Wave-DCP, and LCP Bone Plates for Femoral Osteosynthesis. [online]. ISRN orthopedics, 2013, 1-6.

Martinez, Wendy and Martinez, Angel (2005). Exploratory Data Analysis with MATLAB. CRC Press.

Math Bits (2018). Statistics 2: Correlation Coefficient. [online]. https://mathbits.com/MathBits/TISection/Statistics2/correlation.htm.

MATHWORKS, MATLAB (2017). Unsupervised Learning. [online]. https://uk.mathworks.com/discovery/unsupervised-learning.html.

Maxim, L. D., Niebo, R. and Utell, M. J. (2014). Screening tests: a review with examples. Inhalation toxicology, 26 (13), 811-828.

McGraw, N. H. (1942). Osseosonometry. Archives of surgery, 45 (1), 195-205.

Meyer-Baese, Anke and Schmid, Volker (2014). Pattern Recognition and Signal Analysis in Medical Imaging. 2nd ed., Elsevier.

Milivojević, Zoran (2009). Digital Filter Design. MikroElektronika.

Moheimani, S. O. R. (2003). A survey of recent innovations in vibration damping and control using shunted piezoelectric transducers. Control systems technology, IEEE transactions on, 11 (4), 482-494.

Morgado Ramírez, Dafne Z., Strike, Siobhan and Lee, Raymond Y. W. (2013). Measurement of transmission of vibration through the human spine using skin-mounted inertial sensors. [online]. Medical engineering and physics, 35 (5), 690-695.

Mustafa, M. A. and Al-Bahar, J. F. (1991). Project risk assessment using the analytic hierarchy process. Engineering management, IEEE transactions on, 38 (1), 46-52.

Mustra, M., Grgic, M. and Zovko-Cihlar, B. (2014). Alignment of X-ray bone images. In: Telecommunications (BIHTEL), 2014 X international symposium on, 1-4.

MVSR, Teja, Kumar, A. and Prasanth, C. V. S. (2014). Comparative analysis of windowing techniques in minimizing side lobes in an antenna array. In: 2014 international conference on communications and signal processing (ICCSP).

myDAQ, Datasheet (2010). User Guide and Specifications NI myDAQ. National Instruments.

National Instruments (2018). Aliasing. [online]. http://zone.ni.com/reference/en-XX/help/371361H-01/lvanlsconcepts/aliasing/.

Naylor, Andrew (2014). Can Wood be used as a Bio-mechanical Substitute for Bone during Evaluation of Surgical Machining Tools? Bioresources, 9(4), 5778-5781.

Neale, M. J. (ed.) (1996). Tribology Handbook. 2nd ed., Elsevier Ltd.

NHS National Institute for Health Research (2017). Good Clinical Practice (GCP). [online]. https://www.nihr.ac.uk/our-faculty/clinical-research-staff/learning-and-development/national-directory/good-clinical-practice/#whatgcp.

Nikiforidis, G, Bezerianos, A, Dimarogonas, A, Sutherland, C (1990). Monitoring of Fracture Healing by Lateral and Axial Vibration Analysis. Journal of biomechanics, 23(4), 323-330.

Nokes, L., *et. al.* (1984). Vibration analysis of human tibia: The effect of soft tissue on the output from skin-mounted accelerometers. Journal of biomedical engineering, 6 (3), 223-226.

Nokes, L., *et. al.* (1985). Vibration Analysis in the Assessment of Conservatively Managed Tibial Fractures. Journal of biomedical engineering, 7 (1), 40-44.

Nokes, L. D. M. (1999). The use of low-frequency vibration measurement in orthopaedics. Proceedings of the institution of mechanical engineers. pt. H. Journal of engineering in medicine, 213 (H3), 271-290.

Norouzi, Mohammad and Fleet, David, J. (2013). Cartesian k-means. In: Portland, USA.

O'Brien, Todd (2016). A Novel Method of Fracture Detection Via Smartphone. OBRIEN Medical.

Pang, Marco Y. C. (2010). Whole body vibration therapy in fracture prevention among adults with chronic disease. World journal of orthopedics, 1 (1), 20-25.

Parker, M. (2017). Digital Signal Processing 101. Second ed., Newnes.

Patil, S. S. and Gaikwad, J. A. (2014). Vibration analysis of electrical rotating machines using FFT: A method of predictive maintenance. In: 2013 fourth international conference on computing, communications and networking technologies (ICCCNT), Tiruchengode, India, 4-6 July 2013. IEEE, 6.

Pettit, Joseph, Mayo and Mcwhorter, Malcolm, Myers (1961). Chapter 1: Basic Amplifier Definitions. In: Electronic amplifier circuits: Theory and design (Electrical and electronic engineering series). McGraw-Hill, 1.

Pickering, Paul (2009). A System Designer's Guide to Isolation Devices. Sensors article archives.

Pillai, A. Sivathanu, Joshi, A. and Rao, K. Srinivasa (2002). Performance measurement of R&D projects in a multi-project, concurrent engineering environment. International journal of project management, 20 (2), 165-177.

Placzek, Jeffrey D. and Boyce, David A. (2017). Chapter 17 – Evaluation of Medical Laboratory Tests. In: Orthopaedic Physical Therapy Secrets. 3rd ed., Elsevier, 125-134.

Planell, Josep A. (2009). 2 Bone anatomy, physiology and adaptation to mechanical loading. In: Best, Serena M., Lacroix, Damien and Merolli, Antonio (eds.). Bone Repair Biomaterials. Woodhead Publishing Limited, 25-68.

Public Health England (2008). Guidance Patient dose information: guidance. [online]. Last updated 4 September 2008. https://www.gov.uk/government/publications/medical-radiation-patient-doses/patient-dose-information-guidance.

Qin, Yi (2015). 29 - Measurement, Testing, and Diagnosis for Micromanufacturing Systems. In: Micromanufacturing Engineering and Technology. 2nd ed., Elsevier Inc., 675-704.

R. Ali, A. Offiah and S. Ramlakhan (2016). Fuzzy C-Means clustering to analyze bone vibration as a method of screening fracture. In: 2016 10th international symposium on communication systems, networks and digital signal processing (CSNDSP), Prague, Czech Republic, IEEE, 1-5.

Rao, Singiresu, S. (2007). Vibration of Continuous Systems. 1st ed., John Wiley & Sons.

Razaghi, H., *et. al.* (2014). An investigation of relationship between bone vibration frequency and its mass-volume ratio. In: Acoustics, speech and signal processing (ICASSP), 2014 IEEE international conference on, Florence, IEEE, 3616-3620.

Razaghi, H., *et. al.* (2014). Correlation analysis of bone vibration frequency and bone mineral density in children. In: Communication systems, networks & digital signal processing (CSNDSP), 2014 9th international symposium on, 188-192.

RelayHealth (2017). Summit Medical Group: Fracture Treatment. [online]. https://www.summitmedicalgroup.com/library/adult_health/sma_fracture_treatment/.

Rennie, L., *et. al.* (2007). The epidemiology of fractures in children. Injury, 38 (8), 913-922.

Rizzoli, R., *et. al.* (2001). Protein intake and bone disorders in the elderly. Joint bone spine, 68 (5), 383-392.

Rizzoli, R. and Bonjour, J. (2004). Dietary protein and bone health. J. bone miner. res., 19, 527-531.

Rizzoli, Rene (2010). Chapter 21 - Role of Dietary Protein in Bone Growth and Bone Loss. In: Osteoporosis in Men. 2nd ed., Academic Press.

Roberts, Sydney G. and Steele, Charles R. (2000). Efficacy of Monitoring Long-Bone Fracture Healing by Measurement of either Bone Stiffness or Resonant Frequency: Numerical Simulation. Journal of orthopaedic research, 18 (5), 691-697.

Ryder, D. M., *et. al.* (1993). A possible method of monitoring bone fracture and bone characteristics using a noninvasive acoustic technique. In: Acoustic sensing and imaging, 1993, International conference on, 159-163.

Salem, O., Yaning Liu and Mehaoua, A. (2013). Detection and isolation of faulty measurements in medical Wireless Sensor Networks. In: Future information and communication technologies for ubiquitous HealthCare (ubi-HealthTech), 2013 first international symposium on, Jinhua, 1-3 July 2013. 1-5.

Seeman, E. (2003). The structural and biomechanical basis of the gain and loss of bone strength in women and men. Endocrinol. metab. clin. north. am., 32 (1), 25-38.

Singh, V. R., Yadav, S. and Adya, V. P. (1989). Role of natural frequency of bone as a guide for detection of bone fracture healing. J. biomed eng., 11 (6), 457-461.

Singh, V. R. (1996). Diagnosis of bone abnormalities. In: Engineering in medicine and biology society, 1996. Bridging disciplines for biomedicine. Proceedings of the 18th annual international conference of the IEEE, Amsterdam, Netherlands, IEEE, 161-162.

Slongo, Theddy and Audigé, L. (2010). AO Pediatric Comprehensive Classifi cation of Long-Bone Fractures (PCCF). Switzerland, AO Foundation. AO Pediatric Classification Group, 4-36.

Stádník, Bohumil, Raudeliūnienė, Jurgita and Davidavičienė, Vida (2016). Fourier Analysis for Stock Price Forecasting: Assumption and Evidence. Journal of business economics and management, 17(3), 365-380.

Stearns, Samuel, D. and David, Ruth, A. (1996). Signal Processing Algorithms in MATLAB. United States of America, Prentice Hall.

Stein, Jonathan Y. (2001). John Wiley & Sons, Inc. Digital Signal Processing: A Computer Science Perspective.

Stephan, Gift, J. G. and Maundy, Brent (2015). Versatile composite amplifier configuration. International journal of electronics, 102 (6), 993-1006.

Tan, L. and Jiang, J. (2013). Digital Signal Processing - Fundamentals and Applications. Second ed., Elsevier.

Tan, Lei, *et. al.* (2016). Intermittent low-magnitude high-frequency vibration enhances biological and radiological parameters during fracture healing in sheep. Int J clin exp pathol, 10 (1), 282-289.

Theintz, G., *et. al.* (1992). Longitudinal monitoring of bone mass accumulation in healthy adolescents: evidence for a marked reduction after 16 years of age at the levels of lumbar spine and femoral neck in female subjects. J. clin. endocrinol. metab., 75 (4), 1060-1065.

Thomsen, Jon, Joel (1990). Modelling Human Tibial Structural Vibrations. J. biomechanics, 23 (3), 215-228.

Thomsen, J. S., Brüel, A. and Hauge, E. M. (2012). Human vertebral bone microstructure from infancy to senescence. Bone, 50, Supplement 1 (0), S56.

Tsyrulnik, A. (2015). Emergency department evaluation and treatment of wrist injuries. Emergency medicine clinics of North America, 33 (2), 283-296.

Tutorials Point (2018). Signals Sampling Theorem. [online]. https://www.tutorialspoint.com/signals_and_systems/signals_sampling_theorem.htm.

Vasile, Alexandru, *et. al.* (2014). Electro-magnetic actuated vibrating platform. In: 2013 IEEE 19th international symposium for design and technology in electronic packaging (SIITME), Galati, Romania, 24-27 Oct. 2013. 241-244.

Vijaya, M. S. (2012). Piezoelectric materials and devices.

Applications in Engineering and Medical Sciences. 1st ed., Boca Raton, CRC Press.

Vijayakumar, R. and Gireesh, G. (2013). Quantitative analysis and fracture detection of pelvic bone X-ray images. In: Computing, communications and networking technologies (ICCCNT), 2013 fourth international conference on, Tiruchengode, 4-6 July 2013. 1-7.

Wahab, Magd, Abdel (2008). Dynamics and Vibration - An introduction. Revised ed., John Wiley & Sons Ltd.

Wallisch, Pascal, *et. al.* (2013). Chapter 12. Frequency Analysis Part II: Nonstationary Signals and Spectrograms. In: MATLAB for Neuroscientists: An Introduction to Scientific Computing in MATLAB. 2nd ed., Academic Press, 241.

Welch, Peter D. (1967). The use of fast Fourier transform for the estimation of power spectra: A method based on time averaging over short, modified periodograms. IEEE transactions on audio and electroacoustics, 15 (2), 70-73.

Wilson, J. M. G. and Jungner, G. (1968). Principles and Practice of Screening for Disease. Geneva, World Health Organization. (34).

Xu, Xueyan S., *et. al.* (2016). Vibrations transmitted from human hands to upper arm, shoulder, back, neck, and head. Int J ind ergon, 62, 1-12.

Yaniv, Z. and Joskowicz, L. (2004). Long bone panoramas from fluoroscopic X-ray images. Medical imaging, IEEE transactions on, 23 (1), 26-35.

Yarlagadda, R. K. R. (2010). Chapter 2: Convolution and Correlation. In: Analog and Digital Signals and Systems. Springer Science Business Media, LLC 2010, 39-69.

Yasuda, I. (1953). The classic: Fundamental aspects of fracture treatment. Clin orthop relat res reprinted from J. Kyoto med. soc., 4, 395-406.

Yoganathan, Ajit P., Gupta, Ramesh and Corcoran, William H. (1976). Fast Fourier transform in the analysis of biomedical data. Medical & biological engineering, 14, 239-245.

Yoshizawa, Shingo and Miyanaga, Yoshikazu Yoshizawa, Shingo (2013). Hardware Implementation of FFT Processors for Wireless Communications. IEICE ESS fundamentals review, 7 (2), 116-123.

Zarychta, Piotr and Kawa, Jacek (2011). CT images processing as one of the stages in knee joint alloarthroplasty. In: Mixed design of integrated circuits and systems (MIXDES), 2011 proceedings of the 18th international conference, Gliwice, Poland, 48-51.

Zawistowski, Thomas and Shah, Paras (2009). An Introduction to Sampling Theory. [online]. http://www2.egr.uh.edu/~glover/applets/Sampling/Sampling.html.

Zhang, Z. and Moore, J. (2011). New significance test methods of Fourier analysis of geophysical time series. Nonlinear processes in geophysics, 18, 643-652.

Zhu, Dong, *et. al*. (2010). Low-magnitude, high-frequency mechanical signal appears to prevent osteoporosis in male suspended rats. In: Bone, Shenzhen, China, S411-S411.

Appendices

A.1 Sensor Datasheet

Contact Microphone CM-01

High Sensitivity

Robust

Low Noise

Piezo Film Technology

Shielded Cable

FEATURES

Broad Bandwidth

High Sensitivity

Excellent Impact Resistance

Lightweight

Low Cost

APPLICATIONS

Electronic Stethoscope

Bone-conducted Sound Pickup

General Purpose Contact Microphone

Vibration/Impact Sensing

The CM-01B Contact Microphone

uses sensitive but robust PVDF piezo film combined with a low-noise electronic preamplifier to provide a unique sound or vibration pick-up with buffered output. The design minimises external acoustic noise while offering extremely high sensitivity to vibration applied to the central rubber pad. The CM-01B is ideal for detecting body sounds.

CM-01 Rev 1 www.disensors.com 05/12/2009 1 of 3 **Contact Microphone CM-01** CM-01 Rev 1 www.disensors.com 05/12/2009 **specifications**

CHARACTERISTICS	Min	Typ	Max	Units
Sensitivity		40		V/mm
Lower Limiting Frequency (-3 dB)		8		Hz
Upper Limiting Frequency (+3 dB)		2.2		kHz
Resonance Frequency		5		kHz
Spring Constant		20		N/m
Electronic Noise		1		mV pk-pk
Supply Voltage	4	5	30	V-DC
Supply Current		0.1		mA
Operating Temperature	+5		+60	°C
Storage Temperature	-20		+85	°C

dimensions

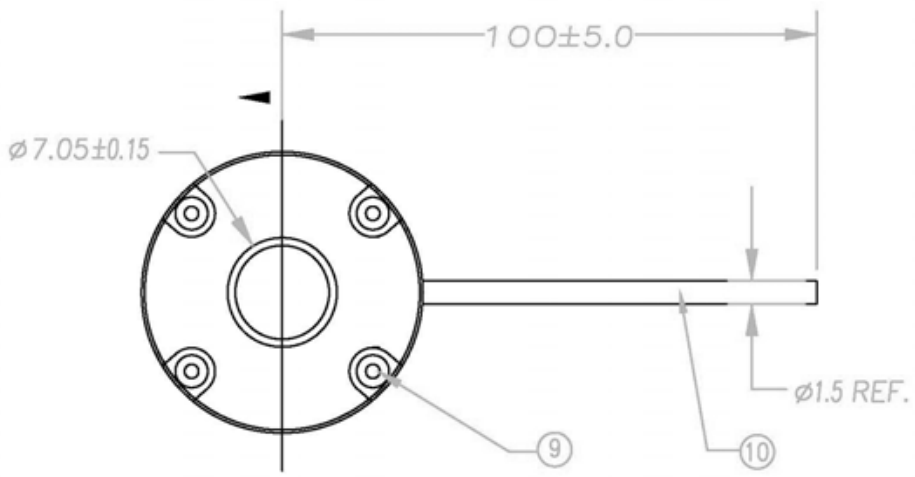

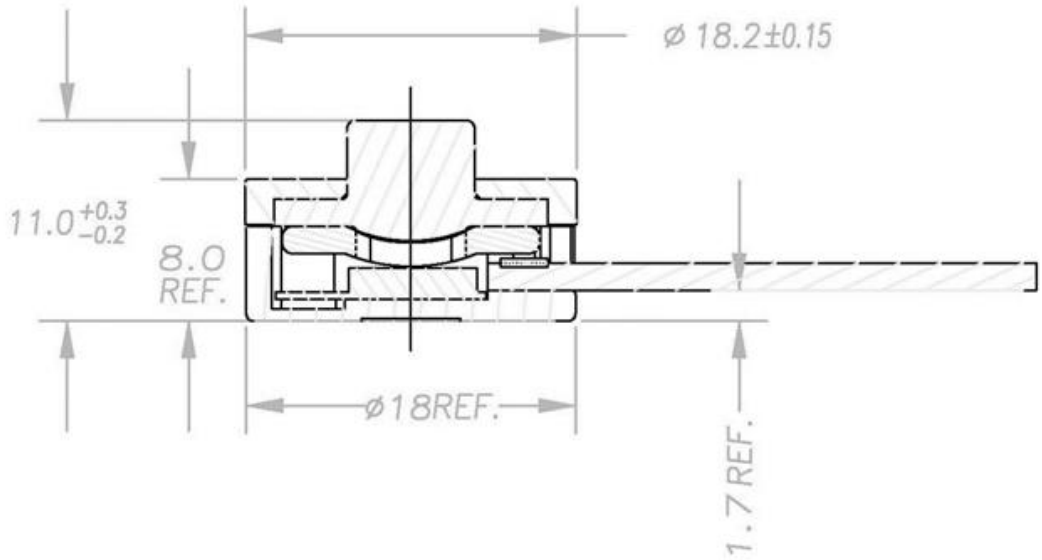

Typical Frequency Response

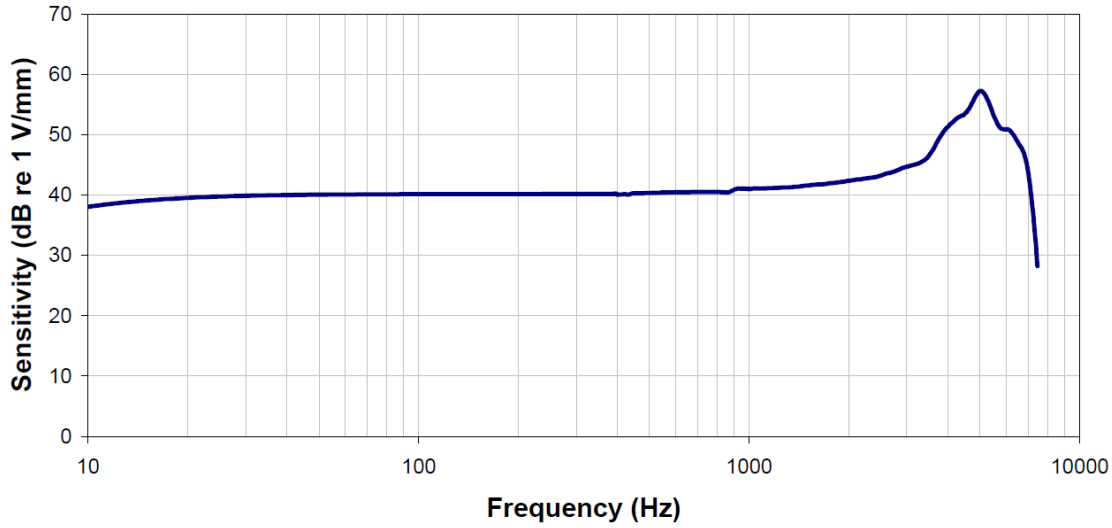

The above plot shows a typical frequency response curve for a device clamped below and subjected to piston-like displacement to the face of the rubber sensing pad.

internal schematic

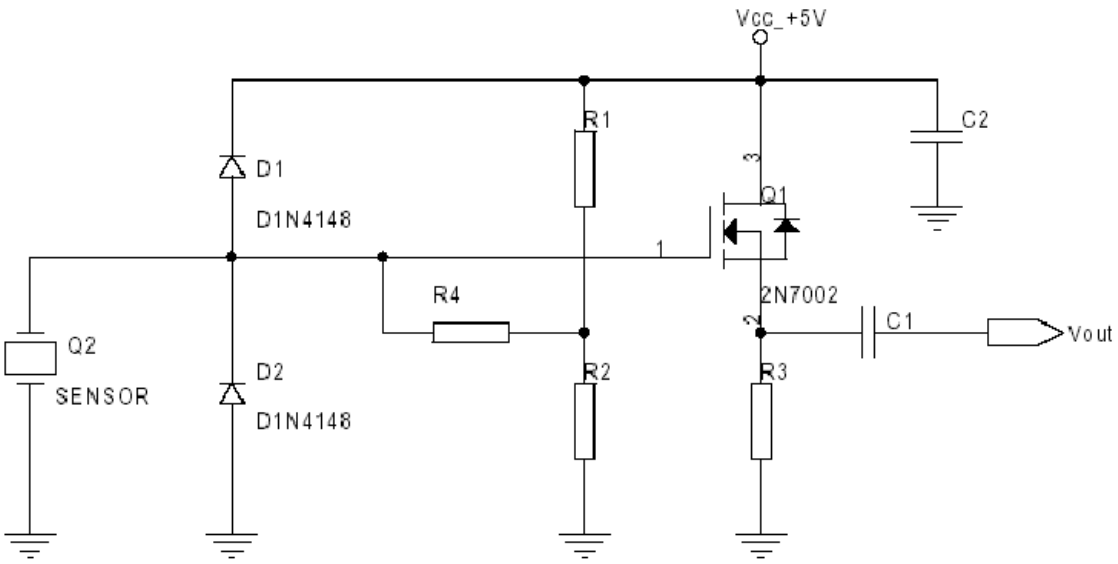

Shield (braid): GND C1 = C2 = 0.1 µF

Red wire: VCC, +5V R1 = R2 = 300K

Yellow wire: Vout R3 = 10K

R4 = 100M

A.2 Graphs for fracturing processes carried on the blocks of wood

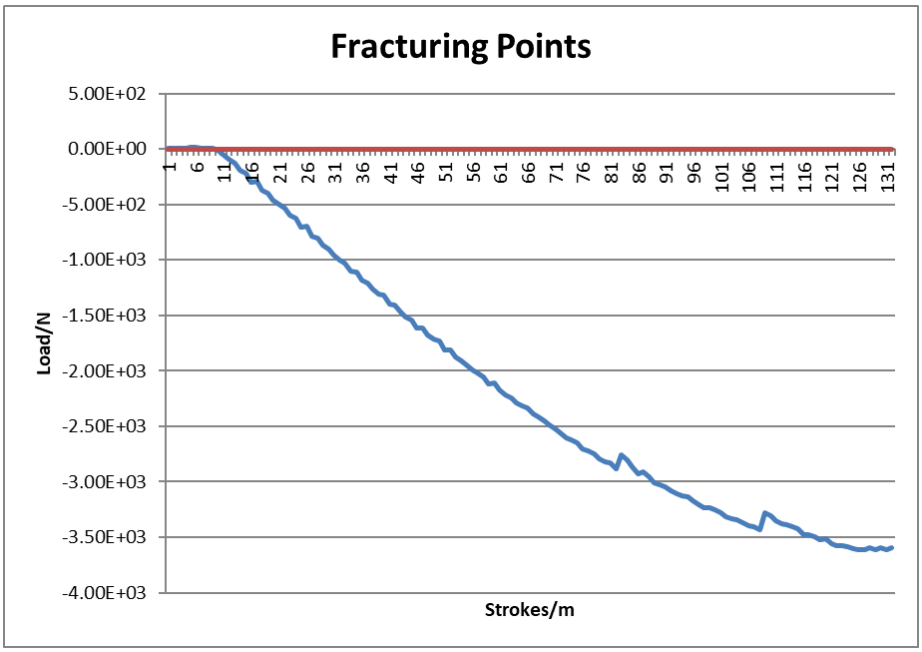

Figure A.2.1: Increase of Load to Walnut wood for fracturing it.

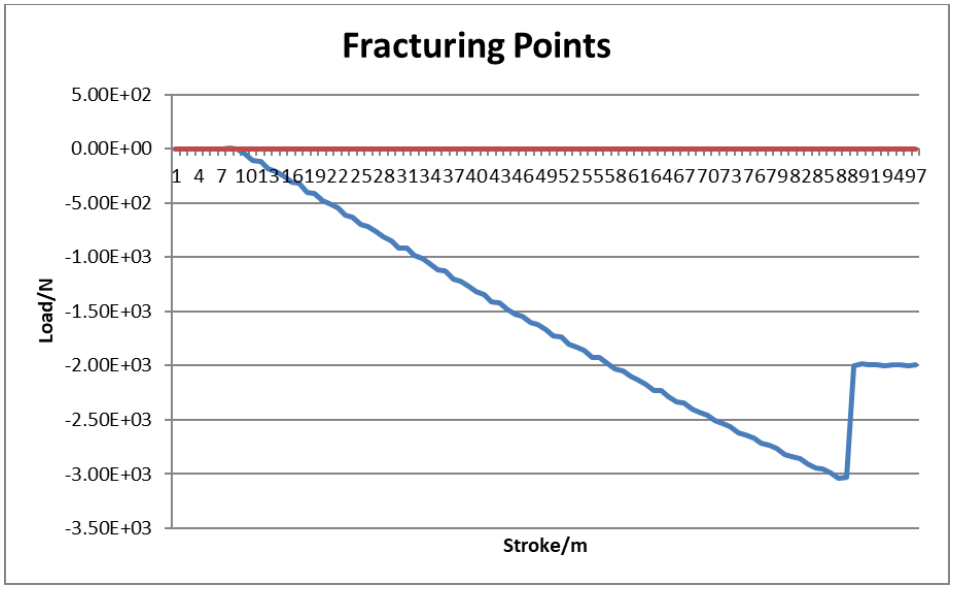

Figure A.2.2: Increase of Load to Maple wood for fracturing it.

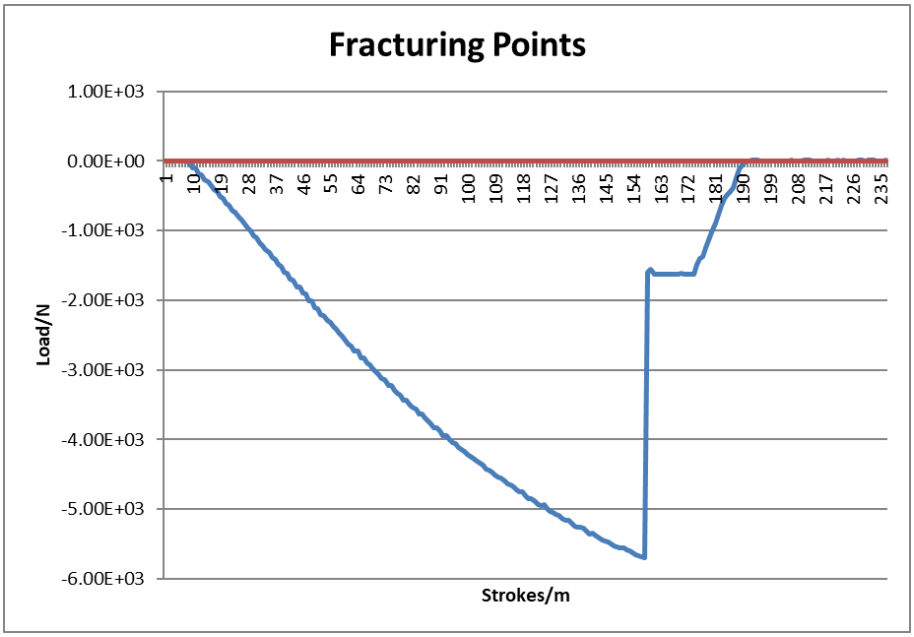

Figure A.2.3: Increase of Load to Beech wood for fracturing it.

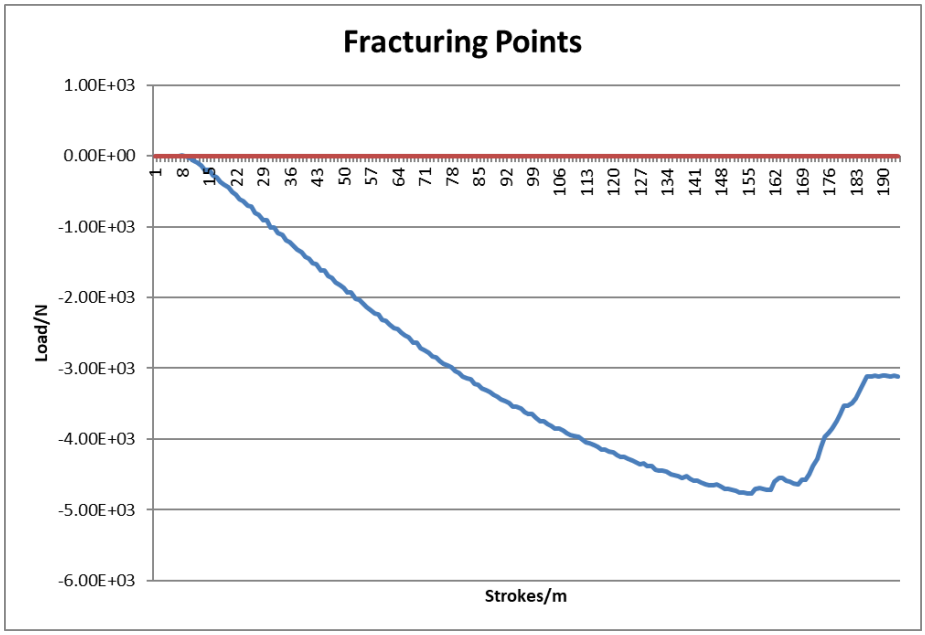

Figure A.2.4: Increase of Load to Oak wood for fracturing it.

A.3 Consent Form from Adult patients

Participant Study Number:

PARTICIPANT CONSENT FORM

Title of project: Bone Vibration as a Novel Screening Tool for Long Bone Fractures: Subjective Discomfort in Adult and Potential Tolerability in Children

Names of researchers: Dr Reza Saatchi[1], Dr Amaka Offiah[2], Dr Shammi Ramlakhan[3], Professor Derek Burke[3], Ms Ridita Ali[1]

[1] Sheffield Hallam University
[2] Sheffield University
[3] Sheffield Children Hospital

Please initial box

1. I confirm that I have read and understood the information sheet for the above study and have had an opportunity to ask questions. ☐
2. I understand that my participation is completely voluntary and that I am free to withdraw at any time, without giving any reason and without my legal rights being affected. ☐
3. I agree to take part in the above study. ☐

Name of the participant	Date	Signature
Name of Person taking consent	Date	Signature

1 copy for researcher; 1 copy to be given to the participant

A.4 Consent Form Parents/Carers of Children Patients

Sheffield Children's NHS
NHS Foundation Trust

Volunteer study number:

PARENT/LEGAL GUARDIAN CONSENT FORM

Title of project: *Vibration as a Method for Fracture Screening in Children*

Names of researchers: Dr Amaka C Offiah, Dr Lyuba Alboul and Professor Derek Burke

Please initial box

1. I confirm that I have read and understand the information sheet dated 21.12.2017 (version 1.0) for the above study and have had the opportunity to ask questions. ☐
2. I understand that my child's participation is voluntary and that I am free to withdraw my child at any time, without giving any reason, without my child's legal rights being affected. ☐
3. I agree to my child taking part in the above study. ☐

Name of Parent/Guardian	Date	Signature
Name of Person taking consent (if different from researcher)	Date	Signature
Researcher	Date	Signature

1 copy for parent; 1 copy for researcher

A.5 Self-organising map (SOM) pictures

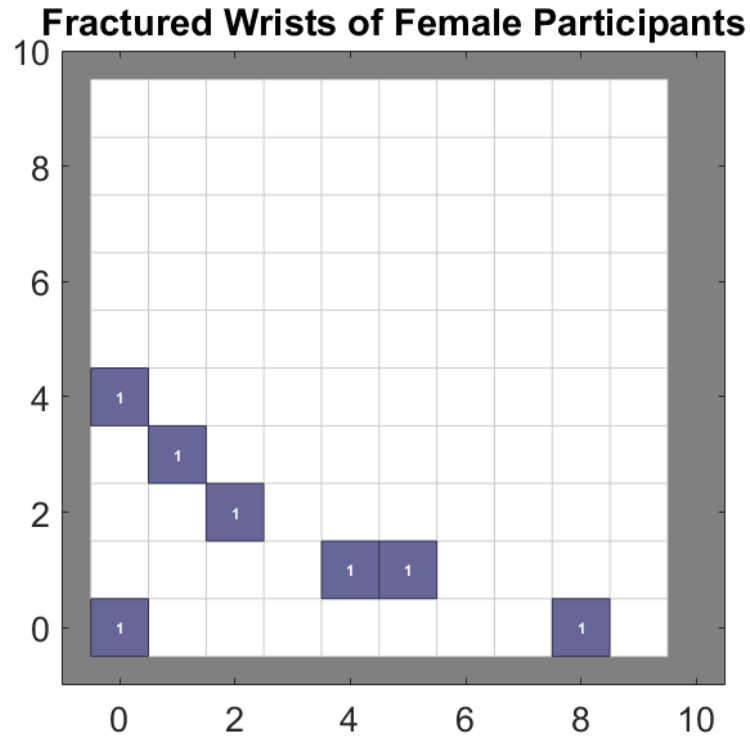

Figure A.5.1: Self-organised map of fractured wrists of female participants.

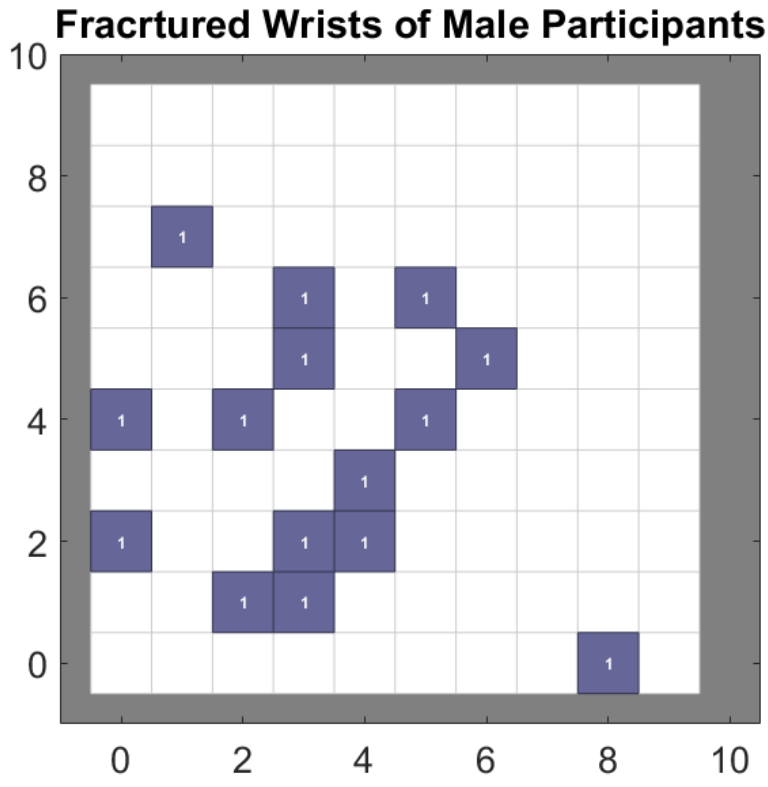

Figure A.5.2: Self-organised map of fractured wrists of male participants.